KICKING BLACK HOLES, CRUSHING NEUTRON STARS, AND THE VALIDITY OF THE ADIABATIC APPROXIMATION FOR EXTREME-MASS-RATIO INSPIRALS

A Dissertation

Presented to the Faculty of the Graduate School

of Cornell University

in Partial Fulfillment of the Requirements for the Degree of

Doctor of Philosophy

by

Marc Favata

August 2006

KICKING BLACK HOLES, CRUSHING NEUTRON STARS, AND THE VALIDITY OF THE ADIABATIC APPROXIMATION FOR EXTREME-MASS-RATIO INSPIRALS

Marc Favata, Ph.D.

Cornell University 2006

Current experiments hope to detect gravitational waves—oscillations of space and time predicted by Einstein. The strongest sources of gravitational waves are compact object binaries—orbiting neutron stars or black holes. Gravitational waves carry away energy, linear momentum, and angular momentum until the binary merges to form a single black hole. This thesis concerns three distinct projects regarding binary coalescence.

The linear momentum radiated when binaries merge imparts a recoil or "kick" to the final black hole. Black hole recoils have important astrophysical consequences: black holes can be displaced or ejected from their host galaxies or globular clusters, affecting black hole growth, quasar activity, and the density structure of galaxies. We compute the kick velocity using black hole perturbation theory, treating the binary as a small mass spiraling into a massive, spinning black hole. We find that the recoil can easily reach $\sim 100 - 200$ km/s but probably does not exceed 500 km/s.

Binary neutron stars are another important source of gravitational waves. Understanding the final coalescence phase of the gravitational wave signal requires

computer simulations. Some numerical simulations have shown that the neutron stars are subject to a crushing force late in the inspiral. This crushing effect has had no explanation and is disputed. We show that a compressive force arises due to a coupling of gravitomagnetic tidal fields to the current-quadrupole moment of the neutron star. However, except in special circumstances, this gravitomagnetic crushing effect is overwhelmed by stabilizing Newtonian tidal interactions.

A small compact object orbiting a massive black hole will be a strong source for space-based gravitational wave detectors. Accurate waveforms for these systems will require computing the self-force on the compact object. The tools to do this do not yet exist. But when the inspiral time is much longer than the orbital period (the adiabatic approximation), approximate waveforms for generic orbits can be computed. We estimate the error in the adiabatic approximation by computing the gravitational wave phase using post-Newtonian theory. We find that, for orbits with small eccentricity, the adiabatic waveforms will be good enough for detection but not for parameter extraction.

BIOGRAPHICAL SKETCH

Marc Favata was born on December 30, 1978 to Vincent and Diana Favata. He spent his early years in Bergen County, New Jersey.

Marc's education began at the Young School, which he attended for one year of pre-kindergarten education. Marc has few memories of his time there, but we surmise that when he was not expressing himself artistically or socializing with the other youngsters, we was undoubtedly pondering the mysteries of gravitation in the school playground. A year later Marc accepted a position at Our Lady of Grace School (OLG), a Catholic elementary school in Fairview, NJ. There he received his kindergarten Diploma in 1988, as well as his Diploma for completing grades 1 through 8 in 1996. Despite occasional set-backs due to "unsatisfactory" conduct, Marc was appointed to the prestigious Honor Roll on numerous occasions. He greatly enjoyed collaborating with his many colleagues at OLG, and during those years he developed a strong interest in physics and astronomy. While he originally considered careers in shoe-sales, insurance, and sanitation engineering, in the fourth-grade Marc decided to pursue a career as an astronaut, but in the sixth grade his interests switched to astrophysics. This was partly motivated by a sci-fi television series featuring an astrophysicist who, when not trying to save the world from aliens, would spend most of the day napping in his office and "thinking."

For his post-elementary studies Marc attended Bergen Catholic (BC) High School in Oradell, NJ. Under the watchful eye of the Irish Christian Brothers, BC provided a thorough and regimented academic environment, free of the unwholesome "distractions" of the fairer sex. Marc worked quite diligently at BC, reaching the peak of his academic prowess before his long spiral into stupidity that

continued through his graduate-school career. In 1996 he received his Diploma and was salutatorian of his graduating class. Marc continued to pursue his interests in physics and mathematics at BC and took a brief summer sabbatical at Columbia University to study physics there. When considering which universities to apply to, Marc's physics teacher, Mr. Felix Rizo, suggested he consider Caltech. Previously unknown to him, Marc discovered that this school was supposed to be a somewhat good place to study physics and astronomy. Around this time he also encountered a book titled *Black Holes and Time Warps: Einstein's Outrageous Legacy*, by Kip S. Thorne. Marc liked this book, and when he discovered that much of the research it discussed was taking place at Caltech, he became intent to go there.

Fortunately Marc was admitted and began his college studies in September 1996. Marc's undergraduate years were spent working on problem sets and enjoying numerous adventures with his Ruddock House cronies. Marc began his research work at Caltech with Tom Prince and Brian Vaughen on low-mass x-ray binaries. He then worked with George Djorgovski on the digitized Palomar observatory sky survey. In his junior year Marc took an eagerly anticipated course with Kip Thorne on general relativity, and after some pestering Thorne agreed to give Marc a summer project concerning tidal energy transfer. He continued to work with Thorne throughout his senior year and was eventually accepted to graduate schools (in no small part due to the undeserved good words put in by his advisers).

Based on the recommendation of Thorne and partly on that of his long-time comrade Daniel Abrams (who argued that you need to live someplace crappy to better appreciate the nicer places), Marc decided to attend graduate school at Cornell University under the tutelage of Éanna Flanagan. In a few months time the veracity of Abrams' argument became apparent, and Marc began plotting his

escape to fairer skies. In the fall of 2002 Marc spent a semester as a graduate fellow at the Kavli Institute for Theoretical Physics (KITP) in Santa Barbara, CA. There he worked with Scott Hughes and Daniel Holz on the kicks black holes receive after they coalesce. After returning to Ithaca for another bitter winter, Marc quickly escaped to Boston for the summer of 2003 to work with Hughes. Finally, after several more years of dwelling in Ithaca Hoovervilles and sweaty (yet freezing) walks up Cornell's hill, Marc defended his thesis on June 1, 2006.

Marc will spend the next few years as a postdoctoral fellow at the KITP. While he will undoubtedly enjoy the sunshine and ocean vista, his thoughts may occasionally drift back to the many cold, snowy nights he spent in Ithaca—a town whose charms he eventually came to appreciate.

This thesis is dedicated to my parents, grandparents, and teachers, as well as to the American taxpayer.

ACKNOWLEDGEMENTS

Where do I begin? Since I've spent nearly my entire life in school, I'll start by thanking the many teachers who have instructed me over the years. In particular the following individuals had an important impact: In elementary school the only stand-out I recall was Joseph Ciccone. Part teacher and part cop, he was one of the few teachers who actually knew something about science and provided some measure of encouragement. Unfortunately, he left teaching and pursued a political career as a county sheriff, a choice that ultimately ended somewhat disastrously.

At Bergen Catholic High School there were many fine-quality teachers. The following individuals particularly stand out in my mind: Felix Rizo was my physics teacher and provided lots of encouragement. In particular I credit him with suggesting that I consider Caltech for college—going there was probably one of the smartest moves I made. Br. Francis Gammaro was a master of many subjects, and in particular was a fine chemistry and computer science teacher. He also provided encouragement to the school science teams and drove us around to our various competitions. Finally, Br. Thomas Jensen, my mathematics teacher for two years, was a teacher and individual of excellence. Almost everything in this thesis (and most of the scientific work that I'll do in the future) rests upon the basic mathematical foundations that I learned from his classes.

My Caltech years are perhaps those on which I look back with the fondest memories. Many instructors there were quite good; many were not (for my own good I won't name names). I skipped a lot of classes, so I really don't remember much about most of them. But there were three classes that I attended religiously. Their instructors had an important role in getting me excited about astrophysics (and also in helping me get into grad school through the many letters that they

wrote for me). The first is George Djorgovski, who taught Ay20 (basic astronomy) my freshman year. I learned a lot about astronomy from his class and enjoyed interacting with him throughout my Caltech years. I also thank him for giving me a summer job when some other opportunities didn't come through, as well as for giving me my first (and so far only) observing experiences. Chuck Steidel was my instructor for Ay21 (galaxies and cosmology) and also for a senior astronomy lab class. He was an excellent teacher and served as my academic adviser for several years—dutifully signing my add card and providing useful advice whenever needed.

And of course there's Kip Thorne, who I, along with several generations of relativists, cannot thank enough. I first learned about Kip while reading his popular book in high school. His book played a big role in getting me interested in gravitational waves and also influenced my decision to attend Caltech. Kip's reputation as a master teacher was well-known, and I experienced this first-hand through his class on general relativity (Ph236) and later in his class (co-taught with Roger Blandford) on the applications of classical physics (Ph136). Most of what I know about relativity I learned from him, either through his classes or through his many books and articles. In addition to being a master teacher, I later learned that he is also a master person and mentor. While taking his Ph236 class, I asked Kip a few times if I could do a SURF (summer undergraduate research fellowship) with him, and he eventually agreed. He managed to pick out a project that was not too hard and not too easy. He was always helpful, encouraging, and generous with his time, and was always looking out for the best interests of his students (even if they be lowly undergraduates). For my senior thesis Kip picked out an interesting project concerning the strange results of neutron star binary simulations. However, perhaps because this project was a little tricky, but more likely because his student

was too stupid or lazy, it was not fully completed until recently. The results are presented in chapter 3 of this thesis. Much of what I know about relativity and how science works in practice I learned while working on this project. (Kip, I'm sorry it took so long.) Kip also played a big role in encouraging me to attend Cornell for graduate school. His friendship and personal and scientific excellence continue to inspire me.

Finally we come to Cornell, and there are many people here whom I should thank. I perhaps didn't take as many classes as I should, but several teachers stand out in my mind: David Hammer taught a class in plasma physics that I enjoyed (although I'm not sure how much of it I remember). I took two classes from Steve Strogatz on nonlinear dynamics and complex systems and found him to be a masterful instructor. I don't think I ever got lost or bored in one of his lectures. A great deal of the little I know about astrophysics I learned from Dong Lai through the many courses or seminars he has taught. I hope I can attain only a fraction of his enthusiasm and insight. I am also very grateful to the members of my special committee: Saul Teukolsky, Dong Lai, Riccardo Giovanelli, and Jim Cordes. Thanks for listening to me blab on about my research and for not abusing me as badly as you easily could have.

I must also thank my collaborators on the gravitational-wave recoil project: Dan Holz, especially for his friendship and advice; and David Merritt and Miloš Milosavljević for discussions about the consequences of black hole kicks and for generously putting my name on a paper on which I did relatively little work.

A special note of thanks is reserved for Scott Hughes. I first met Scott while I was an undergraduate at Caltech and he gave me some helpful grad school advice. Later, Scott served as the primary adviser on the gravitational-wave recoil project,

which we started (along with Dan Holz) when we were all at the Kavli Institute for Theoretical Physics (KITP). It would be hard to pick a more interesting and relevant project, and I'm very grateful to Scott for letting me collaborate with him on it. He has been an excellent mentor and friend on matters both scientific and personal. For whatever small successes I've had in my graduate school career, I owe a great deal to him.

I'd also like to thank Lars Bildsten. I came very close to choosing UCSB for grad school to study with Lars, but I somehow concluded that cold weather would do me some good. Lars was largely responsible for getting me a graduate fellow position at the KITP, and he was later responsible for giving me the KITP postdoctoral position that I will begin once this thesis is completed. Thanks!

And most importantly, I thank my adviser Éanna Flanagan. I came to Cornell largely because I was so impressed by the wide range of interesting topics on which Éanna had worked. While his student I was further impressed not only by his intellect and insightful approaches to problems, but also by the kindness and patience he showed to his sometimes difficult student. Éanna advised me extensively on all the problems I worked on as a graduate student, and although I didn't always follow his advice at first, he usually ended up being correct. I owe him a debt of gratitude for everything that he has done for me, and especially for putting up with me. I am proud to have had Éanna as my adviser, and I only regret that I was not a more diligent student.

While much is learned from teachers and advisers, more important are the lessons learned from family and friends. I'm especially indebted to my Caltech friends and classmates, who are perhaps the most important and lasting asset of my Caltech education. In particular I'd like to give a shout out to the following:

first, to Danny "M1" Abrams, thanks for being my house mate for most of our graduate school careers; likewise to the other members of "Ruddock East," Zach Medin and Ryan Gutenkunst, as well as the other members of the Caltech/Cornell crew, David Fang and Chris Liu. A special thanks to those Caltech peeps who made the trek out to Ithaca to visit my sorry ass: Dr. Hanna Kim, Dr. Kartik Srinivasan, Jeremiah Smith, Teo Der-Stepanians, Matt Dawson, and Jennie Teece. Thanks to Kartik, Matt, and Jennie for letting me crash at your places so many times over the past 6 years. And also thanks to the rest of the Ruddock House crowd: Kanchana, Umesh, Richi, Brian Blood, Lefty, Angela, Andrew, and Kevin. I would also like to thank my Cornell friends and colleagues, especially Steve Drasco, Étienne Racine, and Tanja Hinderer for many discussions about physics and lots of good times in the office or at conferences.

There are few to whom I owe more thanks than Hyun Jung Kang. Her love and support helped to make my final two years of grad school memorable. My fondest memories of Ithaca will be of the times I spent there with her.

Lastly I'd like to thank my parents. Everything I have I owe partly to them, not least of all my expensive education. They have supported me since birth and put up with my desire to study physics and astronomy instead of something practical. Thanks Mom and Dad.

TABLE OF CONTENTS

LIST OF FIGURES

LIST OF TABLES

PREFACE

Welcome to my thesis. In all likelihood you are either a member of my special committee, a close relative, friend or colleague, or a Cornell graduate student perusing the thesis shelves in the Astronomy Department reading room.

If you've made it this far you've probably already read the most interesting parts. If you wish to read on, here are some guidelines: Most of the material presented here appears or will appear in published form elsewhere. While some material here may remain unpublished, the published papers are likely to contain more complete and accurate information, and will probably be written a little better too.

Chapter 1 contains an introductory description of the projects that I worked on in graduate school. It is meant to be understood by someone with little science background. The remaining three chapters contain detailed descriptions of each project.

Chapter 2 and its appendices discuss the gravitational radiation rocket effect. A much shorter account of this work was published in Astrophys. J. Letters [4] (see also [2]). I have added a substantial amount of additional material here including: a detailed summary of the history of recoil calculations, a discussion of work done since our paper was published, many more figures, and details on the various calculations. Some of this material will probably be incorporated in a future publication. Read that instead.

Chapter 3 and its appendices discuss the binary-induced collapse of neutron stars. It is similar to work published in Phys. Rev. D [12].

Chapter 4 and its appendices concern the adiabatic approximation in extreme-mass ratio inspirals. It has not been published at the time of this writing. The

final published version could differ substantially. I refer you to that (hopefully) published version.

Enjoy!

Marc Favata

August 3, 2006

Santa Barbara, CA

Chapter 1
An Introduction to Gravitational Wave Astrophysics and an Overview of this Thesis

> *When you are courting a nice girl an hour seems like a second. When you sit on a red-hot cinder a second seems like an hour. That's relativity.*
> A. Einstein, *News Chronicle*, 14 March 1949

Gravitational waves (GW) are oscillations in the fabric of space and time that are predicted by Einstein's theory of General Relativity. The simplest way to imagine gravitational waves is to think about the ripples generated in a pond as you swirl your finger in a circle. Instead of the surface of the water oscillating up and down, gravitational waves are oscillations of the gravitational field. In Newtonian language, as a gravitational wave passes by, a small mass will oscillate back and forth relative to some reference point. In the language of curved space and time, the passing wave causes oscillations in the ticking rates of clocks or changes the distance between freely falling points.

Gravitational waves exist. We know that they exist because of observations of two neutron stars orbiting around each other [13]. The motion of these two stars causes oscillations in the gravitational field, and these oscillations carry energy away from the system. This energy loss causes the binary separation to shrink and its orbital frequency to increase. This increase in the orbital frequency has been measured, and these measurements agree very well with the predictions of gravitational wave emission as described by Einstein's theory.

However, this evidence for gravitational waves is *indirect*: their existence is inferred by observing the motion of distant objects. We would like to directly

detect gravitational waves in terrestrial laboratories from astrophysical sources in our Galaxy and in the distant Universe. Several experiments are currently trying to do this [14, 15, 16, 17]. The largest of these experiments is the Laser Interferometer Gravitational-Wave Observatory (LIGO). It consists of two installations (one in Hanford, WA, the other in Baton-Rouge, LA) each consisting of two 4-km vacuum tubes in an L-shape. In a simplified description, each tube has two mirrors with a laser beam bouncing back-and-forth. A passing gravitational wave will very slightly change the distance between the mirrors (by a distance of $1/1000^{\text{th}}$ of the diameter of a proton). Through the interference of the laser light in the two tubes, these small changes in length can be detected.

The direct detection of gravitational waves will be interesting for several reasons: It will further confirm that gravitational waves exist and have the properties predicted by Einstein's theory of gravity. Einstein's theory is believed to be a fundamental law of nature, but it has only been tested in limited contexts. The direct detection of gravitational waves will solidify our evidence for Einstein's theory in regimes where it has not been previously tested. Gravitational waves will also tell us about the nature of black holes, the structure of neutron stars, what happens in a supernova explosion, and the earliest moments after the Big Bang. Gravitational waves represent an entirely new kind of radiation that is very different from visible light, x-rays, radio waves, neutrinos, or cosmic rays; this makes their detection challenging and, in some sense, intrinsically interesting. It also means that we will be able to view the Universe in a fundamentally new way, making it likely that we will find something surprising and unexpected.

The most likely source for the first-generation of gravitational-wave detectors will be compact-object binaries: systems of two neutron stars or black holes or-

biting each other. As discussed above, these binaries release gravitational waves as they orbit, and the binary separation slowly shrinks with time. Eventually the neutron stars or black holes get so close that they quickly merge to form a single neutron star or black hole, emitting a giant burst of gravitational waves in the process. This entire scenario—the slow inspiral of the two objects, their rapid merger, and the resulting "ringing" of the remnant black hole—is referred to as binary coalescence.

This thesis consists of three separate projects, each concerning different aspects of binary coalescence. In the remainder of this chapter, I will provide a simple description of these three projects suitable for a reader with little science background. The reader is referred to the introductory sections of each chapter for more technical summaries.

1.1 What are Neutron Stars and Black Holes?

Let's first begin with a brief explanation of what neutron stars and black holes are. Most of the objects that we see when we look up at the night sky are stars. Like people, stars are born, they live, and they die. Also like people, most stars tend to exist in couples or binaries. Neutron stars and black holes are two types of objects that are left behind when stars die. (White dwarfs are another kind of compact-object remnant resulting from the death of low mass stars).

Massive stars (with masses greater than $\sim 5M_{\odot}$, where $M_{\odot}$ is the mass of the Sun) experience supernova explosions at the end of their lives. These explosions happen when the stars are no longer able to sustain nuclear fusion in their cores. Normally, stars are held together by a careful balance between the inward pull of gravity and the outward thermal pressure caused by the intense heat from fusion

reactions in their stellar core. When these fusion reactions cease, there is no longer an outward pressure to balance the pull of gravity, and the star rapidly collapses in on itself. During the collapse the core of the star is compressed to very high densities, and nuclear reactions convert protons to neutrons. For stars with initial masses in the range $\sim 5 - 15 M_\odot$, the collapse is eventually halted by a new kind of pressure that develops—*neutron degeneracy pressure*. The ordinary pressure that we feel from air or water is due to the collision of atoms or molecules. But neutron degeneracy pressure results from a special kind of quantum-mechanical repulsion that comes from neutrons not wanting to be too close to each other.[1] When the stellar core has finished collapsing, it is supported against gravity by neutron degeneracy pressure, and a neutron star is formed.

Neutron stars are extremely dense (up to 10^{15} times as dense as water). They contain about as much mass as the Sun in a sphere with a 20 km diameter. A paper-clip sized volume of neutron star material would weight about as much as Mt. Everest. Extremely massive and dense objects have very strong gravitational fields—they cause large distortions in the space and time around them, making them excellent laboratories for probing general relativity.

Like neutron stars, black holes are also formed in supernova explosions, but in stars with initial masses $\gtrsim 15 M_\odot$. In these stars the force of gravity is much stronger and neutron degeneracy pressure cannot halt the collapse of the star. As

[1]Think of degeneracy pressure as the kind of anxiety or discomfort you feel when cramped together on a very crowded airplane. Everyone is squished together to the extent that the seating allows. But if a few rows of empty seats are made available, a few people will escape from their crowded seats to occupy some fraction of the empty ones. In quantum mechanics, no two neutrons can exist in the same quantum state, just as two passengers can't occupy the same seat. When neutrons are highly compressed, there are less states or "seats" available, so there is a struggle to find an available state. But if more states are made available, the pressure is reduced.

the star continues to collapse, the gravity at the surface of the collapsing core becomes greater and greater. The strength of gravity can be related to a quantity called the escape velocity. On Earth the escape velocity is 11.2 km/s or about 25000 mph: this is the speed you would have to throw a baseball at sea level for it to completely escape the pull of Earth's gravity. In the Newtonian limit, the escape velocity is proportional to $(M/R)^{1/2}$, where M is the mass of the star or planet and R is its radius. If the mass is kept constant but the radius decreases (as in a collapsing star), the escape velocity increases. If the Earth were compressed to a radius of about 1 cm, the escape speed from its surface would equal the speed of light. Since nothing can travel faster than this speed, no information could leave the surface and the Earth would have formed a black hole. The surface of the Earth would have passed through an *event horizon*, a one-way membrane through which matter or information can enter but not escape. The same thing happens in the collapse of a massive star: As the stellar core continues to shrink, it passes through an event horizon and forms a black hole.

Black holes formed in this way are called *stellar mass black holes* because their masses are similar to those of massive stars, $\sim 3 - 100 M_\odot$. But black holes can form through other means as well. The Big Bang may have produced very small black holes with masses $\sim 10^{12}$ kg. Larger black holes might form through the collapse of a cluster of stars, through the swallowing of matter by an initially stellar-mass black hole, or through the merger of one black hole with another. The largest observed black holes are referred to as *supermassive black holes* and can have masses in the range of $\sim 10^5 - 10^9 M_\odot$. Strong observational evidence indicates that most galaxies contain supermassive black holes at their centers.

But what exactly is a black hole? What is it made of? In a very real sense,

a black hole is made almost entirely of the warpage of space and time. All the material that initially formed the black hole has been compressed to nearly infinite density in a nearly zero volume at the center of the black hole.[2] It has no solid surface, only an invisible one-way entrance to its interior. A black hole is, in effect, an extreme distortion of the gravitational field. This distortion manifests itself in several ways: Black holes distort the flow of time. Suppose that two people synchronize their watches far from a black hole, but one person later wanders near the black hole for a time. When the two people meet again far from the black hole, they will find that time has passed more slowly for the person who travelled near the black hole. Black holes also distort the geometry of space around them. This can be determined by measuring lengths and angles near a black hole. For example, near a black hole the circumference of a circle will not equal 2π times its radius, and the sum of the interior angles of a triangle will not add up to 180^o. If a black holes spins, it can also "drag" the fabric of space and time around it, forcing objects to revolve around the black hole or rotate in space.

There is much more that can be said about black holes, but I'd like to finish writing this thesis sometime soon. The internet has a wealth of information (and some disinformation) on black holes. There are also many popular books on the subject. I especially liked Thorne's [18] book, which is one of the things that got me interested in this subject. Now let's discuss what I actually did in graduate school.

[2]A detailed description of the state of matter inside a black hole requires a theory of *quantum gravity* which so far remains elusive.

1.2 How Black Holes Get their Kicks!

As discussed above, one of the main sources of gravitational waves is the coalescence of binary black holes. As the black holes spiral around each other they emit energy, angular momentum, and linear momentum. The linear momentum that is emitted imparts a recoil or "kick" to the black hole. This is similar to the recoil that a bullet imparts to a gun when fired, only in this case the "bullets" are gravitational waves. In a black hole binary, each black hole releases gravitational-wave "bullets" as it orbits. As the binary separation shrinks, the black holes orbit faster and the momentum of the bullets becomes larger.

Understanding how the radiated momentum imparts a kick to the binary is a little subtle since momentum is a vector quantity—it has both a magnitude and a direction associated with it. If the orbiting black holes have equal masses (and are non-spinning), then at each instant each black hole emits momentum with equal magnitudes but opposite directions.[3] Since the total momentum lost by the binary comes from adding up the momentum vectors from each black hole, the net momentum cancels and no kick is imparted to the black hole. Acquiring a net momentum (and a net kick) therefore requires that there be some asymmetry in the system. The simplest kind of asymmetry is for the two black holes to have different masses.[4] In this case the smaller hole is moving faster than its larger companion, and this allows it to emit momentum more strongly in its direction of motion (see Figure 1.1).

[3]The gravitational-wave momentum of each black hole is preferentially emitted in the direction in which the black hole is moving. In an equal-mass binary, each black hole is always moving at an equal speed, but in an opposite direction from the other.

[4]If one or both of the black holes are spinning, this can also be a source of asymmetry even in the equal-mass case.

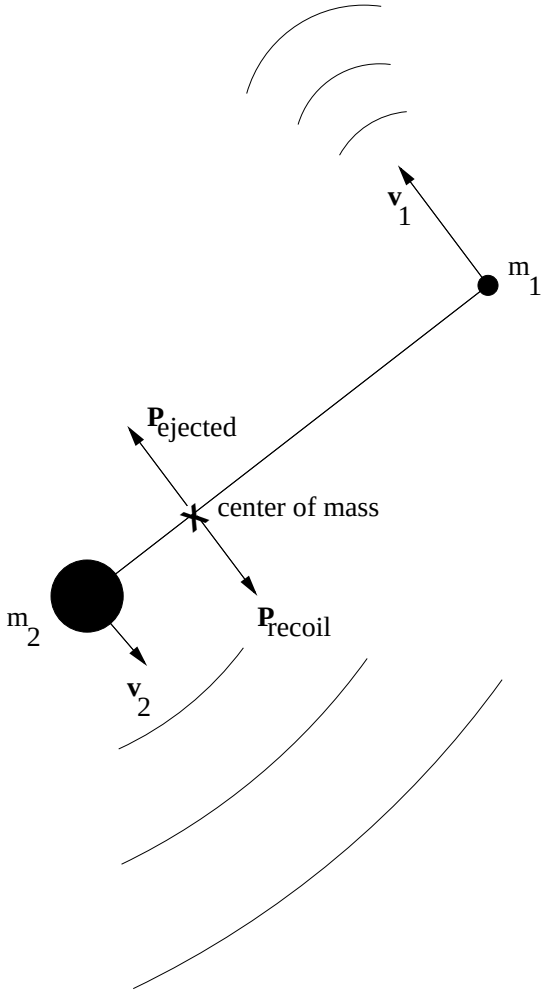

Figure 1.1: Linear momentum ejected by a black hole binary. The smaller black hole moves faster in its orbit and is more effective at "forward-beaming" its radiation. This figure is adapted from figure 3 of Wiseman [1].

However, asymmetry in the masses alone is not enough to give the system a kick. Suppose that at a given instant in a circular orbit, one black hole emits more momentum than the other, so that a net kick results. Half of an orbital cycle later the two holes have switched positions. They have the same velocities as they did half a cycle earlier, but are moving in opposite directions. Likewise, the momentum is emitted in the opposite direction after half of an orbital cycle. This causes the binary's center of mass to move in a constant circle. After one orbit of the binary, the center of mass has returned to its original position; its has undergone no net displacement. Although there is an instantaneous recoil velocity, the time average (over an orbital period) of the recoil is zero.[5] This is analogous to someone who, while floating in empty space, fires a gun in one direction, rotates 180^o and fires the gun in the opposite direction, and repeats with a constant period. After each shot the person experiences a kick in the direction opposite to the direction the gun was fired. But when the next shot is fired, the person moves in the opposite direction. This causes the person to continuously bounce back and forth between two fixed points. Although the person experiences an instantaneous recoil after each shot, there is no net velocity that permanently ejects him from his original position.

To get a net recoil requires not only asymmetry in the masses—the orbit itself must contain some asymmetry. For circular orbits[6] this asymmetry is provided by the fact that the separation between the black holes is decreasing because of the loss of gravitational-wave energy. The orbit traces out a spiral instead of a

[5]For elliptical orbits things are a bit different as the orbit itself is asymmetric along one direction.

[6]While bound binary orbits are generally eccentric, gravitational radiation tends to circularize orbits, so we expect that many comparable-mass black hole binaries will be nearly circular before they merge.

circle (see Figure 1.2). After one complete revolution, the binary has shrunk by a small amount and the momentum radiated is slightly more than it was in the previous cycle. As the orbit spirals in to smaller and smaller radii, the net radiated momentum slowly builds up. This causes a recoil that moves the center of mass of the binary on a circular spiral with increasing radius (see lower left panel of Figure 1.3).

When the black holes get very close together they encounter an instability in their orbit that causes them to rapidly plunge toward each other and merge into a single black hole. During this final plunge phase the orbit executes only a fraction of a revolution (see Figure 1.2). Because only a fraction of an orbit is completed (and the orbit itself is non-circular), the momentum released during the final plunge does not have an opportunity to "cancel," and most of the recoil velocity is accumulated during this phase (see the right panels of Figure 1.3).

The goal of my project was to calculate the final kick velocity imparted to a black hole binary after merger. Previous work on this subject (see Section 2.2) either did not take into account the effects of strong gravity near a black hole, or they did not consider the importance of the final plunge in determining the kick velocity.

While we were all at the Kavli Institute for Theoretical Physics in Santa Barbara, my collaborators (Scott Hughes and Daniel Holz) and I began to look for ways to improve upon previous calculations. Hughes had developed a computer code to calculate the gravitational waves emitted as a small mass slowly inspiralled around a much larger black hole. This code relied on something called *black hole perturbation theory*. The only way to accurately describe the orbit and gravitational waves from two orbiting black holes is to solve all of Einstein's equations

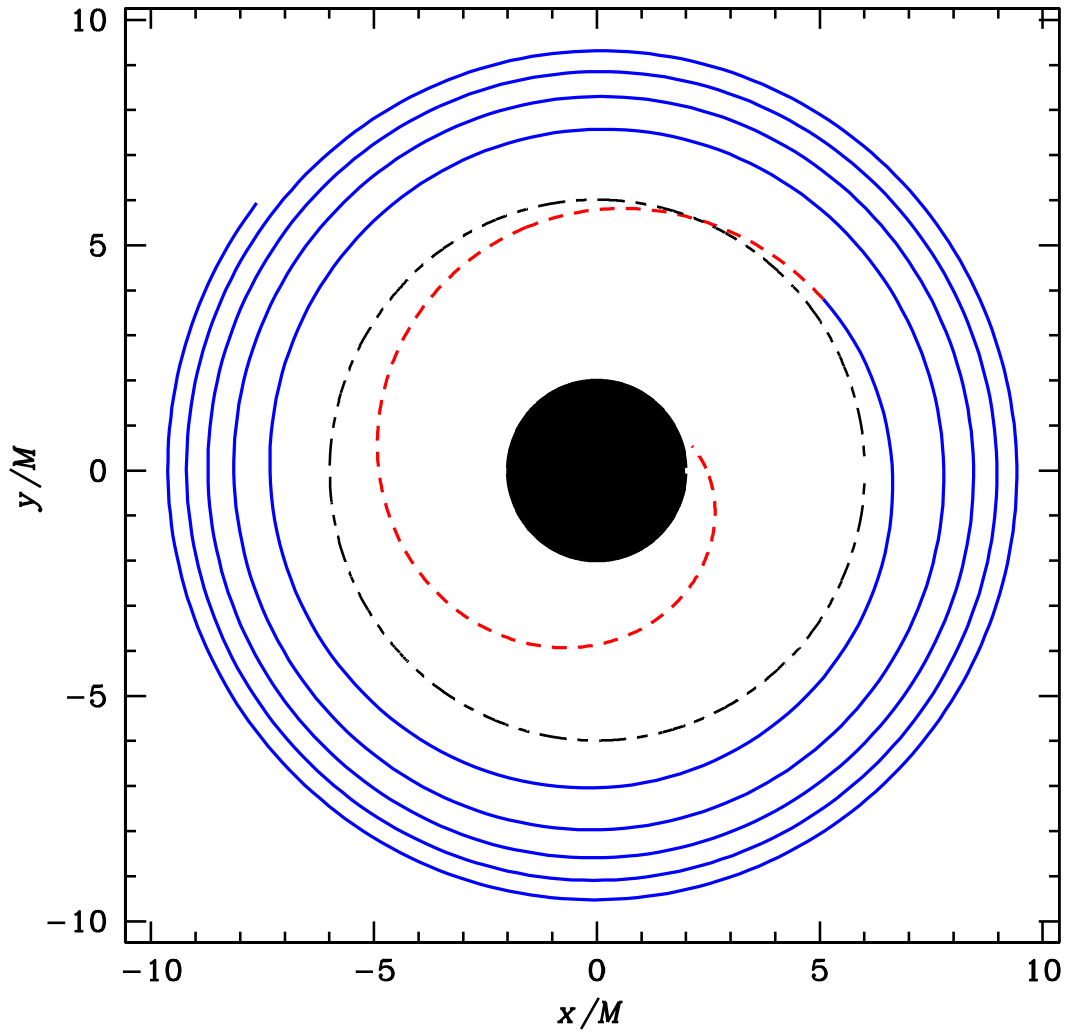

Figure 1.2: Orbit of a point particle spiralling into a non-spinning black hole. The reduced mass ratio is $\eta = 0.1$. The blue (solid) curve represents the slow inspiral part of the orbit. The red (dashed) curve represents the plunge into the hole. The black (dash-dotted) circle is the location of the last stable orbit, which marks the transition from inspiral to plunge.

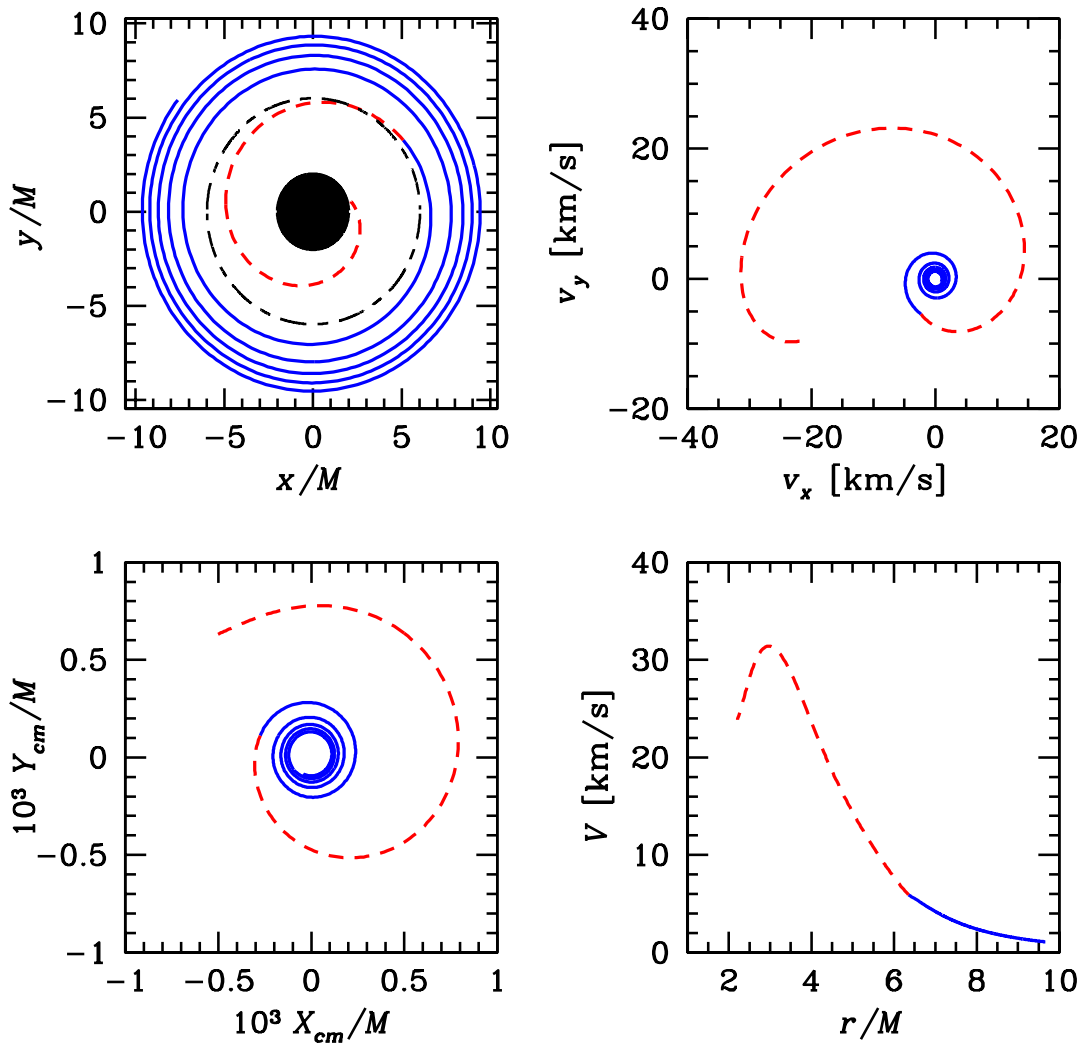

Figure 1.3: Orbit, recoil velocity and center of mass motion for a point particle spiralling into a non-spinning black hole. The reduced mass ratio is $\eta = 0.1$. The upper left panel is the orbit (see Figure 1.2); the upper right panel is the curve traced out by the recoil velocity vector; the lower left panel is the center of mass motion of the binary; the lower right panel is the magnitude of the recoil velocity as a function of orbital separation. The blue (solid) curves are the contributions during the slow, inspiral part of the orbit. The red (dashed) curves are the contributions from the plunge part of the orbit.

(the equations that describe the gravitational field) numerically using a supercomputer. This is very difficult to do, and at the time this project was under taken two black holes could only be evolved in this way for a fraction of an orbit.[7] Black hole perturbation theory simplifies the problem by assuming that one of the black holes is really small and doesn't effect the other black hole very much.[8] Using Hughes' computer code we were able to compute the momentum radiated during the inspiral, correctly accounting for the effects of the strong gravitational field as the black holes get close together. We were also able to do this for spinning black holes, which previous binary recoil calculations had not explored. However, because of the assumptions built into Hughes' code, we could not calculate the contribution to the recoil from the final "plunging" phase of the coalescence.[9] To circumvent this we used a crude approximation: We modelled the plunging orbit accurately,[10] but we computed the radiated momentum using a formula that assumes that gravity is weak and the motion of the black holes is slow. While these assumptions are violated during the plunge, we decided to forge ahead anyway. Since the plunge provides the most important contribution to the kick velocity, even a rough calculation would be useful.

So compute we did, and we found several interesting results: One of our

[7]Recently there has been much progress in the field of numerical relativity, and black holes can now be evolved for many orbits.

[8]Despite the small-mass-ratio assumption, there is some evidence that our results can be "scaled-up" to the comparable mass-ratio case with reasonable accuracy.

[9]The code relies on Fourier transforms of a certain equation (the Teukolsky equation), and this requires orbits with well-defined frequencies. During the final plunge, the orbit is no longer a periodic function of time and thus does not admit a discrete Fourier transform.

[10]This was done by solving the Kerr geodesic equation; this is reasonably accurate because the plunge happens on a very short timescale, and radiation-reaction effects are relatively unimportant.

most important findings was that the gravitational radiation emitted during the "plunge" phase of the coalescence really is *much* more important than any contributions from the other phases of coalescence.[11] While we expected this intuitively, it was not previously demonstrated or fully realized by the community. We also accurately computed the recoil up to the last stable orbit—the point marking the end of the inspiral and the beginning of the plunge. This had previously been done for non-spinning black holes [19], but we extended those results to black holes of any spin. While the recoil up to the last-stable-orbit is generally not as important as the plunge contribution, for rapidly spinning holes it can be of comparable or greater importance.[12] Our main result was a combination of three recoil calculations: the accurate recoil estimate up to the last-stable-orbit using black hole perturbation theory, and two approximate calculations of the plunge contribution to the recoil. Together these approximate calculations established rough upper and lower limits to the final recoil velocity. We found that recoils would be unlikely to exceed 500 km/s, and would typically be in the range of $\sim 10-200$ km/s. Previous estimates of the recoil were much more uncertain, some predicting recoils as large as several thousand km/s, and did not attempt to model the recoil from all the stages of realistic binary coalescence. Gravitational-wave recoil velocities are independent of the total mass of the binary, so our results apply to stellar, supermassive, and intermediate-mass black holes.

Depending on the size of the kick velocity, gravitational-wave recoil can have important astrophysical consequences. We explored some of these consequences in collaboration with David Merritt and Miloš Milosavljević (who did most of the

[11] This has recently been confirmed analytically by Damour and Gopakumar [8].

[12] The is because for rapidly spinning holes and prograde orbits, the last-stable-orbit is very close to the event horizon of the hole, so there is effectively very little contribution from the plunge phase of coalescence.

work) [2]. Black hole binaries are not just floating in completely empty space—they reside inside other structures like galaxies or globular clusters (dense concentrations of stars found within galaxies). Just like the surface of the Earth or a neutron star, these much larger structures also have escape velocities. If black holes receive a kick that exceeds those escape speeds, they will be ejected from the system. This could lead to a population of black holes that wander within a galaxy or in the spaces between galaxies.

Our calculated kick velocities have different consequences for different kinds of systems (see Figure 1.4). Very large elliptical galaxies have high escape velocities ($\gtrsim$ 800 km/s), so they are likely to retain their black holes. However, smaller galaxies and globular clusters have much smaller escape velocities ($<$ 100 km/s) and their black holes could more easily be ejected.

In galactic systems kicks result after a moderately large black hole merges with the supermassive black hole at the galaxy's center. These black hole mergers are ultimately the product of galaxy mergers. Each galaxy brings its own large black hole with it, and after the galaxies collide interactions with the stars in the galaxy tend to bring the smaller hole into orbit around the larger one. When the merger is complete and the newly formed black hole gets a recoil, it is unlikely to escape from a large galaxy. However, it will wander about that galaxy until it is brought back to the galaxy's center by a kind of "frictional" force exerted by all of the stars in the galaxy. During this process the displacement of the black hole from the center of the galaxy will tend to lower the central density of stars. In fact, some of the stars will be bound to the black hole when it gets kicked, and they will travel with the black hole through the galaxy.

More dramatic things can happen when the black holes are embedded in dark

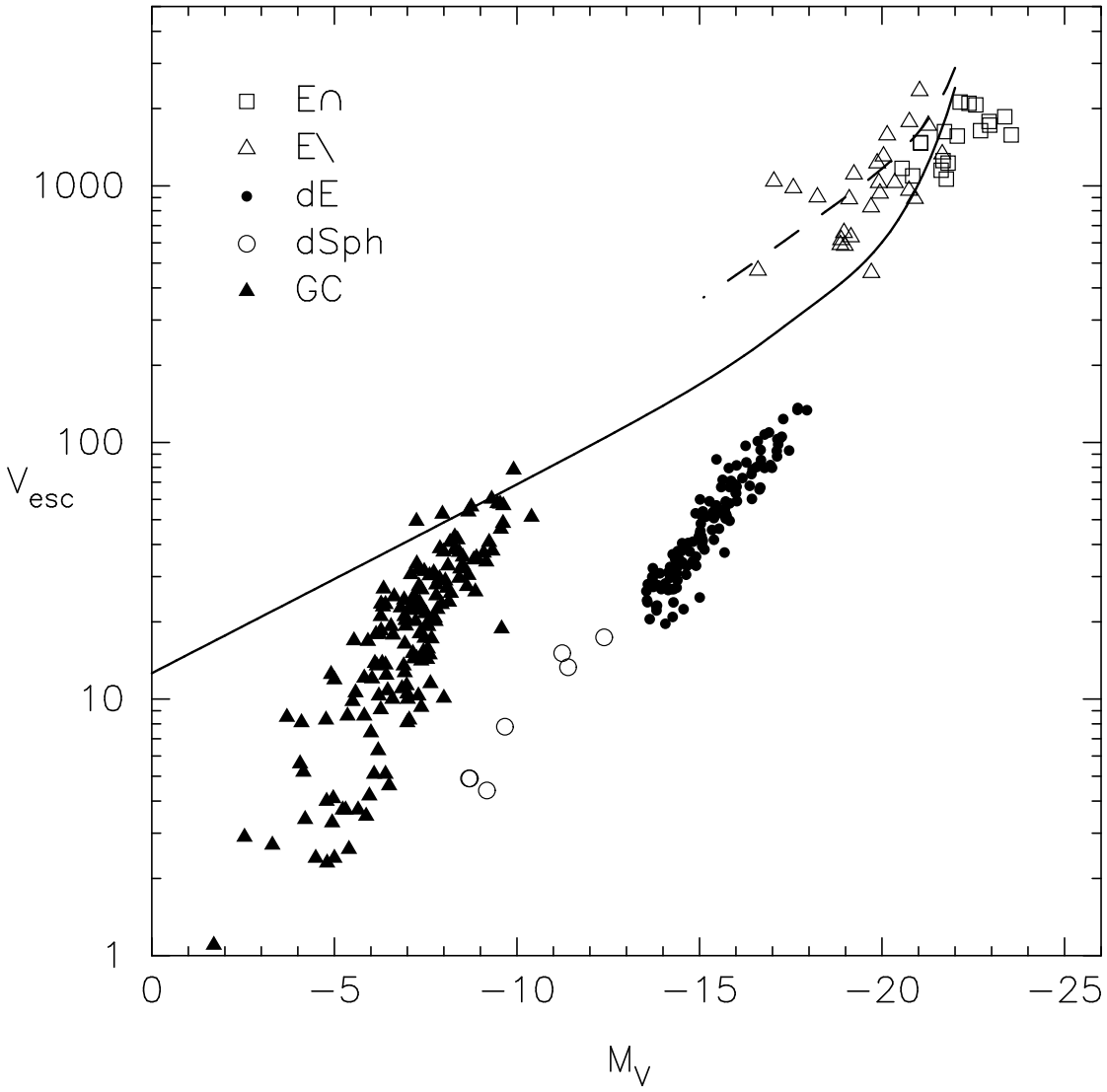

Figure 1.4: Central escape velocities in km/s in four types of stellar systems that could harbor merging black holes (Figure 2 of Merritt et. al. [2]). Data are plotted as a function of absolute visual magnitude. Open squares are core elliptical galaxies, open triangles are power-law elliptical galaxies, closed circles are dwarf elliptical galaxies, open circles are dwarf spheroidal galaxies, and closed triangles are globular clusters. The solid line is the mean escape velocity from the dark matter halos associated with the luminous matter of corresponding M_V. The dashed line is the escape velocity from the combined luminous and dark matter potential for elliptical galaxies.

matter halos, the early precursors of galaxies. The mass of most galaxies is composed primarily of dark matter, an unknown form of matter that is detected only through its gravitational interactions [20]. The early universe was filled with relatively small dark matter halos—galaxy-sized clumps of dark matter and smaller amounts of ordinary matter. Over time these halos merged together and built up the big galaxies that we see today. As these large galaxies were built through a sequence of mergers of smaller structures, the black holes inside these galaxies were also assembled by mergers and through the accretion of gas and stars, eventually forming the supermassive black holes that reside in most present-era galaxies. Black hole kicks have the potential to disrupt the build-up of these supermassive black holes. If at some point during the sequence of mergers a black hole received a kick, it could be ejected completely from the galaxy or dark matter halo. Kicks can thus limit the mass and number of black holes in galaxies. Early in the universe, dark matter halos were small and had low escape velocities. Our results indicated that before a certain time in the universe's history, kicks tended to prevent the growth of supermassive black holes because the smaller "seed" holes that they formed from were ejected from their host halos.

Kicks play a similarly important role in the formation of *intermediate-mass black holes* in globular clusters. Intermediate-mass black holes tend to have masses in the range $10^2 - 10^4 M_\odot$. There is strong, but not conclusive evidence for their existence [21]. They are thought to be formed either from the collapse of very-massive stars early in the Universe's history, or through the growth of stellar mass black holes that reside at the center of globular clusters. In the latter scenario, the capture of stars, gas, or other black holes by the "seed" hole at the dense center of the cluster slowly builds up a stellar-mass black hole into an intermediate-mass

one. Just as in the case of supermassive black holes at the centers of galaxies, kicks could also play an important role in preventing the growth of intermediate-mass black holes. Globular clusters have rather small escape velocities ($\sim 3-100$ km/s), so our calculated kick velocities indicate that stellar-mass seed black holes are quite likely to be ejected unless they can quickly grow to large enough masses through the accretion of gas.

1.3 Are neutron stars crushed?

Another source of gravitational waves that will be important for the first generation of detectors is binaries consisting of two neutron stars. Neutron star binary coalescence progresses in much the same as black hole binary coalescence. The primary difference is that neutron star binaries are in some-sense more "messy": The collision of two black holes proceeds rather cleanly—the two holes essentially absorb each other just as two drops of water absorb each other to become one larger drop. But when neutron stars collide they tend to rip each other apart, spewing matter everywhere, with the remaining matter usually collapsing to form a black hole.

Understanding the gravitational waves from binary neutron stars (and binary black holes) requires that these systems be modelled very accurately. The reason for this is that detecting gravitational waves is much more difficult than other observations in astronomy. To observe a star or a galaxy using electromagnetic radiation we do not need to know very much information about what we are looking at. We can simply point our eyes or our telescopes at some area of the sky, and if something is there and is bright enough, we will see it. Detecting gravitational radiation works rather differently for several reasons. First, unlike electromagnetic

radiation, gravitational radiation does not ionize atoms, excite electrons, move electric charges, or interact with the atomic nucleus. Instead gravitational waves cause distortions on macroscopic scales (although the magnitude of those distortions are generally very small). While electromagnetic waves are generated by the microscopic interactions of atoms and charges,[13] gravitational waves are generated by the large-scale motions of material (via the motion of entire stars in a binary or the bulk motion of the fluid or crust inside a neutron star). Because they are generated by large-scale motions and not small patches of atoms, gravitational waves cannot be used to make images of individual stars or black holes. These properties make gravitational radiation more closely analogous to sound than to electromagnetic radiation: While visible light photons interact with individual molecules and electrons in our eyes, sound causes oscillations of relatively large structures in our inner-ears. Similarly, sound is generated not by atomic or subatomic interactions, but by large-scale mechanical vibrations (the ringing of a bell for example).

Perhaps the most important difference between gravitational waves and electromagnetic radiation is that, even for the strongest of sources, gravitational waves are very weak. This makes them difficult to detect. For Earth-based detectors that operate in a frequency band between $10 - 1000$Hz, several sources of noise (seismic noise, noise associated with the laser light, and several others) will be comparable in size to the largest expected signals. Unless the gravitational wave signal is unexpectedly strong, detecting gravitational waves will require a technique called *matched filtering*. In this technique a *template waveform*—a model of what the gravitational-wave signal will look like—is first generated. This template depends

[13]For example, the individual photons of light that we see from the Sun are generated by individual atoms or the collisions of individual atoms and photons with each other.

on several parameters, such as the masses of the stars in the binary, their spins, and their sky positions. Once a template is generated, the noisy data is compared with the template to see if there is an actual signal from a binary with parameters close to those used in generating the template. Much of the theoretical research in gravitational-wave science concerns the generation of these templates.

When the neutron stars or black holes in a binary are far apart, Einstein's equations are relatively easy to solve, and signal templates can be represented by analytical formulas. But when the binary separation is very small (and for nearly equal-mass binaries), approximate solutions can no longer be found and Einstein's equations must be solved numerically in order to generate waveform templates. Such is the case for two neutron stars shortly before they merge together.

The second part of this thesis concerns numerical simulations of binary neutron star mergers that were performed by James Wilson, Grant Mathews, and Pedro Marronetti in the mid-1990s. At the time their simulations were state-of-the-art. They simulated the final stages of coalescence of two neutron stars by solving Einstein's equation (but subjected to some simplifying approximations). These simulations made a rather surprising prediction: if two neutron stars—each individually stable against gravitational collapse to black holes—were placed in a binary, they could be compressed and collapse to black holes *before the point in the orbit where the neutron stars plunge together and merge* (after merger, collapse to a black hole is expected). This result—referred to as "star-crushing" or binary-induced-collapse—was very surprising as most people expected that the stars would become more stable and not less. In particular Dong Lai [22] showed that Newtonian tidal forces[14] present in a binary will stabilize each neutron star.

[14]Tidal forces are gravitational forces that tend to stretch a star in one direction and compress it along the other two. They arise because the force of gravity gets

Over 15 other papers also argued that the crushing effect in the Wilson-Mathews-Marronetti simulations was unphysical. Eventually Éanna Flanagan [23] found an error in one of the equations used in the Wilson-Mathews-Marronetti simulations. After fixing this error, the compression of the neutron stars in the simulations was significantly reduced but not entirely eliminated.[15]

Are these residual compressions artifacts of the approximations used in the simulations, or is there a physical process that could cause binary-induced compression and collapse? These questions were first suggested to me by Kip Thorne, my undergraduate research adviser, during my senior year at Caltech. He also suggested a possible mechanism: gravitomagnetic tidal forces could couple to certain kinds of velocity currents inside one of the neutron stars, generating a compressional force. Gravitomagnetic tidal forces are a special kind of force that is predicted by general relativity. Just as the motion of electric charges in a wire produces a magnetic field, the motion of masses (in this case the orbital motion of two orbiting neutron stars) produces a *gravitomagnetic field*. When electric charges move through a magnetic field, a force is exerted on them that deflects their motion (in a direction perpendicular to their original velocity and the direction of the magnetic field). Likewise, when neutral matter particle or fluid moves through a gravitomagnetic field it is similarly deflected.

My research showed that gravitomagnetic tidal forces can, in principle, lead to compressional forces. In order for these compressional forces to exist, the fluid

---

weaker as the separation between objects decreases. In a system of two stars or planets, gravity is stronger on one side of an object (the side closer to the second body) and weaker on the farther side, leading to a tidal distortion of the stars or planets.

[15] An overview of the history of this Wilson-Mathews-Marronetti "controversy" is given in section 3.2 and in Kennefick [24].

inside the neutron star has to move in a certain kind of swirly motion (called a current quadrupole). This motion is pictured in Figures 3.1 and 3.2. How can this kind of motion come about in the first place? It turns out that in non-rotating stars, this velocity pattern is itself generated by the gravitomagnetic field. In this situation, the size of the compressional force that results is always less than the Newtonian force that stabilizes the star—so net compression is not possible in practice. One way around this is to suppose that the current quadrupole velocity is generated in a different way (perhaps as an artifact of a numerical simulation). If the magnitude of the velocity is large enough (but not implausibly large), I showed that compression of roughly the size achieved in the revised Wilson-Mathews-Marronetti simulations could be achieved.

It is far from clear that this kind of velocity field was in fact generated in their simulations (certain peculiarities in their simulations suggest that this is possible). Determining this would require access to their computer code or its output. It is also possible that numerical error, an artifact of their computational methods, or some other physical mechanism is responsible for their residual compression. We may never know. After taking a lot of heat from the community, Wilson, Mathews, and Marronetti seem uninterested in pursuing this further. No simulations from other research groups have indicated compression. Except for some details in the way they start their simulations, current methods for simulating neutron star binaries are much more sophisticated than those used by Wilson, Mathews, and Marronetti. It is therefore quite likely (but in my opinion not 100% conclusive) that the compression seen in their simulations is not physical.

1.4 Detecting Inspirals into a Supermassive Black Hole

The final topic of this thesis also concerns binary black hole coalescence, but in the case in which one of the black holes is very big $\sim 10^5 - 10^6 M_\odot$ and the other black hole is very small $\sim 1 - 100 M_\odot$. These sources, referred to as *extreme-mass ratio inspirals* (EMRIs) will be important for the planned space-based gravitational wave detector LISA (the Laser Interferometer Space Antenna).[16]

Because the smaller black hole isn't very massive, it emits gravitational waves very slowly and takes a long time to spiral into the larger hole. This means that while it is in the observing frequency of LISA it will execute many, many orbits very close to the black hole. The gravitational waves that it emits during this time will therefore be very sensitive to the nature of the strong-gravity region near the larger black hole. This will allow the "mapping" of the spacetime around the black hole: [17]: Those waves will contain an imprint of the black hole nature of the source, and they will allow us to determine whether the central object really is a black hole with the properties described by Einstein's theory, or if it is some other

[16] See http://lisa.jpl.nasa.gov.

[17] This spacetime mapping has been given the name "bothrodesy" by Sterl Phinney (see Ref. 4 of Fang and Lovelace [25]). It comes from the Greek word "Bothros" meaning "garbage-pit," and is meant to invoke the idea that black holes are like garbage pits since they "swallow stuff up." Bothros also has a vulgar connotation in the Greek language. I am not a big fan of this term: it is difficult to say and far from self-explanatory. As a replacement I have coined the term "holiodesy." This comes from "hole" and "geodesy," which is the mapping of the structure of the Earth's gravitational field. It has an obvious play on the words "holy odyssey," lending a somewhat inflated importance to the quest to determine the nature of black holes. It also meshes well with the words "periholion" and "apholion," which I believe were originally coined by Kip Thorne and refer to the black hole analogs of perihelion and aphelion (the closest and farthest points in an orbit about the Sun). The bothrodesy equivalents of these words are "peribothron" and "apbothron," which hardly roll off the tongue. Another good substitute for "bothrodesy" would be "spacetime-geodesy" (which, unlike bothrodesy or holiodesy) is in some sense more accurate as it does not presume that the object is a black hole).

kind of exotic object, perhaps described by a different theory of gravity.

The detection of extreme-mass-ratio inspirals by LISA will have other science objectives as well. From the detected gravitational waves the masses and spins of the black holes will be determined with very high accuracy. This will allow a census of supermassive black holes—object that which play a surprisingly important role in the visible properties of galaxies. Measurements of the masses of the inspiralling objects will also allow a census of the kinds of objects that populate the dense stellar concentrations near the supermassive black holes that reside at galaxy centers. Measurements of the black hole spins will give information about the dominant mechanism for black hole growth—through the accretion of gas or through mergers with other large black holes.

Realizing these science goals requires that these binaries be detected and that their parameters (such as their masses and spins) be extracted from the gravitational wave signal with high accuracy. As in the case with neutron star binaries discussed above, this will require matched-filtering, which means an accurate waveform template must be generated. Generating these accurate templates is especially difficult for these sources because they execute very many cycles (around a million) very close to the black hole (where the weak-gravity and slow-motion approximations break down). If the waveform template differs from the actual gravitational wave signal by more than about 1 cycle (out of a million cycles), the detection of the binary will be impeded.

To generate these waveform templates we can use the tools of *black hole perturbation theory*. This is an approximation to Einstein's equations that relies on the fact that the gravitational field in these extreme-mass-ratio systems is dominated by the larger black hole. Since the smaller black hole is much less massive

than its companion, it causes only a very small perturbation to the larger black hole's gravitational field. This small-perturbation assumption greatly simplifies Einstein's equations and is valid even very close to the larger black hole.

Solving the black hole perturbation theory equations consistently—correctly computing the gravitational waves emitted by the small orbiting black hole and the corrections to its motion resulting from this wave emission—is difficult to do. For certain aspects of the calculation we do not yet have the necessary computational tools. However, if we make a certain additional approximation—the *adiabatic approximation*, we can do the calculation. The adiabatic approximation essentially assumes that the orbit of the small black hole evolves slowly—the time it takes the small black hole to orbit once is much shorter than the time it takes the separation between the black holes to decrease significantly. When the separation between the two black holes is large, this approximation is good. But when the black holes are closer together, the separation starts to decrease more quickly (since the gravitational waves emitted are more intense) and the adiabatic assumption begins to break down. The goal of my project was to determine how well the adiabatic approximation works. Can it be used to produce waveforms that remain accurate to within one cycle?

To properly address this question, one would have to generate two kinds of waveforms and compare then: one that uses the adiabatic assumption and one that does a more exact calculation. Unfortunately this more exact calculation is very difficult to do. The only way to get around doing a hard calculation is to make even more approximations. The additional approximation that we make is the *post-Newtonian* approximation. This assumes that the velocity of the small orbiting hole is small (much less than the speed of light) and that the gravity near

the larger hole is weak. Both of these assumptions are grossly violated by extreme-mass-ratio inspiral systems! But since we merely wish to estimate an error and not compute an exact quantity, the hope is that, despite these approximations, we can still get a handle on how large of an error we are making by ignoring the adiabatic assumption.

Using post-Newtonian equations, I derived expressions for the number of cycles in the gravitational waveforms (this is roughly twice the number of times that the small hole revolves around the larger one). Most of these cycles come from the "adiabatic-piece" of the waveform, but a fraction of them come from corrections to the adiabatic approximation. In the case in which the eccentricity[18] of the orbit is small, the adiabatic approximation will be good enough for detecting extreme-mass-ratio inspirals using LISA. However, it cannot be used to determine the parameters of the binary (the masses and spins) with high precision. The large eccentricity case is harder to explore, but preliminary indications [26] suggest that extreme-mass-ratio inspirals with large eccentricities could be difficult to detect with adiabatic waveforms.

[18]Eccentricity is a measure of how "elliptical" the orbit looks. An orbit with an eccentricity of 0 is a perfect circle, while an orbit with an eccentricity near $\lesssim 1$ is a highly elongated ellipse.

Chapter 2
How Black Holes Get Their Kicks: Gravitational Radiation Recoil Revisited

This chapter is based mostly on work performed in collaboration with Scott A. Hughes and Daniel E. Holz. Some portions of the text below were published in Astrophys. J. Letters, **607***, L5, (2004). Smaller portions were excerpted from work published in collaboration with David Merritt and Miloš Milosavljević in Astrophys. J. Letters,* **607***, L9, (2004). Other parts of this chapter and its appendices may appear in a future publication.*

2.1 Introduction and Background

A binary system of compact objects emits gravitational waves (GWs). These waves carry energy and angular momentum away from the source, decreasing the energy and angular momentum of the orbit, and also decreasing the binary separation. When the compact objects—considered to be a system of binary black holes (BHs) here—are widely separated, the objects slowly inspiral in such a way that the orbital evolution is adiabatic. In other words, the radiation-reaction timescale $T_{\rm rr}$ is much than longer the orbital period $T_{\rm orb}$,

$$T_{\rm rr} \sim r/\dot{r} \sim (M/\eta)(r/M)^4 \ll 2\pi/\Omega_{\rm orb} \sim M(r/M)^{3/2} \,, \tag{2.1}$$

where r is the orbital separation, $M = m_1 + m_2$ is the sum of the masses, $\eta = \mu/M$ is the reduced mass ratio, $\mu = m_1 m_2/M$, $\Omega_{\rm orb}$ is the orbital angular frequency, and an overdot denotes a time derivative.[1] Eventually the binary reaches the last stable orbit (LSO), at which point the orbit becomes dynamically unstable and

[1]Here and throughout this thesis we use units in which $G = c = 1$.

the two holes plunge together and merge in a time $T_{\rm plunge} \sim$ few $\times M$.

During this process of binary black hole coalescence, the emitted gravitational waves also carry away linear momentum[27, 28, 29, 30, 31]. Conservation of momentum then demands that the binary center-of-mass (COM) must recoil. This recoil or "gravitational radiation rocket" effect is independent of the system's total mass. Many stellar systems (galaxies, globular clusters, dark matter halos) are thought to contain BHs at the their centers. If these holes undergo binary coalescence with a compact object of comparable mass, the resulting kick velocity could eject or displace the merged remnant from its stellar environment. The astrophysical consequences of kicks have been explored in Merritt et. al. [2] and several other papers. These consequences depend crucially on the magnitude of the kick velocity. Estimating these magnitudes is difficult as the final kick imparted to the merged BH depends sensitively on the details of the merger process and on the effects of strong gravity. Previous estimates of the recoil velocity either did not properly account for relativistic effects, or examined binary configurations that do not represent generic binary BH coalescences. The history of these computations is reviewed in Section 2.2.

Here we will attempt to improve upon past calculations of the kick velocity. Unlike previous analyses, our treatment applies to the strong-gravity, fast-motion regime around spinning BHs undergoing binary coalescence. Using BH perturbation theory we model the dynamics of the binary, the generation of GWs, and the backreaction of those waves on the system during the slow, adiabatic inspiral up to the inner-most stable circular orbit (ISCO). Our results in this regime are accurate only for extreme mass ratio inspirals ($q \ll 1$), but we can extrapolate to $q \sim 0.4$ with modest error. We will then use a cruder "semi-relativistic" or

"hybrid" approximation to model the momentum emitted during the plunge phase of the coalescence. Both of these approaches represent significant improvements over past estimates of the recoil. While our final values for the recoil still contain much uncertainty (see figure 2.4), the previous state of these calculations was even more ambiguous.

2.2 The history of recoil calculations

There has been a long history of recoil calculations. The foundational work in the early 1960's and 1970's derived the basic expressions for the momentum radiated in GWs. Later work extended and applied these expressions to astrophysical situations of increasing levels of realism. In this section I will review this history. Later, in section 2.8, I will discuss recent progress in recoil calculations.

2.2.1 Formal expressions for the momentum flux

Although they only examined a restricted system of two point masses oscillating on the z-axis, Bonnor and Rotenberg [27] were the first to realize that gravitational radiation can carry away linear momentum and lead to a "radiation-rocket" effect. Shortly afterwards, Peres [28] derived a general expression for the momentum flux radiated in GWs in terms of the leading-order multipole moment couplings [the analog of Eq. (2.30b) below].[2] Papapetrou [29, 30] seems to have done something

[2]In a series of papers Cooperstock [32, 33, 34] also considered the momentum flux from GWs. He claimed that in a system of two mass-quadrupole moments (he considered two spinning rods), a recoil arises from a mass-quadrupole/mass-quadrupole coupling that enters at a lower order than the standard quadrupole/octupole coupling. This result is somewhat surprising and not well understood. According to Press' [35] discussion of Cooperstock's result, this appears to result from a break down of the usual quadrupole approximation, which assumes that the source of gravitational waves lies within its own wave zone. Press

similar (although his paper is in French so I can't completely understand it), as did Bekenstein [31]. Booth [36, 37] and Dionysiou [38, 39] derived similar expressions. Campbell and Morgan [40] derived a general expression for the momentum flux valid to all orders, as did Dionysiou [41, 42], Bonnor and Rotenberg [43], and (in more modern notation) Thorne [44]. Bonnor and Piper [45] derived a general metric describing a gravitational-wave rocket—a mass accelerated by the emission of GWs.

2.2.2 Recoil from gravitational collapse

Bekenstein's [31] work is among the most readable of the early papers, and he is also the first to address the astrophysical implications of recoil. He calculated the recoil from the asymmetric collapse of an axisymmetric stellar core to a black hole. He found an upper limit on the recoil of

$$V_{\rm recoil} \leq 300|\epsilon_2\epsilon_3| \text{ km/s} , \tag{2.2}$$

where $\epsilon_l \leq 1$ (for $l = 2, 3$) are proportional to the quadrupole and octupole moments generated during the collapse,

$$\epsilon_l = \frac{\int \rho P_l(\cos\theta) r^l dV}{\int \rho r^l dV} , \tag{2.3}$$

where ρ is the mass density and P_l are the Legendre polynomials. The values of the ϵ_l vary with time, but they are expected to remain small unless the collapse is highly non-spherical.[3] Bekenstein also speculated on other astrophysical consequences of

[35] describes a formalism for computing gravitational waves and their energy and momentum fluxes for sources that extend into their own wave zones.

[3]For the nearly-spherical, pressureless collapse of a core with initial size R_i and mass M, Bekenstein approximates $\epsilon_l \approx \epsilon_{li} R_i/(4M)$, where ϵ_{li} are the initial values of the ϵ_l.

the GW recoil effect including: 1) the disruption of binaries when one member collapses to a BH; 2) the detachment of the newly formed BH from its stellar envelope; 3) escape from globular clusters; 4) escape from galaxies leading to a population of intergalactic BHs, and 5) the depletion of BHs from the galactic disk due to the component of recoil perpendicular to the galactic plane.

Moncrief [46] revisited Bekenstein's collapse calculations. Using the perturbation theory results of Cunningham, Moncrief, and Price [47, 48] he calculated the momentum radiated in a slightly nonspherical, axisymmetric Oppenheimer-Snyder collapse model. He found a recoil velocity of ~ 25 km/s, but speculated that recoils as large as Bekenstein's upper limit might be attained in highly-nonspherical collapse.

There appears to be little or no further work on computing gravitational-wave recoil from stellar collapse (although the work of Brandt and Anninos [49] on distorted holes is somewhat relevant). Gravitational wave recoil is likely to be small in comparison with recoil from other sources such as hydrodynamic effects (mass ejection), or anisotropic electromagnetic or neutrino emission (see [50, 51] and references therein).

2.2.3 Recoil from binaries

The foundational work for recoil calculations in binaries was performed by Fitchett [52]. Modelling the orbital motion with Newtonian gravity (neglecting radiation reaction), he computed the momentum flux using the leading-order terms of a multipole expansion [Eq. (2.30b)]. He evaluated the recoil velocity for the full class of Newtonian binary orbits: circular, elliptical, parabolic, and hyperbolic orbits, as well as the head-on collision of two point-masses.

Fitchett found that the instantaneous recoil for a circular binary with separation r is given by

$$V_F = 1480\text{km/s}\frac{f(q)}{f_{\max}}\left(\frac{2M}{r}\right)^4 , \tag{2.4}$$

where $M = m_1 + m_2$ is the total mass and $q = m_1/m_2 \leq 1$ is the mass ratio. The function

$$f(q) = \frac{q^2(1-q)}{(1+q)^5} \tag{2.5}$$

has a maximum of $f_{\max} = 0.0178885$ at $q_{\max} = 0.381966$. When the mass ratio is small $f(q) \approx q^2$. This scaling function is extremely important for recoil calculations. Post-Newtonian corrections to the recoil's mass-ratio dependence cause only small changes in Fitchett's scaling function $f(q)$. There is also evidence from numerical simulations that perturbative (small q) calculations can be "scaled-up" to large mass ratios by replacing $q^2 \to f(q)$. This was first suggested by Fitchett and Detweiler [19]. It will be convenient to express this scaling function in terms of the reduced mass ratio $\eta = \mu/M = q/(1+q)^2$, where $\mu = m_1 m_2/M$ is the reduced mass:

$$f(\eta) = \eta^2\sqrt{1-4\eta}\,. \tag{2.6}$$

The reduced mass ratio is the quantity that usually appears in post-Newtonian calculations. It allows us to easily perform an "effective-one-body" scaling of perturbative calculations in which $m_2 \to M$, $m_1 \to \mu$, $q \to \eta$, and, in the leading-order mass-ratio dependence of the recoil, $q^2 \to f(\eta)$. We will make use of this scaling-up procedure in our calculations below.

In the absence of radiation reaction, the center of mass of a circular binary moves in a circle with constant speed as the binary orbits at a fixed separation. Fitchett's formula calculates this center of mass speed. However, for this situation, the time-averaged recoil velocity vanishes. Fitchett's formula indicates that

the recoil depends quite sensitively on the binary separation. However, interpreting his formula is not straightforward for several reasons: First, it is not clear what orbital separation to substitute into his equations. If one computes the recoil at the separation corresponding to the inner-most stable circular orbit (ISCO) of a non-rotating BH ($r = 6M$), the maximum recoil is ≈ 18 km/s. At $r = 2M$ Fitchett's formula would predict 1480 km/s, and at $r = 1M$ (the horizon or ISCO of a maximally rotating BH) it could be as large as 23680 km/s! Second, Fitchett's calculation does not account for the slow-inspiral of the orbit (which causes the recoil and center-of-mass motion to slowly increase with time) or the shutting-off of the recoil that occurs when the holes finally merger together. Before this termination of the gravitational wave signal, the holes plunge together on orbits that deviate in important waves from circularity (even for orbits that are nearly circular during the inspiral phase). The non-circular nature of such orbits is obviously not modelled correctly with Fitchett's formula. Finally, Fitchett's calculations do not take into account relativistic effects that are important in the strong-field region. Specifically, Fitchett's model ignores post-Newtonian corrections to the orbital motion (he uses the Newtonian equations of motion); he ignores higher multipole contributions to the recoil [beyond the mass octupole and current quadrupole terms in Eq. (2.30b)]; and he ignores post-Newtonian corrections to the leading-order multipole moments themselves. The $(M/r)^4$ scaling of Fitchett's formula (2.4) indicates that most of the recoil is acquired at small separations, where strong-field effects are especially important.

Following Fitchett's work several groups began examining the recoil problem using the tools of numerical relativity, black hole perturbation theory, and post-Newtonian techniques. Many of these initial recoil calculations focused on the

head-on collision of two BHs.

Nakamura and Haugan [53] used BH perturbation theory to compute the recoil of a point-particle falling into a Kerr BH along its spin axis. For non-spinning BHs they found a recoil of $V = 261q^2$ km/s. Scaling these results to a mass ratio of $q_{\rm max} \approx 0.38$ via Fitchett's scaling function gives $V_{\rm max} = 4.7$ km/s. [In order to facilitate the comparison of recoil computations I will scale all published results to a mass ratio of $q_{\rm max} \approx 0.38$ using Fitchett's scaling function $f(q)$. I will denote such scaled quantities by $V_{\rm max}$.] For a BH with a spin parameter of $a/M = 0.99$, they found $V = 29.2q^2$ km/s, corresponding to $V_{\rm max} = 0.52$ km/s.

Fitchett also computed the recoil for the head-on collision of two point-masses, but his results depend sensitively on the final separation of the masses (his point masses cannot "merge" together like BHs). For a final separation of $r = 2M$ his numbers imply a maximum recoil of $V_{\rm max} = 45$ km/s, while a final separation of $r = 3M$ would give a value of $V_{\rm max} = 9$ km/s.

For the head-on collision, Andrade and Price [54] computed the recoil using the close-limit approximation, which treats the final stage of the merger of two BHs using BH perturbation theory. Their results were highly uncertain as they depended sensitively on the initial separation of the two BHs: For example, their values ranged from ~ 1 km/s for an initial separation (the proper distance between the apparent horizons) of $2M$ to ~ 100 km/s for an initial separation of $4M$. Anninos and Brandt [55] used full numerical relativity to compute the head-on collision recoil and found $V_{\rm max} = 9$ km/s. More recent calculations using BH perturbation theory by Lousto and Price [56] found $V_{\rm max} = 4.5$ km/s, in close agreement with the earlier results of Nakamura and Haugan [53].

Using full numerical relativity Brandt and Anninos [49] computed the recoil

from single black holes that were highly distorted by axisymmetric Brill waves.[4] The resulting recoils spanned the range from $2-500$ km/s depending on the nature of the holes's distortion; but they claimed that the choice of distortion leading to recoils of 150 km/s and 23 km/s (for even and odd perturbations respectively) are the most astrophysically relevant. Still, it is not clear how the amplitudes and shapes of their distorted black holes correspond to the physical parameters of a binary or a collapsing star.

Post-Newtonian corrections were first incorporated into recoil calculations by Pietilä et. al. [57]. They used Fitchett's Newtonian expressions for the momentum flux, but used the 2.5PN equations of motion for the orbit when integrating the momentum flux. They found a kick velocity with the same form as Eq. (2.4), increased by a factor of 1.45. But they also were faced with the problem of choosing a termination separation to plug into Eq. (2.4). They choose a value based on comparisons of the energy radiated in perturbative and numerical relativity calculations of head-on collisions. Their final estimates for the recoil were quite high ($\sim$ 4000 km/s), but they note that this is likely an upper bound, and they limit the recoil to 2000 km/s in their subsequent calculations. Junker and Schäfer [58] used post-Newtonian expressions to compute the energy and angular momentum flux to 3.5PN order, but they did not push their calculations of the momentum flux beyond what Fitchett already calculated. While previous authors computed the recoil by assuming the balance of momentum loss in the system with the momentum carried by GWs, Blanchet [59] directly proved the balance equation for linear momentum. Wiseman [1] performed the first explicit calculations of the 1PN corrections to the momentum flux and binary recoil. To compute the recoil

[4]Brill waves are exact gravitational wave solutions of Einstein equations

he substituted the 2.5PN equations of motion into the momentum flux formula and integrated the equations. However, he noticed that his 1PN expression for the momentum flux breaks down at separations near $\approx 7M - 9M$, so he did not push his calculations far into the strong-field regime. At a separation of $7M$ (in harmonic coordinates) he computed a maximum recoil of $V_{\rm max} \approx 7.5$ km/s. Kidder [60] computed leading-order corrections to the momentum flux due to the spin-orbit interaction, but did not fully investigate its consequences.[5] Spin contributions can be non-zero even in an equal mass binary and can cause recoil out of the equatorial plane.

Black hole perturbation theory has been a quite fruitful approach to the recoil problem as it allows one to explore strong-field effects. As mentioned previously Nakamura and Haugan [53] computed the recoil for the head-on collision. Fitchett and Detweiler [19] computed the momentum flux for circular orbits around a non-spinning BH. They found that relativistic effects mildly enhance the recoil relative to Fitchett's results. At separations of $6M$ and greater this enhancement was small: they predicted a maximum recoil of $V_{\rm max} = 18$ km/s, nearly indistinguishable from Fitchett's formula. But if the ISCO for a comparable mass binary occurs at a smaller separation [they use Clark and Eardley's [61] estimate of the ISCO location at $r \approx 6\max(m_1, m_2)$], Fitchett and Detweiler predict $V_{\rm max} \approx 125$ km/s (where $r/M \approx 4.35$ for $q \approx q_{\rm max}$), while Fitchett's formula predicts 66 km/s. Although they accounted for strong field-effects, like Fitchett [52] they did not account for the effects of radiation-reaction on the orbit and the resulting recoil. They were also restricted to circular orbits and could not examine the final plunge from the

[5] For circular, non-precessing orbits I have used Kidder's results to compute the corrections to Fitchett's formula (2.4) due to the spin-orbit contribution to the momentum flux; see Eq. 2.36 and Appendix A.

ISCO into the horizon.

Among the most important of these early recoil calculations were those performed by Nakamura and collaborators in the early 1980's. Using BH perturbation theory, they computed the gravitational waves emitted as a particle plunged from an infinite distance into a black hole. In addition to the head-on collision, they also examined particles plunging with non-zero orbital angular momentum. While these kinds of plunging orbits differ from the more realistic plunges that start near the ISCO, they are somewhat similar in structure. Their work remains the only recoil calculations that examine very-strong field, non-circular orbits using BH perturbation theory (although we hope to improve upon this in future work). Their work is especially important because the final recoil velocity is strongly dominated by the plunge contribution, which was not treated in the works mentioned above.

For the plunge into a Schwarzschild hole, Oohara and Nakamura [3] computed a kick velocity of

$$V = 2.7q^2 \text{ km/s}(4L_z^2 + 5L_z + 10)^2 \,, \tag{2.7}$$

where the formula above was fit to their computations for different (dimensionless) orbital angular momenta in the range $L_z \in [0, 3.5]$ (the orbital energy $E = 1$ for particles plunging from infinity). At $r = 6M$, a circular orbit about a Schwarzschild BH has a dimensionless angular momentum of $L_z = 3.464$, yielding a maximum recoil of $V_{\rm max} = 274$ km/s. Kojima and Nakamura [62] (see also Nakamura, Oohara, and Kojima [63]) extended these calculations to Kerr holes. Based on their figure 6, I have crudely estimated the maximum kick velocities for a plunging orbit with the dimensionless angular momentum of a particle at the ISCO[6]: For selected values

[6]Keep in mind that while this choice of angular momentum is accurate for orbits that plunge from the ISCO of a Kerr BH, the radiated momentum calculated by Kojima and Nakamura [62] assumed $E = 1$ for the dimensionless orbital energy;

of the dimensionless Kerr spin parameter $\tilde{a} = a/M$, the corresponding maximum recoil velocities (scaled to $q = q_{\rm max} \approx 0.38$) are approximately

$$(\tilde{a}, V_{\rm max}) = \\ (-0.99, 268), (-0.85, 215), (-0.7, 209), (0, 274), (0.7, 80), (0.85, 80), (0.99, 38) \ , \tag{2.8}$$

where the negative spin parameters refer to retrograde orbits and all velocities are in km/s. These quoted numbers have large errors since Kojima and Nakamura did not compute the recoil for the precise values of orbital angular momentum used above (I estimated their values using a ruler and pencil). But they show a general trend indicating that as BH spin is increased the kick velocities decrease for prograde orbits but increase for retrograde orbits. It is not clear if this trend should also be present for binary orbits that slowly inspiral before merging.

Nakamura, Oohara, and Kojima [63] also investigate the momentum radiated for hyperbolic orbits. Their maximum recoils span a large range, from < 1 km/s to ~ 1600 km/s (see their figure 10-14).

2.2.4 This chapter

In this chapter we will improve upon previous recoil calculations in several ways. The primary improvement is the treatment of both the inspiral and plunge phases of the binary coalescence.[7] During the inspiral phase, our work is essentially an

particles plunging from the ISCO would have $E < 1$. For a BH with dimensionless spin parameter $\tilde{a} = a/M = (0, 0.99, -0.99)$, $E_{\rm isco} = (0.943, 0.736, 0.962)$ respectively. Despite our ability to choose the same values for L_z as circular orbits near the ISCO ($L_z = L_{\rm isco}$), the fact that the plunging trajectories studied in Refs. [3, 62, 63] all satisfy $E = 1$ instead of $E \approx E_{\rm isco}$ means that their computed recoils could differ substantially from orbits that plunge from the ISCO.

[7]The ringdown phase of coalescence is ignored in our work. As shown by Damour and Gopakumar [8], the momentum emitted during this phase contributes

extension of the Fitchett and Detweiler's [19] results to spinning BHs. But in addition to treating spins we also account for the effects of radiation reaction on the orbit.[8] While our "semi-relativistic" plunge calculation does not properly account for all relativistic effects, previous fully-relativistic calculations were restricted to binaries in a head-on collision [54, 56, 55, 53] or plunging from infinity [3, 62, 63]. We treat the realistic case of a particle plunging from the last stable orbit of a circular inspiral. In addition to assuming that the orbits are quasi-circular during the inspiral, we assume that only one of our BHs is spinning and that the orbital angular momentum is parallel or antiparallel to the BH spin. This restricts the orbital motion to the equatorial plane of the larger BH.

2.3 Overview of gravitational radiation recoil

2.3.1 Gravitational wave multipole moment formalism

An expression for the radiated momentum flux can be derived in terms of a multipole moment expansion in the same way that such expressions are derived for the energy and angular momentum flux [44]. We will briefly sketch their derivation here (see Chapter 20 of MTW [64], Thorne [44], and Section IVB of Racine and Flanagan [65] for further details).

The starting point for these calculations is a procedure for constructing the 4-momentum P^μ of a gravitating region as an integral over the source: Begin by expressing the Einstein field equations in the form given by Landau & Lifshitz [66]

$$H^{\mu\alpha\nu\beta}_{\mathrm{LL}}{}_{,\alpha\beta} = 16\pi T^{\mu\nu}_{\mathrm{eff}} = (-g)(T^{\mu\nu} + t^{\mu\nu}_{\mathrm{LL}}) \; . \tag{2.9}$$

little ($\sim 15\%$) to the final recoil.

[8] By neglecting this, Fitchett and Detweiler [19] should actually have found that the recoil vanishes for circular orbits.

Here[9] $g = \det(g_{\mu\nu})$, $H_{\rm LL}^{\mu\alpha\nu\beta}$ is given by

$$H_{\rm LL}^{\mu\alpha\nu\beta} \equiv \mathfrak{g}^{\mu\nu}\mathfrak{g}^{\alpha\beta} - \mathfrak{g}^{\alpha\nu}\mathfrak{g}^{\mu\beta} \ , \tag{2.10}$$

where

$$\mathfrak{g}^{\alpha\beta} \equiv (-g)^{1/2} g^{\alpha\beta} \equiv \eta^{\alpha\beta} - \bar{h}^{\alpha\beta} \ , \tag{2.11}$$

$T_{\rm eff}^{\mu\nu}$ is an "effective stress-energy," and $t_{\rm LL}^{\mu\nu}$ is the Landau-Lifshitz pseudotensor given by Eq. (20.22) of MTW [64] or Eq. (96.9) of Landau and Lifshitz [66]. The effective stress-energy satisfies the conservation law

$$T_{\rm eff}^{\mu\nu}{}_{,\nu} = [(-g)(T^{\mu\nu} + t_{\rm LL}^{\mu\nu})]_{,\nu} = 0 \ . \tag{2.12}$$

At constant coordinate time t consider a 3-volume V whose surface $\Sigma = \partial V$ has a spherical topology. We define the 4-momentum P^μ by the following surface integral:

$$P^\mu(t) \equiv \frac{1}{16\pi} \oint_\Sigma H_{\rm LL}^{\mu\alpha 0 j}{}_{,\alpha} \, d^2\Sigma_j \ . \tag{2.13}$$

Here $d^2\Sigma_j$ is the surface element of Cartesian flat-space, and the above integral is a well-defined 4-vector representing the total 4-momentum of the system only when the surface Σ is taken to be in the asymptotically-flat region infinitely far from the source. Using the flat-space Gauss' theorem and the symmetries of $H_{\rm LL}^{\mu\alpha\nu\beta}$, Eq. (2.13) can be expressed as a volume integral over the source

$$P^\mu(t) = \int_V T_{\rm eff}^{\mu 0} \, d^3x \ , \tag{2.14}$$

where d^3x is the Cartesian volume element of flat space. Taking a time-derivative of the above equation, and using the conservation law in Eq. (2.12) and Gauss'

[9] Everywhere in this thesis, Greek indices run over 0,1,2,3, while Latin indices run over 1,2,3. We follow the conventions of Misner, Thorne, and Wheeler (MTW) [64].

theorem, yields

$$\frac{dP^{\mu}}{dt} = -\oint_{\Sigma} (-g) t^{\mu j}_{\rm LL}\, d^2\Sigma_j \ . \tag{2.15}$$

The matter stress-energy does not contribute in the above formula because the surface of integration is far from the source.

Now let's consider gravitational wave solutions to the field equations that are small perturbations to the flat Minkowski metric,

$$h_{\alpha\beta} = g_{\alpha\beta} - \eta_{\alpha\beta} \ , \tag{2.16}$$

where $|h_{\alpha\beta}| \ll 1$. For these solutions and far from the source, $\bar{h}^{\alpha\beta}$ reduces to the trace-reversed metric perturbation $\bar{h}^{\alpha\beta} = h^{\alpha\beta} - \frac{1}{2}\eta^{\alpha\beta}h$. The radiative degrees of freedom of the gravitational field are contained in the transverse-traceless (TT) piece of the spatial parts of the metric perturbation, $h^{\rm TT}_{jk} = \bar{h}^{\rm TT}_{jk}$. The TT piece of the metric perturbation is constructed by applying the projection operator $P_{jk} = \delta_{jk} - n_j n_k$ to the metric perturbation h_{jk}:

$$h^{\rm TT}_{jk} = P_{ja}P_{kb}h_{ab} - \frac{1}{2}P_{jk}(P_{ab}h_{ab}) \ . \tag{2.17}$$

Far from all sources the GW field satisfies the flat-space wave equation,

$$\Box h^{\rm TT}_{jk} = 0 \ . \tag{2.18}$$

The general out-going wave solution to Eq. (2.18) can be expressed as an expansion in symmetric-trace-free (STF) mass and current multipole moments, $\mathcal{I}_{ij}$ and $\mathcal{S}_{ij}$ [44]:

$$h^{\rm TT}_{jk} = \frac{1}{r}\sum_{l=2}^{\infty}\left[\frac{4}{l!}{}^{(l)}\mathcal{I}_{jkA_{l-2}}(t-r)N_{A_{l-2}} + \frac{8l}{(l+1)!}\epsilon_{pq(j}{}^{(l)}\mathcal{S}_{k)pA_{l-2}}(t-r)n_q N_{A_{l-2}}\right]^{\rm TT} , \tag{2.19}$$

where the notation N_{A_l} means $n_{a_1}n_{a_2}\ldots n_{a_l}$, $n_j = x_j/r$ is a unit radial vector, and ${}^{(l)}\mathcal{I}_{jk}$ means to take l-time derivatives of the multipole moment $\mathcal{I}_{jk}$. These

multipole moments can be expressed as complicated integrals over the effective stress-energy tensor $T^{\mu\nu}_{\rm eff}$ (see Section V. of Thorne [44]). For weak-field, slow-motion sources with small internal stresses, these integrals simplify considerably and any pseudotensor contributions can be ignored:

$$\mathcal{I}_{A_l} = \left[\int \rho X_{A_l} d^3x\right]^{\rm STF} , \tag{2.20a}$$

$$\mathcal{S}_{A_l} = \left[\int \epsilon_{a_l pq} x_p (\rho v_q) X_{A_{l-1}} d^3x\right]^{\rm STF} , \tag{2.20b}$$

where ρ is the Newtonian mass density and v_q is the source velocity. For sources with a characteristic mass M, length scale L, and dynamical timescale T, the mass and current moments scale as

$$\mathcal{I}_{A_l} \sim ML^l , \tag{2.21a}$$

$$\mathcal{S}_{A_l} \sim ML^l(L/T) . \tag{2.21b}$$

When the velocities of the system are small, the gravitational-wave field is well described by the first few terms of this multipole expansion in Eq. (2.19),

$$h^{\rm TT}_{jk} = \varepsilon^2 \frac{1}{r}\left[2\,{}^{(2)}\mathcal{I}_{jk} + \varepsilon\left(\frac{2}{3}\,{}^{(3)}\mathcal{I}_{jka}n_a + \frac{4}{3}(\epsilon_{pqj}\,{}^{(2)}\mathcal{S}_{kp} + \epsilon_{pqk}\,{}^{(2)}\mathcal{S}_{jp})n_q\right) + O(\varepsilon^2)\right]^{\rm TT} , \tag{2.22}$$

where $\varepsilon \sim v \sim L/T$ is an expansion parameter that can be set to unity.

We now consider the energy and momentum flux of the gravitational waves. For GW solutions, Isaacson [67] showed that when the Landau-Lifshitz pseudotensor $(-g)t^{\alpha\beta}_{\rm LL}$ is averaged over several wavelengths of the GWs, it becomes a stress-energy tensor $T^{\alpha\beta}_{\rm GW}$ for those waves and has all the properties of a well-defined tensor. In terms of the TT-metric perturbation, it has the form [64]

$$T^{\rm GW}_{\alpha\beta} = \frac{1}{32\pi}\left\langle h^{\rm TT}_{jk,\alpha} h^{\rm TT}_{jk,\beta}\right\rangle . \tag{2.23}$$

The 4-momentum flux in Eq. (2.15) then becomes

$$\frac{dP^\mu}{dt} = -\oint T^{\mu j}_{\rm GW}\, d^2\Sigma_j = -r^2 \oint T^{\mu j}_{\rm GW} n_j\, d\Omega\ , \tag{2.24}$$

where we have used the surface element for a sphere with outward unit normal n_j.

Since GWs are locally planar in the direction $\boldsymbol{n}$ (the unit vector pointing away from the source) and are null, they satisfy $h^{\rm TT}_{jk} \propto e^{-i\omega(t-\boldsymbol{n}\cdot\boldsymbol{x})}$, and the derivatives of $h^{\rm TT}_{ab}$ satisfy $\partial_j = -n_j\partial_t$ and $n_j\partial_j = -\partial_t$. This gives for the rate of change of the source's energy and momentum[10]

$$\frac{dE}{dt} = -\frac{r^2}{32\pi}\oint \langle \partial_t h^{\rm TT}_{ab} \partial_t h^{\rm TT}_{ab}\rangle\, d\Omega\ , \tag{2.25}$$

$$\frac{dP^j}{dt} = -\frac{r^2}{32\pi}\oint \langle \partial_t h^{\rm TT}_{ab} \partial_t h^{\rm TT}_{ab}\rangle n_j\, d\Omega\ . \tag{2.26}$$

Regardless of sign conventions, the energy and momentum fluxes are related by

$$\frac{dP^j}{dt d\Omega} = n^j \frac{dE}{dt d\Omega}\ . \tag{2.27}$$

The expression for the angular momentum flux is more subtle and derived in [44]:

$$\frac{dJ^j}{dt} = -\frac{r^2}{16\pi}\oint \epsilon_{jpq}\langle h^{\rm TT}_{pa}\partial_t h^{\rm TT}_{aq} - \frac{1}{2}x_p\partial_q h^{\rm TT}_{ab}\partial_t h^{\rm TT}_{ab}\rangle\, d\Omega\ , \tag{2.28}$$

where we have added a minus sign to the formula in [44] to agree with our conventions.

Substituting the multipole expansion (2.19) into the above flux formulas, performing the angular integration, and reversing the overall signs, we arrive at the following expansions for the energy, momentum, and angular momentum fluxes

[10]There appears to be an overall sign difference between the formula here and those used in Section IVB. of Thorne [44]. Thorne appears to be using the symbols E and P_j to denote the energy and momentum of the GWs, not the energy and momentum of the source. Eq. (2.24) here describes the rate of change of the source's 4-momentum.

carried by the GWs [44]

$$\frac{dE_{\rm GW}}{dt} = \sum_{l=2}^{\infty}\left[\frac{(l+1)(l+2)}{(l-1)l}\frac{\langle^{(l+1)}\mathcal{I}_{A_l}{}^{(l+1)}\mathcal{I}_{A_l}}{l!(2l+1)!!} + \frac{4l(l+2)}{(l-1)}\frac{\langle^{(l+1)}\mathcal{S}_{A_l}{}^{(l+1)}\mathcal{S}_{A_l}\rangle}{(l+1)!(2l+1)!!}\right] , \tag{2.29a}$$

$$\frac{dP_j^{\rm GW}}{dt} = \sum_{l=2}^{\infty}\left[\frac{2(l+2)(l+3)}{l(l+1)!(2l+3)!!}\langle^{(l+2)}\mathcal{I}_{jA_l}{}^{(l+1)}\mathcal{I}_{A_l}\rangle \right. \\ \left. + \frac{8(l+3)}{(l+1)!(2l+3)!!}\langle^{(l+2)}\mathcal{S}_{jA_l}{}^{(l+1)}\mathcal{S}_{A_l}\rangle + \frac{8(l+2)\langle\epsilon_{jpq}{}^{(l+1)}\mathcal{I}_{pA_{l-1}}{}^{(l+1)}\mathcal{S}_{qA_{l-1}}\rangle}{(l-1)(l+1)!(2l+1)!!}\right] , \tag{2.29b}$$

$$\frac{dJ_j^{\rm GW}}{dt} = \sum_{l=2}^{\infty}\left[\frac{(l+1)(l+2)}{(l-1)l!(2l+1)!!}\langle\epsilon_{jpq}{}^{(l)}\mathcal{I}_{pA_{l-1}}{}^{(l+1)}\mathcal{I}_{qA_{l-1}}\rangle \right. \\ \left. + \frac{4l^2(l+2)\langle\epsilon_{jpq}{}^{(l)}\mathcal{S}_{pA_{l-1}}{}^{(l+1)}\mathcal{S}_{qA_{l-1}}\rangle}{(l-1)(l+1)!(2l+1)!!}\right] . \tag{2.29c}$$

The first few terms of these expressions can be expanded as

$$\frac{dE_{\rm GW}}{dt} = \varepsilon^4\frac{1}{5}\langle^{(3)}\mathcal{I}_{ab}{}^{(3)}\mathcal{I}_{ab}\rangle + \varepsilon^6\left(\frac{1}{189}\langle^{(4)}\mathcal{I}_{abc}{}^{(4)}\mathcal{I}_{abc}\rangle + \frac{16}{45}\langle^{(3)}\mathcal{S}_{ab}{}^{(3)}\mathcal{S}_{ab}\rangle\right) , \tag{2.30a}$$

$$\frac{dP_j^{\rm GW}}{dt} = \varepsilon^5\left(\frac{2}{63}\langle^{(4)}\mathcal{I}_{jab}{}^{(3)}\mathcal{I}_{ab}\rangle + \frac{16}{45}\langle\epsilon_{jpq}{}^{(3)}\mathcal{I}_{pa}{}^{(3)}\mathcal{S}_{qa}\rangle\right) , \tag{2.30b}$$

$$\frac{dJ_j^{\rm GW}}{dt} = \varepsilon^4\frac{2}{5}\langle\varepsilon_{jpq}{}^{(2)}\mathcal{I}_{pa}{}^{(3)}\mathcal{I}_{qa}\rangle + \varepsilon^6\left(\frac{1}{63}\langle\epsilon_{jpq}{}^{(3)}\mathcal{I}_{pab}{}^{(4)}\mathcal{I}_{qab}\rangle + \frac{32}{45}\langle\epsilon_{jpq}{}^{(2)}\mathcal{S}_{pa}{}^{(3)}\mathcal{S}_{qa}\rangle\right) . \tag{2.30c}$$

Since the total 4-momentum is conserved the source's energy changes according to $\dot{E} = -\dot{E}_{\rm GW}$, and the motion of the source is given by

$$\frac{dP^j}{dt} = \frac{d}{dt}(\gamma M V^j) = -\frac{dP^j_{\rm GW}}{dt} , \tag{2.31}$$

where $dP^j_{\rm GW}/dt$ is the momentum flux in gravitational waves, γ is the Lorentz factor, M is the total rest mass of the system, and V^j is the recoil velocity of the source. Since the recoil velocity will be $\ll c$ for astrophysical situations, we can approximate $\gamma \approx 1$.

2.3.2 Scaling estimates for binary recoil

Using the above formula for the momentum flux [Eq. (2.30b)] we can derive the scalings of the recoil velocity for a particle of mass μ orbiting a BH with mass M at a separation L and undergoing motion with a characteristic timescale T. Assuming that $\mu \ll M$ the time-derivatives of the multipole moments have the following scalings:

$$ {}^{(n)}\mathcal{I}_{A_l} \sim \mu \frac{L^l}{T^n} \,, \tag{2.32a} $$

$$ {}^{(n)}\mathcal{S}_{A_l} \sim \mu \frac{L^l}{T^n} \left(\frac{L}{T}\right) \,. \tag{2.32b} $$

From Eq. (2.30b) the momentum flux then scales like

$$ \left|\frac{dP_j^{\rm GW}}{dt}\right| \sim \frac{\mu L^2}{T^3}\frac{\mu L^3}{T^4} \sim \frac{\mu^2 L^5}{T^7}. \tag{2.33} $$

If the source momentum flux scales like $|dP_j/dt| \sim M v_{\rm recoil}/T$, and $T \sim (R^3/M)^{1/2}$ is the orbital timescale, then we recover the extreme-mass-ratio limit of Fitchett's scaling:

$$ v_{\rm recoil,inspiral} \sim \left(\frac{\mu}{M}\right)^2 \left(\frac{M}{L}\right)^4 . \tag{2.34} $$

For $L \sim 6M$ and $\mu \sim 0.3M$, this yields $v_{\rm recoil,inspiral} \sim 20$ km/s, which is not that bad of an estimate. During the final plunge the lengths and timescales are different, $L \sim T \sim M$, and the scaling simply reduces to

$$ v_{\rm recoil} \sim \left(\frac{\mu}{M}\right)^2 . \tag{2.35} $$

2.3.3 Recoil Intuition

From Eqs. (2.29b) and (2.30b) we can see that GW recoil arises from "beating" between different multipoles. This formula is analogous to the beating between the

electric dipole and the electric quadrupole or magnetic dipole that produces recoil in electromagnetic systems (see [50] for an astrophysical application). This beating between adjacent multipoles means that calculations of the momentum flux are more sensitive to phase cancellation effects than calculations of the energy flux. From the leading-order multipole expansion (2.30b) and Newtonian expressions for the multipole moments and the binary orbit, Fitchett's formula for the recoil [Eq. (2.4)] can be easily derived.

Wiseman [1] provides an intuitive description of the recoil: When two non-spinning bodies are in a circular orbit, the lighter mass moves faster and is more effective at "forward beaming" its radiation (see Figure 1.1. Net momentum is ejected in the direction of the lighter mass's velocity, with opposing center-of-mass recoil. When $m_1 = m_2$, the beaming is symmetric and the recoil vanishes. For unequal masses the instantaneous recoil continually changes direction over a circular orbit, so the center-of-mass traces a circle. Neglecting radiation reaction, this circle closes, and the recoil averages to zero over each orbit. With radiative losses, the orbit does not close, and the recoil accumulates. This accumulation proceeds until the holes plunge and merge, shutting off the radiated momentum flux and yielding a net, non-zero kick velocity (cf. Figures 2.5 to 2.10).

Spin complicates this picture by breaking the binary's symmetry. Consider an equal-mass binary, with one member spinning parallel to the orbital angular momentum. Due to spin-induced frame dragging, the non-spinning body's speed—and hence radiation beaming—is enhanced. Kidder [60] has treated this spin-orbit interaction in post-Newtonian theory. Specializing his Eq. (3.31) to a circular, non-precessing orbit, the total kick for two bodies with spins $\mathbf{S}_{1,2} = \tilde{a}_{1,2} m_{1,2}^2 \hat{\mathbf{z}}$ parallel

or antiparallel to the orbital angular momentum is (see Appendix A)

$$V_{\rm kick} = \left| V_F + 883\ \ {\rm km/s}\, \frac{f_{\rm SO}(q,\tilde{a}_1,\tilde{a}_2)}{f_{\rm SO,\,max}} \left(\frac{2M}{r_{\rm term}}\right)^{9/2} \right| , \qquad (2.36)$$

where V_F is given by Eq. (2.4), the spin-orbit scaling function is $f_{\rm SO}(q,\tilde{a}_1,\tilde{a}_2) = q^2(\tilde{a}_2 - q\tilde{a}_1)/(1+q)^5$, and $f_{\rm SO,\,max} \equiv 1/16$. The recoil is directed in the orbital plane of the binary. The correction term in Eq. (2.36) causes significant recoil even when $q = 1$ (and hence $V_F = 0$). The spin-orbit term is largest when $q = 1$ and the spins are maximal and antiparallel ($\tilde{a}_1 = -\tilde{a}_2 = \pm 1$). The recoil vanishes for $q = 1$ and spins equal and parallel ($\tilde{a}_1 = \tilde{a}_2$)—a symmetric binary.

Since we work in the $q \ll 1$ limit, we ignore the smaller body's spin, which incurs an error $\sim q^2\tilde{a}_1$ in the orbital dynamics [60]. Our extreme mass ratio analysis treats the binary in an effective-one-body sense: a non-spinning point particle with mass $\mu = m_1 m_2/M$ orbits a Kerr hole with mass $M = m_1 + m_2$ and spin $\mathbf{S} = \tilde{a}M^2\hat{\mathbf{z}}$. There is an ambiguity, however, in how one translates the physical spin parameter $\tilde{a}_2$ of the hole with mass m_2 to the "effective" spin parameter $\tilde{a}$ of the hole with mass M. Damour [68] provides a relation between these parameters, valid in the post-Newtonian limit for $\tilde{a} < 0.3$: $\tilde{a} = \tilde{a}_2(1 + 3q/4)/(1+q)^2$. Because of this ambiguity, we present our results in terms of the effective-spin-parameter $\tilde{a}$ even when $|\tilde{a}|$ is large. Even if the larger hole's spin is nearly maximal ($\tilde{a}_2 \simeq \pm 1$), finite mass ratios $q \gtrsim 0.1$ restrict our results to spins with $|\tilde{a}| \lesssim 0.8 - 0.9$.

When applied to a perturbation calculation of the head-on collision of two BHs, an effective-one-body scaling of the GW energy flux ($\dot{E}_{\rm GW} \propto q^2$) in which $q \to \eta = \mu/M = q/(1+q)^2$ has been shown to agree with results from full numerical relativity to within $\sim 20\%$ [69]. We use a similar "scaling up" procedure for the momentum flux: In perturbation theory $\dot{P}^j_{\rm GW} \propto q^2$. We then substitute $q^2 \to f(q)$ [19]. [In terms of η, the scaling function is given by $f(q) \to f(\eta) = \eta^2\sqrt{1-4\eta}$,

and is maximized at $\eta = 1/5$.] Using $f(q)$ [or $f(\eta)$] to scale the momentum flux assumes both bodies are non-spinning and that the orbit is quasi-circular. For simplicity, approximate spin corrections to $f(q)$ based on Eq. (2.36) are ignored (incurring errors $\lesssim 30\%$ if $q \lesssim 0.4$) (cf. Merritt, et. al [2] or section 2.6).

2.4 Inspiral recoil from perturbation theory

Our model binary consists of a mass μ in circular, equatorial orbit about a BH with mass M and effective spin $a = \tilde{a}M$ (where a is the spin parameter that appears in the Kerr metric). Since GWs rapidly reduce eccentricity, circularity is a good assumption for many astrophysical binaries. When $\mu \ll M$, binary evolution is well described using BH perturbation theory [70]. We treat the binary's spacetime as a Kerr BH plus corrections obtained by solving the perturbed Einstein equations—the Teukolsky equation. Specifically, we solve a linear wave equation for the complex scalar function Ψ_4 (a component of the Weyl tensor), which describes radiative perturbations to the hole's curvature. Far from the binary, $\Psi_4 = (\ddot{h}_+ - i\ddot{h}_\times)/2$, where h_+ and $h_\times$ are the two GW polarizations; it therefore encodes information about the GW fields in the distant wave zone, as well as the energy, momentum, and angular momentum carried by those fields.

Far from the binary Ψ_4 has the expansion:

$$\Psi_4 = \frac{1}{r}\sum_{l=2}^{\infty}\sum_{m=-l}^{l} Z_{lm} S_{lm}(\theta; a\omega_m) e^{im\phi - i\omega_m t_R} \ . \tag{2.37}$$

In terms of Boyer-Lindquist coordinates (t, r, θ, ϕ), $t_R = t - r$ is retarded time, $\omega_m = m\Omega_{\rm orb}$ is a harmonic of the orbital frequency $\Omega_{\rm orb}$, $S_{lm}(\theta; a\omega_m)$ is a spheroidal harmonic, and Z_{lm} is a complex number found by solving a particular ordinary differential equation [71].[11]

[11] To simplify our notation we have dropped the spin index on the spheroidal

The linear momentum flux can be extracted by combining Eqs. (B.1) and (2.37). The resulting expression is simplest in the "corotating" frame, $\phi^{\rm corot} = \phi(t) - \Omega_{\rm orb} t$:

$$\dot{\mathcal{P}}^{+}_{\rm GW} = \frac{1}{2} \sum_{ll'm} \frac{Z_{lm} \bar{Z}_{l'(m+1)}}{\omega_m \omega_{m+1}} \int_0^\pi S_{lm} S_{l'(m+1)} \sin^2\theta d\theta \ . \tag{2.38}$$

Here, $\dot{\mathcal{P}}^{+}_{\rm GW} = e^{-i\phi(t)}[\dot{P}^{x}_{\rm GW} + i\dot{P}^{y}_{\rm GW}]$, and an overbar denotes complex conjugation. $\dot{P}^{x}_{\rm GW}$ and $\dot{P}^{y}_{\rm GW}$ are the inertial-frame momentum fluxes and $\phi(t)$ is the orbital phase. Similar expressions give the energy and angular momentum fluxes. The details of the derivation of this formula, as well as a review of the necessary BH perturbation theory formalism, is given in Appendix B. The recoil velocity is found by integrating Eq. (2.38), starting at initial time t_0 when the binary has a large separation [and the recoil is well described by Eq. (2.4)], and ending at time T when the GW emission terminates:

$$v_x + i v_y = -\frac{1}{M} \int_{t_0}^{T} e^{i\phi(t)} \dot{\mathcal{P}}^{+}_{\rm GW} \, dt \ . \tag{2.39}$$

Our procedure starts with a point source on a circular geodesic orbit with specified energy E and angular momentum L_z. Solving the Teukolsky equation gives us the energy, momentum, and angular momentum fluxes of GWs to infinity and down the event horizon. The linear momentum flux down the horizon does not affect the recoil. In the adiabatic limit (in which GW backreaction changes the orbit very slowly, $r/\dot{r} \ll 2\pi/\Omega_{\rm orb}$), the energy and angular momentum fluxes $(\dot{E}_{\rm GW}, \dot{L}_{z,\rm GW})$ are used to evolve to a new geodesic with energy $E - \dot{E}_{\rm GW}\Delta t$ and angular momentum $L_z - \dot{L}_{z,\rm GW}\Delta t$. Repeating this procedure for a sequence of geodesics generates a slow inspiral trajectory (see Hughes [71, 72] for details). The momentum flux along this trajectory and the associated recoil velocity are then calculated via Eqs. (2.38) and (2.39).

harmonic functions. We have also dropped the label "H" from the Z_{lm} numbers. See Appendix B for the detailed expressions.

This prescription can be used to calculate the recoil velocity only up to the ISCO. There the slow, adiabatic inspiral of the particle transitions to a rapid "plunge" that terminates when the particle crosses the event horizon (cf. Fig. 2.5a). Our Fourier decomposition of Ψ_4 is no longer valid as there are no well-defined harmonics ω_m for plunging trajectories. Our calculated recoil up to the ISCO for various values of the BH spin parameter are given in Table 2.1 for binaries with reduced mass ratios of $\eta = 0.1$ and $\eta = 0.2$. In our calculation we have included sums up to $l = 12$ in Eq. (2.38), which is sufficient for the calculation to converge. The Fitchett-Detweiler [19] scaling-up procedure, $\eta^2 \to f(\eta)$, has been applied to our recoil values. This scaling function has important errors associated with it: aside from post-Newtonian finite-mass ratio corrections which are small (discussed below), the scaling function is modified in the case of spinning-binaries. For example, spin effects will cause non-zero recoil even when $m_1 = m_2$. During the inspiral phase it is possible to "derive" corrections to $f(q)$ based on the spin-orbit correction terms in Eq. (2.36). These corrections deviate from $f(q)$ by $\sim 10\%$ at $q = 0.38$ and by $\sim 43\%$ at $q = 0.8$. However, it is far from clear what the correct scaling function during the plunge should be for spinning holes. Given these uncertainties (and relatively small corrections for $q \approx 0.38$), we ignore more complicated scaling functions and stick with $f(q)$.

Figure 2.1 shows the perturbation theory calculation of the recoil up to the ISCO for a binary with reduced mass ratio $\eta = 0.1$ ($q = 0.127$). The data in this plot (the solid, blue curve) can be fit as a function of the BH spin parameter a/M by

$$V_{\rm ISCO} = 17.9 \ \ {\rm km/s}\, \frac{f(q)}{f_{\rm max}} \begin{cases} (7.11)^{a/M}\,, & -1 \le a/M < 0.8 \\ 4.95(1-a/M)^{-0.456}\,, & 0.8 \le a/M \le 0.998 \end{cases} . \quad (2.40)$$

This function was fit to the $\eta = 0.1$ inspiral data (Table 2.1) and agrees with it to within $\sim 20\% - 30\%$. Applying this function unchanged to the $\eta = 0.2$ inspiral data shows agreement to $\sim 30\% - 40\%$. (For the values in Table 2.1, Fitchett's scaling function was used in determining the mass ratio dependence.)

The solid curve in Figure 2.1 can be fit with better accuracy by a function of the location of the ISCO,

$$V_{\rm isco} = 422 \ \ {\rm km/s}\, \frac{f(q)}{f_{\rm max}} \left(\frac{2M}{r_{\rm isco}}\right)^{2.63+0.06 r_{\rm isco}/M} , \tag{2.41}$$

where $r_{\rm isco}$ is the spin-dependent ISCO radius [defined for $q = 0$ by Eq. (2.21) of [73]; see also Appendix C]. This function agrees with the calculated data for $\eta = 0.1$ to within about $\lesssim 6\%$, and with the $\eta = 0.2$ data to within $\lesssim 20\%$.

Although our adiabatic assumption is violated for $\eta = 0.1$ (especially for large, prograde spins) our results are still valid since $V_{\rm isco}/f(q)$ is only weakly dependent on q (and is independent of q in the $q \to 0$ limit). This is supported by post-Newtonian analyses [6, 8] that demonstrate this weak mass-ratio dependence. Errors due to the adiabatic approximation (and the neglect of finite-mass ratio effects) scale like $O(\eta)$. These errors will tend to become more important as the ISCO is approached (since $T_{rr} \sim T_{\rm orb}$ there), but we estimate that our results for the recoil up to the ISCO are accurate to better than $\lesssim 20\% - 30\%$. This is crudely based on the fact that post-adiabatic corrections to the recoil scale like $O(\eta)$. Recent post-Newtonian work [6, 8] indicates that these errors are actually much smaller (a few percent). Some part of our error is also due to the fact that we terminate the simulation shortly before the ISCO is reached. While we can compute the radiated momentum at the ISCO, our scheme for implementing radiation reaction does not let us step past the ISCO, so we stop integrating some short distance outside the ISCO.

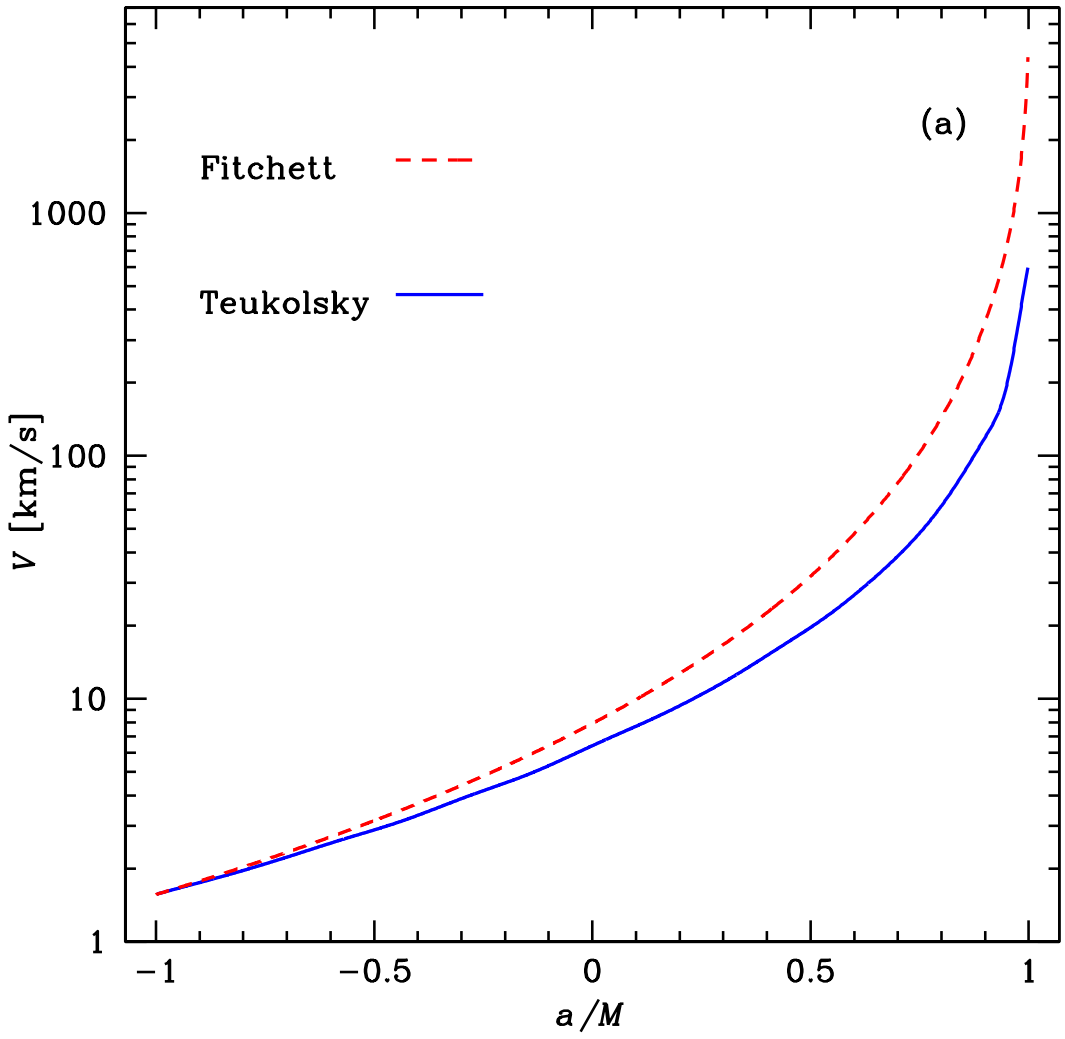

Figure 2.1: Recoil velocity up to the ISCO versus effective spin a/M for $\eta = 0.1$ ($q = 0.127$). The solid (blue) curve is our Teukolsky equation result. The dashed (red) curve shows the Newtonian recoil prediction [Eq. (2.4)], which is substantially higher for large, prograde spins (smaller ISCO radius).

For retrograde orbits around rapidly spinning holes, the ISCO is at large radius ($9M$ for $\tilde{a} = -1$) and Fitchett's Newtonian formula [Eq. (2.4)] agrees well with our result. For prograde inspiral into rapidly spinning holes, the ISCO is deep in the strong field, where relativistic effects become important and suppress the recoil relative to Fitchett's result. Post-Newtonian calculations [1] show a similar suppression, but break down in the strong field region (even when $\eta \ll 1$).

The power law dependence of Eq. (2.41) differs from the $(M/r)^4$ dependence of Fitchett's result. However, Eq. (2.41) is meant to be interpreted merely as a fitting function that approximates our calculated results (to within $\approx 6\%$) (see Table 2.1). It is only valid when evaluated at the ISCO radius. Figures 2.2 and 2.3 show how the recoil accumulates during the inspiral and compares with Fitchett's results. As discussed above, the relativistic corrections to the inspiral recoil are relatively unimportant when the ISCO is at $r_{\rm isco} \gtrsim 6M$, but those corrections become quite important when the ISCO moves to smaller separations.

The accumulated recoil during the inspiral as a function of r (Figures 2.2 and 2.3) has almost the same form regardless of spin. It is therefore useful to look at the accumulated recoil vs. r for $a/M = 0.998$—the case for which the inspiral penetrates to the smallest r-values. A fit to this data is

$$V_{\rm recoil}(a/M = 0.998, r) = \frac{f(q)}{f_{\rm max}} \begin{cases} 939 \ \text{km/s} \left(\frac{2M}{r}\right)^{3.85} , & 10 < r/M \leq 20 , \\ 756 \ \text{km/s} \left(\frac{2M}{r}\right)^{3.72} , & 5 < r/M \leq 10 , \\ 451 \ \text{km/s} \left(\frac{2M}{r}\right)^{3.09} , & 1.35 < r/M \leq 5 . \end{cases} \tag{2.42}$$

This agrees with the $a/M = 0.998, \eta = 0.1$ inspiral data to $\lesssim 10\%$ ($\sim 20\%$ at the low-r end). We can test the universality of this curve by comparing to the accumulated recoil versus radius for another spin value. Comparing the accumulated

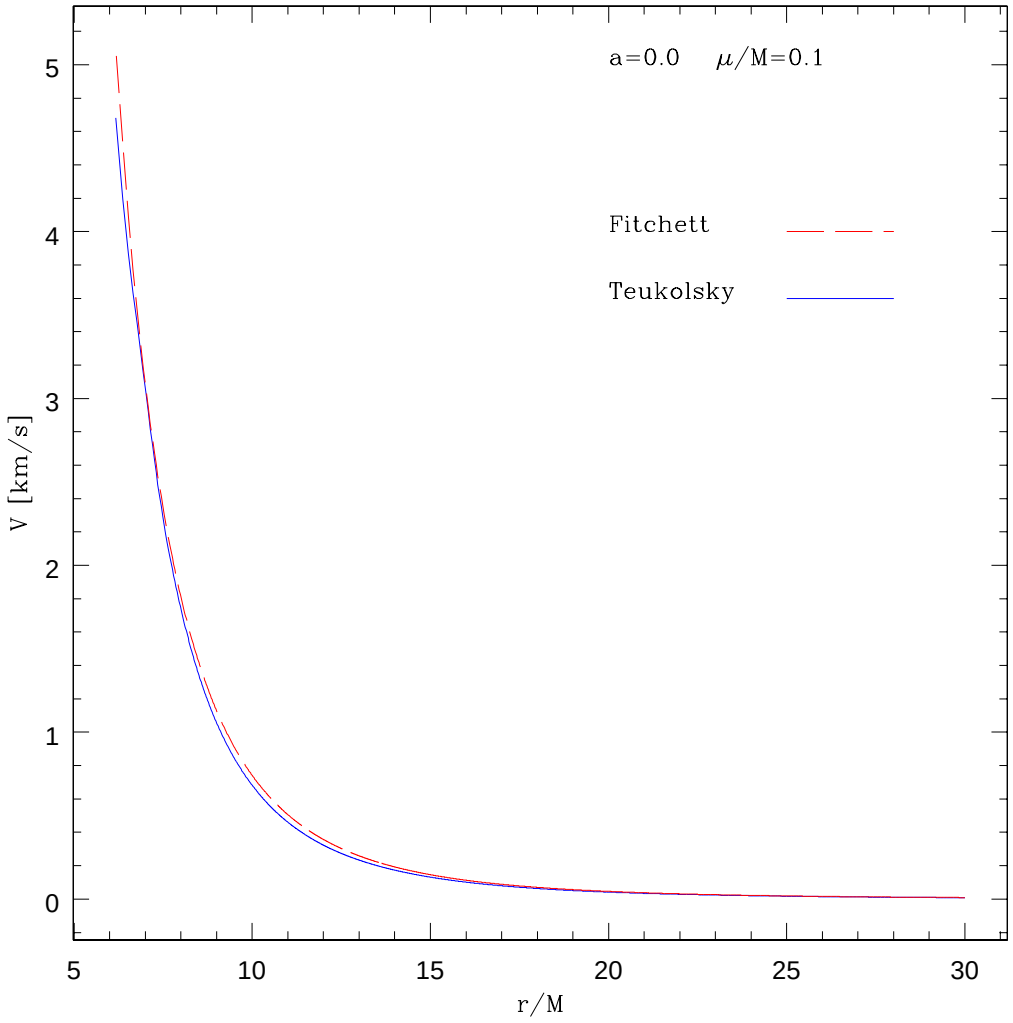

Figure 2.2: Accumulated recoil for a non-spinning black hole up to the ISCO ($r_{\rm isco} = 6M$) as a function of Schwarzschild coordinate radius r. The red (dashed) curve is the prediction from Fitchett's formula [Eq. (2.4)]. The blue (solid) curve is the result of our perturbation theory calculation. Up the ISCO of a non-spinning BH, the recoil is nearly identical but slightly smaller than Fitchett's prediction. The reduced mass ratio of the binary is $\eta = 0.1$.

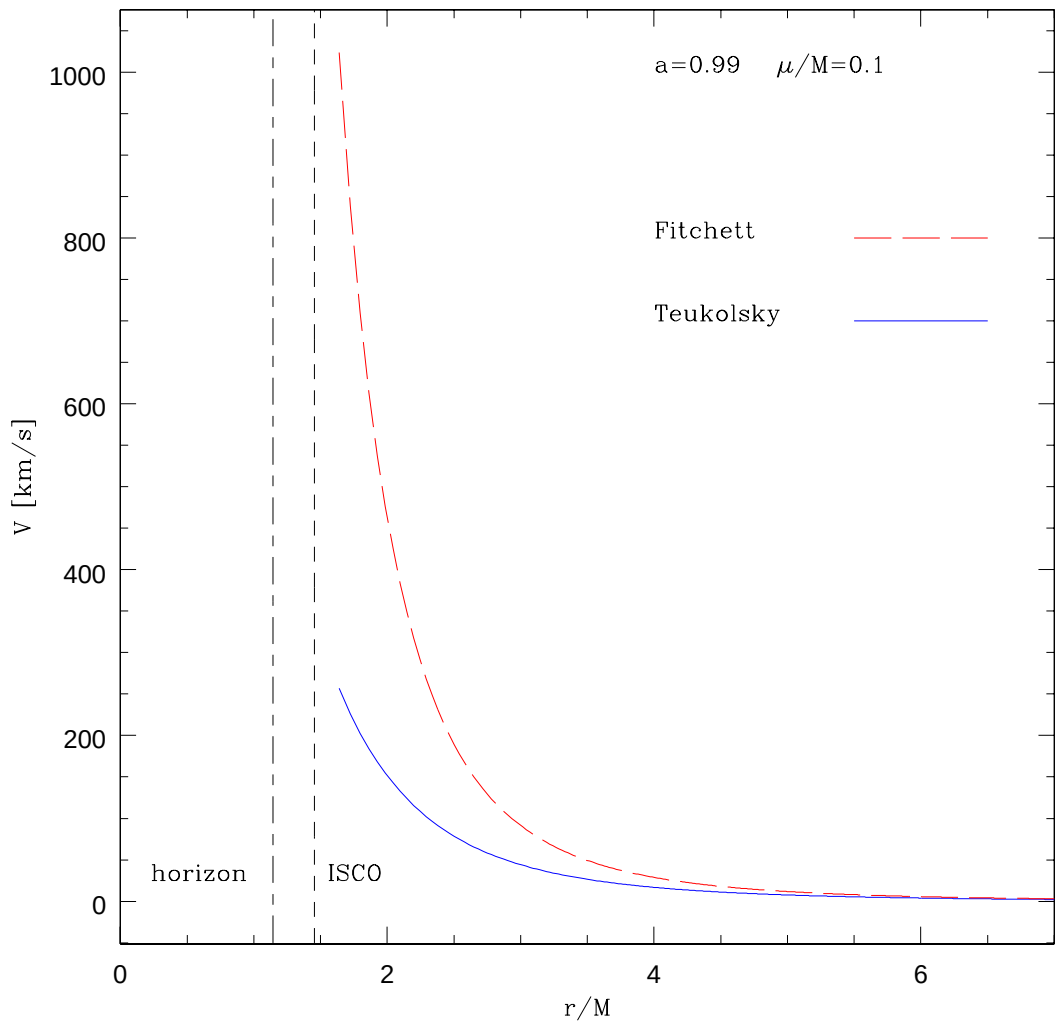

Figure 2.3: Accumulated recoil for a rapidly-spinning black hole (with spin parameter 0.99) up to the ISCO ($r_{\rm isco} \approx 1.45M$) as a function of Boyer-Lindquist coordinate radius r. The curves are labelled as in Figure 2.2. The dashed lines represent the locations of the ISCO and the event horizon. In this case the inspiral penetrates deeper into the strong-field region, and the recoil is significantly suppressed relative to the prediction of Fitchett's formula. The reduced mass ratio of the binary is $\eta = 0.1$.

recoil for $a/M = 0.998$ to that for $a/M = 0.0$ ($\eta = 0.1$ in both cases), shows that these two function agree to within $\sim 20 - 30\%$. This tells us that (aside from the spin-dependence of the ISCO) the accumulated recoil up to the ISCO depends only weakly on the spin of the hole, and is mostly dependent on the radial coordinate value of the ISCO[12]. From the fitting function (2.42) it is interesting to note that at large r the kick velocity approximately follows Fitchett's $1/r^4$ scaling, but as we move to smaller radii, this slowly transitions to an approximately $1/r^3$ scaling.

During the inspiral phase, the recoil is largest for prograde inspirals into a rapidly rotating hole. For these orbits the ISCO moves very close to the horizon and relativistic effects become very important (see figure 2.3). When the hole is very rapidly spinning $a/M > 0.8$ (and orbits are prograde) the recoil up to the ISCO is likely to be very important as the distance the particle must "plunge" to enter the horizon is very short. It is therefore interesting to calculate how large the ISCO recoil can grow by pushing the spin parameter close to its maximum value ($a/M = 1$). Running our Teukolsky code for near-maximal spins gives the following values: for $a/M = 0.998$ the maximum recoil is 597 km/s (for $\eta = 0.1$) and 1410 km/s (for $\eta = 0.2$). For $a/M = 0.99999$ we find that the recoil is 438 km/s for $\eta = 0.1$. Oddly, this is lower than the value for $a/M = 0.998$. The recoil in this case seems to peak at 604 km/s, but then drops down before passing through the ISCO. This sort of peak is also seen in our description of the plunge, but it is rarely present during the inspiral. It is not clear if this behavior is physical or due to numerical error or some other artifact of our computations. For the

[12]This strong dependence on the ISCO radius and weak dependence on spin gives us a hint as to how the inspiral part of the recoil will behave for circular, inclined orbits. It is likely that the recoil up to the last stable orbit (LSO) in this case can be approximated by simply replacing $r_{\rm isco}$ with $r_{\rm LSO}$ in Eq. (2.41), where $r_{\rm LSO}$ is approximately given by Eq. (C.3).

case with $\eta = 0.2$, the recoil is 2325 km/s, and the accumulated recoil increases monotonically. It is not clear what would happen if we were to push the spin parameter even higher. It is possible that the recoil could approach $V_{\rm isco} \sim c$ for nearly extremal Kerr BHs. However, the ISCO recoil for prograde inspiral into BHs with spins $a/M \gtrsim 0.95$ is irrelevant for astrophysical situations: the finite mass and size of the particle will significantly modify the dynamics, either by changing the location of the ISCO or through the formation of a common event horizon.

2.5 Recoil estimates from the final plunge

During the plunge, the small body's motion is dominated by the Kerr effective potential rather than radiation-reaction forces [74]. It is easy to match a plunging geodesic with constant E and L_z onto an inspiral trajectory near the ISCO. The details of this are presented in Appendix D. With a code that does not Fourier expand Ψ_4 [75, 76], one could then properly compute the GW emission and associated recoil along such a plunging trajectory (when $q \ll 1$).

Since we do not have such a code at hand, we must estimate the wave emission more crudely. Our results from the inspiral show that, for a given spin, $\dot{\mathcal{P}}^{+}_{\rm GW}$ is well described by a power law in radius, $\dot{\mathcal{P}}^{+}_{\rm GW} \propto r^{-\alpha}$, from large r up to the ISCO. As an approximate "upper limit" of the recoil, we make the ansatz that this power law can be continued past the ISCO. This must break down at some point: the power-law reflects the circularity of the inspiral orbit and should be suppressed by the increasingly radial motion during the plunge.[13] To prevent the

[13]This method overestimates the recoil partly because it assumes that the "Keplerian" law for the angular velocity that holds for $r > r_{\rm isco}$ is also valid during the plunge. This overestimates the velocity of the particle. Fitchett and Detweiler [19] performed a similar extrapolation past the ISCO, but did not account for the

Table 2.1: Recoil velocities in km/s for different values of the effective spin parameter $\tilde{a}$. Columns two and three are the recoil up to the ISCO for the inspiral calculation, $V_{\rm inspiral}(\eta)$, for the two calculated values of η. The fourth column is the total accumulated recoil $V_{\rm lower}$ for $\eta = 0.1$, based on our lower-limit prescription for computing the plunge contribution. The plunge calculation was matched to the inspiral solution at a radius slightly larger than the ISCO, and it was continued up to a radial cutoff at $r = r_{\rm horizon} + 2\eta M$ when the holes "touch." Column five shows the values in column four, but scaled-up to $\eta = 0.2$ using Fitchett's scaling function [Eq. (2.6)].

$\tilde{a} = a/M$	$V_{\rm inspiral}(\eta = 0.1)$	$V_{\rm inspiral}(\eta = 0.2)$	$V_{\rm plunge}(\eta = 0.1)$	$V_{\rm plunge}(\eta = 0.2)$
-0.998	1.57	3.27	93.9	217
-0.9	1.75	3.68	3.73	8.62
-0.8	1.96	4.08	5.53	12.8
-0.7	2.23	4.61	8.35	19.3
-0.6	2.54	5.24	10.6	24.5
-0.5	2.88	5.99	12.6	29.0
-0.4	3.31	6.86	14.3	33.1
-0.3	3.88	7.98	16.1	37.2
-0.2	4.50	9.33	18.4	42.5
-0.1	5.30	10.8	21.0	48.4
0.0	6.41	12.9	23.9	55.1
0.1	7.70	15.6	27.1	62.5
0.2	9.36	18.8	30.7	71.0
0.3	11.7	23.4	34.8	80.4
0.4	15.1	29.4	39.8	92.0
0.5	19.6	38.7	45.7	105
0.6	26.7	53.0	53.0	122
0.7	38.7	75.0	61.8	143
0.8	62.2	119	68.1	157
0.9	119	227	66.7	154
0.95	196	369	98.5	228
0.998	597	1410	NA	NA

momentum flux from diverging, we truncate the power law at $3M$, replacing it with the condition that $(dt/d\tau)\dot{\mathcal{P}}^{+}_{\rm GW} = \text{constant}$ for $r \leq 3M$, where τ is the proper time along the plunge geodesic.[14] This allows the momentum flux to "redshift away" as the particle approaches the horizon. Using the recoil velocity at the ISCO as initial conditions [Sec. 2.4] and a plunge trajectory with coordinates $[r(t), \phi(t)]$, we use Eq. (2.39) and our truncated-power-law ansatz to compute the accumulated recoil until a cutoff time T when the horizons of the holes come into contact. In a quasi-Newtonian interpretation of the coordinates this occurs when $r = r_{\rm horizon} + 2\mu$, where $r_{\rm horizon}$ is the coordinate location of the BH event horizon. The upper-curve of Figure 2.4 shows the result of this calculation (for $\eta = 0.1$).

We also perform a separate "lower-limit" calculation. A plunge trajectory is computed as before, but in place of the power-law ansatz for $\dot{\mathcal{P}}^{+}_{\rm GW}$, we integrate the truncated, multipole expansion of Eq. (2.30b) instead. We use simple Newtonian point-particle expressions to describe the multipole moments, substituting the coordinates of the particle's plunge orbit. Details of this prescription are discussed in Appendix E. In this calculation the momentum flux initially grows like a power law, but then reaches a maximum and decreases as the plunging trajectory nears the event horizon. This behavior has been confirmed in approaches using post-Newtonian theory [8] and numerical relativity [9]. Because we neglect higher multipoles (which are extremely important in the fast-motion, strong-gravity region)

---

non-circular nature of the plunge orbit. Blanchet et al. [6] also used the wrong Kepler's law when applying their momentum flux formula to the plunge, causing them to overestimate the recoil.

[14] For $a/M = 0$ the point $r = 3M$ is near the peak of the effective potential of the Sasaki-Nakamura equation. Radiation emitted at smaller radii has trouble escaping from this potential. The location of the peak varies as a function of spin, frequency, and harmonic index l, but for the sake of simplicity we choose $3M$ as an approximate cutoff point for all the spins that we examine.

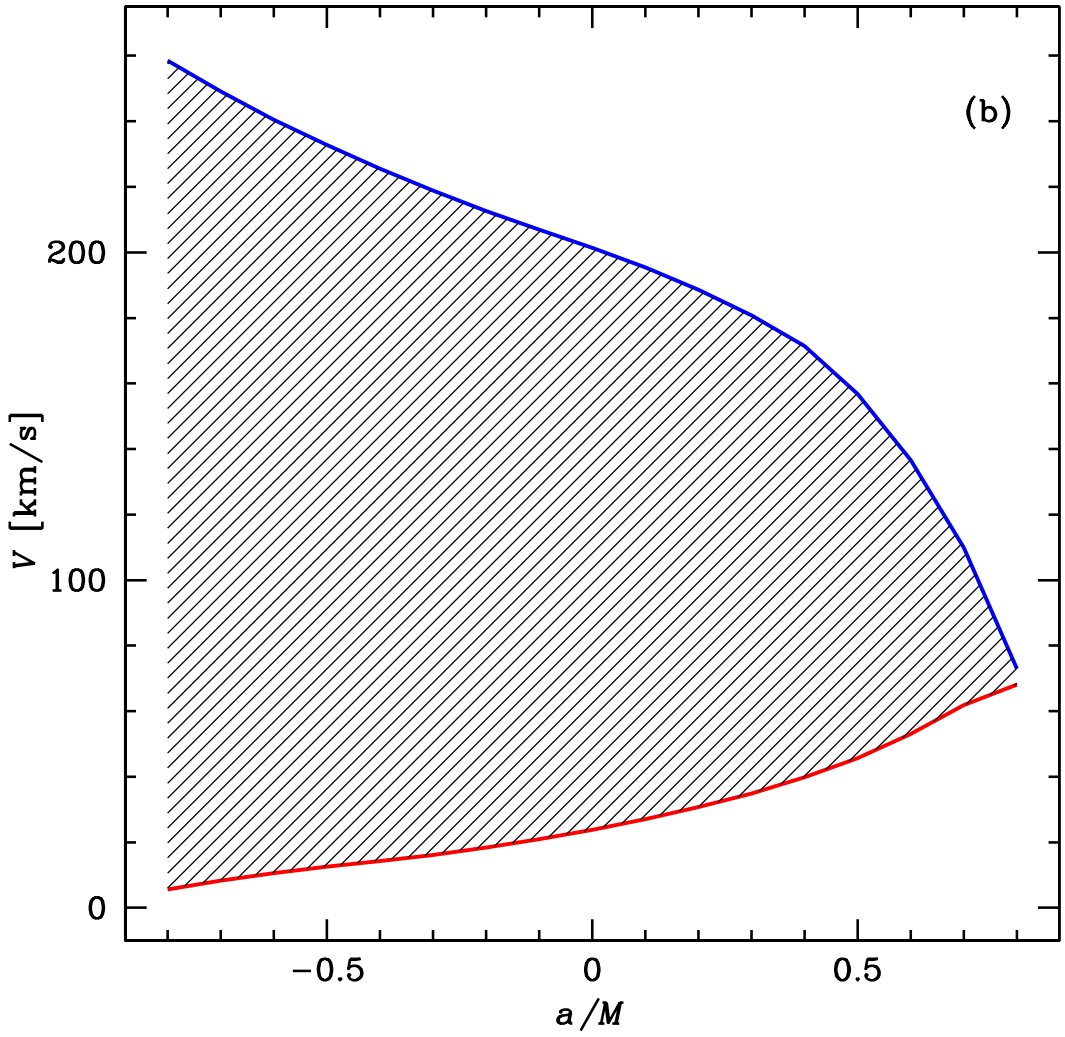

Figure 2.4: Upper and lower limits for the total recoil velocity versus effective spin a/M for $\eta = 0.1$ ($q = 0.127$). The shaded region represents our uncertainty in the final kick velocity. The detailed shape of the upper-limit curve depends on the nature of our truncated-power-law ansatz.

and post-Newtonian corrections to the leading-order multipoles, this method underestimates the recoil. This has been confirmed in the recent analysis by Damour and Gopakumar [8]. The total accumulated recoil at the cutoff time T (determined by when the horizons "touch" as described above) using this method is shown in the lower curve of Figure 2.4.

Figures 2.6 - 2.9 show the orbit, recoil, and center of mass motion for prograde and retrograde coalescence into spinning and non-spinning holes using both our upper- and lower-limit prescriptions. We can see by comparing the lower-right-hand panels of each plot that the accumulation of the recoil behaves quite differently depending on wether the upper- or lower-limit scheme is used. These results are summarized in Figure 2.4.

The shaded region between the two curves in Figure 2.4 represents our uncertainty in the total recoil at the end of the plunge. This uncertainty is largest for retrograde orbits around rapidly spinning holes, in which the distance the particle must "plunge" is greatest. For prograde inspiral into rapidly spinning holes, much of the recoil is due to emission during the slow inspiral phase, for which our BH perturbation techniques are well-suited. Figures 2.7 and 2.8 show the relative contributions from the inspiral and plunge for such a scenario.

Although the two calculations for the plunge recoil give rather different results, useful astrophysical information is contained in the approximate upper and lower bounds that they represent. The estimate $V \sim 120$ km/s bisects the shaded region of Figure 2.4 and represents a typical recoil velocity for this mass ratio. Note also that the numbers in Figure 2.4 can be scaled to higher mass ratios by multiplying by $f(q)/f(\eta = 0.1)$. For $q \approx 0.38$ this implies that our results can be augmented by a factor ≈ 2.3.

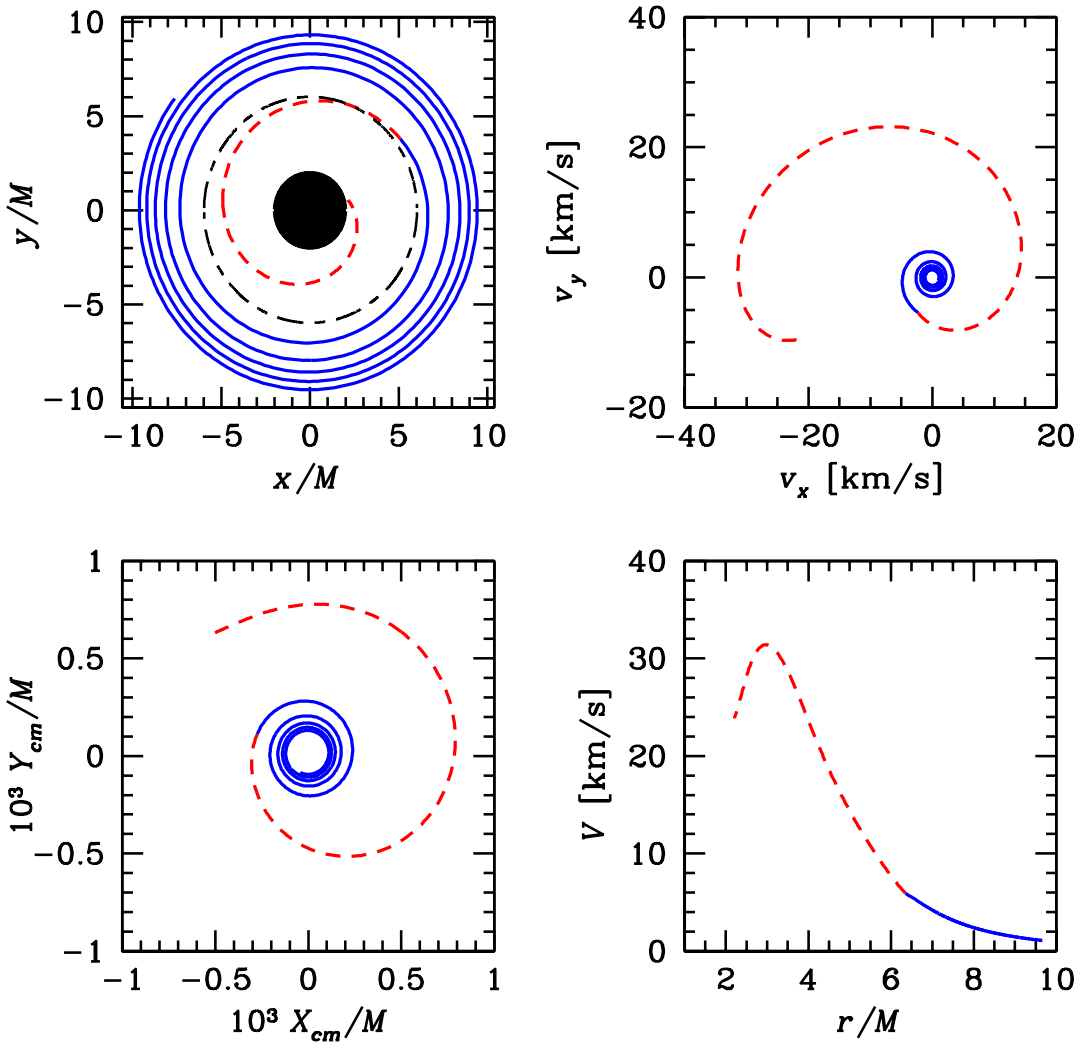

Figure 2.5: Lower-limit recoil calculation for prograde coalescence with $a/M = 0.0$, $\eta = 0.1$ ($q = 0.127$). Solid (blue) lines represent quantities during the inspiral, as calculated using our Teukolsky equation solver. Dashed (red) lines are calculations during the plunge (using the "upper-limit" prescription discussed in section 2.5). The plunge is truncated shortly before the particle enters the event horizon. The different panels are: (upper-left) Orbit of the mass μ about the central spinning hole. The dashed circle is the location of the ISCO. (upper-right) Recoil velocity of the center of mass. The spiral ends when GW emission is cut off. (lower-left) Motion of the binary's center of mass. (lower-right) Total center of mass recoil velocity, $(v_x^2 + v_y^2)^{1/2}$.

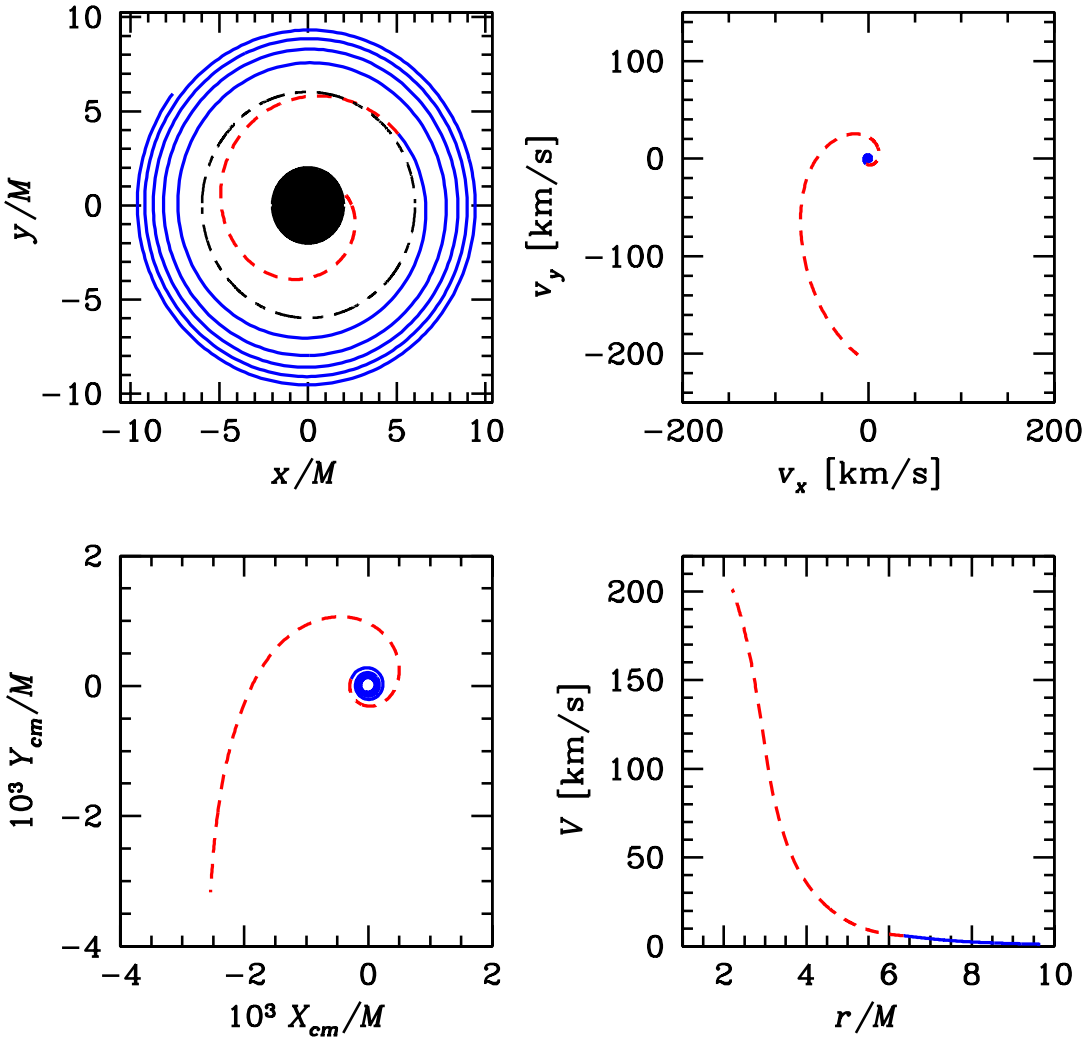

Figure 2.6: Upper-limit recoil calculation for prograde coalescence with $a/M = 0.0$, $\eta = 0.1$ ($q = 0.127$). Details are the same as in figure 2.5.

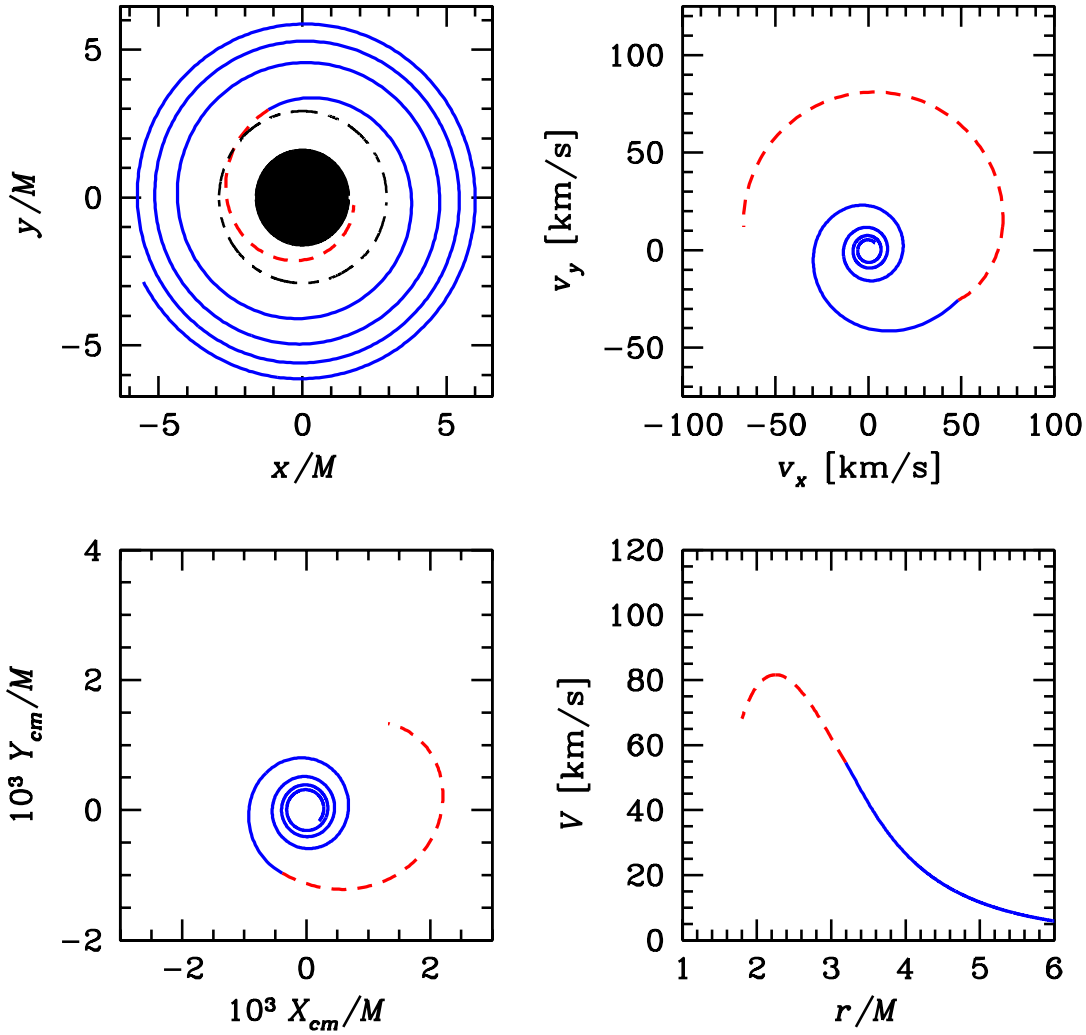

Figure 2.7: Lower-limit recoil calculation for prograde coalescence with $a/M = 0.8$, $\eta = 0.1$ ($q = 0.127$). Details are the same as in figure 2.5.

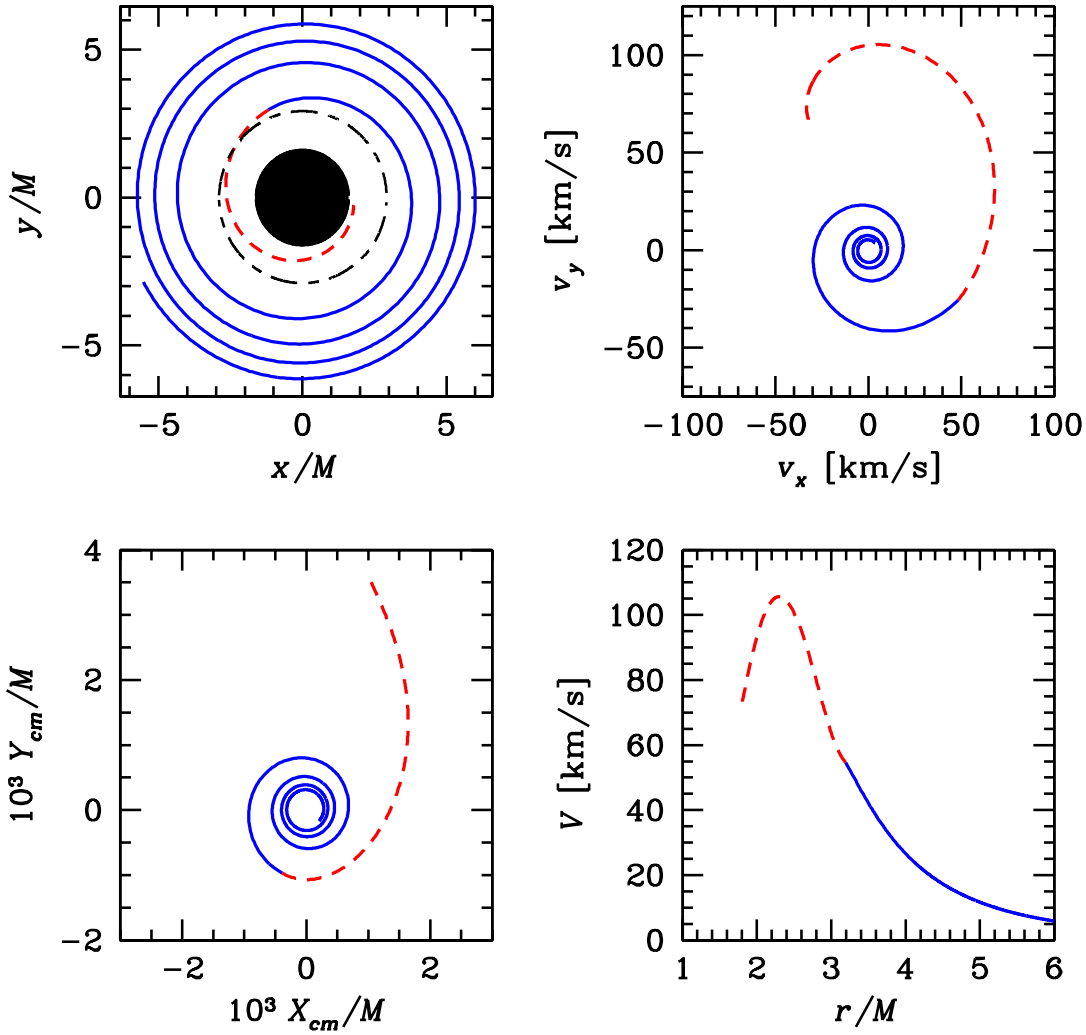

Figure 2.8: Upper-limit recoil calculation for prograde coalescence with $a/M = 0.8$, $\eta = 0.1$ ($q = 0.127$). Details are the same as in figure 2.5.

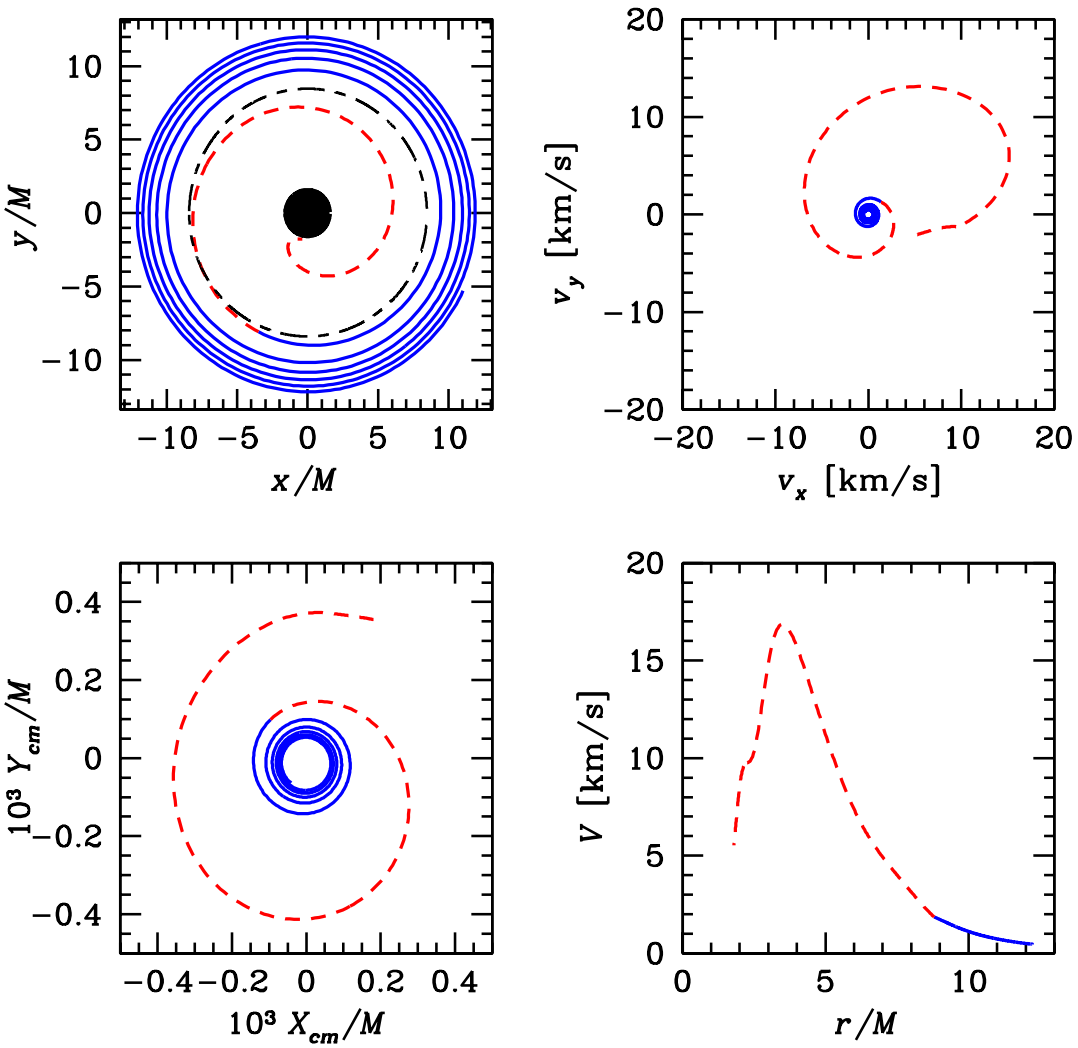

Figure 2.9: Lower-limit recoil calculation for retrograde coalescence with $a/M = 0.8$, $\eta = 0.1$ ($q = 0.127$). Details are the same as in figure 2.5.

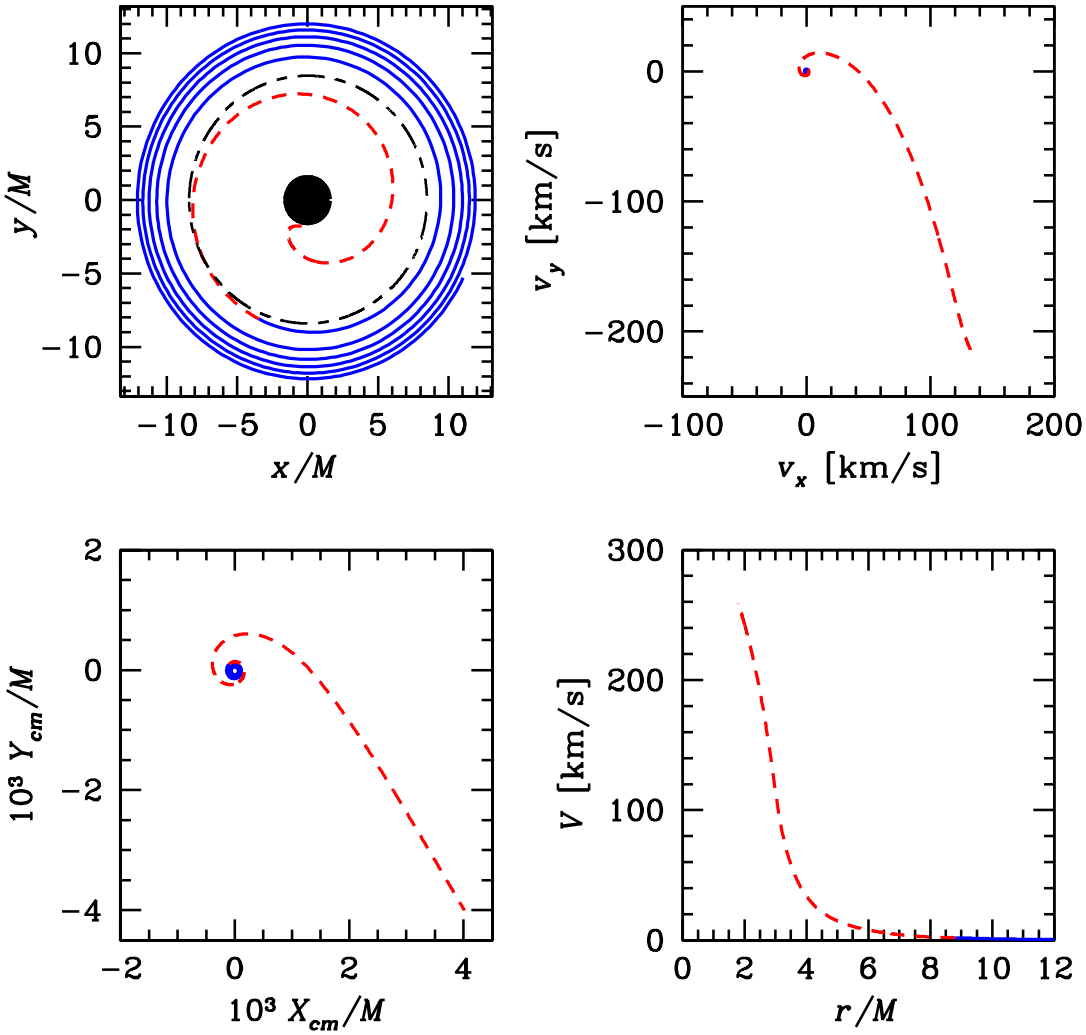

Figure 2.10: Upper-limit recoil calculation for retrograde coalescence with $a/M = 0.8$, $\eta = 0.1$ ($q = 0.127$). Details are the same as in figure 2.5.

Although we only consider the cases where the inclination angle is $\iota = 0$ and $\iota = 180$, the recoil for arbitrary inclination is likely to be bounded between these extreme values. Also, the detailed inclination dependence is unimportant in comparison with the large uncertainty already present in the contribution to the recoil from the final plunge and coalescence. The restriction to equatorial-prograde/retrograde orbits considered here likely encompasses the characteristic range of recoil velocities.

2.6 Fitting functions for the total recoil

The results shown in Figure 2.4 should be interpreted as upper- and lower-limit estimates of the recoil velocity as a function of the *effective spin parameter* $\tilde{a}$ for a reduced mass ratio $\eta = 0.1$. As discussed in section 2.3.3, we have restricted ourselves to $\tilde{a} \lesssim 0.8$ since the finite-mass of the particle complicates the distinction between "inspiral" and "plunge" when the hole is rapidly spinning. Also, because of the neglect of relativistic effects, our errors for the plunge calculations are likely to be very large for holes that are spinning very rapidly $\tilde{a} > 0.8$.

Our upper-limit calculations for $\eta = 0.1$ are well fit in the range $-0.9 \leq \tilde{a} \leq 0.8$ by the following fifth-order polynomial:

$$V_{\rm upper} = 465 \text{ km/s} \frac{f(q)}{f_{\rm max}} (1 - 0.281\tilde{a} - 0.0361\tilde{a}^2 - 0.346\tilde{a}^3 - 0.374\tilde{a}^4 - 0.184\tilde{a}^5). \quad (2.43)$$

Our lower-limit calculations are well fit by

$$V_{\rm lower} = 54.4 \text{ km/s} \frac{f(q)}{f_{\rm max}} (1 + 1.22\tilde{a} + 1.04\tilde{a}^2 + 0.977\tilde{a}^3 - 0.201\tilde{a}^4 - 0.434\tilde{a}^5). \quad (2.44)$$

We can convert these expressions into estimates of the bounds on the total recoil as follows. First we recall the ambiguity in how one translates the physical spin

parameter $\tilde{a}_2$ of the larger hole into the effective spin parameter $\tilde{a}$ of equations (2.43) and (2.44). Here we adopt Damour's [68] relation $\tilde{a} = (1+3q/4)(1+q)^{-2}\tilde{a}_2$. This expression is valid in the post-Newtonian limit for $\tilde{a} < 0.3$; in the absence of anything better, we adopt it for all values of $\tilde{a}$, while keeping in mind that high "effective" spins are suppressed when $q \gtrsim 0.1$.

Second, Fitchett's scaling function assumes that both bodies are non-spinning, and vanishes when $q = 1$. In fact, when $\tilde{a} \neq 0$, significant recoil would occur even for $q = 1$ due to spin-orbit coupling. We can guess the approximate form of a new scaling function by examining the spin-orbit corrections (Kidder [60]) to Fitchett's recoil formula. For equatorial orbits, Eq. (2.36) above suggests that $f(q)$ should be multiplied by the factor $|1 + (7/29)\tilde{a}_2/(1-q)|/|1 + (7/29)\tilde{a}_2/(1-q')|$, where $q' = 0.127$ is the value used in defining $V_{\rm upper}$ and $V_{\rm lower}$ in equations (2.43) and (2.44). Note that the mass ratio where the recoil peaks is now a function of spin, rather than peaking at $q \approx 0.38$ for all values of $\tilde{a}_2$ as in Fitchett's expression.

Figure 2.11 plots the recoil upper and lower limits as functions of $\tilde{a}_2$ and q. The average over $\tilde{a}_2$ of the upper limit estimates are $\sim (138, 444, 154)$ km s^{-1} for $q = (0.1, 0.4, 0.8)$; Figure 2.11 suggests a weak dependence on $\tilde{a}_2$. Lower limit estimates are more strongly spin-dependent but, for moderately large spins ($\tilde{a}_2 \gtrsim 0.8$) and prograde capture, these values exceed 100 km s^{-1} for $0.2 \lesssim q \lesssim 0.6$. For the purpose of determine the astrophysical consequences of kicks we can assume that the recoil is likely to be at least of order $\sim 100-200$ km s^{-1} over a wide range of $(q, \tilde{a}_2)$ values, and that ~ 500 km s^{-1} is an absolute upper limit.

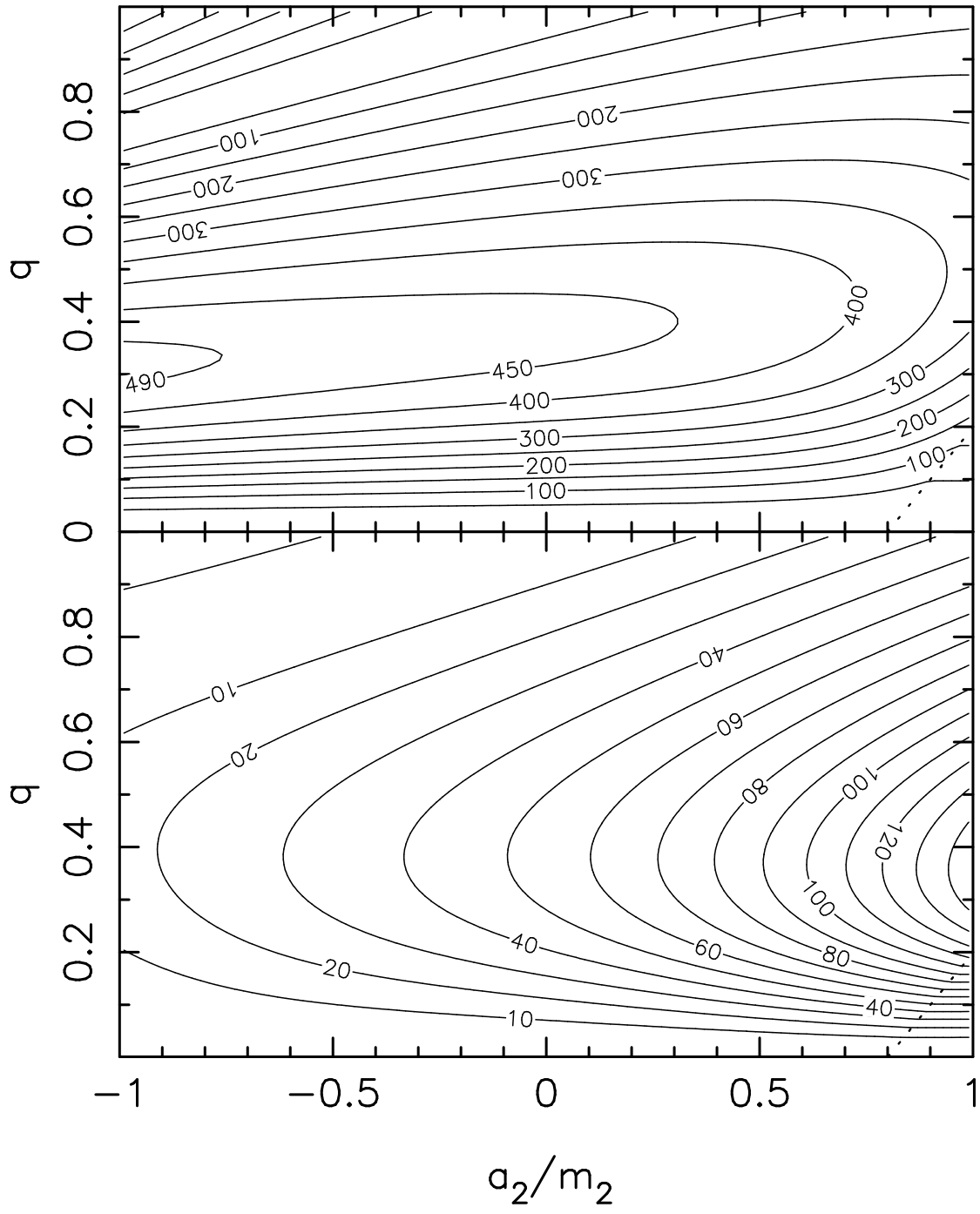

Figure 2.11: Upper limit (top) and lower limit (bottom) estimates of the recoil velocity as functions of mass ratio q and spin of the larger black hole $\tilde{a}_2$ in units of km/s (Figure 1 of Merritt, et al.[2]). Values of $\tilde{a}_2$ and q corresponding to $\tilde{a} > 0.8$ lie in the region to the right of the dotted line. Since Eqs. (2.43) and (2.44) are not valid for $\tilde{a} > 0.8$, $\tilde{a}$ was replaced by 0.8 in this region.

2.7 Discussion

The punchline of our analysis is simple: previous quasi-Newtonian estimates have significantly overestimated the kick velocity from anisotropic GW emission during binary coalescence. The recoil is strongest when the smaller member is deep in the strong-field of the large black hole. General relativistic effects, such as the gravitational redshift and spacetime curvature-scattering, act on the emitted GWs and reduce the recoil.

Though reduced, the recoil remains large enough to have important astrophysical consequences. Recoils with $V \sim 10$–$100\,\mathrm{km/s}$ are likely; kicks of a few hundred km/s are not unexpected; and the largest possible recoils are probably $\lesssim 500$ km/s. These speeds are smaller than most galactic escape velocities, suggesting that BH mergers that follow galaxy mergers will remain within their host structures. However, these recoils are similar to the escape speeds of dwarf galaxies; and they may be sufficient to escape from mergers in high redshift structures ($z \gtrsim 5 - 10$; cf. Barkana and Loeb [77], Figure 8). Binary BH ejection from globular clusters is quite likely, with significant implications for the formation of intermediate mass black holes (IMBH) via hierarchical mergers [21]. Our recoil estimates will also be useful in simulations of supermassive and IMBH evolution in dark halos [78, 79].

Future work will investigate the influence of orbital inclination on the recoil. More work in perturbation theory also remains in addressing the recoil from the plunge and final ringdown of the merging black holes.

Finally, Redmount and Rees [80] have speculated that spin-orbit misalignment could lead to recoil directed out of the orbital plane. This recoil might accumulate secularly rather than oscillate, and would be similar to the "electromagnetic rocket" in pulsars with off-centered magnetic dipole moments [50, 51]. We sus-

pect that this effect occurs but it is likely small compared to the recoil from the final plunge and merger. Firm estimates of the final kick velocity will rely on correctly modelling the final phase of BH coalescence. For comparable mass binaries, full numerical relativity will ultimately be needed to accurately compute the GW recoil.

2.8 Recent recoil calculations

Since our paper was published, there has been a resurgence of interest in recoil calculations. Most of this progress has been in post-Newtonian and numerical relativity calculations.

Blanchet, Qusailah, and Will [6] computed the momentum flux for non-spinning BHs up to 2PN order, including the effects of gravitational wave tails. Their final expression for the momentum is strictly valid only for circular orbits. At the ISCO they compute a maximum kick velocity of $V_{\rm max,isco} = 22.2$ km/s, larger than our calculated value of 15.8 km/s. This difference is possibly due to the neglect of 3PN terms in their calculation[15]. To compute the recoil during the final plunge, they perform a calculation that at first sight is similar to our "lower-limit" calculation: They model the orbital motion using the Schwarzschild geodesic equations, matching a plunging orbit onto a circular one at the ISCO. They then substitute this orbit solution into their 2PN expression for the momentum flux, and integrate (as we do) up to $r = 2(M + \mu)$. Their resulting recoil is $V_{\rm max} = 250 \pm 50$ km/s. This lies in between our upper and lower limits on the recoil for non-spinning holes,

[15]Our computation of the recoil up to the ISCO includes all relativistic corrections in the test-mass limit; all post-Newtonian recoil calculations [1, 6, 8] have demonstrated that the dependence of the momentum flux on the mass ratio is very weak.

465 km/s and 54.4 km/s. While their plunge calculation uses a momentum flux formula that contains 2PN terms that we neglect in our lower-limit calculations[16], their formula makes some important simplifications that we do not: they assume that their momentum flux formula for circular orbits applies also for plunging orbits. In deriving their momentum flux equation, the ϕ-motion is assumed to obey the 2PN Kepler's-law for circular orbits. As shown by Damour and Gopakumar [8], this is not a good approximation during the plunge, and it causes them to overestimate the recoil. This is essentially the same reason why our upper-limit calculation overestimates the recoil. Blanchet et al. [6] make this approximation because it drastically simplifies their momentum flux formula. This is necessary as the expressions would become quite lengthy for general (plunging) orbits, and the 1.5PN tail contribution would probably have to be calculated numerically for such orbits. In contrast, our lower-limit plunge calculation explicitly expands out all the terms in the leading order ("quasi-Newtonian") momentum flux and directly substitutes the equations of motion without simplification.

Damour and Gopakumar [8] improve upon these post-Newtonian calculations by computing the recoil using the effective-one-body (EOB) approach. This models the 2-body dynamics of a binary-BH as taking place in a "deformed" Schwarzschild metric, where these deformations are post-Newtonian corrections proportional to the reduced mass ratio η of the binary. The resulting orbit dynamics is described by the geodesics of this metric (derived from a corresponding Hamiltonian), and are supposed to account for features that go beyond the usual post-Newtonian equa-

[16]Despite the close agreement between their 2PN and 1.5PN estimates (see figure 1 of [6]), Damour and Gopakumar [8] point out that this does not necessarily indicate that their momentum flux calculation has converged, as the PN series demonstrates erratic convergence properties as the PN order increases.

tions of motion. Using the EOB equations of motion, Damour and Gopakumar use a "corrected" 2PN momentum flux formula that incorporates a more-reliable orbital frequency during the plunge. They also explore the use of Padé approximants in the 2PN momentum flux. For their computation of the recoil up to the ISCO, they find values from 16.2 km/s (2PN Padé approximants) up to 22.3 km/s (ordinary 2PN expansion). The former value is much closer to our (nearly) exact result. Damour and Gopakumar also compute the recoil from the plunge and ringdown phases of coalescence. They analytically show that the total recoil is dominated by the plunge, especially near the peak in the momentum flux at $r \simeq 3.5M$. The ringdown contributes very little to the total recoil: including the ringdown decreases the kick velocity by $\sim 15\%$. Their final "best-bet" value for the maximum recoil is 74 km/s, in closer agreement with out lower-limit estimate. In fact, when they remove the 2PN corrections to the momentum flux (keeping the orbital dynamics unchanged) they find a final recoil of 51 km/s, which agrees with our lower limit estimate to within 7%. Their 2PN Padé approximate method also agrees with our results to within 10%.

Campanelli [5] and the University of Texas, Brownsville (UTB) group have computed the recoil using the Lazarus approach to numerical relativity. This models the binary using full-numerical relativity when the holes are near the last-stable-orbit, but then switches to a perturbative calculation (based on the close-limit-approximation) as the holes merge. Because the simulation is started at small separation, and because of uncertainties in the initial data, the recoils generated with this approach are rather uncertain. Their estimates for the rescaled maximum recoil range from 277 ± 160 km/s (rescaled from their values at $q = 0.5$) to 172 ± 95 km/s (rescaled from $q = 0.83$).

Recently there have been several advances in numerical relativity, allowing nearly all research groups to evolve binary BHs for several orbits. Published recoil numbers currently exist from two groups. The Penn State group [7] finds maximum recoils of 118 km/s (rescaled from $q = 0.85$), while the Goddard group [9] gets 163 km/s (rescaled from $q = 0.67$).

The various recoil estimates discussed in this section are summarized in Figure 2.12. They indicate that the maximum recoil velocity from the merger of two non-spinning black holes lies in the approximate range of $\sim 50 - 200$ km/s.

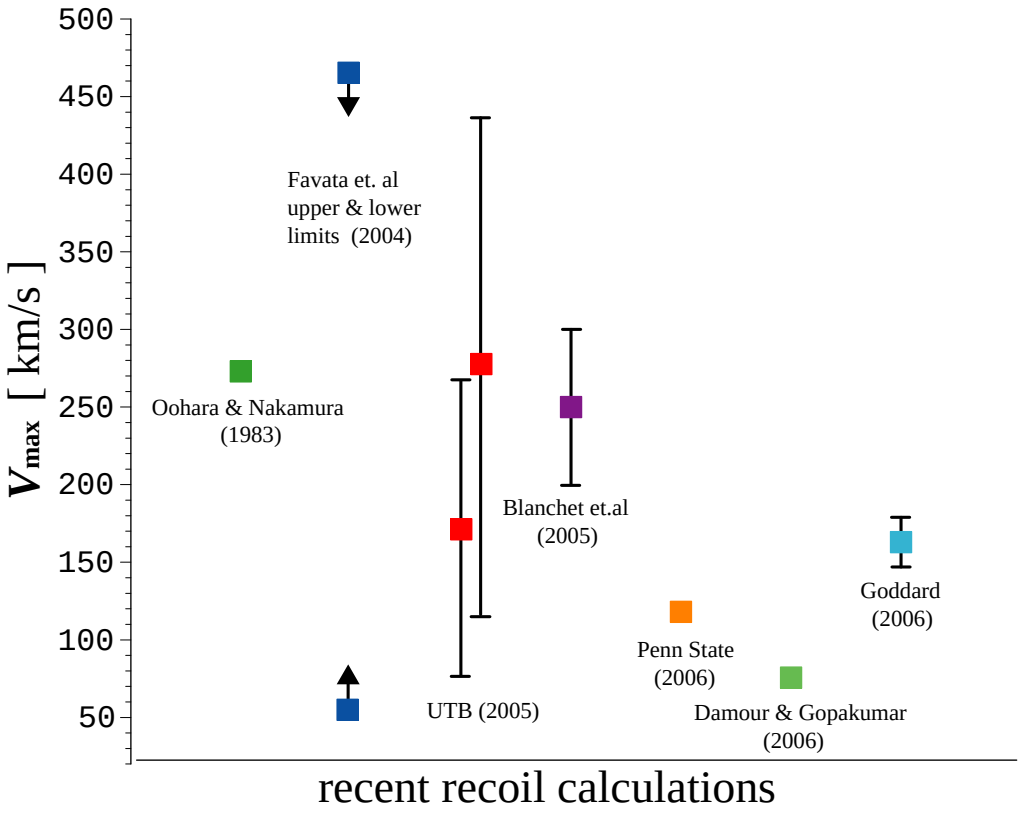

Figure 2.12: Summary of recoil calculations for binary coalescence. All results are for non-spinning holes and have been scaled up to a mass ratio $q \approx 0.38$ using Eq. (2.5). From left to right the different estimates are: Oohara and Nakamura's [3] plunge-from-infinity calculation with $L_z = 3.464$; upper and lower limits from Favata, Hughes, and Holz [4] (this chapter); UTB [5] estimates with error bars, scaled from two different mass ratios (see text); Blanchet, Qusailah, Will [6] with 3PN error bars; Penn State's [7] numerical relativity estimates; Damour and Gopakumar's [8] "best-bet" effective one-body calculation; the NASA Goddard [9] numerical relativity estimates with 10% error bars.

Chapter 3
Are neutron stars crushed? Gravitomagnetic tidal fields as a mechanism for binary-induced collapse

This chapter is based on the following publication: Favata, Phys. Rev. D, **73**, *104005, (2006).*

3.1 Introduction and Summary

Binary systems of two neutron stars (NSs) or a neutron star and a stellar-mass black hole (BH) are possible sources of gravitational waves (GWs) for current [81, 82] and future [83] GW interferometers. To extract information from these waves the stages of the coalescence must be modelled accurately. When the binary separation d is large (such that $d \gg R$, where R is the radius of the NS), analytic post-Newtonian (PN) methods [84] can describe the binary dynamics accurately enough to allow detection and parameter extraction. However, as the binary separation decreases, the PN approximation (which assumes weak gravity and slow motion) becomes less and less accurate. At some point the system must be modelled by numerical simulations that account for strong gravitational fields and hydrodynamic effects. Several groups have developed numerical codes to simulate NS/NS systems (e.g., see [85] and Refs. 7-15 of [86]). The detection of GWs from NS/NS coalescences could yield information about the equation of state (EOS) of ultradense nuclear matter, and about short-duration gamma-ray bursts [87, 88]. Accurate predictions of the GW signal will be important for these purposes.

Wilson, Mathews, and Marronetti (WMM) [89, 11] were one of the first groups

to simulate the hydrodynamics of NS/NS mergers in general relativity. Their simulations made the surprising prediction that relativistic effects can compress neutron stars that are near their maximum mass, initiating collapse to black holes prior to the onset of the dynamical orbital instability that causes the stars to plunge and merge. This prediction, which is referred to by some as "star-crushing" or "binary-induced collapse," was highly controversial and ran counter to intuition obtained from the Newtonian result that a NS in a binary is more stable against collapse [22]. If true, this collapse instability would have important implications for the detection of NS/NS binaries using matched filtering. The energy loss from the collapse process would change the orbital phase and introduce additional EOS-dependent parameters in the inspiral waveform templates. Over 15 papers appeared in the literature refuting WMM's claim. Details of this controversy are reviewed in Sec. 3.2 below and in [87]. Kennefick [24] provides a very interesting and readable account of the controversy from a sociological viewpoint. The WMM controversy largely subsided once Flanagan [23] discovered an error in one of WMM's equations. Although correcting this error caused a substantial decrease in the crushing effect, some compression of the neutron stars remained [10].

Various analytic [90, 22, 91, 92, 93, 94, 95] and numerical [96, 97, 98, 99, 100, 101, 102, 103] studies have claimed to rule out the star-crushing effect. However, none of these studies considered certain post-Newtonian, velocity-dependent tidal couplings or they constrained the NS velocity field to be either initially vanishing, corotating (where the NSs are rigidly rotating at the orbital frequency), irrotational (the NS fluid velocity has vanishing curl), or described by ellipsoidal models (in which the velocity field is a linear function of the distance from the star's center of mass); see Sec. 3.2 for further discussion. These approximations have left open

a loophole in the demonstration that the central density of a neutron star should always *decrease* when placed in a binary system. Specifically, there remains the possibility that gravitomagnetic tidal interactions could couple to complex velocity patterns inside a neutron star, causing the central density to *increase*. The purpose of this paper is to investigate whether such a mechanism can explain the residual compression observed in WMM's revised simulations [10] and, more importantly, to address the following general question: Are there any circumstances under which general-relativistic tidal forces can compress a neutron star?

We find that there is a compression effect which can be briefly summarized as follows: In addition to the familiar Newtonian tidal field of its companion, the fluid of each NS also interacts with a gravitomagnetic tidal field generated by the motion of its companion. If the NS fluid has a nonzero current-quadrupole moment, velocity-dependent tidal forces can lead to compression of the star, increasing its central density in certain circumstances and making it more susceptible to gravitational collapse.

To describe this mechanism in mathematical language, begin by considering a nonrotating neutron star with mass M and radius R interacting with the tidal field of a binary companion with mass M' a distance d away. Introduce the dimensionless book-keeping parameters $\epsilon = M/R$ (which parameterizes the strength of the NS's internal gravity) and $\alpha = R/d$ (which parameterizes the strength of tidal forces). We use units with $G = c = 1$. For our purposes, we can treat the star's internal self-gravity as Newtonian (see Appendix F). Then at leading order in ϵ and α, the metric in the vicinity of the star with mass M can be expanded as

$$g_{00} = -1 - 2\Phi - 2\Phi^{\rm ext} + O(\epsilon^2) + O(\epsilon\alpha^4) \ , \tag{3.1a}$$

$$g_{0i} = \zeta_i^{\rm ext} + O(\epsilon^{3/2}\alpha^{9/2}) + O(\epsilon^{5/2}\alpha^{7/2}) \ , \tag{3.1b}$$

$$g_{ij} = (1 - 2\Phi - 2\Phi^{\rm ext})\delta_{ij} + O(\epsilon^2) + O(\epsilon\alpha^4) \ , \tag{3.1c}$$

where $\Phi = O(\epsilon)$ is the star's self-gravitational Newtonian potential, and $\Phi^{\rm ext} = O(\epsilon\alpha^3)$ and $\zeta_i^{\rm ext} = O(\epsilon^{3/2}\alpha^{7/2})$ are the Newtonian and gravitomagnetic potentials describing the external tidal field. Inside and near the star these potentials satisfy a subset of the first post-Newtonian (1PN) Einstein field equations, $\nabla^2\Phi^{\rm ext} = \nabla^2\zeta_i^{\rm ext} = 0$ and $\nabla^2\Phi = 4\pi\rho$, where ρ is the NS's mass density. Our metric expansion (3.1) is not a complete 1PN expansion but only includes Newtonian and gravitomagnetic terms. A detailed justification of the expansion (3.1) is given in Appendix F. None of the terms that we neglect affect our final results.

The external potentials in (3.1) can be expanded as power series in the spatial coordinates x^i whose origin follows the star's center of mass worldline:

$$\Phi^{\rm ext} = \frac{1}{2}\mathcal{E}_{ab}x^a x^b + O(x^3) \ , \tag{3.2}$$

$$\zeta_i^{\rm ext} = -\frac{2}{3}\epsilon_{ipq}\mathcal{B}^p{}_l x^q x^l + O(x^3) \ , \tag{3.3}$$

where $\mathcal{E}_{ij}(t)$ and $\mathcal{B}_{ij}(t)$ are electric-type and magnetic-type tidal moments. These moments are symmetric and trace-free (STF) tensors. They can be written in terms of the Riemann tensor of the external (tidal) pieces of the metric (3.1) evaluated at the spatial origin via $\mathcal{E}_{ij}(t) \equiv R_{0i0j}$ and $\mathcal{B}_{ij}(t) \equiv \frac{1}{2}\epsilon_{ipq}R^{pq}{}_{j0}$. See Appendix F for further discussion.

In addition to the Newtonian tidal force, magnetic-type tidal fields introduce acceleration terms in the hydrodynamic equations that resemble the vector-potential and Lorentz-force terms from electromagnetism,

$$\boldsymbol{a}^{\rm ext} = -\nabla\Phi^{\rm ext} - \dot{\boldsymbol{\zeta}}^{\rm ext} + \boldsymbol{v} \times \boldsymbol{B} \ . \tag{3.4}$$

Here $\boldsymbol{B} = \nabla \times \boldsymbol{\zeta}^{\rm ext}$ is the gravitomagnetic field, $\boldsymbol{v}$ is the internal fluid velocity measured with respect to an inertial frame who's origin coincides with the star's

center of mass, and an overdot denotes a time derivative.[1] As we will show below (Secs. 3.3 and 3.4), gravitomagnetic tidal forces can compress a star if the angle average of the $\boldsymbol{v}\times\boldsymbol{B}$ Lorentz-like force is nonzero and inward pointing. Such a force can only arise if the star's internal velocity field has a component in the subspace spanned by the $l=2$ magneticlike vector spherical harmonics $\boldsymbol{Y}^{B,lm}\propto\boldsymbol{x}\times\nabla Y^{lm}$. (See Appendix G or Thorne [44] for a discussion of vector spherical harmonics.) The velocity field will have a nonzero component of this type if and only if the star's current-quadrupole moment $\mathcal{S}_{ij}$ is nonzero. In the weak-field, slow-motion limit the current quadrupole is defined by

$$\mathcal{S}_{ij}=\int x_{(i}\epsilon_{j)ab}x_a\rho v_b\,d^3x\ , \tag{3.5}$$

where ρ is the mass density, v_b is the fluid velocity, and the parentheses denote symmetrization. Such a velocity field is depicted in Figures 3.1 and 3.2.

If the gravitomagnetic tidal field $\mathcal{B}_{ij}(t)$ is slowly varying, and if the star is initially static, then the $\dot{\boldsymbol{\zeta}}^{\rm ext}$ term in Eq. (3.4) induces a velocity field given by $\boldsymbol{v}=-\boldsymbol{\zeta}^{\rm ext}$. The corresponding current-quadrupole moment is

$$\mathcal{S}_{ij}=\gamma_2 MR^4\mathcal{B}_{ij}\ . \tag{3.6}$$

Here γ_2 is the *gravitomagnetic Love number*, a dimensionless constant that depends on the NS equation of state (see Sec. 3.3.2 and Appendix I).[2] This process is analogous to the Newtonian tidal distortion of stars, wherein the electric-type

[1] We have dropped other 1PN terms from the tidal acceleration. This is justified in Appendix F. Retaining them does not affect our results.

[2] This gravitomagnetically-induced current-quadrupole moment is related to Shapiro's [104] gravitomagnetic induction of circulation in a NS by the gravitational field of a spinning black hole; see Sec. 3.3.2 and Appendix H. The ellipsoidal model of a NS used in [104] excluded current-quadrupole moments. Our analysis is also applicable to a spinning BH or any other source that produces a $\mathcal{B}_{ij}$ tidal field.

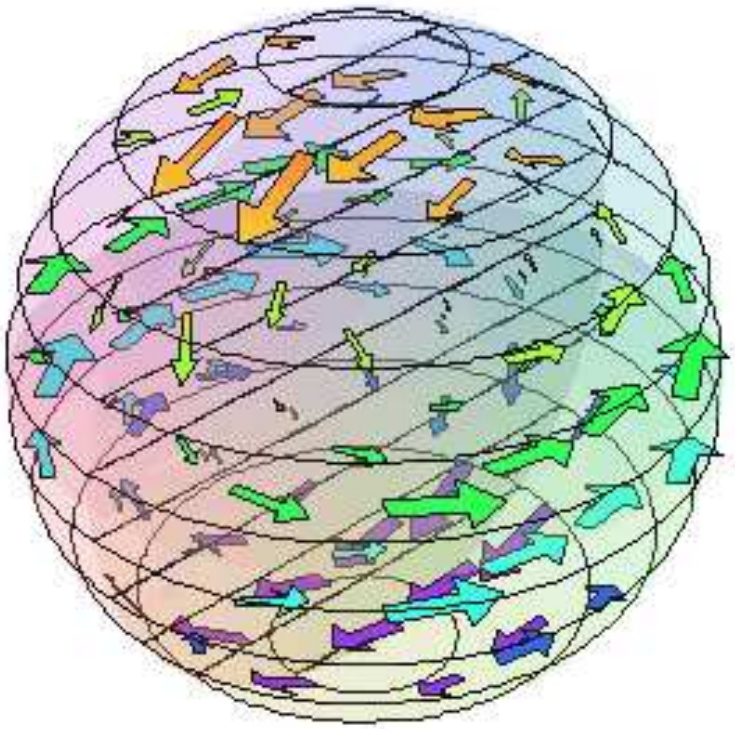

Figure 3.1: Internal velocity field $\boldsymbol{v}$ of a nonrotating neutron star with a current-quadrupole moment induced by the tidal field of an orbiting companion. The arrows denote the velocity vectors and are generated by Eqs. (3.19) and (3.43). The velocity field is stationary in a coordinate frame rotating at the binary's orbital angular velocity (which points perpendicular to the equatorial plane of the star).

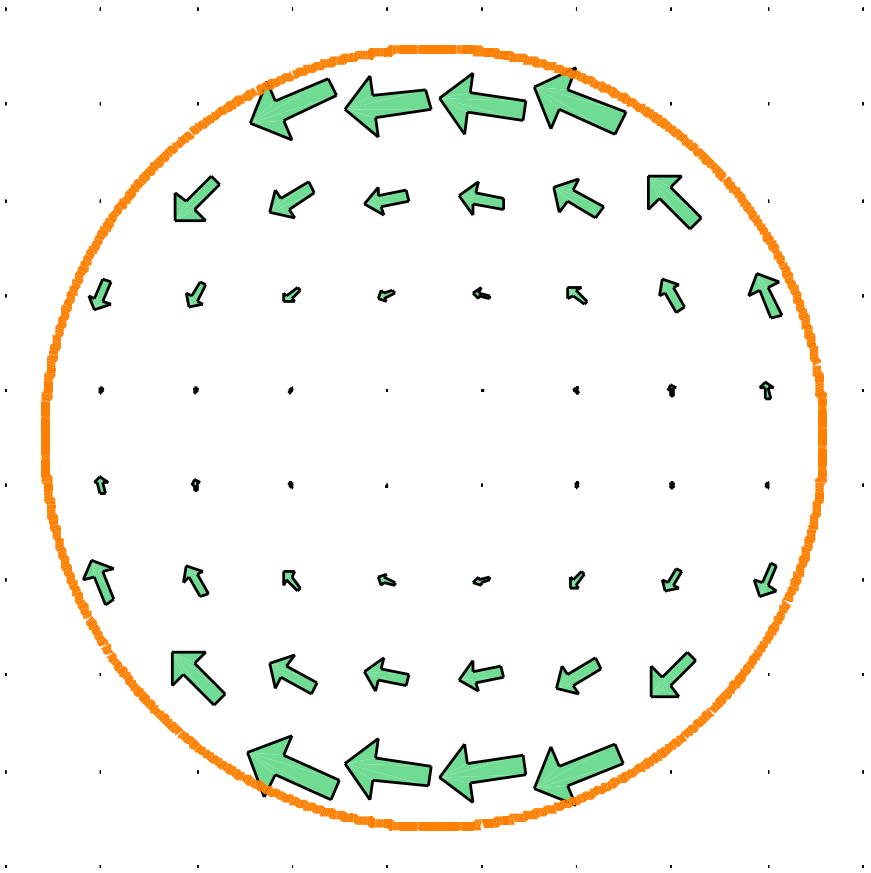

Figure 3.2: Same as Fig. 3.1 but showing only the induced velocity field on a slice through the equatorial plane. The velocity current loops set up in the star are easily seen.

tidal field $\mathcal{E}_{ij}$ induces a mass quadrupole moment $\mathcal{I}_{ij}$ given by

$$\mathcal{I}_{ij} = -\frac{1}{3} k_2 R^5 \mathcal{E}_{ij} \ . \tag{3.7}$$

Here k_2 is the dimensionless Newtonian Love number (see chapter 4.9 of [105] or Appendix I).

As shown in Sec. 3.3, the gravitomagnetically induced velocity field (Figures 3.1 and 3.2) drives the fundamental radial mode of the NS (along which compression and decompression occur) via a combination of the Lorentz $\boldsymbol{v} \times \boldsymbol{B}$ and nonlinear advection $(\boldsymbol{v} \cdot \nabla)\boldsymbol{v}$ terms. (Figure 3.3 shows the total gravitomagnetic tidal acceleration acting on the fluid in an inertial reference frame whose origin instantaneously coincides with the NS center of mass.) Up to order $O(\alpha^7)$, the resulting change in central density is

$$\frac{\delta\rho_c}{\rho_c} = c_1 \mathcal{E}_{ij}(t)\mathcal{E}^{ij}(t) + c_2 \mathcal{B}_{ij}(t)\mathcal{B}^{ij}(t) \ , \tag{3.8}$$

where the constants c_1 and c_2 have units of [length]^4 and depend on M, R, and the equation of state [91]. In a binary, the tidal fields scale as $\mathcal{E}_{ij} \sim M'/d^3$ and $\mathcal{B}_{ij} \sim (M'/d^3)\sqrt{(M+M')/d}$, so the two terms scale as $O(\alpha^6)$ and $O(\alpha^7)$, respectively. The first term in Eq. (3.8) is the Newtonian tidal-stabilization term. Its sign ($c_1 < 0$) has been computed for relativistic stars by Thorne [92]; Lai [22] and Taniguchi and Nakamura [94] have computed its value for Newtonian stars, $c_1 \approx -0.38 R^6/M^2$ (for a $\Gamma = 2$ polytrope). Its derivation is reviewed in Appendix J. One of the main results of this paper is the magnitude and sign of the coefficient c_2: it is positive and has the value $c_2 \approx 0.064 R^5/M$ (also for a $\Gamma = 2$ polytrope). This term therefore tends to compress the star. However, its size is not large enough to overcome the decompressive effect of the first term. Therefore, nonrotating neutron stars with no preexisting velocity fields suffer *no*

net compression when placed in a binary. In Appendix L we briefly discuss how to extend our results to rotating stars.

In Sec. 3.4 we consider the possibility that the neutron star is not initially unperturbed but instead has a *preexisting* current quadrupole. (By "preexisting" we mean that the current quadrupole does not arise through the mechanism of gravitomagnetic tidal induction discussed here.) Viscosity will damp astrophysical sources of a current quadrupole on a timescale $\tau_{\rm vis} < 1$ day.[3] Any velocity currents arising from the formation of the NS will be damped long before the NS comes close to merging. Unless they are generated shortly before coalescence, astrophysical preexisting current quadrupoles are unlikely. However, a current quadrupole could be present as a numerical artifact in a NS/NS simulation. Approximations to the equations of motion, numerical errors, artificial viscosity, or the method of choosing the initial data could possibly lead to a nonzero current-quadrupole moment. It is possible that such a numerical artifact was present in the WMM simulations [11]. In any case, the presence of a preexisting current quadrupole affects the change in central density by replacing the second term in Eq. (3.8) with $c_2' \mathcal{S}_{ij}(t)\mathcal{B}^{ij}(t)$, where $c_2' \approx 2.9R/M^2$ (for a $\Gamma = 2$ polytrope). This term scales like $\alpha^{7/2}$, and at large separations it actually dominates over the Newtonian tidal-stabilization term. The time dependence and sign of this term depends on the unknown functional form of $\mathcal{S}_{ij}(t)$. If we assume that $\mathcal{S}_{ij}(t)$ is constant, the $O(\alpha^{7/2})$ term oscillates in sign at the orbital period, and a net compressive force results during parts of the orbital phase. For plausible values of $\mathcal{S}_{ij}(t)$, the net change in central density is small

[3]The viscous time is $\tau_{\rm vis} \sim \rho R^2/\eta$, where ρ is the density and $\eta \approx 4.7 \times 10^{19}$g cm^{-1}s$^{-1}(T/10^8{\rm K})^{-2}[\rho/(2.8\times10^{14}{\rm g\ cm^{-3}})]^2$ is the coefficient of shear viscosity (this is valid at low temperatures $T \lesssim 10^9$ when protons and neutrons are superfluid and electron-electron scattering dominates [106]). This gives $\tau_{\rm vis} \sim 0.0019\ {\rm day}(R/10{\rm km})^2(T/10^6{\rm K})^2(\rho/10^{15}\ {\rm g\ cm^{-3}})^{-1}$

for Newtonian stars, $\lesssim 1\%$ (see Fig. 3.6), but it could be large enough to cause collapse if the NS is close to its maximum mass.

In the remainder of this article and in its appendices, we provide the details of the analysis summarized above. But first we give further motivation for our analysis by reviewing the history of the WMM star-crushing controversy (Sec. 3.2).

Throughout this paper we follow the notations and conventions of Misner, Thorne, and Wheeler [64] (MTW). We assume geometric units with $G = c = 1$. Time and space coordinates are denoted by $x^\alpha = (t, x^j)$. Spatial indices (in a Cartesian basis) are raised and lowered using δ_{ij}. Repeated spatial indices are summed, whether or not they are up or down. Spatial partial derivatives are denoted by ∇_i and time derivatives are denoted by an overdot, $\dot{f} = \partial f/\partial t$. Spacetime indices and covariant derivatives are rarely used.

3.2 A brief history of a controversy

To help motivate our analysis, it is useful to review the history of the star-crushing controversy, focusing on the arguments for and against crushing and the approximations that are assumed in the various arguments. We begin by reviewing the original WMM simulations.

WMM's simulations [89, 11] relied on two important assumptions, which have come to be called the Wilson-Mathews approximation[4]: First, the spatial metric satisfies the spatial conformal flatness (SCF) condition, $\gamma_{ij} = \phi^4 \delta_{ij}$, where γ_{ij} is the 3-metric of a spacelike hypersurface and ϕ is the conformal factor. The SCF condition simplifies the form of the hydrodynamic and field equations, ne-

[4]A self-contained description of the WMM simulations is also found in their recent book [107]. For a shorter review of their work, see Ref. [108].

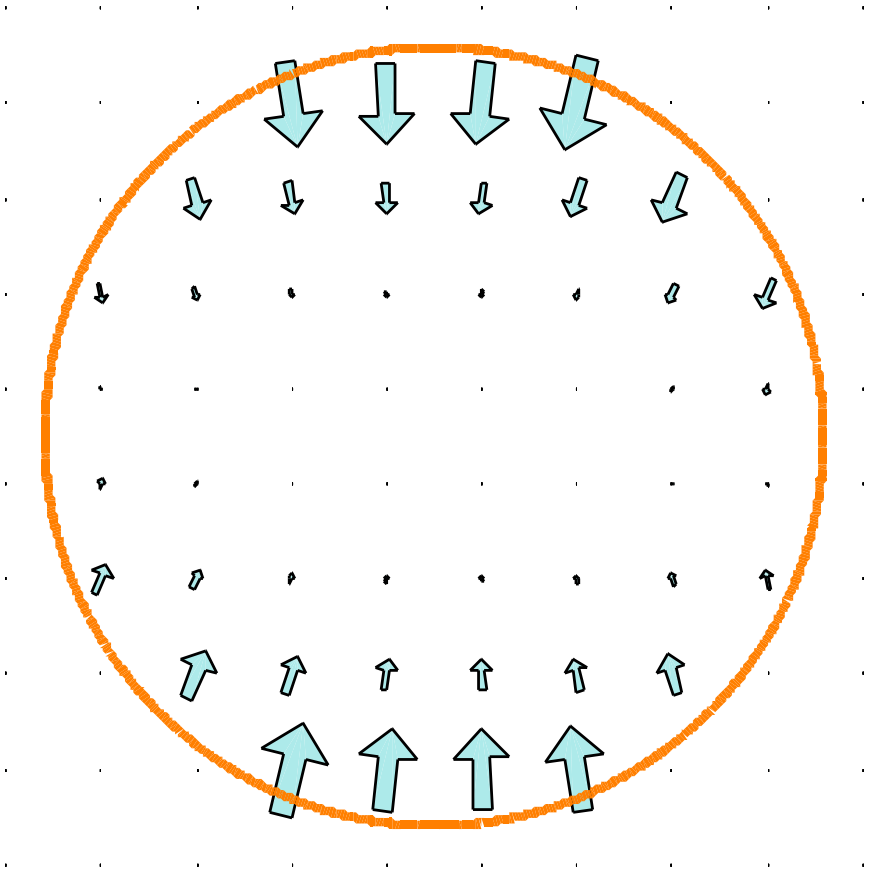

Figure 3.3: The total gravitomagnetic tidal acceleration of a nonrotating neutron star interacting with a binary companion. Only a slice through the equatorial plane is shown. The arrows represent the acceleration vectors in an inertial reference frame centered on the star's center of mass and are given by Eqs. (3.26) and (3.43). Their magnitude vanishes at the center of the star. As in Figs. 3.1 and 3.2 the acceleration field rotates at the binary's orbital angular velocity. The radially-inward pointing acceleration indicates that the gravitomagnetic tidal interaction causes compression.

glects gravitational radiation in the spatial 3-metric, and is generally accurate only to 1PN order. However, it is exact for situations with spherical symmetry and very accurate for rapidly rotating relativistic stars [109]. Although widely used by many groups, the SCF condition was suspected by some to be the source of WMM's crushing effect (but see Sec. 3.2.1 below). The second assumption is a quasiequilibrium approximation in which the terms involving the time derivatives of the gravitational degrees of freedom (the spatial metric γ_{ij} and extrinsic curvature K_{ij}) are dropped from the equations of motion. This is thought to be a good approximation at large separations when GWs hardly modify the orbital dynamics. Combined with the SCF condition, this assumption reduces the equations for the gravitational field to flat-space elliptic equations. Given an initial matter distribution, WMM first solve the momentum and Hamiltonian constraint equations for the gravitational field. The hydrodynamics equations (coupled to the gravitational field) are then evolved to the next time slice. Instead of also evolving the gravitational field variables, the constraint equations are solved again at that time slice and the process is iterated. Gravitational waves are calculated via a multipole expansion and their effect on the neutron stars is accounted for by adding a radiation-reaction potential to the hydrodynamics equations. WMM also employ what they refer to as a "realistic equation of state". This zero-temperature, zero-neutrino-potential EOS [110, 111, 11] is softer (smaller values of M/R) than polytropic equations of state used by other groups and shows greater compression in their simulations. This EOS was motivated by matching models of SN 1987A to the observed neutrino signal [112].

Unlike most other NS/NS simulations of that time, the WMM simulations used *unconstrained hydrodynamics*—they did not constrain the binary to be coro-

tating or irrotational. Even though more recent NS/NS simulations also use unconstrained hydrodynamics ([86] and references therein), they all constrain the stars in their initial data sets to be either corotating or irrotational. In the WMM simulations, the initial data is formulated differently (Sec. III of [11]): An initial "guess" solution from the Tolmen-Oppenheimer-Volkoff equation for each star is placed on the grid in a corotating configuration. The stars are then allowed to relax to an equilibrium configuration. This is accomplished by solving the field equations and evolving the hydrodynamics without radiation reaction. An artificial damping of the fluid motion is imposed and slowly removed as stars reach an equilibrium state. The resulting equilibrium configurations are neither corotational nor irrotational, but result in stars with almost no intrinsic spin (Sec. IV E of [113]). As discussed in Sec. 3.4, this method of choosing the initial data sets could possibly be the source of compression.

The main result of the initial WMM simulations was that initially stable neutron stars could be highly compressed: a star $\sim 12\%$ from its maximum mass has a change $\delta\rho_c$ of its central density ρ_c given by $\delta\rho_c/\rho_c \approx 0.51$ at a proper separation of 68 km [10]. The simulations indicated that the central density increased according to $\rho_c \propto U^4$, where $U^2 = U_i U^i$ and U_i are the spatial components of the 4-velocity (see Fig. 2 of [113]). WMM also found that the binary's orbit would become unstable at an orbital separation that was larger (by a factor of ~ 1.4) than the PN prediction [89].

In the years following WMM's initial publications, several papers appeared claiming that neutron stars in a binary should be stabilized and not compressed. These were followed by a rebuttal paper by WMM [113]. Lai [22] used an energy variational principle (including 1PN corrections to the star's self-gravity) to show

that a Newtonian tidal field decreases the central density according to $\delta\rho_c/\rho_c = -2.7(M'/M)^2(R/d)^6$ (for an $n = 3/2$ polytrope at its maximum mass in isolation; see also [94] and Appendix J of this paper). Wiseman [93] showed that there was no change in central density in a binary at 1PN order, but he neglected tidal effects. Brady and Hughes [90] examined a point particle with mass $\mu \ll M$ orbiting a static, spherical NS and showed that there is no change in central density at linear order in μ. Thorne [92] showed that fully-relativistic, static or rotating NSs are stabilized by an electric-type tidal field. Although these papers [93, 90, 92] consistently applied their approximations, they did not include the velocity-dependent forces that WMM attribute their compression to [113], and they did not consider the gravitomagnetic interactions that we investigate here. Shibata and Taniguchi [114] and Lombardi et al. [95] both examined equilibrium sequences of compressible ellipsoids at 1PN order. Shibata and Taniguchi considered corotating binaries while Lombardi et al. considered corotating and irrotational ones. Both also found that the NSs were stabilized, but WMM claim that they also ignored the relevant velocity-dependent terms [113]. Shibata et al. [101] performed 1PN hydrodynamics simulations for corotating and irrotational binaries and also saw no signs of compression. WMM speculated that this was due to the unrealistically soft EOS (with $M/R \approx 0.023$) used by Shibata et al. [101]. For the very close separations examined in that paper, WMM claimed that the tidal stabilization overwhelms any compression effect [113].

In a series of papers, Baumgarte et al. [96, 97, 98] simulated corotating NS/NS binaries using the SCF and quasiequilibrium conditions, finding that the stars were stabilized. However, their simulations did not contradict the WMM results since the centrifugal force tends to stabilize the star in corotating binaries. Further,

WMM showed analytically that their compression effect vanishes for corotation [113]. This indicated to WMM that the compression was probably due to the nonrigidly-rotating motion set up in the NS fluid [113].

A matched-asymptotic-expansion analysis of the crushing effect was performed by Flanagan [91]. He showed that, to all orders in the strength of internal gravity of each NS, the leading-order terms in a tidal expansion of the change in central density are given by Eq. (3.8) above. Flanagan also showed that the coefficient c_1 of the leading $O(\alpha^6)$ term has the form $F_0[1+F_1\epsilon+F_2\epsilon^2+\cdots]$, where $F_0, F_1, F_2, \ldots$ are constants. His analysis did not determine the overall sign of c_1, but he concluded that since F_0 was shown by Lai's [22] Newtonian analysis to be negative, the central density of a NS in a binary will decrease unless $F_1, F_2, \ldots$ are negative and large. Thorne's [92] relativistic analysis showed that the entire coefficient c_1 is negative, thus excluding the possibility of a sign flip. Flanagan did not determine the sign or magnitude of the coefficient c_2 in Eq. (3.8), which is one of the main results of this paper (although, in contrast to Flanagan, the internal gravity of each NS is Newtonian in our treatment). Flanagan's analysis accounts for gravitomagnetic tidal fields and velocity-dependent corrections to the hydrodynamics that are induced by tidal interactions. It neglects, however, any crushing that could be caused by preexisting velocity fields. WMM indicate that such velocity fields may be responsible for their observed compression [113]. We address this in Sec. 3.4.

Despite the numerous claims that NSs in binaries are stabilized against collapse, there are a few analyses that hint that the binary-induced collapse of compact objects is possible. Shapiro [115] considered a system of a "compact object" made up of a test particle in a close orbit around a nonrotating BH, perturbed by the

Newtonian tidal field of a distant binary companion. Although the test particle has a stable orbit in isolation, the tidal field could cause the test particle to plunge into the BH. Duez et al. [116] extended this analysis to a swarm of particles and included relativistic effects neglected by Shapiro, confirming his conclusions. Alvi and Liu [117] also examined the stability of a swarm of test particles but included the effects of magnetic-type tidal fields. They found that including magnetic-type tidal fields did not strongly affect the average radius of the cluster, but it did destabilize individual particles that were stable in the absence of magnetic-type tidal fields.

Despite indications of binary-induced collapse, it seems unlikely that these models are relevant to situations where hydrodynamic forces are present. For circular orbits, the test particles in these simulations lie at the stable minimum of the effective potential of the Schwarzschild geometry (see chapter 25 of MTW, especially Fig. 25.2). For particles close to the last stable orbit, this minimum is only marginally stable. The external tidal forces perturb the test particles about this minimum. The direction and size of the perturbing tidal force depends on the relative orientation and separation of the particle and the tidal field. When the tidal perturbation is small the particle rolls "up the hill" of the potential and then rolls back to the stable minimum. But if the tidal perturbation is large enough, the particle can be forced over the local maximum of the potential, causing it to plunge into the BH's event horizon. Adding additional (magneticlike) tidal fields simply provides an additional force that will cause more particles to become unstable. The binary-induced collapse of a star is different because pressure and not orbital angular momentum supports the star against collapse. Collapse can only occur if the *angle average* of the tidal force points radially inward. This is harder to

achieve than accelerating a single particle to smaller radii.

The controversy appeared to be resolved when Flanagan [23] found an error in one of WMM's equations and showed that this error could account for the observed compression. The error was an incorrect definition of the momentum density in the momentum constraint equation. Wilson and Mathews [10] corrected this error and showed that the compression was reduced (by about a factor ~ 10) but not eliminated. (They also noted that the frequency of the last stable orbit moved closer to the post-Newtonian value.) For a $\Gamma = 2$ polytrope, $\delta\rho_c/\rho_c$ was reduced from 0.14 (at a 138 km separation) to 0.008 (at a 118 km separation). Using their realistic EOS and stars with a gravitational mass of $1.39M_\odot$, $\delta\rho_c/\rho_c$ was reduced from 0.51 (at a 68 km separation) to 0.03 (at a 61 km separation). Stars closer to the last stable orbit showed a compression of $\sim 10\%$ but did not collapse (as they did in the uncorrected simulations; see Figure 3.4). But for stars close to their maximum mass ($\lesssim 9\%$ for their realistic EOS) and for very close (but stable) orbits, collapse to BHs could still occur. (In this case the coordinate separation between the stars was 2.4 times their coordinate radii.) The $\rho_c \propto U^4$ scaling of the central density also remained in their revised simulations. Wilson and Mathews also state that the question remains as to whether their residual compression "is real or an artifact of the numerics" or the SCF approximation [10].

Wilson and Mathews continue to identify the observed compression as arising from enhanced self-gravity terms proportional to the square of the fluid velocity [118, 113]. These terms originate from the $\Gamma^{\mu}{}_{\mu\lambda}T^{\mu\lambda}$ term of the hydrodynamics equations (here $\Gamma^{\mu}{}_{\mu\lambda}$ is a connection coefficient and $T^{\mu\lambda}$ is the energy-momentum tensor). Although they claim that tidal effects do not cause the compression [113], the conventional understanding of the equivalence principle suggests that all gravi-

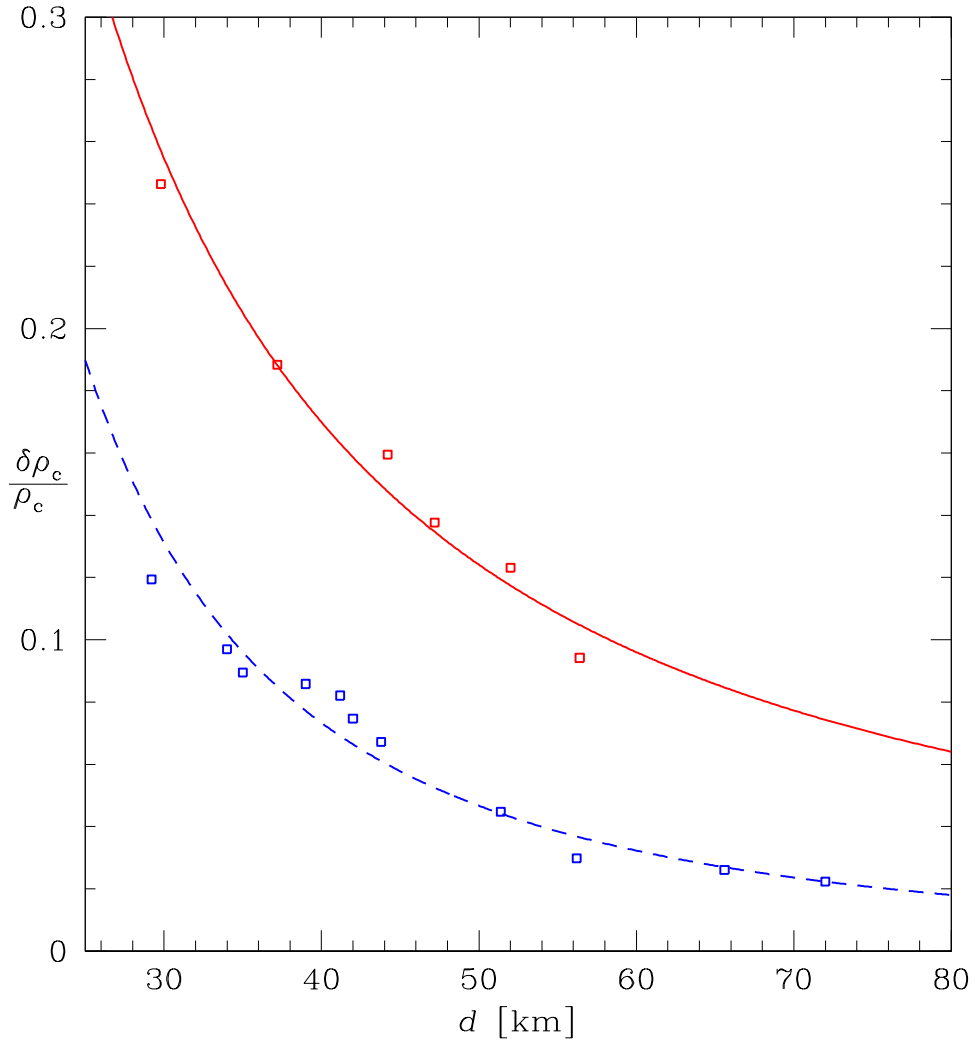

Figure 3.4: Change in central density for the revised Wilson-Mathews simulations as a function of proper distance between the neutron star centers. The lower set of points (Table III of [10]) corresponds to stars that are 12% from their maximum mass (in isolation). These stars were compressed, but did not collapse before the last stable orbit. A fit to these points (dashed, blue curve) indicates the scaling $\delta\rho_c/\rho_c \propto \alpha^{2.0}$. The upper set of points (Table IV of [10]) corresponds to stars that are 8.6% from their maximum mass (in isolation). In this case the stars did collapse (not shown here) and the orbit remained stable. A fit to these points (solid, red curve) indicates the scaling $\delta\rho_c/\rho_c \propto \alpha^{1.4}$. In both cases, a "realistic" equation of state was used (see [10, 11]).

tational interactions of a NS with an external body are tidal interactions. The analyses of Thorne [92] and Flanagan [91] support this argument, as does the present paper. This suggests that the residual compression in [10] might be an artifact of the computational scheme they have chosen. If the revised Wilson-Mathews [10] simulations contain some fluid circulation in their initial data, compression could occur via the mechanism discussed in Sec. 3.4 below. We also note that, despite skepticism of their compression effect, Wilson and Mathews continue to invoke it as a mechanism to explain gamma-ray bursts [112, 119] and, recently, to propose a new class of Type I supernovae [118].

3.2.1 Compression in irrotational simulations

Because of the controversial nature of their results, WMM developed an independent numerical code using the irrotational approximation [120]. (The hydrodynamics was unconstrained in their previous simulations.) In the irrotational approximation the fluid vorticity is zero.[5] These simulations also show a small increase in central density (1.5% at 30 km separation for a $\Gamma = 2$ polytrope) that is larger than the numerical errors estimated in [120] but is within the possible error induced by the SCF condition. WMM [120] also claim that this compression is consistent with the irrotational simulations of Bonazzola et al. [99, 122]. In this section, we review the results of irrotational NS/NS simulations from two independent groups which show no evidence for compression. This indicates that the small compression seen in WMM's irrotational simulations is unphysical. The

[5]More precisely, the specific momentum density per baryon is expressed as the gradient of a potential, $hu_\mu = \nabla_\mu \Psi$, where u_μ is the 4-velocity, ∇_μ is a covariant derivative, and h is the relativistic enthalpy [120]. See Teukolsky [121] for a discussion of the irrotational approximation in NS/NS simulations; see also Appendix H of this paper.

observed compression is possibly due to the inaccurate treatment of a boundary condition or insufficient grid resolution.

Other numerical groups have shown that no central compression occurs for NS/NS binaries in the irrotational approximation. Although WMM claim that Bonazzola et al. [99, 122] also see a small compression of order $\lesssim 0.3\%$ (see Figs. 12 and 13 of [122]), the central density decreases with decreasing orbital separation in their simulations (in contrast to WMM [120]) and is within the error induced by the SCF approximation. Uryū et al. [102, 103] also performed irrotational simulations and see a decrease in central density at small separation. While they also see oscillations in which the central density increases by $\sim 0.5\%$ (see Fig. 6 of [103]), they claim that this is due to the errors of their finite-difference scheme and of their Legendre expansion of the gravitational field (Sec. III D of [103]). Furthermore, after improving their method of determining the stellar surface, the slight increase in central density seen in [99, 122] is removed and the central density decreases monotonically (by $\sim 1\%$) with decreasing separation (see Fig. 2 and footnote 3 of Taniguchi and Gourgoulhon [100]; see also Figs. 12-14 of [123]).

The source of compression in WMM's irrotational simulations [120] is most likely not the SCF or quasiequilibrium assumptions. The French [99, 100, 124, 123] and Japanese [102, 103] numerical groups also make these assumptions but do not see compression. Further, Wilson [125] examined the head-on collision of two NSs using two separate simulations: one in full general relativity and the other using the SCF condition. He found similar levels of compression in both cases, indicating that the SCF condition is not a likely culprit. See Appendix B of Baumgarte and Shapiro [85] for a further discussion of the validity of the SCF condition.

The primary difference between the irrotational simulations of WMM and those

of the other groups is the numerical technique used: The Japanese group used a multidomain, finite-difference method with surface-fitted spherical coordinates (which allow accurate resolution of the stellar fluid and surface). The French group used an even more accurate multidomain spectral method, also with surface-fitted spherical coordinates. WMM's technique is the least accurate: a single-domain finite-difference method with Cartesian coordinates. Both the French and Japanese groups point out a likely source of error in the WMM [120] simulations: the use of Cartesian coordinates and an approximate treatment of the boundary condition for the velocity potential Ψ that treats the stellar surface as spherical [see Eq. (19) of [126] and the discussion in Sec. V A of [102] and Sec. VII A of [124]]. This issue is also discussed in Sec. 9.3 of [85].

It is also possible that low grid resolution is the source of the WMM compression [127]. Since they were using the best grid size possible at the time, it was not possible to estimate the error due to poor resolution in [120]. Regardless of the precise source of error, the fact that more accurate simulations do not observe compression strongly suggests that the compression seen in WMM's irrotational simulations is unphysical. If poor grid resolution is the source of the compression in their irrotational simulations, then it seems plausible that low resolution may also be the source of compression in the revised Wilson-Mathews simulations [10] using unconstrained hydrodynamics. However, we will also discuss in Sec. 3.4 the possibility that the compression in [10] is related to the fact that the initial data sets in those simulations were neither corotational nor irrotational.

Many numerical groups use the irrotational approximation to either simplify the evolution equations, or to determine the initial data when solving the constraint equations. The irrotational approximation is frequently motivated by the

findings of Kochanek [128] and Bildsten and Cutler [129] that the NS viscosities are too small to allow binaries to be tidally locked. However, this is more an argument against corotation than it is one in favor of irrotation. The irrotational assumption is also motivated by Kelvin's circulation theorem—in the absence of viscosity, initially irrotational flows remain irrotational; see Appendix H for discussion. Irrotation is widely adopted primarily because it simplifies the hydrodynamic equations. However, there are physically well-motivated reasons to consider more general fluid configurations. Although realistic NSs will not be corotating, they will have some intrinsic spin, thus violating the irrotation assumption.[6] The much studied r-modes in rotating stars are another example of a velocity configuration that does not fit into the corotation or irrotation class. The excitation of these r-modes could lead to small effects on the GW signal, even in the low frequency ($10\text{Hz} \lesssim f \lesssim 100\text{Hz}$) regime [131]. Although recent NS/NS simulations use unconstrained hydrodynamics and full general relativity (see [86] and references therein), they constrain the initial data sets to be corotational or irrotational. The WMM simulations [89, 11, 10] do not make this assumption. This provides further motivation for our examination in Sec. 3.4 of the coupling of preexisting current quadrupoles to tidal fields.

[6] See Marronetti and Shapiro [130] for recent work that treats NS/NS binaries with arbitrary spin.

3.3 Gravitomagnetic contribution to the change in central density

3.3.1 Equations of motion

To determine if a NS interacting with external tidal fields is compressed, we will compute the change in central density of the star by solving the fluid equations of motion. Begin by considering a star with mass M and radius R (in isolation) interacting with the external gravitational field of a binary companion (characterized by a mass M' at a distance d). Assume that the star is *initially static* in the following sense: when the binary separation is very large the stellar fluid configuration is that of an unperturbed, nonrotating star in hydrostatic equilibrium. If one expands the metric in the local proper reference frame of the star [as in Eqs. (3.1)] and substitutes into the conservation of energy-momentum equation for a perfect fluid, the leading-order response of the star to the external gravitational field can be described by

$$\frac{\partial \rho}{\partial t} + \nabla_i(\rho v^i) = 0\,, \tag{3.9a}$$

$$\frac{\partial v_i}{\partial t} + (v^k \nabla_k) v_i = -\frac{\nabla_i P}{\rho} - \nabla_i \Phi + a_i^{\rm ext}\,, \tag{3.9b}$$

$$\nabla^2 \Phi = 4\pi\rho\,. \tag{3.9c}$$

These are just the continuity, Euler, and Poisson equations for a star with baryon density ρ, internal velocity v_i, pressure P, and Newtonian self-gravity Φ, augmented by an external driving force which is the 1PN point-particle acceleration (see chapter 9 of Weinberg[132]),

$$a_i^{\rm ext} = -\nabla_i \Phi^{\rm ext} - \dot{\zeta}_i^{\rm ext} + (\boldsymbol{v} \times \boldsymbol{B})_i + 3 v_i \dot{\Phi}^{\rm ext} - v^2 \nabla_i \Phi^{\rm ext} + 4 v_i (v^k \nabla_k) \Phi^{\rm ext}\,, \tag{3.10}$$

where $\boldsymbol{B} = \nabla \times \boldsymbol{\zeta}^{\rm ext}$. We also assume a barotropic EOS $P = P(\rho)$. In the above equations we have ignored all PN corrections to the fluid equations except for the terms in the external acceleration $a_i^{\rm ext}$. This is justified in Appendix F. None of the terms that we drop will affect the leading-order corrections to the change in central density. The potentials $\Phi^{\rm ext}$ and $\zeta_i^{\rm ext}$ that appear in Eqs. (3.1) and (3.10) can be expressed in terms of the electric and magnetic-type tidal moments as in Eqs. (3.2) and (3.3). We will ignore the tidal octupole moment contribution, $\Phi^{\rm ext} = \frac{1}{6}\mathcal{E}_{ijk}x^i x^j x^k$ and higher moments; they will affect the central density at order $O(\alpha^8)$ and higher.

For our purposes we will only need to consider the lowest order tidal expansion of the first three terms in Eq. (3.10):

$$a_i^{\rm ext} = -\varepsilon_{\mathcal{E}}\mathcal{E}_{ij}x^j + \varepsilon_{\mathcal{B}}\left(\frac{2}{3}\epsilon_{ijk}\dot{\mathcal{B}}_l^j x^k x^l - 2\epsilon_{ijk}\mathcal{B}^{kl}v^j x^l\right) + O(x^3)\,, \tag{3.11}$$

where $\varepsilon_{\mathcal{E}}$ and $\varepsilon_{\mathcal{B}}$ are dimensionless book-keeping constants proportional to their respective tidal moments. They will be set to unity at the end of the calculation. One can explicitly show that for nonrotating stars, the terms in Eq. (3.10) that we have neglected will affect neither the change in central density up to order $O(\alpha^7)$ nor the leading-order contribution to the induced current-quadrupole moment; see Appendix F.

3.3.2 Second-order Eulerian perturbation theory

To determine the influence of the external tidal fields on the structure of our star, we treat the tidal acceleration as a small perturbation whose size is parameterized by a dimensionless book-keeping parameter ε. The density, pressure, internal

gravitational potential, and stellar velocity field are then expanded as

$$\rho(t,\boldsymbol{x}) = \rho^{(0)} + \varepsilon\rho^{(1)} + \varepsilon^2\rho^{(2)} + \cdots \,, \tag{3.12a}$$

$$P(t,\boldsymbol{x}) = P^{(0)} + \varepsilon P^{(1)} + \varepsilon^2 P^{(2)} + \cdots \,, \tag{3.12b}$$

$$\Phi(t,\boldsymbol{x}) = \Phi^{(0)} + \varepsilon\Phi^{(1)} + \varepsilon^2\Phi^{(2)} + \cdots \,, \tag{3.12c}$$

$$\boldsymbol{v}(t,\boldsymbol{x}) = \boldsymbol{v}^{(0)} + \varepsilon\boldsymbol{v}^{(1)} + \varepsilon^2\boldsymbol{v}^{(2)} + \cdots \,, \tag{3.12d}$$

and substituted into the fluid equations (3.9). Each equation is then solved order by order in ε. For an initially static star $\boldsymbol{v}^{(0)} = 0$.[7]

In a general analysis one could pick $\varepsilon = \alpha$ and use the full expression for $a_i^{\rm ext}$ in Eq. (3.10). However, one would find that the contribution to $\delta\rho_c/\rho_c$ at $O(\alpha^6)$ would come solely from the leading-order Newtonian tidal term proportional to $\mathcal{E}_{ij}$, while the $O(\alpha^7)$ contribution to $\delta\rho_c/\rho_c$ and the leading contribution to $\mathcal{S}_{ij}$ would only come from the gravitomagnetic terms in $a_i^{\rm ext}$. It is therefore much simpler for our purposes to expand separately in either $\varepsilon_{\mathcal{E}}$ or $\varepsilon_{\mathcal{B}}$. To compute the $O(\alpha^6)$ tidal-stabilization term, one would set $\varepsilon = \varepsilon_{\mathcal{E}}$, $\varepsilon_{\mathcal{B}} = 0$ in Eqs. (3.9), (3.11), and (3.12), and expand to $O(\varepsilon_{\mathcal{E}}^2)$. This leading-order tidal-stabilization term is actually more difficult to compute than the $O(\alpha^7)$ destabilization term that we compute below. The tidal-stabilization term has also been computed by other methods [22, 94]; this is reviewed in Appendix J. We will simply use the result of Taniguchi and Nakamura [94] for the change in central density of a $\Gamma = 2$ Newtonian polytrope,

$$\frac{\delta\rho_c}{\rho_c} = -\frac{45}{2\pi^2}\left(\frac{M'}{M}\right)^2\left(\frac{R}{d}\right)^6 \,. \tag{3.13}$$

To compute the gravitomagnetic destabilization term, we set $\varepsilon = \varepsilon_{\mathcal{B}}$, $\varepsilon_{\mathcal{E}} = 0$ in Eqs. (3.9), (3.11), and (3.12), expand, and solve the fluid equations order by order

[7] For a slowly-rotating star in a tidal field, one would choose $\boldsymbol{v}^{(0)} = \boldsymbol{\Omega}\times\boldsymbol{x}$ and expand the fluid variables in both the tidal expansion parameter ε and the angular velocity Ω; see Appendix L for an analysis of this case.

in $\varepsilon_{\mathcal{B}}$. At order $O(\varepsilon_{\mathcal{B}}^0)$ we have the standard equations for a star in hydrostatic equilibrium,

$$\nabla_i P^{(0)} = -\rho^{(0)} \nabla_i \Phi^{(0)} \ , \quad \dot{\rho}^{(0)} = 0 \ . \tag{3.14}$$

[Poisson's equation is also satisfied at each order in the expansion: $\nabla^2 \Phi^{(n)} = 4\pi \rho^{(n)}$.]

At order $O(\varepsilon_{\mathcal{B}}^1)$ we have

$$\frac{\partial \rho^{(1)}}{\partial t} + \nabla_i [\rho^{(0)} v_i^{(1)}] = 0 \ , \tag{3.15}$$

and

$$\rho^{(0)} \frac{\partial v_i^{(1)}}{\partial t} = -\nabla_i P^{(1)} - \rho^{(1)} \nabla_i \Phi^{(0)} - \rho^{(0)} \nabla_i \Phi^{(1)} - \rho^{(0)} \dot{\zeta}_i^{\rm ext} \ . \tag{3.16}$$

Combining the time derivative of (3.15) with the divergence of (3.16) and Poisson's equation gives

$$\frac{\partial^2 \rho^{(1)}}{\partial t^2} = 8\pi \rho^{(0)} \rho^{(1)} + \nabla^2 P^{(1)} + \nabla_i \rho^{(0)} \nabla^i \Phi^{(1)} + \nabla_i \rho^{(1)} \nabla^i \Phi^{(0)} \ , \tag{3.17}$$

where we have used $\nabla^i [\rho^{(0)} \dot{\zeta}_i^{\rm ext}] = 0$ from Eq. (3.3) and $\rho^{(0)} = \rho^{(0)}(r)$. If our initial conditions state that there are no fluid perturbations at early times [so that at order $O(\varepsilon_{\mathcal{B}}^1)$ and higher, ρ, P, Φ, and $\boldsymbol{v}$ and their first time derivatives vanish as $t \to -\infty$], then the solution to Eq. (3.17) is

$$\rho^{(1)} = P^{(1)} = \Phi^{(1)} = 0 \ . \tag{3.18}$$

Equation (3.16) then reduces to $\dot{v}_i^{(1)} = -\dot{\zeta}_i^{\rm ext}$. In an inspiralling binary $\mathcal{B}_{ij} \to 0$ as $t \to -\infty$, and the leading-order velocity becomes

$$v_i^{(1)} = -\zeta_i^{\rm ext} = \frac{2}{3} \epsilon_{ijk} \mathcal{B}^j{}_l x^k x^l \ . \tag{3.19}$$

This induced velocity shows that, in the absence of viscosity, a nonrotating star responds to the gravitomagnetic vector potential without resistance (like a spring

with a vanishing spring constant). In rotating stars the Coriolis effect provides a restoring force, and the gravitomagnetic field excites an r-mode [131]; the velocity (3.19) is the zero-rotation limit of the r-mode excitation. (See Figures 3.1 and 3.2 for a graphical depiction of this velocity field.) The velocity field (3.19) can be expressed as a sum of $l = 2$ magnetic-type vector spherical harmonics

$$v_i^{(1)} = \sum_{m=-2}^{2} B_v^{2m}(t,r) Y_i^{B,2m} \,, \tag{3.20}$$

with

$$B_v^{2m}(t,r) = -\frac{8\pi}{15}\sqrt{\frac{2}{3}} r^2 \mathcal{B}_{ij} \mathcal{Y}_{ij}^{2m*} \tag{3.21}$$

(see Appendix G for definitions). Such a velocity field would be excluded by numerical simulations that enforce corotation. It would also be excluded in analyses that model each NS as an ellipsoid with an internal fluid velocity that is a linear function of the coordinates. However, such a velocity field would be permitted in a relativistic irrotational simulation. This seems puzzling at first because $v_i^{(1)}$ has nonvanishing Newtonian vorticity, $\omega_i = [\nabla \times \boldsymbol{v}^{(1)}]_i = 2\mathcal{B}_{ij} x^j$. The resolution is that the 1PN limit of the relativistic irrotational condition, $\nabla \times (\boldsymbol{v}^{(1)} + \boldsymbol{\zeta}^{\rm ext}) = 0$, is satisfied [104]. In contrast, a rotating star or a nonzero frequency r-mode would not satisfy the relativistic irrotational condition. See Appendix H for further discussion.

The velocity field (3.19) endows the NS with an induced current-quadrupole moment. Substituting Eq. (3.19) into Eq. (3.5) gives $\mathcal{S}_{ij} = \gamma \mathcal{B}_{ij}$, where

$$\gamma = \frac{8\pi}{15} \int_0^R \rho r^6 \, dr = \gamma_2 M R^4 \,, \tag{3.22}$$

and γ_2 is the *gravitomagnetic Love number*. For a uniform density Newtonian star, $\gamma_2 = 2/35$; for a $\Gamma = 2$ polytrope $\gamma_2 = 2(\pi^4 - 20\pi^2 + 120)/(15\pi^4) \approx 0.0274$ (see Appendix I).

At order $O(\varepsilon_{\mathcal{B}}^2)$ we have the equations necessary to compute the change in central density at $O(\alpha^7)$:

$$\frac{\partial \rho^{(2)}}{\partial t} + \nabla_i[\rho^{(0)} v_i^{(2)}] = 0 \ , \tag{3.23}$$

and

$$\frac{\partial v_i^{(2)}}{\partial t} + \frac{\nabla_i P^{(2)}}{\rho^{(0)}} + \nabla_i \Phi^{(2)} + \frac{\rho^{(2)}}{\rho^{(0)}} \nabla_i \Phi^{(0)} = a_i^{\rm tot} \ , \tag{3.24}$$

where

$$a_i^{\rm tot} = [\boldsymbol{v}^{(1)} \times \boldsymbol{B}]_i - [\boldsymbol{v}^{(1)} \cdot \nabla] v_i^{(1)} \ . \tag{3.25}$$

This acceleration term shows that the second-order perturbations are driven by a combination of the Lorentz-type gravitomagnetic and the nonlinear convective derivative terms. (See Figure 3.3 for a graphical depiction of $a_i^{\rm tot}$.) Both terms are generated by the first-order velocity perturbation to the star. Using Eq. (3.19), the acceleration term $a_i^{\rm tot}$ can be expressed explicitly in terms of the gravitomagnetic tidal field,

$$a_i^{\rm tot} = H_{ijkl} x^j x^k x^l \ , \tag{3.26}$$

where

$$H_{ijkl} = \frac{8}{9} \left(\mathcal{B}_{ik} \mathcal{B}_{jl} - \mathcal{B}_{ak} \mathcal{B}_{al} \delta_{ij} - \frac{1}{2} \epsilon_{caj} \epsilon_{ibl} \mathcal{B}_{ak} \mathcal{B}_{bc} \right) \ . \tag{3.27}$$

3.3.3 Radial Lagrangian perturbations

To compute the change in central density, we first note that, since the first-order perturbations to the density, pressure and self-gravity vanish, Eqs. (3.23) and (3.24) can be recast as the equation for a linear Lagrangian perturbation of an initially static star. This is done by relabelling $\rho = \rho^{(0)}$, $P = P^{(0)}$, $\Phi = \Phi^{(0)}$, $\delta\rho = \rho^{(2)}$, $\delta P = P^{(2)}$, $\delta\Phi = \Phi^{(2)}$, and $\delta \boldsymbol{v} = \boldsymbol{v}^{(2)}$, and using $\Delta = \delta + \xi_i \nabla^i$, $\delta\Phi = 4\pi\delta\rho$, and $\Delta v_i = \dot{\xi}_i$. Here δ refers to an Eulerian perturbation, Δ refers to a Lagrangian

perturbation, and ξ_i is the Lagrangian displacement. The result is the standard perturbed fluid equations with the forcing term $a_i^{\rm tot}$ (chapter 6 of [133]):

$$\rho\frac{\partial^2\xi_i}{\partial t^2} - \frac{\Delta\rho}{\rho}\nabla_i P + \nabla_i\Delta P + \rho\nabla_i\Delta\Phi = \rho a_i^{\rm tot} \ , \tag{3.28}$$

and

$$\frac{\Delta\rho}{\rho} = -\nabla^i\xi_i \ . \tag{3.29}$$

Equation (3.28) can be reexpressed as

$$\ddot{\boldsymbol{\xi}} + \mathcal{L}[\boldsymbol{\xi}] = \boldsymbol{a}^{\rm tot} \ , \tag{3.30}$$

where $\mathcal{L}$ is a differential operator [see Eq. (K.2)]. This equation can be solved by expanding $\boldsymbol{\xi}(t,\boldsymbol{x})$ in terms of a chosen basis of modes $\boldsymbol{\xi}_\alpha(\boldsymbol{x})$ and their time-dependent amplitudes $q_\alpha(t)$,

$$\boldsymbol{\xi}(t,\boldsymbol{x}) = \sum_\alpha q_\alpha(t)\boldsymbol{\xi}_\alpha(\boldsymbol{x}) \ , \tag{3.31}$$

where $\alpha = (n,l,m)$ label the modes. The basis functions can be further expanded in terms of vector spherical harmonics (Appendix G),

$$\boldsymbol{\xi}_\alpha(\boldsymbol{x}) = E_\xi^\alpha(r)\boldsymbol{Y}^{E,lm} + B_\xi^\alpha(r)\boldsymbol{Y}^{B,lm} + R_\xi^\alpha(r)\boldsymbol{Y}^{R,lm} \ . \tag{3.32}$$

The index $n = 0\cdots\infty$ is the number of radial nodes, and $l = 0\cdots\infty$ and $m = -l\cdots l$ are the familiar angular indices in a spherical harmonic decomposition. We also define the inner product and mode normalization

$$\langle\boldsymbol{\xi}_\alpha,\boldsymbol{\xi}_\beta\rangle \equiv \int\rho(\boldsymbol{x})\boldsymbol{\xi}_\alpha^*\cdot\boldsymbol{\xi}_\beta\,d^3x = MR^2\delta_{\alpha\beta} \ . \tag{3.33}$$

In the absence of external driving ($a_i^{\rm tot} = 0$), employing the standard $e^{-i\omega_\alpha t}$ ansatz for the mode time dependence yields the eigenvalue equation for the modes,

$$-\omega_\alpha^2\boldsymbol{\xi}_\alpha(\boldsymbol{x}) = \mathcal{L}[\boldsymbol{\xi}_\alpha(\boldsymbol{x})] \ . \tag{3.34}$$

Inserting Eq. (3.31) into (3.30) and using Eq. (3.33) yields the equation of motion for the mode amplitudes,

$$\ddot{q}_\alpha(t) + \omega_\alpha^2 q_\alpha(t) = \frac{\langle \boldsymbol{\xi}_\alpha, \boldsymbol{a}^{\rm tot}\rangle}{MR^2} \ . \tag{3.35}$$

To compute the change in central density we need only consider the evolution of the fundamental radial mode $q_0(t)\boldsymbol{\xi}_0(\boldsymbol{x})$. [Here and below the subscript 0 refers to $\alpha = (0,0,0)$.] To see this, substitute Eqs. (3.31) and (3.32) into (3.29). This yields

$$\frac{\Delta\rho}{\rho} = \sum_\alpha q_\alpha(t) \left[\sqrt{l(l+1)}\frac{E_\xi^\alpha}{r} - 2\frac{R_\xi^\alpha}{r} - \frac{dR_\xi^\alpha}{dr}\right] Y^{lm} \ . \tag{3.36}$$

In the $r \to 0$ limit, $\Delta\rho/\rho$ must be independent of direction (θ, ϕ), so it can only be affected by $l = m = 0$ radial modes [90]. Further, the radial eigenfunctions near the center of the star have the form $R_\xi^{n00}(r) \propto r^{n+1}$, so only the fundamental $(n = 0)$ radial mode can change the central density. This radial mode function can be expressed as

$$\boldsymbol{\xi}_0(\boldsymbol{x}) = R_\xi^{000}(r) Y^{00} \boldsymbol{n} = C/(\sqrt{4\pi})\tilde{\xi}_0^r \boldsymbol{n} \ , \tag{3.37}$$

where C is a normalization constant determined by Eq. (3.33), $\boldsymbol{n}$ is a unit radial vector, and $\tilde{\xi}_0^r = r[1 + O(r)]$ near $r = 0$. From Eq. (3.36) the change in central density is

$$\frac{\delta\rho_c}{\rho_c} = \lim_{r\to 0}\frac{\Delta\rho}{\rho} = -\frac{3C}{\sqrt{4\pi}} q_0(t) \tag{3.38}$$

(the Eulerian and Lagrangian density perturbations at the center of the star are identical).

We therefore need to solve Eq. (3.35) with $\alpha = (0,0,0)$ for $q_0(t)$. This involves computing the inner product

$$\langle \boldsymbol{\xi}_0, \boldsymbol{a}^{\rm tot}\rangle = \int \rho r^2 \frac{C}{\sqrt{4\pi}} \tilde{\xi}_0^r(r) \left(\oint \boldsymbol{n}\cdot\boldsymbol{a}^{\rm tot}\, d\Omega\right) dr \ . \tag{3.39}$$

Using Eqs. (3.26) and (3.27), and the STF integrals in Appendix G, the angular integral becomes

$$\oint \boldsymbol{n}\cdot\boldsymbol{a}^{\rm tot}\,d\Omega = -\frac{32\pi}{45}r^3\mathcal{B}_{ij}\mathcal{B}^{ij}\ . \tag{3.40}$$

The negative sign shows that the angle-averaged radial force is inward pointing, leading to compression.

For a $\Gamma = 2$ polytrope, $\omega_0^2 = A\pi^2 M/R^3$, with $A \approx 0.3804$, and $C \approx 4.756$. The radial integrals are computed numerically using the eigenfunction $\tilde{\xi}_0^r = (R/\pi)\xi(u)$ from Appendix K [Eq. (K.11)], giving

$$\langle \boldsymbol{\xi}_0, \boldsymbol{a}^{\rm tot}\rangle \approx -0.05996 M R^4 \mathcal{B}_{ij}\mathcal{B}^{ij}\ . \tag{3.41}$$

3.3.4 Change in central density

We now have all the tools needed to compute the change in central density at $O(\alpha^7)$. We will specialize to a circular binary, for which the tidal fields have the form (see Appendix F)

$$\mathcal{E}_{ij} = \mathcal{E}\begin{bmatrix} 3\sin^2\omega_{\rm orb}t - 2 & -3\cos\omega_{\rm orb}t\sin\omega_{\rm orb}t & 0 \\ -3\cos\omega_{\rm orb}t\sin\omega_{\rm orb}t & 3\cos^2\omega_{\rm orb}t - 2 & 0 \\ 0 & 0 & 1 \end{bmatrix} \tag{3.42}$$

and

$$\mathcal{B}_{ij} = \mathcal{B}\begin{bmatrix} 0 & 0 & \cos\omega_{\rm orb}t \\ 0 & 0 & \sin\omega_{\rm orb}t \\ \cos\omega_{\rm orb}t & \sin\omega_{\rm orb}t & 0 \end{bmatrix}\ , \tag{3.43}$$

where $\mathcal{E} \equiv M'/d^3$, $\mathcal{B} \equiv 3(M'/d^3)V_{\rm orb}$, $\omega_{\rm orb} = [(M+M')/d^3]^{1/2}$ is the Keplerian orbit angular velocity, and $V_{\rm orb} = \omega_{\rm orb}d$ is the relative orbital velocity. Note that the tidal fields contracted with themselves do not depend on the orbital phase:

$\mathcal{E}_{ij}\mathcal{E}^{ij} = 6(M'/d^3)^2$ and $\mathcal{B}_{ij}\mathcal{B}^{ij} = 18(M'/d^3)^2(M+M')/d$. Since d evolves very slowly compared to the orbital and stellar oscillation frequencies, we can ignore its time dependence when solving Eq. (3.35) for $q_0(t)$. The initial conditions that q_0, $\dot{q}_0$, and $\mathcal{B}_{ij}$ vanish at very early times (when the binary is widely separated) yield the simple solution $q_0(t) = \langle \boldsymbol{\xi}_0, \boldsymbol{a}^{\rm tot}\rangle/(\omega_0^2 M R^2)$. Equations (3.38) and (3.41) then yield the gravitomagnetic contribution to the change in central density,

$$\frac{\delta\rho_c}{\rho_c} = 0.06427\frac{R^5}{M}\mathcal{B}_{ij}\mathcal{B}^{ij} \ . \tag{3.44}$$

This equation is valid for any slowly-varying magnetic-type tidal field, not just the specific form given above.[8] The formula (3.43) for $\mathcal{B}_{ij}$ along with Eq. (3.13) then gives the total change in central density up to order $O(\alpha^7)$,

$$\frac{\delta\rho_c}{\rho_c} = -2.280\left(\frac{M'}{M}\right)^2\left(\frac{R}{d}\right)^6 + 1.157\left(\frac{M}{R}\right)^2\left(1+\frac{M'}{M}\right)\left(\frac{M'}{M}\right)^2\left(\frac{R}{d}\right)^7 \ . \tag{3.45}$$

This formula shows that there is a critical orbital separation,

$$\frac{d_{\rm crit}}{R} = 0.5074\left(\frac{M}{R}\right)^2\left(1+\frac{M'}{M}\right) \ , \tag{3.46}$$

where the gravitomagnetic crushing force can overwhelm the Newtonian tidal stabilization. This separation can be large if one considers not only NS/NS binaries but also NS/massive BH binaries. However, one must compare this separation with an estimate for the onset of tidal disruption, or, in the case of massive BHs, the separation when the inner-most stable circular orbit (ISCO) or event horizon is reached (see Fig. 3.5). The tidal disruption radius is approximately $d_{\rm tidal}/R = 2.4(1+M'/M)^{(1/3)}$ [129]. For equatorial orbits the ISCO occurs at

[8] As another example, consider the magnetic-type tidal field of a spinning black hole with spin parameter $\hat{a} = a/M'$. Far from the hole $\mathcal{B}_{ij}\mathcal{B}_{ij} = 18\hat{a}^2M'^4/d^8$ [from Eqs. (3.36) and (5.45b) of [134]], and the resulting change in central density is still compressive, with magnitude $\delta\rho_c/\rho_c = 1.157\hat{a}^2(M/R)^3(M'/M)^4(R/d)^8$.

a separation of $d_{\rm isco}/R = \beta_{\rm isco}(a)(M/R)(M'/M)$, while the event horizon is at a separation of $d_{\rm horizon}/R = \beta_{\rm horizon}(a)(M/R)(M'/M)$ (these formulas are strictly valid only in the limit where $M'/M \gg 1$, but we apply them for all mass ratios). Here $\beta_{\rm isco}(a)$ and $\beta_{\rm horizon}(a)$ are dimensionless functions of the BH spin parameter a and vary from 1 to 9 and 1 to 6, respectively [135]. When one compares these critical separations to the onset of crushing, one finds that, for any plausible value of compaction ($M/R \leq 1$) or mass ratio ($M'/M \geq 1$), either the tidal disruption, ISCO, or horizon radius is reached *before* the gravitomagnetic crushing force dominates over tidal stabilization. Therefore, an increase in central density by this mechanism cannot occur.

The effects of gravitomagnetic compression on the stability of *relativistic* NSs could be treated by applying the second-order perturbation methods of this section to an initially static and spherically symmetric relativistic star. A simpler approach would be to modify Thorne's [92] "local-asymptotic-rest-frame" analysis. This modification would supplement Thorne's potential energy function for the star [his Eq. (7)] with the following terms: (1) the gravitomagnetic contribution to the rate of tidal work performed on the NS by a distant tidal field,[9]

$$\frac{dW}{dt} = -\frac{1}{2}\mathcal{E}_{ij}\frac{d\mathcal{I}_{ij}}{dt} - \frac{2}{3}\mathcal{B}_{ij}\frac{\mathcal{S}_{ij}}{dt} \; ; \tag{3.47}$$

and (2) current-quadrupole contributions to the star's internal energy. Extending Thorne's analysis to gravitomagnetic interactions confirms the main result of this section: the weaker gravitomagnetic compression cannot overwhelm the electric-type tidal stabilization of an initially static neutron star.

[9]Equation (3.47) was first derived by Zhang [136]. The electric-type contribution to the tidal work [the first term on the right-hand-side of (3.47)] was shown to be gauge and energy-localization invariant by Purdue [137], Favata [138], and Booth and Creighton [139]. Although it has not been explicitly calculated, these properties should also hold for the gravitomagnetic term in (3.47).

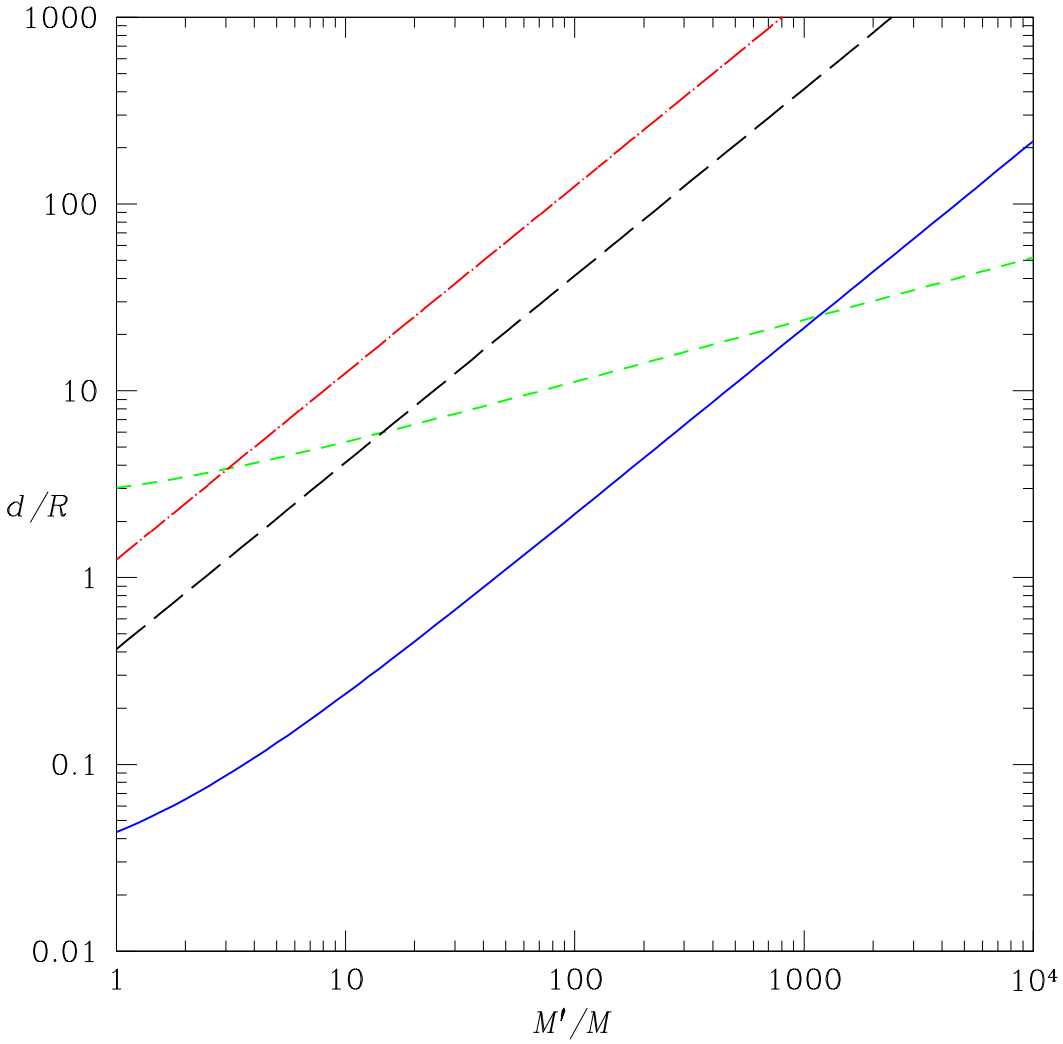

Figure 3.5: Critical orbital separation for compression to overwhelm stabilization. The solid (blue) curve shows, as a function of mass ratio, the critical orbital separation $d_{\rm crit}$ (in units of the NS radius) where the compression and stabilization terms in Eq. (3.45) are equal. The short-dashed (green) curve shows the tidal disruption limit $d_{\rm tidal}/R$. The dashed-dotted (red) curve shows the ISCO $d_{\rm isco}/R$ while the long-dashed (black) curve shows the event horizon $d_{\rm horizon}/R$ of a non-spinning black hole with mass M'. This plot shows that in an inspiralling binary, either the tidal disruption limit, the ISCO, or the event horizon is reached before the critical separation where compression dominates. This is also true for rapidly spinning black holes: as the spin parameter a/M' varies, the lines corresponding to the ISCO and horizon would shift up or down, but they would always remain above the curve for $d_{\rm crit}$. These curves assume a neutron star with $M = 1.4M_\odot$, $R = 10$ km, and a $\Gamma = 2$ polytropic equation of state.

A possible exception is a situation in which a magnetic-type tidal field is present but the electric-type tidal field is absent or very small. A (somewhat contrived) example of such a situation would be a judicious arrangement of at least two less massive bodies (planets) orbiting a star, with their masses, distances, inclinations, and orbital phases carefully chosen, leading to a nearly vanishing $\mathcal{E}_{ij}$ but nonzero $\mathcal{B}_{ij}$. Although it is very unlikely that such situations exist in nature, they show that stars can in principle undergo a net compression due to tidal effects.

3.4 Change in central density from a preexisting velocity field

In the previous section we considered the change in central density caused by a current-quadrupole moment that is induced by an external tidal field. Now we consider the case in which a current-quadrupole moment or other velocity field is *preexisting* in the star rather than induced by tidal interactions. This velocity field then couples to the external tidal field to change the central density. As discussed in Sec. 3.1, viscosity will damp most astrophysical velocity perturbations, but a velocity field might arise as an artifact of a numerical simulation.[10] In the WMM simulations [89, 11, 10] it is possible that a current-quadrupole moment arises in the formulation of the initial data. In those simulations, two initially-corotating single NS solutions are placed on the computational grid and are allowed to relax (using

[10] r-modes driven unstable by radiation reaction in rotating hot neutron stars [140, 141, 142] are an additional source of a preexisting current quadrupole, but their magnitudes are too small to be of interest here: For an r-mode in a star with angular speed Ω, the characteristic velocity of the current quadrupole $\delta v \sim \mathcal{S}_{ij}/(MR^2)$ is approximately $\delta v \sim \hat{\alpha} R\Omega \sim \hat{\alpha}(M/R)^{1/2}(\Omega/\Omega_c)$, where $\Omega_c \equiv (M/R^3)^{1/2}$ and $\hat{\alpha} \ll 1$ parameterizes the r-mode amplitude. Also, the rotation of the star provides additional support against collapse.

artificial viscosity) to a two-body equilibrium state which is neither corotating nor irrotational. Indications of a current quadrupolar velocity pattern can be seen in the original WMM simulations (see Figure 4b of [11] and associated discussion). However it is not clear how that current quadrupole is generated.

Begin by considering an approximately spherical, nonrotating star that satisfies the fluid equations (3.9) augmented by the 1PN external acceleration (3.10), and that contains a preexisting velocity $\boldsymbol{v}_0$. This velocity field can generally be expressed as a sum over vector harmonics as in Eq. (3.32),

$$\boldsymbol{v}_0(t,\boldsymbol{x}) = \sum_{lm} E_v^{lm}(t,r)\boldsymbol{Y}^{E,lm} + B_v^{lm}(t,r)\boldsymbol{Y}^{B,lm} + R_v^{lm}(t,r)\boldsymbol{Y}^{R,lm} \ . \tag{3.48}$$

In isolation, Eqs. (3.9) are satisfied with $a_i^{\rm ext} = 0$ and $\boldsymbol{v} = \boldsymbol{v}_0$. If we further impose the condition that the density is time-independent in the absence of tidal fields, the velocity field must satisfy $\nabla\cdot(\rho\boldsymbol{v}_0) = 0$. If we assume that the background density ρ is spherically symmetric, $\rho = \rho(r)$, then $\boldsymbol{v}_0$ must also satisfy $\boldsymbol{n}\cdot\boldsymbol{v}_0 = \nabla\cdot\boldsymbol{v}_0 = 0$; it is therefore proportional to a magnetic-type tidal field, $\boldsymbol{v}_0 = \sum_{lm} B_v^{lm}\boldsymbol{Y}^{B,lm}$. The magnitude of $\boldsymbol{v}_0$ is not known, but we will assume that it is small enough to satisfy $v_0^2 \ll M/R$. Since the $(\boldsymbol{v}_0\cdot\nabla)\boldsymbol{v}_0$ term is small in this approximation, $\dot{\boldsymbol{v}}_0 \approx 0$, and the structure of the star in isolation is adequately described by the ordinary equations of hydrostatic equilibrium [Eq. (3.14)]. This also implies that $B_v^{lm}(t,r)$ is independent of t. Assuming that order $O(v_0^2)$ terms are small allows us to neglect various 1PN terms in the hydrodynamics equations. Other 1PN terms are dropped for the reasons discussed in Appendix F.

Now allow the external tidal fields to perturb this star. Since the background velocity $\boldsymbol{v}_0$ negligibly affects the structure of the star in isolation, Lagrangian perturbations of the star are described by Eqs. (3.28) and (3.29). The methods used in Sec. 3.3.3 can then be used to compute the change in central density. The

main step is to compute the fundamental radial mode evolution via Eq. (3.35) [with $\alpha = (0,0,0)$], using $\langle \boldsymbol{\xi}_0, \boldsymbol{a}^{\rm ext}\rangle$ for the inner product. Since $\boldsymbol{v}_0$ is small, we ignore terms of order $O(v_0^2)$ in $a_i^{\rm ext}$.

Substituting the expansion (3.48) for $\boldsymbol{v}_0$ into $a_i^{\rm ext}$, expressing the vector spherical harmonics in terms of STF-l tensors [Eqs. (G.8)], and performing the angular integration, we find that the only piece of the velocity field that can change the central density is proportional to an $l = 2$ magnetic-type vector harmonic, $\boldsymbol{Y}^{B,2m}$, which couples to the $\boldsymbol{v}_0 \times \boldsymbol{B}$ piece of the external acceleration.[11] The result for the inner product is

$$\langle \boldsymbol{\xi}_0, \boldsymbol{a}^{\rm ext}\rangle = \frac{C}{\sqrt{\pi}}\frac{4\pi}{5}\sqrt{\frac{2}{3}}\mathcal{B}_{ij}\sum_{m=-2}^{2}\left[\mathcal{Y}_{ij}^{2m}\int \rho r^3 \tilde{\xi}_0^r(r) B_v^{2m}(t,r)\,dr\right] . \tag{3.49}$$

A current-quadrupole moment is also proportional to $\boldsymbol{Y}^{B,2m}$: substituting Eq. (3.48) into (3.5) yields

$$\mathcal{S}_{ij} = -\frac{4\pi}{5}\sqrt{\frac{2}{3}}\sum_{m=-2}^{2}\left(\int \rho r^4 B_v^{2m}(t,r)dr\right)\mathcal{Y}_{ij}^{2m} . \tag{3.50}$$

If we approximate $\tilde{\xi}_0^r(r) = r[1 + O(r)] \approx r$ in Eq. (3.49) (incurring an error $\lesssim 20\%$ for a $\Gamma = 2$ polytrope) and combine with (3.50), the inner product simplifies to

$$\langle \boldsymbol{\xi}_0, \boldsymbol{a}^{\rm ext}\rangle = -\frac{C}{\sqrt{\pi}}\mathcal{S}_{ij}\mathcal{B}^{ij} . \tag{3.51}$$

Since $\dot{\boldsymbol{v}}_0 \approx 0$ we can assume that $\mathcal{S}_{ij}$ is a constant and parameterize the magnitude of its components by $|\mathcal{S}_{ij}| \sim MR^2V_{\mathcal{S}}$, where $V_{\mathcal{S}}$ is the characteristic velocity

[11] There is also a contribution to the inner product $\langle \boldsymbol{\xi}_0(\boldsymbol{x}), \boldsymbol{a}^{\rm ext}\rangle$ from a velocity component proportional to $\boldsymbol{Y}^{R,2m}$ coupling with the $3v_i\dot{\Phi}^{\rm ext}$ piece of the external acceleration; but this piece is excluded by our condition that $\nabla\cdot(\rho\boldsymbol{v}_0) = 0$ when the star is in isolation. If we expand the gravitational potentials to higher powers of α (including octupole and higher tidal moments), other velocity couplings that could change the central density are possible, but would be smaller in magnitude.

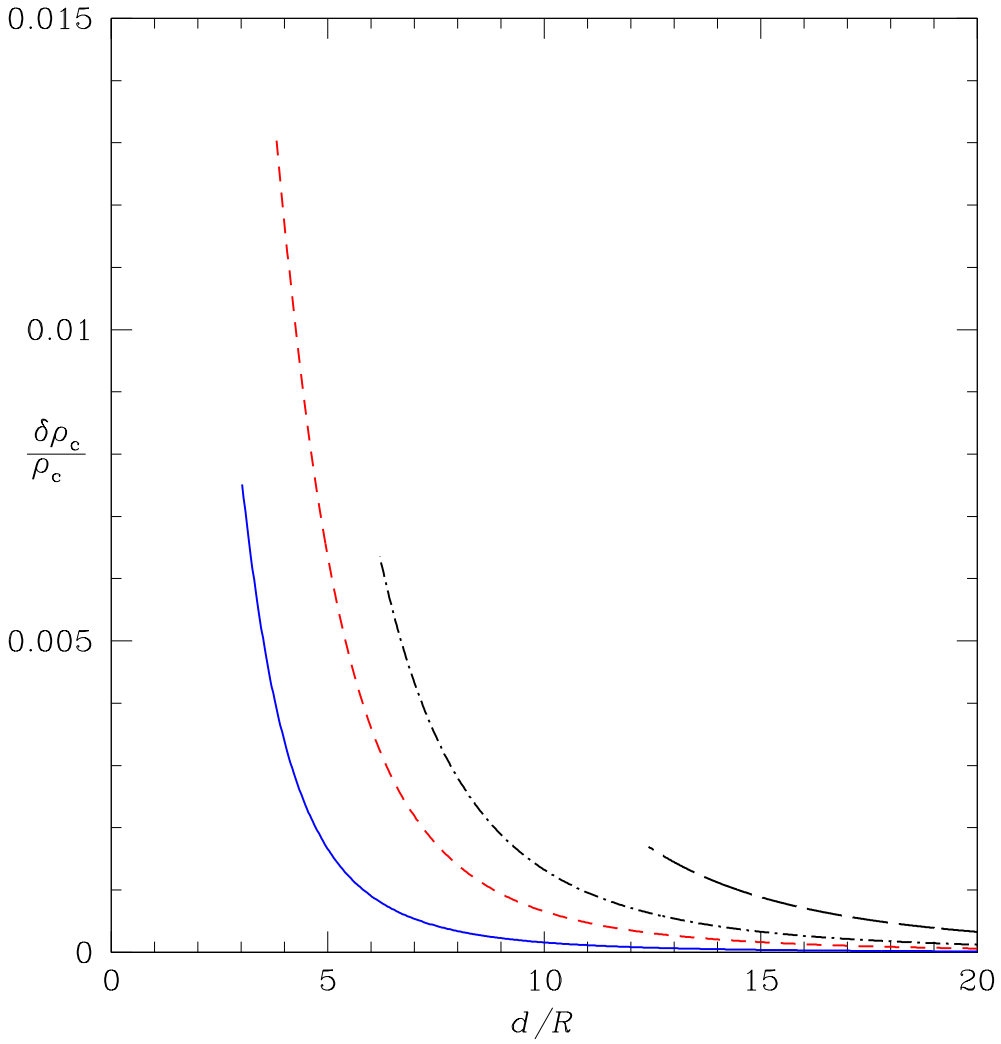

Figure 3.6: Change in central density of a neutron star with a preexisting velocity field [Eq. (3.53) with the cosine term set to +1]. The size of the current quadrupole is fixed at $V_{\mathcal{S}} = 0.1(M/R)^{1/2}$. All curves are for a NS with mass $M = 1.4M_\odot$ and radius $R = 10\,\mathrm{km}$. From left to right, the first two curves are for a NS companion with $M'/M = 1(\text{blue,solid}), 3(\text{red,short-dashed})$ and are terminated at the tidal disruption radius. The next two (black) curves are for a black hole companion with $M'/M = 5(\text{dot-dashed}), 10(\text{long-dashed})$ and are terminated at the innermost stable circular orbit. For the value of $V_{\mathcal{S}}$ used here, compression dominates over stabilization before tidal disruption or orbit instability occurs.

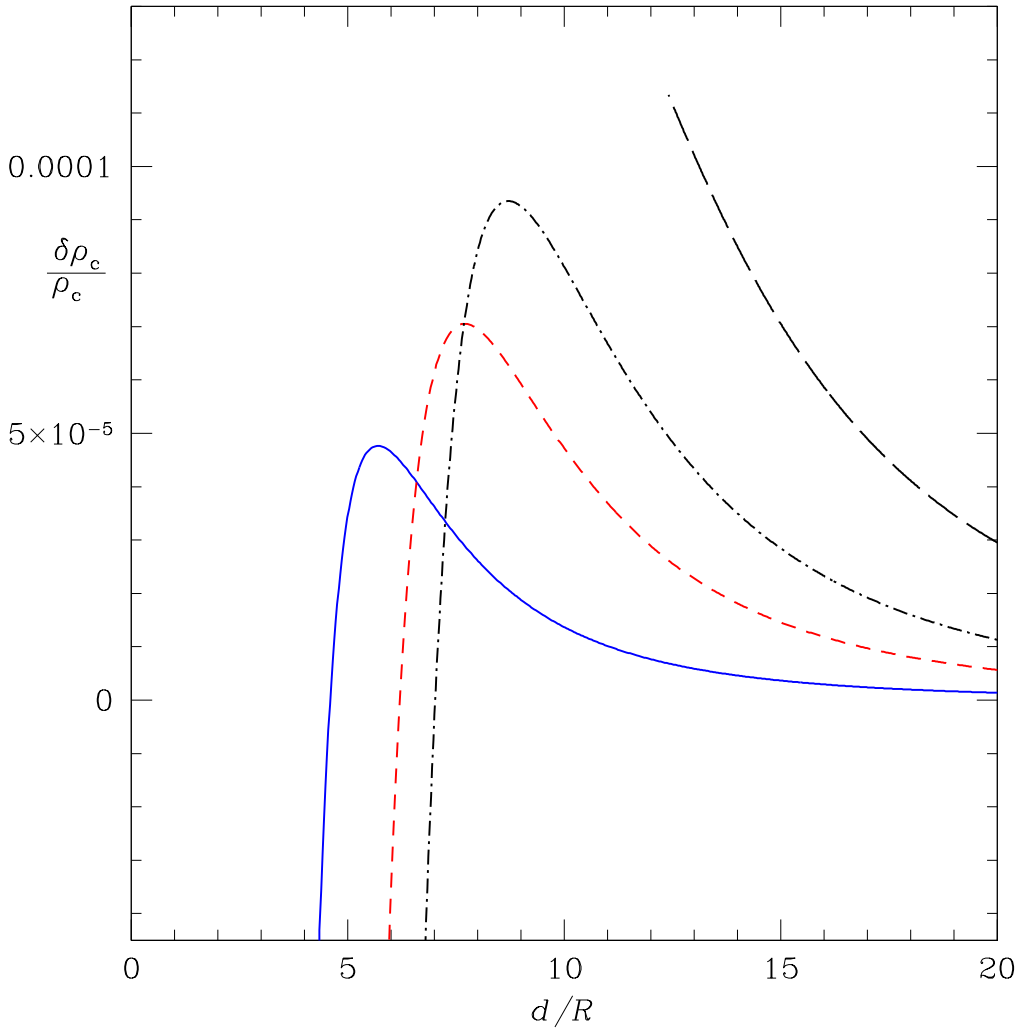

Figure 3.7: Same as Figure 3.6 except that the size of the current-quadrupole moment is smaller, $V_{\mathcal{S}} = 0.01(M/R)^{1/2}$. The compression is much smaller in this case and, for three of the stars, is eventually dominated by the tidal stabilization. For the $M'/M = 3$ binary the neutron star central density decreases by $\lesssim 0.5\%$ before tidal disruption.

associated with the current quadrupolar motions. Integrating Eq. (3.35) using (3.51) and (3.43), assuming that d varies slowly compared with the orbital and stellar oscillation periods, and using the condition that $q_0, \dot{q}_0 \to 0$ as $t \to -\infty$, we get

$$q_0(t) = -\frac{6C}{\sqrt{\pi}} \frac{M'}{d^3} \left(\frac{M+M'}{d}\right)^{1/2} \frac{V_{\mathcal{S}} \cos(\omega_{\rm orb} t + \delta)}{(\omega_0^2 - \omega_{\rm orb}^2)} \,, \tag{3.52}$$

where ω_0 is the angular frequency of the fundamental radial mode, $V_{\mathcal{S}} \equiv (\mathcal{S}_{xz}^2 + \mathcal{S}_{yz}^2)^{1/2}/(MR^2)$, and $\tan\delta \equiv -\mathcal{S}_{yz}/\mathcal{S}_{xz}$. Since the fundamental mode frequency $\omega_0/2\pi \approx 4.2\,$kHz (for a canonical $M = 1.4M_\odot$, $R = 10$ km NS with a $\Gamma = 2$ EOS) is several times larger than the orbital frequency ($\approx 590\,$Hz at $d/R \sim 3$ for two NSs), we can usually approximate $\omega_0^2 - \omega_{\rm orb}^2 \approx \omega_0^2$. Using Eqs. (3.38) and (3.13), the total change in central density is

$$\begin{aligned}\frac{\delta\rho_c}{\rho_c} = &-2.280 \left(\frac{M'}{M}\right)^2 \left(\frac{R}{d}\right)^6 \\ &+ 17.26 V_{\mathcal{S}} \left(\frac{M}{R}\right)^{1/2} \left(\frac{M'}{M}\right) \left(1 + \frac{M'}{M}\right)^{1/2} \left(\frac{R}{d}\right)^{7/2} \cos(\omega_{\rm orb} t + \delta) \,. \end{aligned} \tag{3.53}$$

Because of the cosine term in (3.53), the change in central density oscillates in sign. Compression or stabilization depends on the orbital phase. Since we are interested in the possibility of crushing forces and how they compare with the Newtonian tidal stabilization, we will set the cosine term to $+1$ in our discussion below and in Figures 3.6 and 3.7.

In contrast to the case treated in Sec. 3.3, when the current-quadrupole moment is preexisting the gravitomagnetic crushing contributes to the change in central density with a *lower* power of α than the stabilizing term. This means that at large values of $d/R = 1/\alpha$, crushing will dominate over stabilization even if $V_{\mathcal{S}}$ is small. In Fig. 3.6, we plot the total change in central density for a $1.4M_\odot$, 10 km NS with $V_{\mathcal{S}} = 0.1(M/R)^{1/2}$ in a binary with mass ratios of $M'/M = 1, 3, 5,$ and 10.

The gravitomagnetic term clearly dominates, leading to compression. If the size of the current quadrupole is reduced by a factor of 10 to $V_{\mathcal{S}} = 0.01(M/R)^{1/2}$, the change in central density becomes much smaller (Fig. 3.7). While compression still dominates at large separations, the tidal stabilization eventually overwhelms the gravitomagnetic compression. For the stars treated here significant compression would require rather large current-quadrupole moments, with $V_{\mathcal{S}} > 0.1(M/R)^{1/2}$.

Although the changes in central density shown in Figures 3.6 and 3.7 are small, the gravitomagnetic crushing could be enhanced by an orbital resonance with the fundamental mode. Although we have made the approximation that $\omega_0^2 \gg \omega_{\rm orb}^2$, this is generally true only for Newtonian stars, which do not have a maximum mass. For relativistic stars, the fundamental mode frequency approaches zero as the mass of the star approaches the maximum mass of its EOS. This means that for stars sufficiently close to their maximum mass, the fundamental frequency could be low enough to be in resonance with the orbital period before tidal disruption occurs. This resonance would amplify the change in central density. Even if a resonance does not occur, a relativistic star that is close to its maximum mass is more easily perturbed past the critical point of its potential for radial oscillations (see Thorne [92]). If compressed enough such stars could undergo gravitational collapse to BHs—although their masses would have to be very close to the maximum mass for this to happen.

3.5 Discussion and Conclusions

Is the binary-induced compression and collapse of a neutron star possible? In the simplest and most realistic case of two nonrotating, initially unperturbed stars in a binary, the answer is *no*. Although there is a compressional force on the star it

is *always* smaller than the Newtonian force that stabilizes the star. The compressional force is small because it arises through a nonlinear fluid interaction with a post-Newtonian tidal field: the gravitomagnetic field induces a current quadrupolar velocity field which then couples to itself and to the gravitomagnetic field to produce compression. The Newtonian stabilization force also arises through a nonlinear fluid interaction, but it is induced by a Newtonian tidal field instead. This stabilization force is also small, but not as small as the post-Newtonian compressional force. Although we only consider first post-Newtonian effects, it seems unlikely that effects at 2PN and higher orders will be large enough to change the sign of the change in central density. For a NS/NS binary the parameters $\epsilon = M/R \sim 0.2$ and $\alpha = R/d \lesssim 0.3$ are sufficiently small that higher order terms in an expansion of the central density in ϵ and α are unlikely to be important (unless the coefficients of those terms are much larger than unity).

However, there are certain physical situations in which a net compression is possible in principle. For configurations of masses in which the Newtonian tidal field nearly cancels, the gravitomagnetic compression dominates over tidal stabilization. Such configurations probably do not occur very frequently in nature. A somewhat more likely possibility arises when a velocity field is already present in the neutron star and does not need to be induced by tidal interactions. If the velocity field has a current quadrupolar component, a net compression due to gravitomagnetic forces is possible. In Newtonian stars this compression is small for plausible values of the internal fluid velocity. Nevertheless, stars that are close to their maximum mass could, in principle, be pushed beyond their stability limit and made to collapse to black holes.

The implications of our results for the revised Wilson-Mathews [10] simula-

tions are unclear. As discussed in Sec. 3.2.1, other groups appear to have ruled out compression in NS/NS simulations that enforce irrotation. It therefore seems very likely that the compression seen in the irrotational simulations of Marronetti, Mathews, and Wilson [120] is unphysical and possibly related to their method of implementing certain boundary conditions, or is due to insufficient resolution. If low resolution is the cause of the compression in their irrotational simulations, then it may also be the source of the small residual compression in their unconstrained hydrodynamics simulations [10]. If low resolution is not the source (as maintained by Wilson [143]), then there remains the possibility that the compression is caused by Wilson and Mathews' method of determining the initial data or the use of artificial viscosity. Our analysis in Sec. 3.4 shows that compression can arise if the initial velocity configuration has a current quadrupolar component. For current quadrupolar velocities of size $V_{\mathcal{S}} \approx 0.1(M/R)^{1/2}$ we predict central compressions of order $\delta\rho_c/\rho_c \lesssim 1\%$. This is roughly a factor of $\sim 5 - 80$ times smaller than the compression seen in Wilson and Mathews' revised simulations [10]. Using a larger value of $V_{\mathcal{S}}$ could bring our estimates closer to the Wilson-Mathews' values, but would begin to violate our assumption that $V_{\mathcal{S}}$ is small. The actual size of the current-quadrupole moment in the revised Wilson-Mathews simulations is not clear. If it is very small, then our approach might not be a plausible explanation for compression. Higher values for the central compression (possibly leading to gravitational collapse) could be attained by extending our calculations to include relativistic stars near their maximum mass or the effects of orbital resonances. While the scenario discussed here is plausible in the context of binary neutron star simulations, in nature a preexisting current quadrupole will be rapidly damped and so will be irrelevant for observations unless it is generated shortly before coa-

lescence.

The claims made in this paper should be testable in a numerical simulation. Using a binary neutron star simulation in full general relativity, one could artificially impose a current quadrupolar velocity field on the stars and see if compression results. In a simulation with no initial current-quadrupole moment, it should be possible to extract information about the gravitomagnetic Love number by decomposing the late-time velocity field into vector spherical harmonics. Our claims could also be verified using simpler Newtonian and relativistic codes that model the hydrodynamics of a single neutron star. Such codes have been useful in studying the nonlinear evolution of r-modes [144, 145, 146]. These codes could presumably be modified to treat binary systems by adding tidal acceleration terms [as in Eq. (3.10)] to the hydrodynamics equations. This would also allow the effects of magnetic-type and electric-type tidal interactions to be tested separately by turning those specific terms on or off, something that is harder to do in fully relativistic binary NS simulations.

The revised Wilson-Mathews simulations [10] were performed over five years ago. It would be interesting to reexamine those simulations using higher resolutions than were possible at that time. If low resolution or some other computational artifact is not the cause of the Wilson-Mathews compression, definitively determining the compression's source will require isolating those pieces of physics that are contained in the Wilson-Mathews simulations but are not contained in other NS/NS codes (none of which indicate compression). The Wilson-Mathews method of choosing the initial data (which is neither corotational nor irrotational) and their soft equation of state appear to be two areas that are worth further investigation. In particular further work on generalizing the range of initial data

sets for NS/NS binaries is encouraged. Real neutron stars are likely to have some spin and could be differentially rotating. Such stars could not be modelled in simulations that constrain the initial data to be corotating or irrotational. Restricting the initial data to these two classes could neglect potentially observable effects such as spin-interactions and r-mode excitation [131].

As this paper was nearing completion, a new analysis of the compression effect by Miller [147] appeared. Miller performed binary NS simulations in full general relativity and found that the central density decreases with decreasing orbital separation according to $\delta\rho_c/\rho_c \propto \alpha^{1.4}$. Because the NSs in his simulations were initially corotating, Miller's results do not directly contradict those of Wilson and Mathews (their stars relax to a configuration of almost no intrinsic spin; see Sec. 3.2). Furthermore, Miller's discrepancy with the $\delta\rho_c/\rho_c \propto \alpha^6$ scaling for tidal stabilization is not necessarily surprising since calculations of the α^6 scaling [22, 91, 94] assume that the neutron stars are nonrotating. It is interesting to compare Miller's results with the central density scalings shown in Fig. 2 of Taniguchi and Gourgoulhon: A rough fit to those curves shows that $\delta\rho_c/\rho_c \propto \alpha^{5.7}$ for their irrotational simulation (with values of order $|\delta\rho_c/\rho_c| \sim 0.002 - 0.01$) and $\delta\rho_c/\rho_c \propto \alpha^3$ for their corotating simulation (with values of order $|\delta\rho_c/\rho_c| \sim 0.02 - 0.1$). This indicates that the smaller central density changes in irrotational simulations are dominated by tidal-stabilization effects scaling as $\delta\rho_c/\rho_c \propto \alpha^6$, while the larger central density changes in corotating simulations are dominated by rotational stabilization effects scaling as $\delta\rho_c/\rho_c \propto \Omega^2 \propto \alpha^3$ [where Ω is the orbital and rotational angular frequency; see Eq. (L.6)]. Although probably coincidental, it is also interesting to note that the revised Wilson-Mathews simulations also found a $\delta\rho_c/\rho_c \propto \alpha^{1.4}$ scaling, although with the sign appropriate for compression (see Table IV of [10] or

our Figure 3.4). Miller's $\delta\rho_c/\rho_c \propto \alpha^{1.4}$ scaling remains puzzling, but we speculate that it may arise from his use of initially-corotating neutron stars. Examining the central density scaling in fully-relativistic simulations of initially irrotational or arbitrarily spinning neutron stars could help to resolve the issues discussed here.

Chapter 4
The validity of the adiabatic approximation for extreme-mass-ratio inspirals

This chapter represents work performed in collaboration with Éanna Flanagan. Some version of it may appear in a future publication.

4.1 Introduction

Extreme-mass-ratio inspirals (EMRIs) are compact object binaries consisting of a small stellar mass compact object (a neutron star, white dwarf, or black hole) orbiting a much more massive black hole. These systems will be an important source of gravitational waves (GWs) for LISA (Laser Interferometer Gravitational Antenna). The detection of these systems relies on the process of matched filtering, which requires the generation of GW templates that can accurately describe the observed signal. The generation of these templates has been the focus of a great deal of research.

Because the ratio of the compact object mass m_2 (which we will idealize as a point-mass) to the black hole (BH) mass m_1 is a small number, $\varepsilon \equiv m_2/m_1 \ll 1$, EMRI systems can be studied using perturbative techniques. Much of the research for modelling EMRIs has focused on the so-called *self-force* problem: computing the order $O(\varepsilon)$ deviations from geodesic motion that arise from the interaction of the compact object with its own gravitational field. However, the self-force can be quite difficult to calculate for several reasons: 1) the standard expression for the self-force diverges at the location of the particle, 2) its evaluation requires knowledge of the entire past history of the particle, and 3) there are other technical

issues involved in computing the metric perturbations appearing in the self-force formula from the curvature perturbations that are often used in formulations of BH perturbation theory.

Because of these difficulties waveform templates have so far only been successfully computed by adding an additional simplify assumption: that the evolution of the particle's motion proceeds *adiabatically*—the timescale on which the orbital parameters (for example the semi-latus rectum p) change is much longer than the orbital period $T_{\rm orb}$. In the weak-field, slow-motion regime the radiation-reaction time scales like $T_{\rm rr} \sim (M^2/\mu)(p/M)^4$, where $M = m_1 + m_2$ and $\mu = m_1 m_2/M$, and the orbital period scales like $T_{\rm orb} \sim M(p/M)^{3/2}$. The adiabaticity assumption translates into the condition $\eta \equiv \mu/M \approx \varepsilon \ll (p/M)^{5/2}$, or equivalently the condition $\varepsilon v^5 \ll 1$, where $v \sim (M/p)^{1/2}$ is a typical orbital speed. In the slow motion region ($v \ll 1$) the adiabaticity condition is satisfied for any mass ratio. When EMRI sources are in the LISA frequency band, they will execute many orbital cycles in the $v \sim 1$ region, and the adiabaticity condition becomes $\varepsilon \ll 1$. For non-spinning holes Cutler, Kennefick, and Poisson [148] showed that the reduced mass ratio is constrained by $\eta \ll (p - 6 - 2e)^2$ when the semi-latus rectum satisfies $p \ll 6(1 + e)$. Hughes [71] derives similar constraints for spinning holes (but restricted to circular orbits). Generally, the mass ratio is more tightly constrained as the orbital separation approaches the last stable orbit.

The adiabatic assumption greatly simplifies the calculation of EMRI templates (see Section 4.1.2 below). However, because the particle undergoes so many orbits in the highly-relativistic region close to the BH, small deviations between the signal and the template due to *post-adiabatic* corrections could accumulate. Furthermore, recent work by Pound, Poisson, and Nickel [26] has indicated that post-adiabatic

corrections might be especially important for eccentric orbits. The goal of this chapter is to investigate the range of validity of the adiabatic approximation for eccentric orbits.

4.1.1 Overview of EMRI sources

EMRI sources for LISA typically consist of compact objects with masses $m_2 \sim 1 - 10^2 M_\odot$ orbiting supermassive-black holes (SMBHs) with masses $m_1 \sim 10^5 - 10^9 M_\odot$. EMRI sources for LIGO might consist of stellar mass compact objects inspiralling into intermediate-mass BHs ($m_2 \sim 10^3 - 10^4$). Typical mass ratios for these systems are $\varepsilon \sim 10^{-3} - 10^{-9}$. We will take as our "fiducial" EMRI a system with masses $m_1 \sim 10^6 M_\odot$ and $m_2 \sim 10 M_\odot$.

To form an EMRI the small compact object is first captured from the stellar cusp surrounding the SMBH. This capture occurs when other stars in the cusp perturb the compact object into a highly eccentric orbit around the black hole. These capture orbits can have initial eccentricities $1 - e_0 \sim 10^{-6} - 10^{-3}$ and initial periholion distances of $\sim 8m_1 - 100m_1$ [149]. The orbits decay by GW emission until the *last stable orbit* (LSO) is reached. The orbits then become unstable and rapidly plunge into the SMBH. Some of these EMRI sources will undergo $\sim 10^5 - 10^6$ orbits during the last year of the inspiral [150]. During this time the orbits will be close to the LSO and highly relativistic ($v \sim c$). While gravitational radiation tends to circularize orbits [151], substantial eccentricities can still remain up to the last stable orbit (LSO). Barack and Cutler [152] estimate that about half of the capture orbits will have $e \gtrsim 0.2$ at the LSO. Gair et. al [153] estimated the LISA event rates for EMRI sources and found that $\gtrsim 1000$ events are expected during LISA's mission lifetime.

The detection of EMRIs by LISA will have several scientific payoffs [154]: The masses and spins of the central BH will be measured to fractional accuracies of 10^{-4} [152]. This will provide information about the growth history of SMBHs, and will help determine if SMBHs grow mostly through accretion or mergers [155]. Measurements of the inspiralling compact object's mass to similar accuracies, combined with the measured event rate, will provide a census of the central parsec of galactic nuclei. The many orbital cycles in the highly-relativistic region near the BH will contain information on the multipole moment structure of the BH, allowing us to perform "holiodesy"—the mapping of the spacetime near the BH. This mapping will test general relativity in the strong field regime and help determine if black holes have the precise properties predicted by Einstein's theory.

4.1.2 Methods and requirements for computing templates

To meet these science goals we must face several technical challenges. To compute accurate waveform templates we need to precisely model the binary dynamics for fully-generic orbits (orbits with arbitrary eccentricity and inclination angle) around rapidly-spinning BHs. The generation of GWs for generic EMRI orbits has not been completed until recently [156].

In order to maintain phase coherence in the matched-filtering process, the phase evolution of the templates must match that of the signal to less than one cycle, $\delta\Psi \sim 1$. In order to extract the system parameters (the masses and spins for example) with high precision, this phase accuracy must be maintained for roughly the mission life time (~ 1 yr). This corresponds to a fractional phase accuracy of $\delta\Psi/\Psi \sim 1/N_{\rm cycles} \sim \varepsilon \sim 10^{-5}$, where $N_{\rm cycles}$ is the number of cycles. If one wishes only to detect the signal, computation costs limit a matched filter search to data

spans over a shorter time ($\sim$ 3 weeks) [153].

Several approaches for computing GW templates are being pursued. Full-numerical relativity is impractical for the EMRI problem as very large numbers of orbits would have to be evolved. Post-Newtonian (PN) expansions of the GW phase could be used, but they are unreliable in the strong-gravity, fast-motion region near the LSO. However PN theory has been useful for estimating event rates [153] and in determining LISA's ability to measure binary parameters [152]. We will make extensive use of PN theory in this paper to crudely estimate the error associated with the adiabatic approximation. Numerical "kludge" waveforms [157, 158] are another alternative that slowly evolve instantaneous geodesic trajectories with PN expressions for the fluxes of GW energy and angular momentum; but these methods are also limited by the use of formulas that are valid only in the weak field.

In the extreme-mass-ratio limit ($\varepsilon \ll 1$), BH perturbation theory provides the necessary tools to generate templates in the fast-motion, strong-field regime. The most general and accurate method for computing templates is the *self-force approach*. To compute the worldline of the point mass m_2 the 4-acceleration is expanded in powers of ε,

$$a^\alpha \equiv \frac{d^2x^\alpha}{d\tau^2} + \Gamma^\alpha{}_{\beta\gamma} u^\beta u^\gamma = 0 + \varepsilon a^\alpha_{(1)} + \varepsilon^2 a^\alpha_{(2)} + O(\varepsilon^3) \,, \tag{4.1}$$

where u^β is the particle's 4-velocity, $\Gamma^\alpha{}_{\beta\gamma}$ are the connection coefficients, and $a^\alpha_{(n)}$ represent corrections to the geodesic motion due to the particle's self-force

$$\frac{f^\alpha_{\rm self}}{m_2} = a^\alpha_{\rm self} = \varepsilon[a^\alpha_{(1)} + \varepsilon a^\alpha_{(2)} + O(\varepsilon^2)] \,, \tag{4.2}$$

At leading order $f^\alpha_{\rm self} \propto O(m_2^2)$. A formula for the leading-order piece $f^\alpha_{(1)}$ of the self-force in harmonic gauge has been derived by Mino, Sasaki, and Tanaka [159]

and Quinn and Wald [160] (the so-called MiSaTaQWa force):

$$f^{\alpha}_{(1)}(\tau) \equiv m_2 \varepsilon a^{\alpha}_{(1)} = \frac{1}{2} m_2 \left(g^{\alpha\beta}_{\rm kerr} + u^{\alpha} u^{\beta} \right) \left(\nabla_{\beta} h^{\rm tail}_{\lambda\sigma} - \nabla_{\lambda} h^{\rm tail}_{\beta\sigma} - \nabla_{\sigma} h^{\rm tail}_{\lambda\beta} \right) u^{\sigma} u^{\lambda} \ , \tag{4.3a}$$

$$h^{\rm tail}_{\alpha\beta} = m_2 \int_{-\infty}^{\tau_-} d\tau' \, G^{\rm ret}_{\alpha\beta\alpha'\beta'}[z(\tau), z(\tau')] u^{\alpha'}(\tau') u^{\beta'}(\tau') = h^{\rm ret}_{\alpha\beta} - h^{\rm sing}_{\alpha\beta} \ , \tag{4.3b}$$

where $g^{\alpha\beta}_{\rm kerr}$ is the background Kerr metric, $G^{\rm ret}_{\alpha\beta\alpha'\beta'}(x, x')$ is the harmonic gauge retarded Green's function, $z(\tau) \equiv z^{\alpha}(\tau)$ is the worldline of the particle as a function of its proper time τ, and τ_- is the limit of τ from below (this limit is important for removing the singular contribution $h^{\rm sing}_{\alpha\beta}$ to the particle's retarded metric perturbation $h^{\rm ret}_{\alpha\beta}$; see Poisson [161] and references therein for further discussion).

Although this formal expression can be written down, evaluating it is difficult. The difficulty primarily resides in the computation of the Green's function, which must be evaluated over the entire past history of the particle. The self-force is also divergent at the location of the point mass and this divergence must be carefully regularized. In this regularization the retarded and singular fields are decomposed in a mode sum, and the singular piece $f^{\alpha}_{l,\rm sing}$ of the total self-force is subtracted from the remaining "bare" part $f^{\alpha}_{l,\rm bare}$ of the full self-force,

$$f^{\alpha}_{(1)} = \sum_{l=0}^{\infty} f^{\alpha}_{l,\rm bare} - f^{\alpha}_{l,\rm sing} \ , \tag{4.4}$$

where $f^{\alpha}_{l,\rm bare}$ is constructed from modes of the retarded field $\nabla_{\gamma} h^{\rm ret}_{\alpha\beta}$, and $f^{\alpha}_{l,\rm sing}$ is constructed from modes of the singular field $\nabla_{\gamma} h^{\rm sing}_{\alpha\beta}$ (see Poisson [162] for a brief discussion of these issues). For the Kerr spacetime the singular piece of the force has been calculated by Barack and Ori [163]. Aside from computing the singular piece of the self-force, there are also difficulties associated with computing the retarded metric field. While this can be done in the Schwarzschild spacetime, all the necessary pieces of the metric field are not easily extracted from the Teukolsky

equation (the $l = 0$ and $l = 1$ pieces in particular). Ultimately, we wish to calculate waveforms that properly encode corrections to the particle motion due to the first-order self-force. Computing these waveforms will require second-order perturbation theory.

An alternative scheme to generate GW templates, the conservation law approach, bypasses many of the difficulties of evaluating the self-force. Using linear BH perturbation theory this approach computes the time-averaged fluxes of energy E and angular momentum L_z carried by GWs to infinity and through the event horizon. The use of time-averaged fluxes explicitly assumes the adiabatic approximation. The conservation law approach is implemented in the following way: Starting with a geodesic orbit with given values for E and L_z, the Teukolsky equation is solved and fluxes $\langle dE/dt \rangle$ and $\langle dL_z/dt \rangle$ are computed (where $\langle\rangle$ means to time-average over the period of the geodesic orbit). These fluxes are used to compute the change in the original values of E and L_z. The particle then moves to a new geodesic described by these updated values for E and L_z, and the process is iterated. The energy and angular momentum fluxes and the gravitational waveform can then be computed along this inspiral sequence [71, 72, 164, 150]. For a review of this approach see Glampedakis [165].

The conservation-law approach is limited in two important ways: First, it neglects the conservative pieces of the self-force. The self-force can be split into time-even and time-odd pieces. The conservative piece is time-even and rapidly varying, while the dissipative piece (which is responsible for the decay of the binary orbit) is time-odd and contains both rapidly varying and slowly varying pieces. While the dissipative piece first enters the post-Newtonian equations of motion at 2.5PN order, the conservative self-force enters at Newtonian order (see Appendix

M). Conservative self-forces cause corrections to the frequencies of motion, effecting the rates of periholion precession and the precession of the orbital plane about the spin axis of the BH.

Second, the conservation-law approach is limited in its ability to treat generic orbits. Orbits in the Kerr spacetime are parameterized by three constants of the motion, $E = \xi^{(t)}_\alpha u^\alpha$, $L_z = \xi^{(\phi)}_\alpha u^\alpha$, and the Carter constant $Q = K_{\alpha\beta} u^\alpha u^\beta$, where $\xi^{(t,\phi)}_\alpha$ and $K_{\alpha\beta}$ are the Killing vectors and Killing tensor of the Kerr spacetime. There is no conservation law for the infamous third-constant of the motion (there is no obvious "flux of Carter constant" carried by GWs). For circular or eccentric orbits in the equatorial plane, $Q = 0$, and a formula for the evolution of Q is not needed since such orbits remain equatorial [164]. Similarly, for circular but inclined orbits the Carter constant flux can be simply related to the time-averaged fluxes of E and L_z. But the evolution of orbits that are both inclined and eccentric requires a direct evaluation of the rate of change of the Carter constant, which requires a direct evaluation of the self-force.

Recently Mino [166] has developed an approach that allows the computation of adiabatic-order waveforms for generic orbits. His prescription for evolving the constants of the motion can be summarized as follows: Given an expression for the self-acceleration $a^\alpha_{\rm self}$ (or any non-zero 4-acceleration for that matter), the instantaneous rates of change of the constants of the motion with respect to proper time can be expressed as

$$\frac{dE}{d\tau} = \xi^{(t)}_\alpha a^\alpha_{\rm self}[h^{\rm tail}] \,, \tag{4.5a}$$

$$\frac{dL_z}{d\tau} = \xi^{(\phi)}_\alpha a^\alpha_{\rm self}[h^{\rm tail}] \,, \tag{4.5b}$$

$$\frac{dQ}{d\tau} = 2K_{\alpha\beta} u^\alpha a^\beta_{\rm self}[h^{\rm tail}] \,. \tag{4.5c}$$

In the above equations $a^{\alpha}_{\rm self}[h^{\rm tail}]$ is determined using the first-order self-force expressions in Eqs. (4.2) and (4.3). Using symmetry properties of the Kerr spacetime and the self-force, Mino [166] showed that if only the time-averages of the expressions in Eqs. (4.5) are needed (which is the case if one is using the adiabatic approximation), then these time-averaged fluxes can be computed using the radiative metric perturbation $h^{\rm rad}_{\alpha\beta} = \frac{1}{2}(h^{\rm ret}_{\alpha\beta} - h^{\rm adv}_{\alpha\beta})$ instead of $h^{\rm tail}_{\alpha\beta}$:

$$\left\langle \frac{dE}{d\tau} \right\rangle = \xi^{(t)}_{\alpha} a^{\alpha}_{\rm self}[h^{\rm rad}] \,, \tag{4.6a}$$

$$\left\langle \frac{dL_z}{d\tau} \right\rangle = \xi^{(\phi)}_{\alpha} a^{\alpha}_{\rm self}[h^{\rm rad}] \,, \tag{4.6b}$$

$$\left\langle \frac{dQ}{d\tau} \right\rangle = 2K_{\alpha\beta} u^{\alpha} a^{\beta}_{\rm self}[h^{\rm rad}] \,. \tag{4.6c}$$

Here $h^{\rm ret}_{\alpha\beta}$ and $h^{\rm adv}_{\alpha\beta}$ are the retarded and advanced solutions of the linearized-curved-spacetime wave equation

$$\nabla^{\mu}\nabla_{\mu}\bar{h}_{\alpha\beta} + 2R_{\alpha\gamma\beta\delta}\bar{h}^{\gamma\delta} = -16\pi T_{\alpha\beta} \,, \tag{4.7}$$

where $\bar{h}_{\alpha\beta} = h_{\alpha\beta} - \frac{1}{2} g^{\rm kerr}_{\alpha\beta} h^{\gamma}{}_{\gamma}$ is the traced-reversed metric perturbation, $R_{\alpha\gamma\beta\delta}$ is the Riemann tensor, and the harmonic gauge conditions $\nabla_{\alpha}\bar{h}^{\alpha\beta} = 0$ have been applied [167]. The self-acceleration $a^{\alpha}_{\rm self}[h^{\rm rad}]$ in Eq. (4.6) is computed by substituting $h^{\rm rad}_{\alpha\beta}$ into Eq. (4.3) in place of $h^{\rm tail}_{\alpha\beta}$. The advantage of using Mino's prescription, which we shall refer to as *adiabatic radiation reaction*, is that computing $h^{\rm rad}_{\alpha\beta}$ is much simpler than computing $h^{\rm tail}_{\alpha\beta}$. Like the conservation-law approach (in which Mino's prescription is implicit), adiabatic radiation reaction also neglects the conservative pieces of the self-force. But it has the advantage of allowing generic orbit evolutions within the adiabatic limit. Explicit expressions for the time rate of change of the Carter constant have been derived for scalar [154, 168] and gravitational [169, 170] radiation reaction. These expressions have forms similar to those for the energy

and angular momentum fluxes obtained from frequency-domain decompositions of the Teukolsky equation [cf. Eq.(B.17d) of Appendix B]:

$$\left\langle \frac{dQ}{dt} \right\rangle = \sum_{lmn_r n_\theta} F[Z^H_{lmn_r n_\theta}, Z^\infty_{lmn_r n_\theta}, \omega_{lmn_r n_\theta}] \,, \tag{4.8}$$

where the $Z_i^{\mathrm{H},\infty}$ are the coefficients in a mode-expansion of Ψ_4, the ω_i are the harmonics of the orbital frequencies of the Kerr spacetime, F is some known function of its arguments, and the indices l, m, n_r, n_θ are associated with the spheroidal harmonic and orbital decompositions of the Weyl scalar Ψ_4.

4.1.3 Adiabatic and post-adiabatic scalings

Adiabatic radiation reaction gives the correct prescription for computing the leading-order piece of gravitational waveforms in an expansion in $T_{\mathrm{orb}}/T_{\mathrm{rr}} \sim \varepsilon$. Recently, Hinderer and Flanagan [171] have determined which pieces of the self-force are required for computing the adiabatic and post-adiabatic contributions to the gravitational waveforms. We summarize their result below.

Begin by expanding the self-acceleration in powers of ε,

$$a^\mu = \varepsilon \left[a^\mu_{1,\mathrm{diss}} + a^\mu_{1,\mathrm{cons}} + \varepsilon a^\mu_{2,\mathrm{diss}} + \varepsilon a^\mu_{2,\mathrm{cons}} + O(\varepsilon^2) \right] \,, \tag{4.9}$$

where $a^\mu_{1,\mathrm{diss}}$ and $a^\mu_{1,\mathrm{cons}}$ are the leading-order dissipative and conservative pieces of the self-acceleration, and the other terms are their higher-order corrections. The leading-order piece $a^\mu_{(1)} = a^\mu_{1,\mathrm{diss}} + a^\mu_{1,\mathrm{cons}}$ is known and is given by Eqs. (4.3). The second-order self-acceleration $a^\mu_{(2)} = a^\mu_{2,\mathrm{diss}} + a^\mu_{2,\mathrm{cons}}$ is not yet known. The piece $a^\mu_{1,\mathrm{diss}}$ depends only on $h^{\mathrm{rad}}_{\alpha\beta}$ and is what contributed to the $a^\alpha_{\mathrm{self}}[h^{\mathrm{rad}}]$ terms in Eqs. (4.6).

Using a two-timescale expansion of an action-angle formulation of the equations of motion in the Kerr spacetime [including the self-acceleration terms in Eq. (4.9)],

Hinderer and Flanagan [171] showed that (in the $\varepsilon \to 0$ limit) the dynamical angle variables [for example the orbital phase $\phi(t)$)] can be expanded as

$$\phi(t;\varepsilon) = \frac{1}{\varepsilon}\left[\phi_1 + \varepsilon^{1/2}\phi_{1.5} + \varepsilon\phi_2 + O(\varepsilon^2)\right] \ . \tag{4.10}$$

They further showed that ϕ_1 only depends on $a^{\mu}_{1,\mathrm{diss}}$ while ϕ_2 depends on *both* $a^{\mu}_{1,\mathrm{cons}}$ and $a^{\mu}_{2,\mathrm{diss}}$ (see also [168]). The $\phi_{1.5}$ piece arises from resonances that occur when at least two of the orbital frequencies of the particle motion are related by a factor that is the ratio of two integers. Hinderer and Flanagan [171] have found that the $\phi_{1.5}$ term depends on $a^{\mu}_{1,\mathrm{diss}}$ and could depend on $a^{\mu}_{1,\mathrm{cons}}$ as well. Further investigation of this $O(\varepsilon^{-1/2})$ resonance term is ongoing, but preliminary results indicate that it is small [171]. Because it is small, and because it does not appear in the post-Newtonian equations of motion, we will ignore the $\phi_{1.5}$ contribution to the post-adiabatic phase in this chapter. These relations between the orbital phase and the pieces of the self-force are important because a great deal of work by the radiation-reaction community is focused on calculating $a^{\mu}_{1,\mathrm{cons}}$, with the expectation that it will allow the computation of post-adiabatic [O(1)] pieces of the waveform. While the first-order self-force formalism will allow the computation of both adiabatic waveforms and the small order $O(\varepsilon^{-1/2})$ resonance contributions, the second-order piece of the self-force will also be needed to compute the post-adiabatic corrections to order $O(1)$. For the non-resonant case this observation has also been made by Burko [172].

4.1.4 This chapter

The phase of the gravitational wave Ψ is proportional to the orbital phase $\phi(t)$. Equation (4.10) tells us that while the leading-order (adiabatic) piece of the GW

phase is large, $\Psi_1 \sim O(1/\varepsilon)$, the (non-resonant) post-adiabatic contributions are of order unity over the entire inspiral, $\Psi_2 \sim O(1)$. Since matched filtering requires $O(1)$ phase accuracy, these post-adiabatic corrections could potentially limit the detectability of EMRI sources. To accurately estimate the errors associated with ignoring these post-adiabatic terms, we would need to compute the self-force to second order in ε. Since the tools to do this are not available, we will use post-Newtonian theory to crudely estimate these errors.

Post-Newtonian theory is not well-suited to computing these post-adiabatic errors. It is accurate only when $(v/c)^2 \sim (M/r) \ll 1$. This condition is violated for EMRIs in the LISA band, which spend many orbital cycles [$N_{\rm cycles} \sim 1/(\varepsilon v^5)$] in the region where $v \sim c$. Nevertheless, since we are only interested in a rough estimate to help gauge the validity of the adiabatic approximation, we will apply post-Newtonian theory regardless of its deficiencies.

There is a further subtlety that must be addressed concerning the meaning of the words "adiabatic approximation." (In the following discussion and throughout this chapter we ignore the $O(\varepsilon^{-1/2})$ resonant contribution to the post-adiabatic error.) There are three separate but related ways in which this phrase is used in the context of relativistic binary dynamics: (1) The first meaning is that there exists a separation of time scales in a binary inspiral: Namely that the radiation reaction timescale is much longer than the orbital timescale, $T_{\rm rr} \gg T_{\rm rr}$. This in turn implies the condition $\varepsilon v^5 \ll 1$ (see Sec. 4.1). In post-Newtonian theory $\varepsilon \lesssim 1$, but $v^2 \ll 1$, so the adiabatic condition (1) is always satisfied where ever PN theory is valid; but fulfilling the adiabatic condition does not imply that PN theory must be valid. In fact, when the binary mass ratio ε is only moderately small, the upper bound on the adiabatic condition $\beta \equiv \varepsilon v^5 \ll 1$ must be extremely small for

the upper bound on the PN condition $\alpha \equiv v^2 \ll 1$ to be satisfied. This can be summarized by: "post-Newtonian implies adiabaticity, but adiabaticity does not imply post-Newtonian".

(2) The second meaning of "adiabaticity" is that used in the context of modelling EMRIs with BH perturbation theory. It is simply the specialization of condition the $T_{\rm rr} \gg T_{\rm orb}$ to situations where $v \sim 1$: namely the condition $\varepsilon \ll 1$. Definition (2) implies that definition (1) is satisfied, but not vice-versa. This simply says that neither the PN approximation nor the separation of timescales $T_{\rm rr} \gg T_{\rm orb}$ implies that mass ratios must be small ($\varepsilon \ll 1$).

(3) The third use of "adiabatic approximation" is that which occurs in the post-Newtonian literature and refers to the distinction between effects that are "secular" (building up over a long time) and those that are "periodic" or "dynamical" (rapidly varying effects that average to zero over long timescales). In this context, "adiabatic radiation reaction" refers to secular changes of the orbital elements due to dissipative self-forces (which enter at 2.5PN, 3.5PN, and higher orders) and their corresponding effects on the gravitational waveform. Unlike the definition (2) of adiabaticity, definition (3) does not require that ε be small. In this PN context, "post-adiabatic" effects refer to periodic variations in the orbital elements induced by dissipative radiation-reaction terms; these variations average to zero over several orbital timescales.

There are a few important things to note concerning these three definitions of the adiabatic approximation. Definition (1) is the most general while (3) is the least general. Definition (2) is the most restrictive in the sense that neither (1) nor (3) imply that (2) must be true. We can summarize the relationships between

these definitions as follows:

$$\begin{aligned}
(1) &\nrightarrow (2) \\
(1) &\rightarrow (3) \\
(2) &\rightarrow (1) \\
(2) &\rightarrow (3) \\
(3) &\rightarrow (1) \\
(3) &\nrightarrow (2)\,,
\end{aligned} \tag{4.11}$$

where our notation means "definition (p) implies ($\rightarrow$) or does not imply ($\nrightarrow$) that definition (q) is true." Definition (3) can be especially confusing because it implies that there are "adiabatic" and "post-adiabatic" corrections within PN theory, while definition (1) implies that all of PN theory operates under the adiabatic assumption (since $v^2 \ll 1$ must always be satisfied). There is a further confusion when definitions (3) and (2) are compared. In PN theory the "post-adiabatic" corrections according to definition (3) affect the waveform at $O(\varepsilon)$; but according to definition (2), post-adiabatic corrections affect the waveform at $O(\varepsilon^0)$. This is discussed further in Appendix N.

Since we are interested in EMRIs—systems in which definition (2) is always satisfied, we will consistently mean definition (2) whenever we refer to "adiabatic" or "post-adiabatic" effects. We will use definition (2) even when dealing with post-Newtonian theory, despite the widespread use of definition (3) in the literature. Whether we are working in the language of BH perturbation theory and self-forces, or in the language of PN theory, "adiabatic" will always refer to effects that occur at leading order in the mass ratio ε, and "post-adiabatic" will always refer to the

next order term in an expansion in ε.[1]

For circular orbits around spinning BHs, Drasco, Flanagan, and Hughes (DFH) [154] have used a post-Newtonian expansion of the GW phase to 3.5PN order to estimate the errors cause by ignoring post-adiabatic terms. They found errors of $\lesssim 1$ cycle over the last year of inspiral, concluding that adiabatic waveforms will not be accurate enough for extracting the system parameters from the GW signal with high precision. Adiabatic waveforms will, however, be accurate enough to be used as detection templates. Here, we will extend their calculations to orbits with small eccentricity e by calculating the additional eccentricity-dependent $[O(e^2)]$ corrections to the GW phase up to 2PN order. We will ignore any spin-dependence to these eccentricity corrections. We will find that the conclusions of DFH [154] can be extended to orbits with mild eccentricity ($e \lesssim 0.2$).

In the next section (4.2 we will discuss how the GW phase is defined in post-Newtonian theory and give general expressions for computing its adiabatic and post-adiabatic pieces. A brief discussion of the adiabatic and post-adiabatic pieces of the post-Newtonian equations of motion is found in Appendix M. In Section 4.3 we explicitly compute the GW phase for orbits with small eccentricity, and then examine the resulting post-adiabatic phase error in Section 4.4.

The extension to eccentric orbits was partly motivated by recent results by Pound, Poisson, and Nickel [26]. They examined a toy-model of a point mass with an electric charge orbiting a much more massive star. The electric charge was influenced by the Newtonian gravity of the star and the particle's own electromagnetic

[1]Note that this definition of "post-adiabatic" ignores the resonant contribution that enters at order $O(\varepsilon^{-1/2})$. As such a term does not appear in the post-Newtonian expansion of the GW phase, we ignore it in the calculations in this chapter.

self-force. They found that ignoring the conservative pieces of the electromagnetic self-force (as is done in the adiabatic approximation) causes very large errors in the orbital phase when the orbit is eccentric. For orbits with moderate or large eccentricities, our low-eccentricity results are no longer valid, and it is not clear if the adiabatic approximation will be sufficient to detect EMRIs with substantial eccentricity. We discuss these issues further in Section 4.5, and give our conclusions in Section 4.6.

4.2 The gravitational wave phase in the post-Newtonian approximation

4.2.1 Derivation of the GW phase

We begin by deriving the phase $\Psi(f)$ of the Fourier transform of the dominant, $n = 2$ harmonic of the gravitational waveform. For nearly circular binaries the measured strain produced by the gravitational wave at the detector is given by [173]

$$h(t) = A(t) \cos \phi_{\rm gw}(t) \ , \tag{4.12}$$

where $A(t)$ depends on the sky-position and orientation angles of the binary, the distance to the source, the masses, and the orbital frequency; and $d\phi_{\rm gw}/dt = 2\pi f$, where $\phi_{\rm gw}(t)$ is the phase of the GW as a function of time and f is the GW frequency. Up to a constant, $\phi_{\rm gw}$ is twice the orbital phase. For eccentric orbits this formula has the more general form

$$h(t) = \sum_{n=1}^{\infty} A_n(t) \cos[\frac{n}{2}\phi_{\rm gw}(t) + \delta_n] \ , \tag{4.13}$$

where n is the harmonic of the fundamental GW frequency (twice the azimuthal or ϕ-orbital frequency), and A_n and δ_n have a complicated dependence on the eccentricity and other system parameters. There are post-Newtonian corrections to the GW amplitude that we are ignoring in Eqs. (4.12) and (4.13). These corrections cause power to be emitted in orbital harmonics with $n \neq 2$ even in the case of circular orbits [173]. We ignore these small corrections to the amplitude, but we include post-Newtonian corrections to the gravitational wave phase. For small eccentricity ($e \lesssim 0.2$) most of the GW power is still radiated into the $n = 2$ harmonic of the orbital frequency, so we can ignore the harmonics with $n \neq 2$ and simply use Eq. (4.12).

To compute the Fourier transform of $h(t)$,

$$\tilde{h}(f) \equiv \int_{-\infty}^{\infty} h(t) e^{2\pi i f t}\, dt \,, \tag{4.14}$$

we use the stationary phase approximation [173],

$$\tilde{h}(f) \approx \frac{1}{2} A(t) \Big(\frac{df}{dt}\Big)^{-1/2} \exp[i\Psi(f)] \,, \tag{4.15}$$

where

$$\Psi(f) = 2\pi f t(f) - \phi_{\rm gw}(f) - \pi/4 \tag{4.16}$$

is the phase of the Fourier transform of the GW signal—the quantity we wish to calculate[2].

[2]Droz et. al [174] have computed corrections to the stationary phase approximation. They found that the leading order correction to the GW phase is $\delta\Psi = \frac{92}{45} v^5$, where $v \equiv (\pi \mathcal{M} f)^{1/3}$ and $\mathcal{M} = (m_1 m_2)^{3/5}/(m_1 + m_2)^{1/5}$ is the chirp mass. These corrections are therefore at order $\delta\Psi = O(\varepsilon)$ and contribute to the post-post-adiabatic corrections. However, there are additional corrections $\delta\Psi_w$ that come from the truncation of the time interval over which the Fourier transform is performed (the "windowing" of the time series). These corrections can enter at lower orders than $\delta\Psi$. Their scaling with mass ratio is more complicated, but they can scale as low as $\delta\Psi_w \sim O(\varepsilon^{1/10})$ and as high as $\delta\Psi_w \sim O(\varepsilon^{7/10})$. Since these errors

Using $d\phi_{\rm gw}/df = 2\pi f/(df/dt)$, $dt = df/(df/dt)$, and integrating from some reference GW frequency f_i gives

$$\phi_{\rm gw}(f) = \int_{f_i}^{f} \frac{2\pi f'}{df'/dt}\, df' + \phi_i \ , \quad \text{and} \tag{4.17}$$

$$t(f) = \int_{f_i}^{f} \frac{df'}{df'/dt} + t_i \ , \tag{4.18}$$

where ϕ_i and t_i are the GW phase and time at the detector when the GW frequency is f_i. Plugging these expressions into Eq. (4.16) gives the expression for the phase (see Appendix A of [175]):

$$\Psi = 2\pi f t_i - \phi_i - \pi/4 - 2\pi \int_{f_i}^{f} \tau(f') \left(1 - \frac{f}{f'}\right) df' \ , \tag{4.19}$$

where $\tau = f/(df/dt)$. Choosing the reference frequency, time, and phase to be their values at coalescence [$t_i = t_c, \phi_i = \phi_c, f_i = f_c = \infty$], the GW phase becomes

$$\Psi = 2\pi f t_c - \phi_c - \pi/4 + 2\pi \int_{f}^{\infty} \frac{f'}{df'/dt} \left(1 - \frac{f}{f'}\right) df' \ . \tag{4.20}$$

To match the conventions in Appendix A of DFH we transform the coalescence phase, $\phi_c \to \phi_c' = -\phi_c - \pi/4$, and get

$$\Psi = 2\pi f t_c + \phi_c + 2\pi \int_{f}^{\infty} \frac{f'}{df'/dt} \left(1 - \frac{f}{f'}\right) df' \ . \tag{4.21}$$

The GW phase for circular binaries can also be derived by differentiating Eq. (4.16) and using $d\phi_{\rm gw}/df = 2\pi f(dt/df)$ to get

$$\frac{d\Psi}{df} = 2\pi t(f) \ . \tag{4.22}$$

---

are no larger than the $O(1)$ post-adiabatic terms we seek to estimate, and because our estimates are already limited by our use of the post-Newtonian approximation, we will ignore all of these corrections here.

Differentiating again to get $d^2\Psi/df^2 = 2\pi(dt/df)$, and using $df/dt = \dot{E}/(dE/df)$ (where E is the orbit energy) and the GW luminosity $\mathcal{L}_{\rm GW} = -\dot{E}$ gives[3]

$$\frac{d^2\Psi}{df^2} = -2\pi \frac{dE/df}{\mathcal{L}_{\rm GW}(f)} \,. \tag{4.23}$$

Integrating twice yields an expression equivalent to Eq. (4.21).

4.2.2 Adiabatic and post-adiabatic pieces of the GW phase

Once an expression for the GW phase is in hand, we need to isolate the leading and sub-leading order pieces in ε. To do this we begin by writing the GW phase in Eq. (4.21) as

$$\Psi(f) = 2\pi f t_c + \phi_c + \frac{3}{128\eta\xi_\phi^{5/3}}\mathcal{F} \,, \tag{4.24}$$

where $\xi_\phi = (\pi M f)$, $M = m_1 + m_2$, and $\mathcal{F}$ is a function of the frequency, masses, spins, eccentricity, and other intrinsic quantities that describe the binary. For circular binaries where one member is taken to be a spinning BH, the PN expansion of $\mathcal{F}$ up to 3.5PN order (and including the 1.5PN term for the BH's spin) is given (in different notation) by Eq. (A9) of DFH[4]:

$$\mathcal{F}(\xi_\phi, \eta) = 1 + \xi_\phi^{2/3}\left(\frac{3715}{756} + \frac{55}{9}\eta\right) + \xi_\phi\left[-16\pi + \frac{a}{3}\left(113\nu^2 + 75\eta\right)\right]$$

[3]Note that Eq. (A.7) of DFH differs by a (-) sign due to a different choice of conventions.

[4]Because of recently discovered errors in the equation for the GW luminosity [176, 177], Eqs. (A.9) and (A.10) of DFH contain errors. The corrected formula is given in Eq. (4.25) above. In the notation of DFH the following terms in their Eq. (A.9) should be modified: the coefficient of the $\pi\eta y^7$ term should be $+378515/1512$ instead of $1014115/3024$; the coefficient of the $\pi\eta^2 y^7$ term should be $-74045/756$ instead of $-36865/378$; and the coefficient of the $\pi y^5 \eta \log(y)$ term should be $-65/3$ instead of $+5$. In our notation $y \equiv \xi_\phi^{1/3}$. These changes lead to $\sim 15\%$ changes in the quoted values for the error in the number of cycles and in their Figure 2, but they do not change their overall conclusions.

$$+\xi_\phi^{4/3}\left(\frac{15293365}{508032}+\frac{27145}{504}\eta+\frac{3085}{72}\eta^2\right)+\pi\xi_\phi^{5/3}\ln\xi_\phi\left(\frac{38645}{756}-\frac{65}{9}\eta\right)$$
$$+\xi_\phi^2\left[\frac{6848}{21}\left(\frac{11583231236531}{1530761379840}-\gamma-\frac{70\pi^2}{107}-2\ln 2-\frac{1}{3}\ln\xi_\phi\right)\right.$$
$$\left.+\left(\frac{2255\pi^2}{12}-\frac{15737765635}{3048192}\right)\eta+\frac{76055}{1728}\eta^2-\frac{127825}{1296}\eta^3\right]$$
$$+\xi_\phi^{7/3}\left(\frac{77096675\pi}{254016}+\frac{378515\pi}{1512}\eta-\frac{74045\pi}{756}\eta^2\right)\,. \quad (4.25)$$

In this expression $\gamma \approx 0.5772156649\ldots$ is Euler's constant, a is the BH's dimensionless spin parameter, and $\nu = m_1/M = 1/2 + \sqrt{1/4-\eta}$. The equivalent expression for binaries with small eccentricity (and ignoring spins) will be derived in Sec. 4.3 below up to 2PN order.

Consider a change in the phase of the form $\Psi(f) \to \Psi(f) + \Psi_0 + 2\pi f \Delta t$: such changes are not related to intrinsic properties of the binary—Ψ_0 is an arbitrary constant that simply causes an overall phase shift, while Δt corresponds to a change in the time of arrival of the signal (eg., resulting from the relative motion of the source and observer). We will therefore focus on the observable quantity $\Psi - 2\pi f t_c - \phi_c$, or equivalently on

$$\frac{d^2\Psi}{df^2} \equiv G(f, m_1, m_2)\,. \quad (4.26)$$

Now we can consider the adiabatic and post-adiabatic pieces of the GW phase. Expanding G in powers of the small mass m_2 at fixed f and m_1 yields

$$G(f, m_1, m_2) = \frac{1}{m_2}[G_0(f, m_1) + G_1(f, m_1)m_2 + G_2(f, m_1)m_2^2 + \cdots]\,. \quad (4.27)$$

G can also be expanded in powers of μ at fixed M and f as

$$G(f, m_1, m_2) = \frac{1}{\mu}[\hat{G}_0(f, M) + \hat{G}_1(f, M)\mu + \hat{G}_2(f, M)\mu^2 + \cdots]\,; \quad (4.28)$$

this defines the functions $\hat{G}_n$. Note that G_0 and $\hat{G}_0$ coincide. Equation (4.27) can be computed from (4.28) by substituting $M = m_1(1+\varepsilon)$, $\eta = \varepsilon/(1+\varepsilon)^2$, and $\mu = m_2/(1+\varepsilon)$, and expanding in ε.

The adiabatic approximation to the phase consists of keeping only the leading order piece of (4.27),

$$G_{\rm ad} = \frac{G_0(f, m_1)}{m_2} \ . \tag{4.29}$$

This is simply calculated by substituting $\eta = \varepsilon/(1+\varepsilon)^2$ and $\xi_\phi = (1+\varepsilon)\tilde{\xi}_\phi$ (where $\tilde{\xi}_\phi = \pi m_1 f$) into Eq. (4.24), series expanding $\Psi \sim O(\varepsilon^{-1}) + O(1) + O(\varepsilon) + O(\varepsilon^2) + \cdots$, and taking the limit

$$\Psi_{\rm ad} = \frac{1}{\varepsilon} \lim_{\varepsilon \to 0}(\varepsilon \Psi) \ . \tag{4.30}$$

The phase error due to the adiabatic approximation can be calculated by twice integrating the function

$$\begin{aligned} \Delta G &= G(f, m_1, m_2) - G_{\rm ad} = G_1(f, m_1) + G_2(f, m_1) m_2 + \cdots & \text{(4.31a)} \\ &= \hat{G}_1(f, M) + \hat{G}_2(f, M)\mu + \cdots + \frac{G_0(f, M)}{\mu} - \frac{G_0(f, m_1)}{m_2} \ , & \text{(4.31b)} \end{aligned}$$

or equivalently by calculating

$$\Delta\Psi = \Psi - \Psi_{\rm ad} \ . \tag{4.32}$$

The piece of this phase error due only to post-1-adiabatic [$O(\varepsilon^0)$] terms is found by taking the limit

$$\Delta\Psi^{(1)} = \lim_{\varepsilon \to 0} \Delta\Psi \ . \tag{4.33}$$

The quantity ΔG (or $\Delta\Psi$) describes the total phase error that results from using an adiabatic waveform instead of a post-adiabatic one, assuming that the binary parameters (e.g., the masses and spins) are known.

When detecting a GW, the masses (m_1', m_2') of the best-fit template will generally be different from the true masses (m_1, m_2). The total phase error due to the adiabatic approximation can therefore be split into two pieces, $\Delta G = \Delta G_1 + \Delta G_2$, where

$$\Delta G_2 = \frac{G_0(f, m_1')}{m_2'} - \frac{G_0(f, m_1)}{m_2} \tag{4.34}$$

is the piece of the error that comes from using the measured rather than the true values of the masses in the adiabatic waveform. The remaining error in the GW phase ΔG_1 is given by combining Eqs. (4.31) and (4.34):

$$\Delta G_1 = \hat{G}_1(f, M) + \hat{G}_2(f, M)\mu + \cdots + \frac{G_0(f, M)}{\mu} - \frac{G_0(f, m_1')}{m_2'} \ . \tag{4.35}$$

Now consider the choice of masses $m_1' = M$ and $m_2' = \mu$, which results in[5]

$$\Delta G_1(f, m_1, m_2) = G(f, m_1, m_2) - \frac{G_0(f, M)}{\mu} = \hat{G}_1(f, M) + \hat{G}_2(f, M)\mu + \cdots \ , \tag{4.36}$$

$$\text{and} \quad \Delta G_2(f, m_1, m_2) = \frac{G_0(f, M)}{\mu} - \frac{G_0(f, m_1)}{m_2} \ . \tag{4.37}$$

This choice does not change the ability of the phase function to act as an efficient template. While ΔG_2 makes a large contribution to the total phase error ΔG, it will not impede detection. The two functions ΔG and ΔG_1 simply change which mass parameters are measured: a template based on the phase function constructed from ΔG will measure the mass combination (m_1, m_2), while a template constructed from ΔG_1 will measure the combination (M, μ). Each set of mass parameters can be determined if the other is known. The choice ΔG_1 is somewhat

[5]Note that in DFH, m_2 should be replaced by μ in the denominator of the last term in Eq. (A.5) and in the denominator of the second term in Eq. (A.6). These errors were only in the description of the derivation and did not affect the final results.

easier to construct from a post-Newtonian expansion of the GW phase. The explicit phase error corresponding to ΔG_1 can simply be computed by removing the pieces of $\mathcal{F}$ that contain no η-dependence:

$$\Delta\Psi_1 = \frac{3}{128\eta\xi_\phi^{5/3}}\left[\mathcal{F}(\xi_\phi,\eta) - \mathcal{F}(\xi_\phi,\eta=0)\right] . \tag{4.38}$$

The contribution to $\Delta\Psi_1$ due only to post-1-adiabatic [$O(\varepsilon^0)$] terms is found from the limit

$$\Delta\Psi_1^{(1)} = \lim_{\eta\to 0}\Delta\Psi_1 . \tag{4.39}$$

4.3 Gravitational wave phase for orbits with small eccentricity

We now explicitly calculate the GW phase for eccentric orbits. We will compute the Newtonian, 1PN, 1.5PN, and 2PN pieces of $\mathcal{F}$ in the limit of small orbital eccentricity ($e \ll 1$). The Newtonian piece of this phase error is computed in Appendix A of [175]; we will extend that derivation to 2PN order. The final expression for the phase will depend only on the GW frequency f, the masses, and the initial eccentricity e_0 at some initial frequency f_0.

To describe eccentric, equatorial orbits up to 2PN order, we make use of the "generalized quasi-Keplerian" formalism [178, 179, 180] as described by Damour, Gopakumar, and Iyer (DGI) [181]. This formalism has recently been extended to 3PN order by Memmesheimer, Gopakumar, and Schäfer [182]. By ignoring dissipative effects at 2.5PN and 3.5PN order, the generalized quasi-Keplerian formalism provides an analytic description of the conservative aspects of the orbital motion in a bound binary system. The effects of radiation reaction can be accounted for by allowing the constants of motion that appear in the quasi-Keplerian description to

vary with time. The time variation of these constants is related to the 2.5PN and 3.5PN terms in the PN equations of motion. Including radiation reaction effects allows the calculation of changes in the orbital parameters and the resulting GW signal. These computations, focusing on computing the phase of the GW signal to 2.5PN order, have been performed by DGI. Their work has recently been extended to 3.5PN order by Königsdörffer and Gopakumar [183]. In Appendix N we briefly review some aspects of this formalism and list formulas that we will make use of in the rest of this chapter.

The computation of the GW phase $\Psi(f)$ in the $e \ll 1$ limit essentially involves computing the integral in Eq. (4.21). This requires an expression for the rate of change of the GW frequency df/dt as a function of the frequency f. Such an expression was first derived by Peters [151] at lowest order (he actually derived the rates of change of the semimajor axis and eccentricity, from which the change in the orbital frequency is easily deduced), and is available up to 2PN order in Refs. [181, 183]. The necessary expressions for the evolution of the orbital frequency and eccentricity are given in Eqs. (N.8).

The frequency that appears in those expressions is the radial angular frequency or the "mean motion" $n = 2\pi/P \equiv \omega_r$, where P is the radial orbit period (time from periastron to periastron). But for small eccentricities ($e \lesssim 0.2$), most of the GW power is emitted at twice the azimuthal (ϕ) orbital frequency ω_ϕ. This is the frequency that arises from Fourier transforms of the GW polarizations, which depend directly on the sines and cosines of $2\phi(t)$, where $\phi(t)$ is the orbital phase. Our first step is therefore to relate the frequencies ω_r and ω_ϕ. These are related by the periastron advance rate [see Eqs. (N.14)–(N.16)]. Since the GW frequency is related to the ω_ϕ by $f = \omega_\phi/\pi$, we define the dimensionless an-

gular frequencies $\xi_\phi = \pi M f = M\omega_\phi$ and $\xi = Mn$. These variables scale like $\xi \sim \xi_\phi \sim (M/r)^{3/2} \sim v^3$, where r is the orbital separation and v is the orbital velocity. The dimensionless angular frequencies will naturally serve as our post-Newtonian expansion parameters[6].

Differentiating Eq. (N.14) with respect to time relates the rates of change of ξ, ξ_ϕ, and the time eccentricity e_t (see Appendix N for definitions):

$$\frac{d\xi_\phi}{dt} = \left[1 + \frac{5\xi^{2/3}}{(1-e_t^2)} + \frac{7}{12}\xi^{4/3}\frac{78 - 28\eta + (51-26\eta)e_t^2}{(1-e_t^2)^2}\right]\frac{d\xi}{dt} + \left\{1 + \frac{\xi^{2/3}}{(1-e_t^2)}\left[\frac{69}{4} - \frac{41}{6}\eta + \left(\frac{17}{4} - \frac{13}{6}\eta\right)e_t^2\right]\right\}\frac{6e_t\xi^{5/3}}{(1-e_t^2)^2}\frac{de_t}{dt}\,, \quad (4.40)$$

where we have kept terms up to 2PN order. We also need to invert the relation between the two frequencies in Eq. (N.14), which yields

$$\xi = \xi_\phi\left\{1 - \frac{3\xi_\phi^{2/3}}{(1-e_t^2)} - \frac{15\xi_\phi^{4/3}}{(1-e_t^2)^2}\left[\frac{3}{10} - \frac{7}{15}\eta + \left(\frac{17}{20} - \frac{13}{30}\eta\right)e_t^2\right]\right\}\,. \quad (4.41)$$

Combining Eqs. (4.40) and (4.41) with Eqs. (N.8) and expanding to 2PN order gives the rate of change of the GW frequency and the time eccentricity,

$$\begin{aligned}\frac{d\xi_\phi}{dt} = \frac{96}{5}\frac{\eta}{M}\xi_\phi^{11/3}\Bigg\{&\frac{1 + \frac{73}{24}e_t^2 + \frac{37}{96}e_t^4}{(1-e_t^2)^{7/2}} + \frac{\xi_\phi^{2/3}}{5376(1-e_t^2)^{9/2}}\Big[-(11888 + 14784\eta) \\ &+ (87720 - 159600\eta)e_t^2 + (171038 - 141708\eta)e_t^4 + (11717 - 8288\eta)e_t^6\Big] \\ &+ \frac{\xi_\phi^{4/3}}{580608(1-e_t^2)^{11/2}}\Big[-360224 - 92846560e_t^2 + 783768e_t^4 + 83424402e_t^6 \\ &+ 3523113e_t^8 - 18(-250832 - 859152e_t^2 + 11511348e_t^4 + 6839357e_t^6 + 181110e_t^8)\eta \\ &+ 84(22656 + 729548e_t^2 + 1982215e_t^4 + 771772e_t^6 + 23384e_t^8)\eta^2 \\ &- 3024\sqrt{1-e_t^2}(96 + 4268e_t^2 + 4386e_t^4 + 175e_t^6)(2\eta - 5)\Big]\Bigg\} + M\left(\frac{d\bar{n}}{dt}\right)\Big|_{\text{Tail}} \quad (4.42)\end{aligned}$$

[6]In the equations in this chapter the symbols n and e_t refer to the secularly varying pieces of those quantities, denoted by $\bar{n}$ and $\bar{e}_t$ in Appendix N. Also the n used in the rest of this chapter is not to be confused with the harmonic index used in Section 4.2.1.

and

$$\frac{de_t}{dt} = -\frac{\eta}{M} e_t \xi_\phi^{8/3} \Bigg\{ \frac{304 + 121 e_t^2}{15(1-e_t^2)^{5/2}} + \frac{\xi_\phi^{2/3}}{2520(1-e_t^2)^{7/2}} \Bigg[-(67608 + 228704\eta) + (718008 - 651252\eta) e_t^2 + (125361 - 93184\eta) e_t^4 \Bigg] - \frac{\xi_\phi^{4/3}}{30240(1-e_t^2)^{9/2}} \Bigg[15198032 + 36993396 e_t^2 - 46579718 e_t^4 - 3786543 e_t^6 + 6(-2251560 + 5930538 e_t^2 + 13018711 e_t^4 + 724142 e_t^6)\eta - 84(54144 + 579897 e_t^2 + 509644 e_t^4 + 32840 e_t^6)\eta^2 + 1008\sqrt{1-e_t^2}(2672 + 6963 e_t^2 + 565 e_t^4)(2\eta - 5) \Bigg] \Bigg\} + \frac{1}{2\bar{e}_t} \left(\frac{d\bar{e}_t^2}{dt} \right) \Bigg|_{\text{Tail}} . \quad (4.43)$$

In the tail terms in the above equations we can simply replace $\xi \to \xi_\phi$ in their expressions in Appendix A [Eqs. (N.10)]. PN corrections to the relation for $\xi = \xi(\xi_\phi)$ will not effect the tail terms unless we want accuracy to 2.5PN order.

Because the eccentricity as well as the orbital frequency evolves with time, we need to substitute a relation that describes how the eccentricity depends on frequency, $e_t = e_t(\xi_\phi)$. To determine this relationship we first compute $de_t/d\xi_\phi = (de_t/dt)/(d\xi_\phi/dt)$ and expand in ξ_ϕ to 2PN order:

$$\frac{de_t}{d\xi_\phi} = -\frac{e_t(1-e_t^2)}{3\xi_\phi} \Bigg\{ \frac{304 + 121 e_t^2}{96 + 292 e_t^2 + 37 e_t^4} + \frac{\xi_\phi^{2/3}}{(96 + 292 e_t^2 + 37 e_t^4)^2} \Bigg[\left(\frac{181312}{7} - 50432\eta \right) + \left(-\frac{922774}{7} + \frac{234776}{3}\eta \right) e_t^2 + \left(\frac{383996}{7} - \frac{129524}{3}\eta \right) e_t^4 + \left(-\frac{64181}{28} + \frac{7844}{3}\eta \right) e_t^6 \Bigg] + \frac{5(1-e_t^2)^{5/2}\xi_\phi}{(96 + 292 e_t^2 + 37 e_t^4)^2} \Bigg[3 g_{1.5\text{PN}} (96 + 292 e_t^2 + 37 e_t^4) - (1-e_t^2)(304 + 121 e_t^2) f_{1.5\text{PN}} \Bigg] + O(\xi_\phi^{4/3}) \Bigg\} , \quad (4.44)$$

where

$$f_{1.5\text{PN}} = \frac{384}{5}\pi\kappa_{\text{E}} , \quad (4.45)$$

$$g_{1.5\text{PN}} = \frac{128}{5}\frac{\pi}{e_t^2}\left\{ (1-e_t^2)\kappa_{\text{E}} - \sqrt{1-e_t^2}\kappa_{\text{J}} \right\} , \quad (4.46)$$

and $\kappa_{\rm E}$ and $\kappa_{\rm J}$ are given by Eqs. (N.11). We calculated, but did not write out, the 2PN terms in Eq. (4.44).

At Newtonian order we can solve Eq. (4.44) exactly for $\xi_\phi(e_t)$ [151, 181]:

$$\frac{\xi_\phi(e_t)}{\xi_0} = \left(\frac{e_0}{e_t}\right)^{18/19} \left(\frac{1-e_t^2}{1-e_0^2}\right)^{3/2} \left(\frac{304+121e_0^2}{304+121e_t^2}\right)^{1305/2299} , \tag{4.47}$$

where ξ_0 is the angular frequency when the eccentricity is e_0. At 1PN and higher orders an exact analytic solution cannot be found. When the eccentricity is small, we can expand Eq. (4.44) as

$$\frac{de_t}{d\xi_\phi} = -\frac{19}{18}\frac{e_t}{\xi_\phi}\left[1+\xi_\phi^{2/3}\left(\frac{2833}{3192}-\frac{197}{114}\eta\right)+\frac{377}{152}\pi\xi_\phi \right. \\ \left. +\xi_\phi^{4/3}\left(-\frac{1392851}{508032}+\frac{(97611-11662\eta)\eta}{19152}\right)\right] , \tag{4.48}$$

where we have used the expansions for $\kappa_{\rm E}$ and $\kappa_{\rm J}$ in Eqs. (N.12). Eq. (4.48) can be directly integrated using

$$\int \frac{(1+c_1\xi_\phi^{2/3}+c_2\xi_\phi+c_4\xi_\phi^{4/3})}{\xi_\phi}\, d\xi_\phi = \ln\xi_\phi + \frac{3}{2}c_1\xi_\phi^{2/3} + c_2\xi_\phi + \frac{3}{4}c_3\xi_\phi^{4/3} , \tag{4.49}$$

where c_1, c_2 and c_3 are constants. The result is

$$e_t = K_1\xi_\phi^{-19/18}\exp\left[\xi_\phi^{2/3}\left(-\frac{2833}{2016}+\frac{197}{72}\eta\right)-\frac{377}{144}\pi\xi_\phi \right. \\ \left. +\xi_\phi^{4/3}\left(\frac{26464169}{12192768}-\frac{32537}{8064}\eta+\frac{833}{1728}\eta^2\right)\right] , \tag{4.50}$$

and expanding to 2PN order gives

$$e_t \approx K_1\xi_\phi^{-19/18}\left[1+\xi_\phi^{2/3}\left(-\frac{2833}{2016}+\frac{197}{72}\eta\right)-\frac{377}{144}\pi\xi_\phi \right. \\ \left. +\xi_\phi^{4/3}\left(\frac{77006005}{24385536}-\frac{1143767}{145152}\eta+\frac{43807}{10368}\eta^2\right)\right] , \tag{4.51}$$

where K_1 is a constant determined by the initial condition $e_t(\xi_0) = e_0$.

To calculate the phase using Eq. (4.21) we must next compute the 2PN limit of $\tau = f/(df/dt) = \xi_\phi/(d\xi_\phi/dt)$ using Eq. (4.42). For arbitrary eccentricity this can only be written in simple form up to 1PN order:

$$\tau = \frac{5}{96}\frac{M}{\eta\xi_\phi^{8/3}}\frac{(1-e_t^2)^{7/2}}{(1+\frac{73}{24}e_t^2+\frac{37}{96}e_t^4)}\Bigg\{1+\frac{\xi_\phi^{2/3}}{56(1-e_t^2)(96+292e_t^2+37e_t^4)}\Bigg[(11888 + 14784\eta) + (-87720+159600\eta)e_t^2 + (-171038+141708\eta)e_t^4 + (-11717+8288\eta)e_t^6\Bigg]\Bigg\} + 1.5\text{PN \& 2PN terms}\,. \quad (4.52)$$

If we keep only the terms to leading order in the eccentricity e_t then τ can be expanded up to 2PN order:

$$\tau = \frac{5}{96}\frac{M}{\eta\xi_\phi^{8/3}}\Bigg\{1-\frac{157}{24}e_t^2+\xi_\phi^{2/3}\Bigg[\left(\frac{743}{336}+\frac{11}{4}\eta\right)+\left(-\frac{142319}{4032}+\frac{73}{12}\eta\right)e_t^2\Bigg] + \xi_\phi\left(-4\pi+\frac{59}{16}\pi e_t^2\right)+\xi_\phi^{4/3}\Bigg[\frac{3058673}{1016064}+\frac{5429}{1008}\eta+\frac{617}{144}\eta^2 + \left(-\frac{1459438879}{24385536}-\frac{917381}{48384}\eta+\frac{7735}{3456}\eta^2\right)e_t^2\Bigg]\Bigg\}. \quad (4.53)$$

Plugging Eq. (4.51) into (4.53) and keeping the relevant 2PN terms gives

$$\tau = \frac{5}{96}\frac{M}{\eta\xi_\phi^{8/3}}\Bigg\{1+\xi_\phi^{2/3}\left(\frac{743}{336}+\frac{11}{4}\eta\right)-4\pi\xi_\phi+\xi_\phi^{4/3}\left(\frac{3058673}{1016064}+\frac{5429}{1008}\eta+\frac{617}{144}\eta^2\right) - \frac{157}{24}\frac{K_1^2}{\xi_\phi^{19/9}}\Bigg[1+\xi_\phi^{2/3}\left(\frac{409133}{158256}+\frac{25673}{5652}\eta\right)-\frac{65561}{11304}\pi\xi_\phi + \xi_\phi^{4/3}\left(\frac{22212973}{9766656}+\frac{33013763}{2848608}\eta+\frac{2137631}{203472}\eta^2\right)\Bigg]\Bigg\}\,. \quad (4.54)$$

Note that the exponents of ξ_ϕ in the eccentricity-dependent terms do not follow the same PN counting sequence as the zero-eccentricity terms. This requires one to be careful in computing the series expansions consistently. Plugging (4.54) into the integral in Eq. (4.21) and using $f = \xi_\phi/(\pi M)$, we get the expression for the expansion of the GW phase to 2PN order:

$$\Psi = 2\pi f t_c + \phi_c + \frac{3}{128\eta\xi_\phi^{5/3}}\Bigg\{1 + \xi_\phi^{2/3}\left(\frac{3715}{756} + \frac{55}{9}\eta\right) - 16\pi\xi_\phi + \xi_\phi^{4/3}\left(\frac{15293365}{508032} + \frac{27145}{504}\eta + \frac{3085}{72}\eta^2\right) - \frac{2355}{1462}\frac{K_1^2}{\xi_\phi^{19/9}}\Bigg[1 + \xi_\phi^{2/3}\left(\frac{299076223}{81976608} + \frac{18766963}{2927736}\eta\right) - \frac{2819123}{282600}\pi\xi_\phi + \xi_\phi^{4/3}\left(\frac{16237683263}{3330429696} + \frac{24133060753}{971375328}\eta + \frac{1562608261}{69383952}\eta^2\right)\Bigg]\Bigg\}\,. \tag{4.55}$$

In the $K_1 \to 0$ limit this expression agrees with the 2PN phase formula for circular orbits. The leading term proportional to $K_1^2\xi_\phi^{-19/9}$ agrees with the results from [175]. The remaining PN corrections terms proportional to K_1^2 are new and will be useful for investigating post-adiabatic corrections to the phase for mildly eccentric orbits. To express the phase explicitly in terms of the eccentricity e_0 when the dimensionless frequency $\xi_\phi = \xi_0$, we solve Eq. (4.51) for K_1^2 and expand to 2PN order:

$$K_1^2 = e_0^2\xi_0^{10/9}\Bigg[1 + \xi_0^{2/3}\left(\frac{2833}{1008} - \frac{197}{36}\eta\right) + \frac{377}{72}\pi\xi_0 - \xi_0^{4/3}\left(\frac{1193251}{3048192} + \frac{66317}{9072}\eta - \frac{18155}{1296}\eta^2\right)\Bigg]\,. \tag{4.56}$$

Plugging this into Eq. (4.55) and keeping only terms up to 2PN order in ξ_ϕ and ξ_0 gives

$$\Psi = 2\pi f t_c + \phi_c + \frac{3}{128\eta\xi_\phi^{5/3}}\Bigg\{1 + \xi_\phi^{2/3}\left(\frac{3715}{756} + \frac{55}{9}\eta\right) - 16\pi\xi_\phi + \xi_\phi^{4/3}\left(\frac{15293365}{508032} + \frac{27145}{504}\eta + \frac{3085}{72}\eta^2\right) - \frac{2355}{1462}e_0^2\left(\frac{\xi_0}{\xi_\phi}\right)^{19/9}\Bigg[1 + \xi_0^{2/3}\left(\frac{2833}{1008} - \frac{197}{36}\eta\right) + \xi_\phi^{2/3}\left(\frac{299076223}{81976608} + \frac{18766963}{2927736}\eta\right) + \frac{377}{72}\pi\xi_0 - \frac{2819123}{282600}\pi\xi_\phi - \xi_0^{4/3}\left(\frac{1193251}{3048192} + \frac{66317}{9072}\eta - \frac{18155}{1296}\eta^2\right) + \xi_\phi^{4/3}\left(\frac{16237683263}{3330429696} + \frac{24133060753}{971375328}\eta + \frac{1562608261}{69383952}\eta^2\right) + \xi_0^{2/3}\xi_\phi^{2/3}\left(\frac{847282939759}{82632420864} - \frac{718901219}{368894736}\eta - \frac{3697091711}{105398496}\eta^2\right)\Bigg]\Bigg\}\,. \tag{4.57}$$

Instead of using Eq. (4.21) as our starting point, we could also have calculated the GW phase $\Psi(f)$ by starting from Eq. (4.23) and using the expressions for the orbital energy and GW luminosity given in Appendix N.

Eq. (4.57) gives the GW phase to 2PN order for orbits with small eccentricity. While this formula should be extendible to higher PN orders once the necessary expressions are derived [higher PN expansions to Eqs. (N.8)], fully-analytic extensions to higher orders in the eccentricity are not likely to be found. To compute templates for large eccentricity orbits one must make use of the more complicated formalism to compute the phasing in the time domain as discussed in Refs. [181, 183]. That formalism would also be needed to consistently calculate post-post-adiabatic corrections to the waveform. In addition to investigating the post-adiabatic corrections to EMRI templates (which is the goal of this chapter), the phase expansion in Eq. (4.57) should also be useful for investigating the GW phase evolution of mildly eccentric but comparable-mass binary sources, especially compact object binaries that are sources for ground-based GW interferometers.

4.4 Estimating the post-adiabatic phase error for low-eccentricity orbits

The total post-1-adiabatic phase error is found by substituting Eq. (4.57) into Eq. (4.33). The result is

$$\begin{aligned}\Delta\Psi^{(1)} = \frac{1}{128\tilde{\xi}_\phi^{5/3}}\Bigg[1 + \frac{8335}{252}\tilde{\xi}_\phi^{2/3} - 64\pi\tilde{\xi}_\phi + \frac{158553305}{508032}\tilde{\xi}_\phi^{4/3} \\ - \frac{2355}{1462}e_0^2\left(\frac{\tilde{\xi}_0}{\tilde{\xi}_\phi}\right)^{19/9}\Bigg(1 + \frac{824551187}{27325536}\tilde{\xi}_\phi^{2/3} - \frac{2683}{336}\tilde{\xi}_0^{2/3} - \frac{2819123}{70650}\pi\tilde{\xi}_\phi\end{aligned}$$

$$+\frac{377}{18}\pi\tilde{\xi}_0+\frac{2305899288421}{23313007872}\tilde{\xi}_\phi^{4/3}-\frac{72813791}{3048192}\tilde{\xi}_0^{4/3}+\frac{3753313079627}{82632420864}\tilde{\xi}_\phi^{2/3}\tilde{\xi}_0^{2/3}\Bigg)\Bigg]\,, \tag{4.58}$$

where $\tilde{\xi}_\phi=\pi m_1 f$, $\tilde{\xi}_0=\pi m_1 f_0$, and f_0 is the GW frequency when the eccentricity is e_0. The post-1-adiabatic phase error corresponding to the term ΔG_1 in Eq. (4.36) is given by substituting Eq. (4.57) into Eq. (4.39):

$$\Delta\Psi_1^{(1)}=\frac{3}{128\xi_\phi^{5/3}}\Bigg[\frac{55}{9}\xi_\phi^{2/3}+\frac{27145}{504}\xi_\phi^{4/3}+e_0^2\left(\frac{\xi_0}{\xi_\phi}\right)^{19/9}\Bigg(-\frac{128365}{12432}\xi_\phi^{2/3}$$
$$+\frac{154645}{17544}\xi_0^{2/3}-\frac{165068815}{4124736}\xi_\phi^{4/3}+\frac{3062285}{260064}\xi_0^{4/3}+\frac{4917245}{1566432}\xi_\phi^{2/3}\xi_0^{2/3}\Bigg)\Bigg]\,. \tag{4.59}$$

Before examining these two phase errors, we first take advantage of the fact that we can transform the phase via $\Psi(f)\to\Psi(f)+\Psi_i+2\pi f\Delta t$ without altering any physical information about the binary (see Sec. 4.2.2). This freedom allows us to choose $\Psi(f_i)=\Psi'(f_i)=0$, where f_i is some fixed frequency. This choice sets the coalescence time t_c and the coalescence phase ϕ_c, and the total post-1-adiabatic phase error then becomes

$$\delta\Psi(f)=\Delta\Psi^{(1)}(f)-\Delta\Psi^{(1)}(f_0)-\Delta\Psi^{(1)'}(f_0)(f-f_0)\,, \tag{4.60}$$

where $\Delta\Psi^{(1)}$ is calculated from Eq. (4.33). A similar equation defines $\delta\Psi_1(f)$, the error corresponding to $\Delta\Psi_1^{(1)}$ [Eq. (4.39)].

We are free to pick whatever f_i (or alternatively t_c and ϕ_c) that we like, so we will choose a value that will minimize the phase errors. For the range of masses and frequencies that we examined, this can be accomplished by determining the value of f_i in between our initial (f_1) and final (f_2) observing frequencies that satisfies $\delta\Psi(f_1,f_i)=\delta\Psi(f_2,f_i)$. An analogous equation holds for $\delta\Psi_1$.

We now examine the different types of adiabatic phase errors that we have calculated. We consider as our "fiducial EMRI" a binary with $m_1=10^6M_\odot$,

$m_2 = 10M_\odot$, and spin parameter $a = 0.0$. We examine the evolution of the error in the number of cycles $\Delta N_{\rm cyc} = \delta\Psi/(2\pi)$ (and likewise for $\delta\Psi_1$) for a 1-year observation period ending when the binary reaches its last-stable-orbit. Since the eccentricity is small we approximate this final frequency f_2 as the GW frequency at the innermost-stable-circular orbit (ISCO), defined by

$$f_{\rm isco} = \frac{m_1^{1/2}}{\pi(r_{\rm isco}^{3/2} \pm a m_1^{3/2})} \,, \tag{4.61}$$

where $r_{\rm isco}$ is the ISCO radius in Boyer-Lindquist coordinates [see Eqs. (2.16) & (2.21) of Bardeen, Press, & Teukolsky [73] or Eqs. (C.1) here]. The initial GW frequency f_1 at a time $\delta t \approx 1$ yr before the ISCO is reached is approximated by the circular orbit formula

$$f(\delta t) = f_{\rm isco}(1 + \delta t/\tau_{\rm rr})^{-3/8} \,, \tag{4.62}$$

where $\tau_{\rm rr} = (5/256)\mathcal{M}^{-5/3}(\pi f_{\rm isco})^{-8/3}$ and $\mathcal{M} = \mu^{3/5}M^{2/5}$ is the chirp mass. These circular-orbit expressions should be adequate for orbits with small eccentricity.

We focus on binaries that have eccentricities $e_0 = 0.0$, 0.1, and 0.2 at the start of the observing frequency, $f_0 = f_1$. In the plots shown here we have not included the 2.5PN and 3PN corrections to the circular piece of the GW phase. Those pieces can be found in Eq. (4.25). Including those corrections changes the phase errors by a factor $\sim 2 - 4$ (the sign of the change depends on which error is considered) but does not change their overall behavior or our conclusions.

In Figure 4.1 we plot the post-1 adiabatic phase error (expressed as a change in the number of cycles). This corresponds to the error calculated in Eq. (4.58), with coalescence time and phase chosen so that the error is zero when the binary enters the observing frequency, $f_i = f_0 = f_1$. Over the last year of inspiral a phase error of about one-tenth of a cycle builds up. Orbits with small eccentricity have

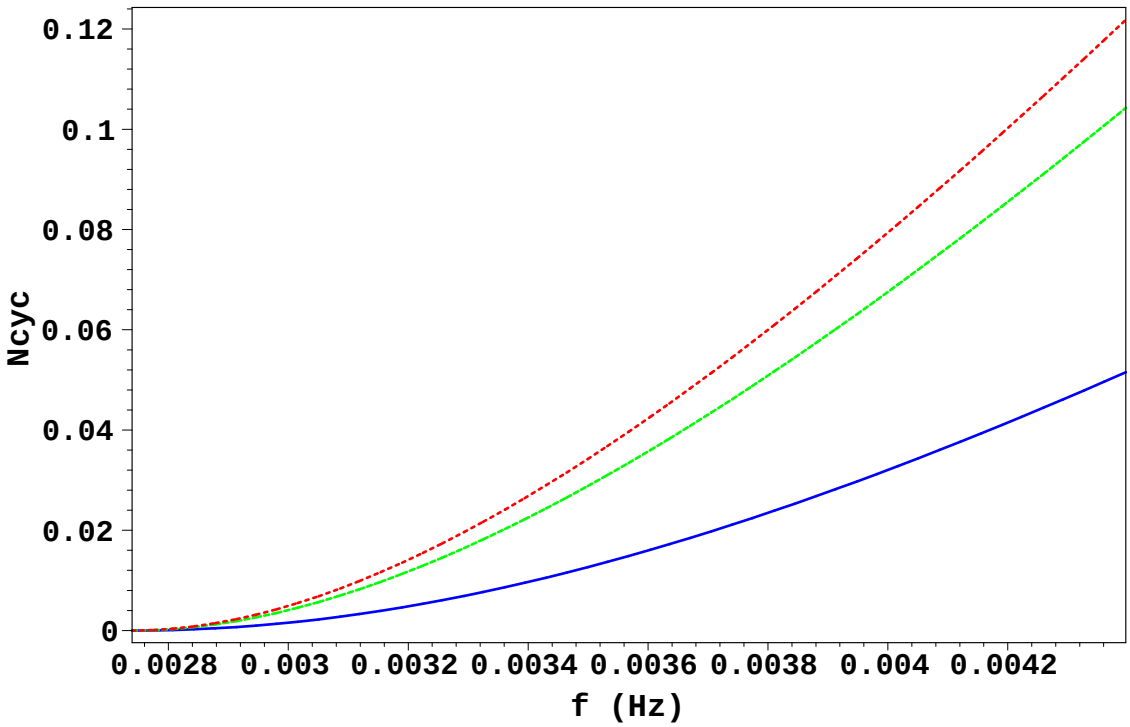

Figure 4.1: Total adiabatic phase error in number of cycles [$\delta\Psi/(2\pi)$; Eqs. (4.58) and (4.60)] for a binary with $m_1 = 10^6 M_\odot$, $m_2 = 10 M_\odot$. Both black holes are non-spinning. The frequency range spans one year before the ISCO is reached. The red (top) line plots an eccentricity of $e_0 = 0$, the green (middle) is $e_0 = 0.1$, and blue (bottom) is $e_0 = 0.2$. The frequency f_i was chosen so that the phase error is zero at the start of the observation time, $f_i = f_0 = f_1$.

a lower adiabatic phase error. Figure 4.2 shows that these errors are lowered by a factor ~ 5 by adjusting the value of the frequency f_i. In Figure 4.3 we show the piece of the phase error constructed from ΔG_1 [Eq. (4.59)]. In this case the phase error is actually larger than in Figure 4.1. However, this plot shows that the eccentricity has almost no effect when this phase error is used. Figure 4.4 shows the same error, but with the frequency f_i varied so as to reduce the error. Varying the frequency again reduces the error by about a factor of 5.

For a one-year observation time, the approximate phase errors that we have calculated are all $\lesssim 1$, but are $\gtrsim 0.01$. These errors are small enough to allow detection of EMRIs using adiabatic waveforms, provided that the eccentricities are

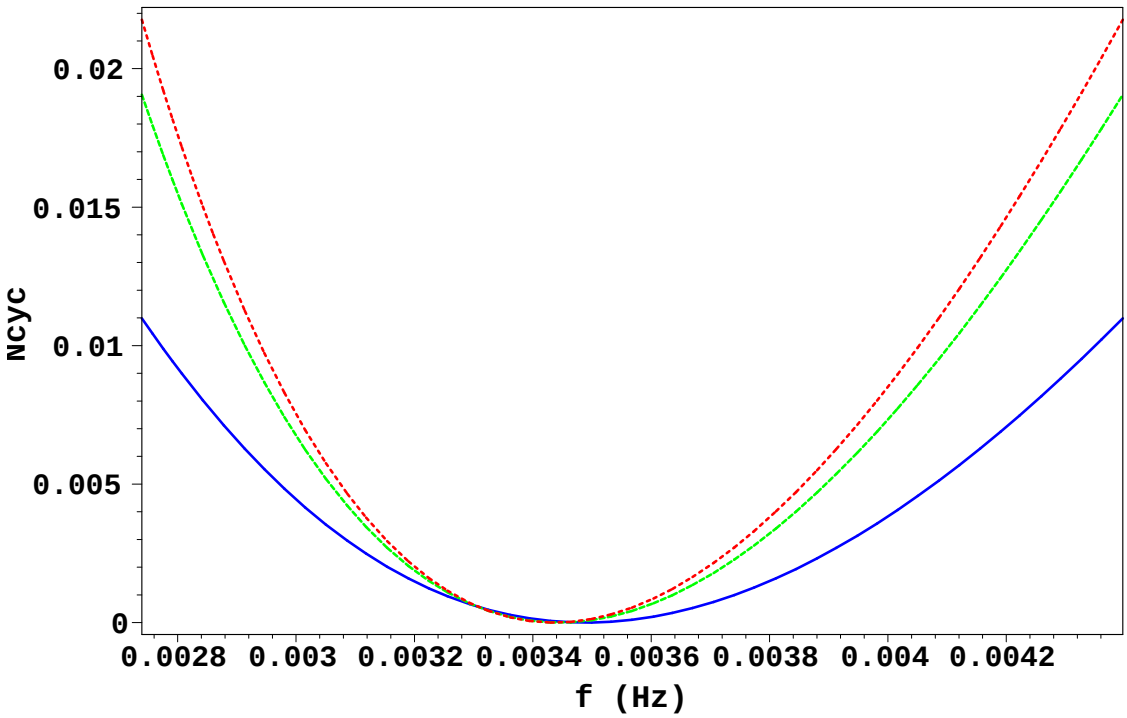

Figure 4.2: Same as Figure 4.1 except the frequency f_i is chosen to minimize the error in the number of cycles.

small. These phase errors are much smaller over the shorter intervals ($\sim$ 3 weeks) that will be used to match the LISA data to detection templates. However, these phase errors are still large enough that they will impede the precise determination of the masses and spins of the BHs.

4.5 The adiabatic approximation for orbits with large eccentricity

When the eccentricity is large there is reason to suspect that adiabatic waveforms will no longer be sufficient as detection templates. Part of this suspicion comes from recent work by Pound, Poisson, and Nickel [26]. They examined a toy model of a point electric charge moving slowly in the weak field of a central mass. In the absence of self-forces this charge follows a Keplerian ellipse described by three

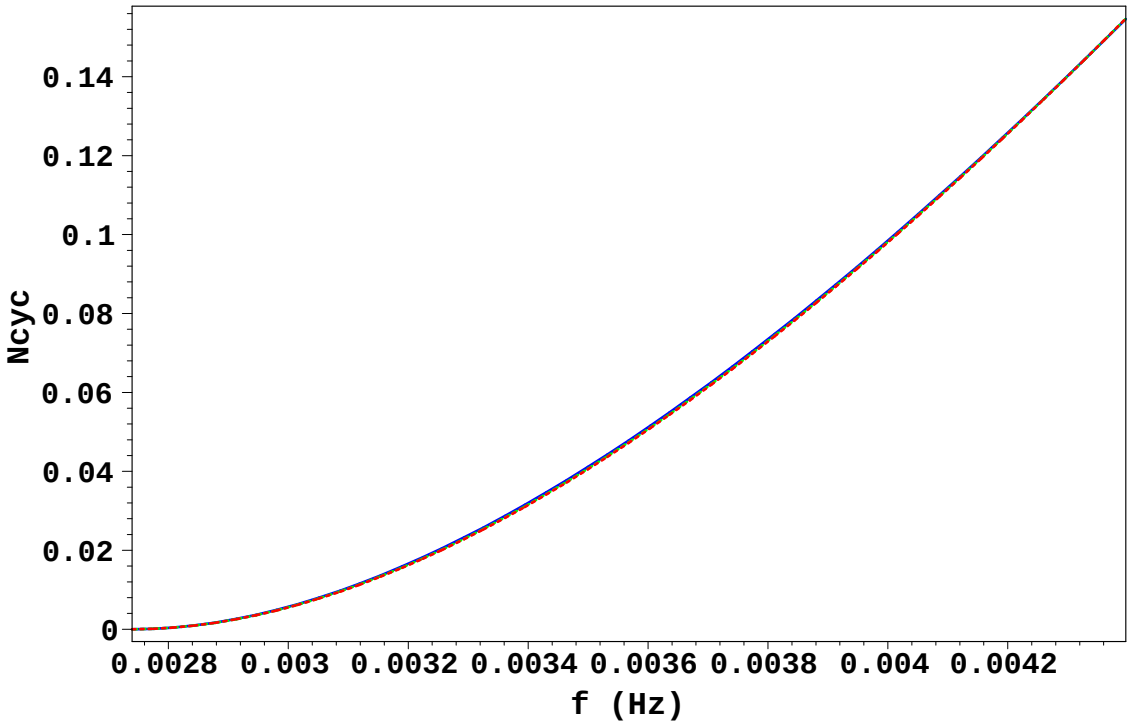

Figure 4.3: Phase error in number of cycles due to the adiabatic approximation, $[\delta\Psi_1/(2\pi)$; Eqs. (4.59) and (4.60)]. This is the same as Figure 4.1 except we only plot the piece of the error corresponding to ΔG_1 or equivalently $\Delta\Psi_1^{(1)}$. The frequency f_i is set to the initial observing frequency, $f_i = f_0 = f_1$. The same three eccentricities are plotted, but the orbits with eccentricities of 0.1 and 0.2 have nearly the same errors as circular orbits.

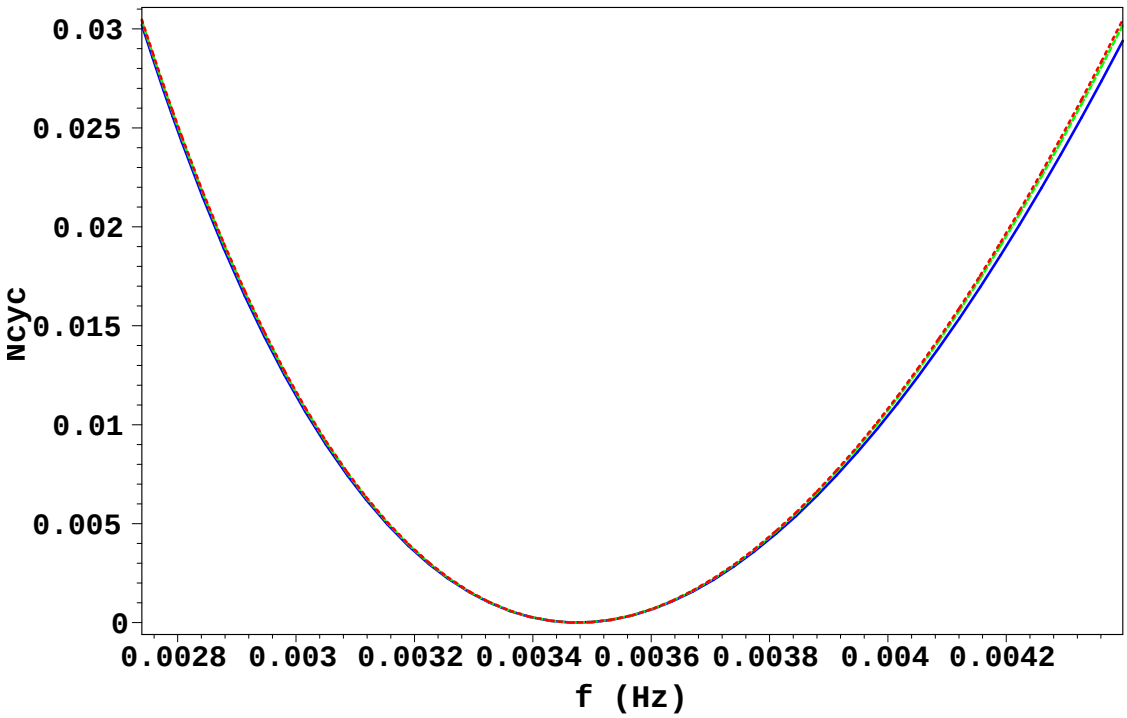

Figure 4.4: Same as Figure 4.3 except the frequency f_i is chosen to minimize the error in the number of cycles.

orbital elements: a semi-latus rectum p, a eccentricity e, and a pericenter angle ω (an angle, not an angular frequency). When the electromagnetic self-force acts on the point charge, it causes these orbital elements to evolve with time. Ref. [26] shows that the time averaged evolution, $\langle \dot{p} \rangle$ and $\langle \dot{e} \rangle$, of p and e are determined solely by the radiation-reaction piece of the weak-field self-force, while the evolution $\langle \dot{\omega} \rangle$ of ω depends only on the conservative piece. They further show that including the effects of the conservative evolution of ω has a large effect on the phasing of the magnetic field.

In the gravitational case we can make a rough estimate of the effect of the conservative self-force terms on the orbital phase. The corresponding effect on the GW phase should be of the same order. Let's focus on the contribution to the orbital phase that comes from periastron precession. This is approximately

given by $\Delta\phi \sim \omega_{\rm peri}\tau$, where $\omega_{\rm peri}$ is given by Eq.(N.15) and τ is the radiation-reaction time and is approximately given by Eq. (4.52) for eccentric orbits. Using the relation between the orbital frequencies in Eq. (4.41), the pericenter precession rate to 2PN order becomes

$$M\omega_{\rm peri} = \frac{3\xi_\phi^{5/3}}{(1-e_t^2)}\left\{1 + \frac{3\xi_\phi^{2/3}}{2(1-e_t^2)}\left[\left(1-\frac{14}{9}\eta\right) + e_t^2\left(\frac{17}{6}-\frac{13}{9}\eta\right)\right]\right\} . \quad (4.63)$$

Multiplying by Eq. (4.52) gives

$$\Delta\phi \sim \frac{15(1-e_t^2)^{5/2}}{\eta\xi_\phi(96+292e_t^2+37e_t^4)}\Big[1 + f_1(e_t)O(\xi_\phi^{2/3}) + f_2(e_t)O(\eta\xi_\phi^{2/3}) + f_3(e_t)O(\xi_\phi^{4/3}) + f_4(e_t)O(\eta\xi_\phi^{4/3})\Big] , \quad (4.64)$$

where the $f_i(e_t)$ are functions of the eccentricity. Since ξ_ϕ contains a hidden factor of $1+\varepsilon$, at first glance the above equation indicates that the phase error due to the adiabatic approximation should scale like

$$\Delta\phi_{\rm ad} \sim \left(\frac{p}{M}\right)^{3/2} , \quad (4.65)$$

where we have used $\xi_\phi \approx [M(1-e_t^2)/p]^{3/2}$. Such a phase error would be large for post-Newtonian situations when $p/M \gg 1$, but would imply order unity corrections $\Delta\phi_{\rm ad} \sim O(1)$ in EMRI situations ($p/M \gtrsim 1$). The adiabatic phase error can actually be made smaller than this estimate (which was given in Ref. [26]) if one ignores those order $O(\varepsilon)$ corrections that only cause small adjustments to the masses of the particles[7]. This is the piece of the adiabatic phase error embodied by the ΔG_1 term in Eq. (4.36). Computing this piece of $\Delta\phi_{\rm ad}$ involves keeping only the leading-order terms in an expansion in η,

$$\Delta\phi_{\rm ad,1} \sim \lim_{\eta\to 0}\frac{1}{\eta}\Big[\eta\Delta\phi(\eta) - \eta\Delta\phi(\eta=0)\Big] . \quad (4.66)$$

[7]Specifically, these are the corrections embedded in terms containing factors of m_1+m_2, such as $\xi_\phi = (1+\varepsilon)m_1\pi f$.

The result is

$$\Delta\phi_{\rm ad,1} \sim \frac{600\sqrt{1-e_t^2}}{(96+292e_t^2+37e_t^4)\xi_\phi^{1/3}}\Bigg[1+\frac{2881}{60}e_t^2-\frac{179}{48}e_t^4-\frac{5231}{120}e_t^6 \\ -\frac{407}{240}e_t^8+\xi_\phi^{2/3}\bigg(-\frac{149}{60}+\frac{180433}{840}e_t^2+\frac{138751}{210}e_t^4+\frac{144659}{320}e_t^6+\frac{72733}{2688}e_t^8\bigg)\Bigg]. \tag{4.67}$$

In contrast to Eq. (4.65), this error has the scaling

$$\Delta\phi_{\rm ad,1} \sim \left(\frac{p}{M}\right)^{1/2}, \tag{4.68}$$

which suggests that the post-adiabatic phase errors will in practice be less severe than implied by Eq. (4.65) and the analysis of [26]. The phase error in Eq. (4.68) is analog of the GW phase error $\Delta\Psi_1^{(1)}$ that was computed for low-eccentricity orbits. Examining the eccentricity dependence of Eq. (4.67) indicates that larger eccentricities ($e_t \sim 0.4-0.8$) can increase the phase error in $\Delta\phi_{\rm ad,1}$ by factors of $\sim 2-10$, possibly impeding detection However, this analysis is very approximate (for example we have ignored all time variations in the orbital frequencies and eccentricities) and the high-eccentricity case needs to be examined more carefully.

4.6 Conclusions

The main results of this chapter are the following: We have computed to 2PN order an analytic expression for the GW phase for orbits will small initial eccentricity [Eq. (4.57)]. As far as we know, such an expression has not been previously derived, and it should be useful for studying inspiralling binary GW sources with relatively small ($e \lesssim 0.2$) orbital eccentricities. We applied this expression to EMRI systems in order to estimate the error in the GW phase that results from post-adiabatic

effects. In an expansion of the phase in powers of the mass ratio ε, these "post-adiabatic" corrections are expected to result in phase errors that scale like $O(\varepsilon^{-1/2})$ and $O(\varepsilon^0)$ [see Eq. (4.10)], but their magnitudes are not well understood. The order $O(\varepsilon^{-1/2})$ piece of the phase arising from orbital resonances cannot be treated with post-Newtonian theory, but has been shown to be small [171]. For circular orbits Drasco, Flanagan, and Hughes [154] estimated the magnitudes of the order $O(\varepsilon^0)$ phase error, and we have extended their calculations to orbits with small eccentricity. Over one year of inspiral for a typical EMRI source with $m_1 = 10^6 M_\odot$ and $m_2 = 10 M_\odot$, post-1-adiabatic effects result in an error of about $1/10$ of a cycle. Adjusting the coalescence time and phase reduces these errors by a factor of ~ 5. Orbits with small eccentricities have post-adiabatic phase errors that are smaller or nearly equal to the phase errors for circular orbits. These phase errors are large enough that they will prevent the precise determination of the masses and spins of the inspiralling black holes. But they are small enough to ensure that adiabatic waveforms will be useful for detection templates, at least for orbits with low eccentricities.

Our results rely on two significant assumptions that should be relaxed in future work: We use post-Newtonian theory to treat orbits near their last stable orbits, and we assume small eccentricities. Both of these assumptions will be violated for EMRI sources. Nevertheless, our results should still be good enough for getting an approximate handle on the size of the post-adiabatic corrections to the GW phase. While still working entirely within the post-Newtonian approximation, it should be relatively straight forward to examine the case of eccentric orbits. This could be done by directly solving the post-Newtonian equations of motion numerically, or by using the recent results of Refs. [181, 183] which are based on the generalized

quasi-Keplerian parametrization of PN orbits. Using either of these approaches, orbital solutions and their corresponding waveforms could be generated, and terms corresponding to post-adiabatic corrections could be manually turned on or off. It should also be possible to further reduce the reliance on post-Newtonian techniques. This would involve directly solving the Kerr geodesic equations, but supplemented by self-force correction terms. For now these self-force terms are not available for realistic orbits. Post-Newtonian approximations to those self-force terms would need to be used in the orbit evolutions. This geodesic/PN hybrid technique should provide a better estimate of the post-adiabatic contributions to the GW phase. Future work will focus on this technique, with an emphasis on examining the phase errors for orbits with moderate to large eccentricities. Pound, Poisson, and Nickel [26] have indicated that adiabatic waveforms will be severely hampered in their ability to detect eccentric EMRIs. While our rough estimates indicate that the situation might be somewhat improved over the estimates in Ref. [26], a more careful analysis of the eccentric case is urgently needed.

Appendix A
Spin-orbit corrections to the recoil velocity

In this appendix we derive the spin-orbit corrections to Fitchett's recoil formula [Eq. (2.4)]. Kidder [60] gives the following expressions for the Newtonian and spin-orbit contributions to the momentum flux:

$$\dot{\mathbf{P}}^{\rm com}_{\rm N} = -\frac{8}{105}\frac{\delta m}{m}\eta^2\left(\frac{m}{r}\right)^4\left\{\dot{r}\hat{\mathbf{n}}\left[55v^2-45\dot{r}^2+12\frac{m}{r}\right]+\mathbf{v}\left[38\dot{r}^2-50v^2-8\frac{m}{r}\right]\right\}\ , \tag{A.1}$$

$$\dot{\mathbf{P}}^{\rm com}_{\rm SO} = -\frac{8}{15}\frac{\mu^2 m}{r^5}\left\{4\dot{r}(\mathbf{v}\times\boldsymbol{\Delta})-2v^2(\hat{\mathbf{n}}\times\boldsymbol{\Delta})-(\hat{\mathbf{n}}\times\mathbf{v})[3\dot{r}(\hat{\mathbf{n}}\cdot\boldsymbol{\Delta})+2(\mathbf{v}\cdot\boldsymbol{\Delta})]\right\}\ , \tag{A.2}$$

where $\delta m = m_1 - m_2$, $m = m_1 + m_2$ $\hat{\mathbf{n}} = \mathbf{x}/r$, $\mathbf{x} = \mathbf{x}_1 - \mathbf{x}_2$, $\mathbf{v} = d\mathbf{x}/dt$, and $\boldsymbol{\Delta} = m(\mathbf{S}_2/m_2 - \mathbf{S}_1/m_1)$. If we specialize to circular orbits with spins perpendicular to the orbital plane, we can simplify these expressions using

$$\dot{r} = \hat{\mathbf{n}}\cdot\mathbf{v} = \hat{\mathbf{n}}\cdot\boldsymbol{\Delta} = \mathbf{v}\cdot\boldsymbol{\Delta} = 0\ . \tag{A.3}$$

The first equation (A.1) reduces to Fitchett's result, and only the $-2v^2(\hat{\mathbf{n}}\times\boldsymbol{\Delta})$ term remains in (A.2). There is no precession or motion out of the orbital plane in this case. This can be verified by examining the equations of motion and precession [Eqs. (2.2c) and (2.5) of [60]]. Since the spin-orbit momentum flux is proportional to $\hat{\mathbf{n}}\times\boldsymbol{\Delta}$ when the orbits are circular and $\boldsymbol{S}_{1,2} \propto \hat{\boldsymbol{z}}$, the kick velocity will be directed in the plane of the binary, perpendicular to the line connecting the two masses.

For circular orbits we can set $\hat{\mathbf{n}} = [\cos\phi, \sin\phi, 0]$, where ϕ is the orbital phase and $\mathbf{v} = r\dot{\phi}[-\sin\phi, \cos\phi, 0]$. At 1PN order

$$\mathbf{v} = \sqrt{\frac{m}{r}}\left[1-\frac{3-\eta}{2}\frac{m}{r}\right][-\sin\phi, \cos\phi, 0]\ , \tag{A.4}$$

but we will ignore the 1PN correction and just use the regular Kepler law $\dot{\phi} = v/r = \sqrt{m/r^3}$. We can also simplify the $\mathbf{\Delta}$ term by defining $\mathbf{S}_{1,2} = \tilde{a}_{1,2} m_{1,2}^2 \hat{\mathbf{z}}$, where $-1 \leq \tilde{a}_{1,2} \leq 1$ (each hole can have any spin but must be directed along the orbital angular momentum direction $\hat{\mathbf{z}}$; $\tilde{a} > 0$ points parallel to the orbital angular momentum, while $\tilde{a} < 0$ points antiparallel.) The spin-orbit term then reduces to

$$\dot{\mathbf{P}}_{\mathrm{SO}}^{\mathrm{com}} = \frac{16}{15} f_{\mathrm{SO}}(q, \tilde{a}_1, \tilde{a}_2) \left(\frac{m}{r}\right)^6 [\sin\phi, -\cos\phi, 0] \ , \tag{A.5}$$

where

$$f_{\mathrm{SO}}(q, \tilde{a}_1, \tilde{a}_2) = \frac{q^2(\tilde{a}_2 - q\tilde{a}_1)}{(1+q)^5} \ . \tag{A.6}$$

It is somewhat more convenient to define a "relative-spin parameter" $\alpha = \tilde{a}_1/\tilde{a}_2 \in [-1, 1]$ and a new function

$$f_{\mathrm{SO}}(q, \alpha) = \frac{q^2(1 - q\alpha)}{(1+q)^5} \tag{A.7}$$

which is related to the previous equation by $f_{\mathrm{SO}}(q, \tilde{a}_1, \tilde{a}_2) = \tilde{a}_2 f_{\mathrm{SO}}(q, \alpha)$. On the domain $q \in [0, 1]$ and $\alpha \in [-1, 1]$, $f(q, \alpha)$ has a maximum value of $1/16$ at $q = 1$ and $\alpha = -1$ (equal masses, spins maximal and anti-parallel). The total change in the center of mass momentum is therefore

$$\begin{aligned} \dot{\mathbf{P}}_{\mathrm{TOT}}^{\mathrm{com}} = \Bigg\{ \frac{464}{105} f(q) \left(\frac{m}{r}\right)^{11/2} \left[1 - \left(\frac{5583 + 182\eta}{522}\right)\left(\frac{m}{r}\right)\right] \\ + \frac{16}{15} \tilde{a}_2 f_{\mathrm{SO}}(q, \alpha) \left(\frac{m}{r}\right)^6 \Bigg\} [\sin\phi, -\cos\phi, 0] \ , \end{aligned} \tag{A.8}$$

where I have also included the 1PN contribution to the momentum flux (see Wiseman [1]). The magnitude of the momentum flux can be written as

$$\begin{aligned} |\dot{\mathbf{P}}_{\mathrm{TOT}}^{\mathrm{com}}| = \frac{464}{105} f(q) \left(\frac{m}{r}\right)^{11/2} \Bigg[1 + \frac{7}{29} \tilde{a}_2 \left(\frac{1 - q\alpha}{1 - q}\right)\left(\frac{m}{r}\right)^{1/2} \\ - \left(\frac{5583 + 182\eta}{522}\right)\left(\frac{m}{r}\right)\Bigg] , \end{aligned} \tag{A.9}$$

which shows that the spin-orbit terms formally enters at a lower order than the 1PN correction. We treat only the case of one spinning particle where $\tilde{a}_1 = \alpha = 0$. If we assume that $(m/r)^{1/2} \sim 1$ and $\alpha = 0$, we see that the corrections due to the spin-orbit term can be significant: $\sim 0.27\tilde{a}_2$ for $q = 0.1$, $\sim 0.40\tilde{a}_2$ for $q = 0.4$, and $\sim 1.2\tilde{a}_2$ for $q = 0.8$.

For exactly circular orbits we can naively calculate the recoil velocity by simply integrating $[\sin\phi, -\cos\phi, 0]$ with respect to time and bringing down a factor $1/\dot{\phi}$. This gives

$$\mathbf{V}^{\rm rec}_{\rm TOT} = -\frac{464}{105} f(q) \left(\frac{m}{r}\right)^4 \left[1 - \left(\frac{5583 + 182\eta}{522}\right)\left(\frac{m}{r}\right) + \frac{7}{29}\tilde{a}_2 \left(\frac{1-q\alpha}{1-q}\right)\left(\frac{m}{r}\right)^{1/2}\right] [\cos\phi, \sin\phi, 0] \ . \quad \text{(A.10)}$$

We can write the magnitude of the total recoil as (we ignore the η correction in the 1PN term as it's entirely negligible)

$$|V^{\rm rec}_{\rm TOT}| = \left| (23700 \text{ km/s}) \frac{f(q)}{f_{\rm max}} \left(\frac{m}{r}\right)^4 \left[1 - 10.7\left(\frac{m}{r}\right)\right] + (20000 \text{ km/s})\tilde{a}_2 \frac{f_{\rm SO}(q,\alpha)}{f^{\rm max}_{\rm SO}} \left(\frac{m}{r}\right)^{9/2} \right|, \quad \text{(A.11a)}$$

$$= \left| (1480 \text{ km/s}) \frac{f(q)}{f_{\rm max}} \left(\frac{2m}{r}\right)^4 \left[1 - 5.4\left(\frac{2m}{r}\right)\right] + (883 \text{ km/s})\tilde{a}_2 \frac{f_{\rm SO}(q,\alpha)}{f^{\rm max}_{\rm SO}} \left(\frac{2m}{r}\right)^{9/2} \right| \ . \quad \text{(A.11b)}$$

The above equation is equivalent to Eq. (2.36) in the main text. It indicates that spin contributions to the recoil, although suppressed by a factor of $\tilde{a}_2(v/c)$, have the potential to be important. This is especially true for nearly equal mass binaries where the leading-order contribution to the recoil vanishes. A forthcoming paper by Whitbeck and Owen [184] will address further issues regarding spin effects in radiation recoil calculations.

Appendix B
Derivation of Linear Momentum Flux in Black Hole Perturbation Theory

In this appendix we derive the expression for the linear momentum flux using black hole perturbation theory [Eq. (eq:pplusminus)] and give other formulas necessary for its implementation. It is based on the unpublished notes of Scott Hughes. Portions of this appendix or its generalization will later be published as part of a paper exploring the recoil for circular, inclined orbits. The reader is referred to that future publication for updated expressions.

B.1 Overview and formalism

The rate at which a system radiates linear momentum in gravitational waves is given by integrating its momentum flux $T^{\rm GW}_{0i} = -T^{\rm GW}_{00} n^i$ over a large radius sphere encompassing the system. The tensor $T^{\rm GW}_{ab}$ is Isaacson's stress-energy tensor for gravitational waves [67]; n^i is the unit vector in the i-th direction. Using Isaacson's result yields

$$\frac{dP^k_{\rm GW}}{dt} = \frac{r^2}{32\pi} \int d\Omega \left\langle \partial_t h^{\rm TT}_{ab} \partial_t h^{\rm TT}_{ab} \right\rangle n^k \ . \tag{B.1}$$

(Repeated indices are summed in this expression.) The angle brackets mean that this result only makes sense when averaged over several wavelengths, and arises from the fact that one cannot localize gravitational energy. This averaging is an essential part of the tensor $T^{\rm GW}_{ab}$. By global conservation of momentum, the recoil of the system $dP^a_{\rm sys}/dt = -dP^a_{\rm GW}/dt$. Note that $h^{\rm TT}_{ab}$ is a transverse and traceless tensor.

Inserting a standard multipolar decomposition of the gravitational wave field (see, e.g., Ref. [44] or Section 2.3.1 of Chapter 2), one can write down the radiated

momentum as a function of the source's multipole moments. The leading order terms are

$$\frac{dP^k_{\rm GW}}{dt} = \frac{2}{63}\left\langle \frac{d^4\mathcal{I}^{ijk}}{dt^4}\frac{d^3\mathcal{I}^{ij}}{dt^3}\right\rangle + \frac{16}{45}\left\langle \epsilon^{kpq}\frac{d^3\mathcal{I}^{pj}}{dt^3}\frac{d^3\mathcal{S}^{qj}}{dt^3}\right\rangle \ . \tag{B.2}$$

In this expression, the tensors $\mathcal{I}^{ij}$, $\mathcal{S}^{ij}$, and $\mathcal{I}^{ijk}$ are the symmetric, trace-free mass quadrupole, current quadrupole, and mass octupole moments, respectively. See Ref. [44] for precise definitions of these quantities.

For much of our analysis, we will treat our binary as a small object that orbits a massive black hole. We will thus wish to extract the recoil from a radiation field built from a solution of the Teukolsky equation. The Teukolsky solution directly provides the Newman-Penrose Weyl curvature perturbation Ψ_4. In the distant wave zone of the binary, this perturbation is simply related to the gravitational waves the binary generates:

$$\Psi_4 = \frac{1}{2}\left(\frac{\partial^2 h_+}{\partial t^2} - i\frac{\partial^2 h_\times}{\partial t^2}\right) \ ; \tag{B.3}$$

where $h_{+,\times}$ are the two polarizations for gravitational waves. In this distant wave zone, Ψ_4 is expanded into harmonics and multipoles as follows:

$$\begin{aligned}\Psi_4 &= \frac{1}{(r-ia\cos\theta)^4}\int_{-\infty}^{\infty} d\omega \sum_{lm} R_{lm\omega}(r)\,{}_{-2}S_{lm}(\theta;a\omega)e^{im\phi}e^{-i\omega t} \\ &= \frac{1}{r}\int_{-\infty}^{\infty} d\omega \sum_{lm} Z^H_{lm\omega}\,{}_{-2}S_{lm}(\theta;a\omega)e^{im\phi}e^{-i\omega(t-r_*)} \qquad \text{as } r\to\infty \ . \end{aligned} \tag{B.4}$$

The real function ${}_sS_{lm}(\theta;a\omega)$ is a spin-weighted spheroidal harmonic, used to expand tensor functions of spin weight s in a non-spherical geometry. A detailed discussion of how to calculate ${}_sS_{lm}(\theta;a\omega)$ can be found in Appendix A of Ref. [71]. The spin-weighted spheroidal harmonics are orthonormal functions:

$$\int d\Omega \left[{}_{s'}S_{l'm'}(\theta;a\omega)e^{-im'\phi}\right]\left[{}_sS_{lm}(\theta;a\omega')e^{im\phi}\right] = \delta_{ss'}\delta_{ll'}\delta_{mm'} \ . \tag{B.5}$$

Their orthogonality can be proved by noting that the equation defining them can be written in the form

$$[\mathcal{L}(a\omega, s) + \lambda]\, {}_sS_{lm}(\theta; a\omega) = 0 \ , \tag{B.6}$$

where $\mathcal{L}(a\omega, s)$ is a self-adjoint operator and λ is an eigenvalue. Hence, by Sturm-Liouville theory, the functions ${}_sS_{lm}(\theta; a\omega)$ are orthogonal. With the normalization chosen, the spin-weighted spheroidal harmonic reduces to a spin-weighted spherical harmonic in the Schwarzschild limit:

$${}_sS_{lm}(\theta; a\omega)e^{im\phi} = {}_sY_{lm}(\theta, \phi) \quad \text{as} \quad a \to 0 \ . \tag{B.7}$$

When in addition $s = 0$, this function becomes the "usual" spherical harmonic. For gravitational radiation, the spin weight $s = \pm 2$. For reasons of calculational convenience, we use $s = -2$. Since the functions ${}_sS_{lm}(\theta; a\omega)$ do not depend on ϕ, the condition Eq. (B.5) implies

$$\int_{-1}^{1} d\cos\theta \Big[{}_{s'}S_{l'm'}(\theta; a\omega')\Big]\Big[{}_sS_{lm}(\theta; a\omega)\Big] = \frac{\delta_{ss'}\delta_{ll'}\delta_{mm'}}{2\pi} \ . \tag{B.8}$$

The complex function $R_{lm\omega}(r)$ is often called the "Teukolsky function", and is found by solving the Teukolsky equation (cf. Ref. [71] for extended discussion). On the second line, we have used the fact that as $r \to \infty$, $R_{lm\omega} \to r^3 Z^H_{lm\omega} e^{i\omega r_*}$, where $Z^H_{lm\omega}$ is a complex number. The function r_* is the "tortoise coordinate", which often appears in studies of radiation in black hole spacetimes:

$$r_*(r) = r + \frac{2Mr_+}{r_+ - r_-} \ln\frac{r - r_+}{2M} + \frac{2Mr_-}{r_+ - r_-} \ln\frac{r - r_-}{2M} \ . \tag{B.9}$$

This is derived from the rule $dr_*/dr = (r^2 + a^2)/\Delta$, where $\Delta = (r - r_+)(r - r_-)$ and $r_\pm = M \pm \sqrt{M^2 - a^2}$. Note that r_+ is the coordinate radius of the hole's event horizon. The difference $t - r_*$ is the retarded time. The time dependence of all

quantities in the distant wave zone always appears in this form, so for all practical purposes the r_* dependence can be ignored.

When we specialize to periodic orbits, the coefficient $Z^H_{lm\omega}$ can be expanded in harmonics of the orbital periods: denoting N as some set of harmonic indices, and ω_{mN} as a particular harmonic of the fundamental frequencies, we can write

$$Z^H_{lm\omega} = \sum_N Z^H_{lmN}\delta(\omega - \omega_{mN}). \tag{B.10}$$

If we now specialize to circular orbits, with two orbital frequencies, Ω_ϕ and Ω_θ, the harmonic frequency is

$$\omega_{mk} = m\Omega_\phi + k\Omega_\theta \ . \tag{B.11}$$

In the Schwarzschild limit, $\Omega_\phi = \Omega_\theta$ due to spherical symmetry. Kerr black holes do not share this property due to the oblateness of their geometry and the effect of frame dragging. For circular orbits, Ω_ϕ and Ω_θ can be expressed in closed form using elliptic integrals; see Ref. [71].

Putting all of this together, we finally find

$$\begin{aligned}\Psi_4 &= \frac{1}{r}\sum_{lmk} Z^H_{lmk\,-2}S_{lm}(\theta; a\omega_{mk})e^{im\phi}e^{-i\omega_{mk}(t-r_*)} \\ &\equiv \frac{1}{r}\sum_{lmk}\psi_{lmk} \ .\end{aligned} \tag{B.12}$$

If we considered eccentric orbits, we would require an index n labelling harmonics of the radial frequency Ω_r.

Combining Eqs. (B.1), (B.3), and (B.12) yields the following general expression for the binary recoil:

$$\frac{dP^j_{\rm GW}}{dt} = \frac{1}{4\pi}\int d\Omega \sum_{lmk}\sum_{l'm'k'} n^j \frac{\left\langle \psi_{lmk}\bar{\psi}_{l'm'k'}\right\rangle}{\omega_{mk}\omega_{m'k'}} \ . \tag{B.13}$$

The overbar on $\bar{\psi}_{l'm'k'}$ denotes complex conjugation.

B.2 Evaluating the energy flux

As a simple warm-up exercise before turning to the evaluation of the recoil, let us evaluate the energy flux that corresponds to the curvature perturbation (B.12). We will do so in two ways: a straightforward evaluation in which we do all averaging in the "obvious" time-domain manner, and an evaluation based on a somewhat more sophisticated averaging using action-angle variables.

In either case, we begin with an expression for the energy flux that is built from Isaacson's stress-energy tensor. It is almost exactly Eq. (B.1), but without the direction vector under the integral:

$$\frac{dE_{\rm GW}}{dt} = \frac{r^2}{32\pi} \int d\Omega \left\langle \partial_t h^{\rm TT}_{ab} \partial_t h^{\rm TT}_{ab} \right\rangle \ , \tag{B.14}$$

leading to the following formula for the energy flux in terms of the curvature perturbation:

$$\frac{dE_{\rm GW}}{dt} = \frac{1}{4\pi} \int d\Omega \sum_{lmk} \sum_{l'm'k'} \frac{\left\langle \psi_{lmk} \bar{\psi}_{l'm'k'} \right\rangle}{\omega_{mk} \omega_{m'k'}} \ . \tag{B.15}$$

B.2.1 Time averaging

The simple-minded time-domain method of averaging a function $f(t)$ is to integrate over one period T and divide by that period:

$$\langle f \rangle = \frac{1}{T} \int_0^T dt \, f(t) \ . \tag{B.16}$$

Unfortunately, this procedure can be somewhat ambiguous as Kerr black hole orbits are multiply periodic. This turns out not to be a problem in this case, as will be shown in a moment.

Inserting the definition of ψ_{lmk} from Eq. (B.12) yields

$$\frac{dE_{\rm GW}}{dt} = \frac{1}{4\pi}\int d\Omega \sum_{lmk}\sum_{l'm'k'} \frac{Z^H_{lmk}\bar{Z}^H_{l'm'k'}}{\omega_{mk}\omega_{m'k'}} {}_{-2}S_{lm}(\theta; a\omega_{mk})\,{}_{-2}S_{l'm'}(\theta; a\omega_{m'k'}) \times e^{i(m-m')\phi}\langle e^{-i(\omega_{mk}-\omega_{m'k'})t}\rangle \quad \text{(B.17a)}$$

$$= \frac{1}{4\pi}\int 2\pi\, d\cos\theta \sum_{lmk}\sum_{l'k'} \frac{Z^H_{lmk}\bar{Z}^H_{l'mk'}}{\omega_{mk}\omega_{mk'}} {}_{-2}S_{lm}(\theta; a\omega_{mk})\,{}_{-2}S_{l'm}(\theta; a\omega_{mk'}) \times \langle e^{-i(k-k')\Omega_\theta t}\rangle \quad \text{(B.17b)}$$

$$= \frac{1}{4\pi}\int 2\pi\, d\cos\theta \sum_{lmk}\sum_{l'} \frac{Z^H_{lmk}\bar{Z}^H_{l'mk}}{\omega^2_{mk}} {}_{-2}S_{lm}(\theta; a\omega_{mk})\,{}_{-2}S_{l'm}(\theta; a\omega_{mk}) \quad \text{(B.17c)}$$

$$= \frac{1}{4\pi}\sum_{lmk}\frac{|Z^H_{lmk}|^2}{\omega^2_{mk}}\,. \quad \text{(B.17d)}$$

To go from (B.17a) to (B.17b), we used the rule

$$\int_0^{2\pi} d\phi\, e^{i(m-m')\phi} = 2\pi\delta_{mm'}\,. \quad \text{(B.18)}$$

This forces $m = m'$, simplifying the time dependence from $(\omega_{mk} - \omega_{m'k'})t$ to $(\omega_{0k} - \omega_{0k'})t = (k - k')\Omega_\theta t$. The only remaining time dependence thus is periodic at harmonics of T_θ, so we clearly want to average with respect to that period. Going from (B.17b) to (B.17c) we averaged over the period T_θ, using

$$\frac{1}{T_\theta}\int_0^{T_\theta} dt\, e^{i(k-k')\Omega_\theta t} = \delta_{kk'}\,. \quad \text{(B.19)}$$

Finally, to go from (B.17c) to (B.17d) we use the normalization (B.8).

B.2.2 Averaging with action-angle variables

Action-angle variables are very useful in detangling issues that arise in multiperiodic systems. One treats the accumulated phase associated with each particular periodic motion separately from all the other phases, even though they of course each accumulate at a rate proportional to time t. For circular orbits of Kerr black

holes, this means that we replace $\Omega_\phi t$ with the accumulated ϕ-angle variable $2\pi w_\phi$, and likewise we replace $\Omega_\theta t$ with $2\pi w_\theta$. We then treat w_ϕ and w_θ as separate, independent variations. See Ref. [185, 186] for further discussion and application of this technique to a study of the motion of generic Kerr black hole orbits. In the action-angle variable paradigm, one averages with respect to each variable:

$$\langle f \rangle = \int_0^1 dw_\phi \int_0^1 dw_\theta \, f(w_\phi, w_\theta) \; . \tag{B.20}$$

In the action-angle variables formulation, the energy flux is

$$\frac{dE_{\rm GW}}{dt} = \frac{1}{4\pi} \int d\Omega \sum_{lmk} \sum_{l'm'k'} \frac{Z^H_{lmk} \bar{Z}^H_{l'm'k'}}{\omega_{mk}\omega_{m'k'}} {}_{-2}S_{lm}(\theta; a\omega_{mk}) {}_{-2}S_{l'm'}(\theta; a\omega_{m'k'}) \times e^{i(m-m')\phi} \left\langle e^{-2\pi i (m-m') w_\phi} e^{-2\pi i (k-k') w_\theta} \right\rangle \; . \tag{B.21}$$

The averaging operators separately force $m = m'$ and $k = k'$, leaving us with the same result as Eq. (B.17d).

In the next section, we will continue to average using action-angle variables. Note that for this particular problem there is nothing intrinsically superior to the "old-fashioned" time averaging. However, the action-angle variables make manifestly clear the separation of the various periodic motions of the system and the way in which they are averaged away.

B.3 Evaluating the recoil

Return now to the formula for the recoil, expressed in terms of Teukolsky equation variables:

$$\frac{dP^j_{\rm GW}}{dt} = \frac{1}{4\pi} \int d\Omega \sum_{lmk} \sum_{l'm'k'} n^j \frac{\left\langle \psi_{lmk} \bar{\psi}_{l'm'k'} \right\rangle}{\omega_{mk}\omega_{m'k'}} \; . \tag{B.22}$$

Let us begin by first focusing on orbits that are purely equatorial (more general orbits will be treated elsewhere [187]). In this case, the k index can be ignored

— the orbit does not oscillate in the latitudinal direction, so $\psi_{lmk} = 0$ for $k \neq 0$. Equation (B.22) then simplifies to

$$\frac{dP^j_{\rm GW}}{dt} = \frac{1}{4\pi}\int d\Omega \sum_{lm}\sum_{l'm'} n^j \frac{\left\langle \psi_{lm}\bar{\psi}_{l'm'}\right\rangle}{\omega_m \omega_{m'}} \ . \tag{B.23}$$

The components of n^a that we are interested in are, in an asymptotically spherical coordinate system,

$$n^x = \sin\theta\cos\phi \ , \tag{B.24a}$$

$$n^y = \sin\theta\sin\phi \ , \tag{B.24b}$$

$$n^z = \cos\theta \ . \tag{B.24c}$$

By symmetry, we expect there to be no momentum ejection along z, so we will ignore that direction for now. For calculational convenience, it is useful to work with $n^\pm = e^{\pm i\phi}\sin\theta$. Insert this into Eq. (B.22) and expand:

$$\frac{dP^\pm_{\rm GW}}{dt} = \frac{1}{4\pi}\int d\Omega \sum_{lm}\sum_{l'm'}\left[\frac{Z^H_{lm}\bar{Z}^H_{l'm'}}{\omega_m\omega_{m'}} {}_{-2}S_{lm}(\theta;a\omega_m)\,{}_{-2}S_{l'm'}(\theta;a\omega_{m'})\sin\theta \right.$$
$$\left. \times e^{i(m\pm1-m')\phi}\left\langle e^{-2\pi i(m-m')w_\phi}\right\rangle\right] \ . \tag{B.25}$$

Performing the averaging over the action-angle variables, we force $m' = m$, so this becomes

$$\frac{dP^\pm_{\rm GW}}{dt} = \frac{1}{4\pi}\int d\Omega \sum_{ll'm}\frac{Z^H_{lm}\bar{Z}^H_{l'm}}{\omega^2_m} {}_{-2}S_{lm}(\theta;a\omega_m)\,{}_{-2}S_{l'm}(\theta;a\omega_m)\sin\theta e^{\pm i\phi} = 0 \ . \tag{B.26}$$

The zero comes from integrating over ϕ. This forces us to the following conclusion: *The averaged recoil from gravitational radiation emission is zero.*

Does this result make sense? Yes — but, it is telling us that *we just computed the wrong quantity.* We are doing an adiabatic calculation, treating the orbit as a truly periodic, geodesic orbit of a black hole. Because it is periodic, the x and

y components of the recoil of course oscillate sinusoidally over the course of the orbit. Naturally, the averaged recoil turns out to be zero — until we include the effect of radiation reaction, we do not expect to see any effect.

Far more interesting is the recoil computed in a frame that corotates at the average ϕ frequency of the orbit. In coordinates attached to an observer in this frame, the instantaneous kick always points in the same direction (modulo some oscillations). In essence, working in this frame makes it possible for us to compute the *magnitude* of the sinusoidally varying recoil, rather than the components of the vectorial recoil itself.

The components of the radial unit vector n^a in the corotating frame are found by applying a rotation by the angle $\Omega_\phi t = 2\pi w_\phi$ about the z axis,

$$R_{eq}(\text{inertial} \to \text{corotating}) = \begin{pmatrix} \cos 2\pi w_\phi & \sin 2\pi w_\phi & 0 \\ -\sin 2\pi w_\phi & \cos 2\pi w_\phi & 0 \\ 0 & 0 & 1 \end{pmatrix} ; \tag{B.27}$$

using this matrix tells us that the basis vectors in the corotating frame are

$$n^x_{\rm co} = n^x \cos 2\pi w_\phi + n^y \sin 2\pi w_\phi \,, \tag{B.28a}$$

$$n^y_{\rm co} = -n^x \sin 2\pi w_\phi + n^y \cos 2\pi w_\phi \,, \tag{B.28b}$$

$$n^z_{\rm co} = n^z \,. \tag{B.28c}$$

Writing $n^\pm_{\rm co} = n^x_{\rm co} \pm i n^y_{\rm co}$, we find

$$n^\pm_{\rm co} = e^{\mp 2i\pi w_\phi} n^\pm \,. \tag{B.29}$$

The recoil for equatorial orbits, projected onto this corotating basis, is

$$\left.\frac{dP^\pm_{\rm GW}}{dt}\right|_{\rm co} = \frac{1}{4\pi}\int d\Omega \sum_{lm}\sum_{l'm'} \left[\frac{Z^H_{lm}\bar{Z}^H_{l'm'}}{\omega_m \omega_{m'}} {}_{-2}S_{lm}(\theta; a\omega_m) {}_{-2}S_{l'm'}(\theta; a\omega_{m'}) \sin\theta \right.$$

$$\times e^{i(m\pm1-m')\phi'}\left\langle e^{-2\pi i(m\pm1-m')w_\phi}\right\rangle\Big] \ . \quad \text{(B.30)}$$

Averaging over w_ϕ forces $m' = m \pm 1$. Continuing the analysis,

$$\left.\frac{dP^{\pm}_{\rm GW}}{dt}\right|_{\rm co} = \frac{1}{4\pi}\int d\Omega \sum_{ll'm} \frac{Z^H_{lm}\bar{Z}^H_{l'(m\pm1)}}{\omega_m\omega_{(m\pm1)}} {}_{-2}S_{lm}(\theta;a\omega_m)\,{}_{-2}S_{l(m\pm1)}(\theta;a\omega_{(m\pm1)})\sin\theta \quad \text{(B.31a)}$$

$$= \frac{1}{2}\int_{-1}^{1} d\cos\theta \sum_{ll'm} \frac{Z^H_{lm}\bar{Z}^H_{l'(m\pm1)}}{\omega_m\omega_{(m\pm1)}} {}_{-2}S_{lm}(\theta;a\omega_m)\,{}_{-2}S_{l(m\pm1)}(\theta;a\omega_{(m\pm1)})\sin\theta \quad \text{(B.31b)}$$

$$\equiv \frac{1}{4\pi}\sum_{ll'm} \frac{Z^H_{lm}\bar{Z}^H_{l'(m\pm1)}}{\omega_m\omega_{(m\pm1)}} I_{(-2)ll'm(m\pm1)}(a\omega_m;a\omega_{(m\pm1)}) \ . \quad \text{(B.31c)}$$

On the last line, we've hidden the integral over θ by defining a number $I_{(-2)ll'm(m\pm1)}$; techniques for evaluating it are described in Section B.4. Notice that *this recoil does not vanish.* By evaluating the recoil in a corotating frame, we compute the recoil's magnitude, eliminating the oscillations that cause it to average to zero.

In the end, the quantity that we really want to understand is the recoil velocity that accumulates in an adiabatic inspiral. We must allow the frequency Ω_ϕ and the complex amplitudes Z^H_{lm} to slowly evolve with time. "Slowly" means that the rates of change of these numbers is much less than Ω times these numbers:

$$\frac{dZ^H_{lm}}{dt} \ll \Omega_\phi \times Z^H_{lm} \ , \quad \text{(B.32)}$$

$$\frac{d\Omega_\phi}{dt} \ll \Omega_\phi \times \Omega_\phi \ . \quad \text{(B.33)}$$

If this condition is *not* met, then the frequencies and complex amplitudes vary so quickly that we cannot treat them as constants in the averaging integrals.

Because we in fact treat these quantities as though they are constant under the integrals, we are making some error. Let $A_{\rm exact}$ be the average computed by treating the time variation of all quantities exactly, and let $A_{\rm adiabatic}$ be the average

computed by treating the slowly evolving quantities as constants. You should be able to convince yourself that

$$\frac{A_{\rm exact} - A_{\rm adiabatic}}{A_{\rm exact}} \approx \frac{d\Omega_\phi/dt}{\Omega_\phi^2} \equiv \frac{1}{2\pi\mathcal{N}_\phi} \ . \tag{B.34}$$

The number $\mathcal{N}_\phi$ represents the number of ϕ orbits that the orbit accumulates before the frequency changes significantly. When it is large, the orbit evolves adiabatically, and approximating the slowly evolving quantities as constant when averaging works OK.

With this in mind, we now can see how to "integrate up" the recoil force to obtain the accumulated recoil velocity: we make the frequencies and the numbers Z^H_{lm} slowly varying functions of time, we invert all of the transformations, and then integrate. Let $\phi(t)$ be the accumulated azimuthal angle over the course of an inspiral, and define

$$\dot{\mathcal{P}}^{\pm}(t) \equiv \frac{e^{\pm i\phi(t)}}{4\pi} \sum_{ll'm} \frac{Z^H_{lm}(t)\bar{Z}^H_{l'(m\pm1)}(t)}{\omega_m(t)\omega_{(m\pm1)}(t)} I_{(-2)ll'm(m\pm1)}[a\omega_m(t); a\omega_{(m\pm1)}(t)] \ , \tag{B.35}$$

where $\dot{\mathcal{P}}^{\pm} = \dot{P}^x_{\rm GW} + i\dot{P}^y_{\rm GW} = e^{\pm i\phi(t)}\dot{\mathcal{P}}^{\pm}_{\rm GW}$. The expression in Eq. (2.38) is equivalent to $\dot{\mathcal{P}}^{+}_{\rm GW}$, but we have dropped the spin-weight indices on the spheroidal harmonic functions in section 2.4. The recoil velocity is then given by

$$M\Delta v^x_{\rm GW} = \frac{1}{2}\int dt \ \left[\dot{\mathcal{P}}^{+}(t) + \dot{\mathcal{P}}^{-}(t)\right] \ , \tag{B.36a}$$

$$M\Delta v^y_{\rm GW} = \frac{1}{2i}\int dt \ \left[\dot{\mathcal{P}}^{+}(t) - \dot{\mathcal{P}}^{-}(t)\right] \ , \tag{B.36b}$$

which are equivalent to Eq. (2.39).

B.4 Angular integrals

The numbers Z^H_{lmk} are found by solving for the Teukolsky equation Green's function and integrating over a source function constructed from the stress-energy tensor

of the orbiting particle; a detailed description of this calculation is given in Sec. IV of Ref. [71]. We compute these numbers using the code that was developed for that analysis, as well as the analysis of Ref. [72]. Note, though, that we need to couple Z^H components with different values of l, rather than just evaluating $|Z^H_{lmk}|^2$. Because of this, we need to make sure that the phase of those numbers is computed very accurately.

Our remaining task is to evaluate the θ integrals. Written generally, the integrals in Eqs. (2.38) are

$$\begin{aligned} I_{sll'mm'}(a\omega, a\omega') &= 2\pi \int_0^\pi {}_sS_{lm}(\theta, a\omega)\,{}_sS_{l'm'}(\theta, a\omega') \sin^2\theta\, d\theta\ , \qquad m' = m \pm 1 \\ &= 0 \qquad \text{all other } m' \end{aligned} \tag{B.37}$$

$$J_{sll'm}(a\omega) = 2\pi \int_0^\pi {}_sS_{lm}(\theta, a\omega)\,{}_sS_{l'm}(\theta, a\omega) \cos\theta \sin\theta\, d\theta \tag{B.38}$$

Begin by specializing to the Schwarzschild limit, and put $\cos\theta = \xi$. The spin-weighted spheroidal harmonics then reduce to spin-weighted spherical harmonics: ${}_sS_{lm}(\theta) \to {}_s\hat{Y}_{lm}(\theta)$. [The hatted harmonic is the usual spherical harmonic without the ϕ dependence: ${}_sY(\theta,\phi) = {}_s\hat{Y}(\theta)e^{im\phi}$.] It is convenient at this point to adopt Dirac notation, so that ${}_s\hat{Y}_{lm}(\theta) \to |slm\rangle$. In this notation, the integral of two spherical harmonics and a third function $f(\xi)$ is written as follows:

$$2\pi \int_{-1}^{1} {}_s\hat{Y}_{lm}(\xi) f(\xi) {}_s\hat{Y}_{l'm'}(\xi)\, d\xi = \langle slm|f|sl'm'\rangle\ . \tag{B.39}$$

The factor of 2π included in this definition is because we really should define these integrals as being over solid angle 4π rather than over $-1 \le \cos\theta \le 1$. However, for all cases that are of interest to us, the ϕ dependence has already been washed away by the averaging procedure. The ϕ piece of that integral then only contributes an overall factor of 2π. We write this out explicitly here in order to avoid confusion.

In the Schwarzschild limit, the integrals that we want to know for the recoil are then

$$I_{sll'mm'}(0,0) = \langle slm|\sqrt{1-\xi^2}|sl'm'\rangle \ , \tag{B.40}$$

$$J_{sll'm}(0) = \langle slm|\xi|sl'm)\rangle \ . \tag{B.41}$$

These quantities can be expressed as

$$\begin{aligned} 2\pi \int_0^\pi \sin\theta d\theta \, {}_s\hat{Y}_{lm} \, {}_s\hat{Y}_{l'm'} \, {}_0\hat{Y}_{1\mu} &= \left[\frac{3}{4\pi}\frac{2l'+1}{2l+1}\right]^{1/2} \langle l', 1, m', \mu | l, m\rangle \\ &\qquad \times \langle l', 1, -s, 0 | l, -s\rangle \delta_{m'+\mu,m} \\ &= \left[\frac{3}{4\pi}\frac{2l'+1}{2l+1}\right]^{1/2} \langle l', 1, m', \mu | l, m\rangle \langle l', 1, -s, 0 | l, -s\rangle \delta_{m',m-\mu} \ , \end{aligned} \tag{B.42}$$

where the numbers $\langle j_1 j_2 m_1 m_2 | JM\rangle$ are Clebsch-Gordan coefficients. We have written them here using the notation of Ref. [188]. Note that the Clebsch-Gordan coefficients enforce $l' \in [|l-1|, l, |l+1|]$.

To evaluate Eq. (B.40), we use

$$\sin\theta = -\sqrt{\frac{8\pi}{3}} \, {}_0\hat{Y}_{1,1} \tag{B.43}$$

for $\mu = 1$ (that is, for $m' = m - 1$). We use

$$\sin\theta = \sqrt{\frac{8\pi}{3}} \, {}_0\hat{Y}_{1,-1} \tag{B.44}$$

for $\mu = -1$ ($m' = m + 1$).

Putting all of this together, we finally obtain

$$\begin{aligned} I_{sll'mm'}(0,0) &= \pm\sqrt{\frac{4l'+2}{2l+1}} \langle l', 1, m', \mp 1 | l, m\rangle \langle l', 1, -s, 0 | l, -s\rangle \qquad \text{for } m' = m \pm 1 \, , \\ &= 0 \qquad \text{for all other } m'. \end{aligned} \tag{B.45}$$

The second integral has been used extensively before [cf. Eq. (A5) of Ref. [71], correcting an error in the prefactor]:

$$J_{sll'm}(0) = \sqrt{\frac{2l'+1}{2l+1}}\langle l', 1, m, 0|l, m\rangle\langle l', 1, -s, 0|l, -s\rangle \tag{B.46}$$

This result was originally taken from Ref. [189], who in turn took it from Ref. [40].

Turn now to the generalization of these quantities for orbits of Kerr holes. These integrals can be expressed in a fairly simple form using the fact that the spheroidal harmonics are nicely decomposed into spherical harmonics:

$$\begin{aligned} {}_sS_{lm}(\theta; a\omega) &= \sum_{k=l_{\min}}^{\infty} b^l_k(a\omega)\,{}_s\hat{Y}_{km}(\theta) \\ &= \sum_{k=l_{\min}}^{\infty} b^l_k(a\omega)|skm\rangle\ . \end{aligned} \tag{B.47}$$

The expansion coefficients $b^l_k(a\omega)$ are simple to compute; see Appendix A of Ref. [71]. Also, $l_{\min} = \max(|s|, |m|)$. For a Schwarzschild hole, $b^l_k = \delta_{kl}$. For non-zero spin, it is typically peaked at $k = l$, but has some interesting and important breadth beyond there.

To proceed, we insert the expansion (B.47) into the momentum flux integrals (2.38). Let us evaluate $J_{sll'm}(a\omega)$:

$$\begin{aligned} J_{sll'm}(a\omega) &= 2\pi \int_{-1}^{1} {}_sS_{lm}(\xi; a\omega)\,{}_sS_{l'm}(\xi; a\omega)\xi\, d\xi \\ &= \sum_{k=l_{\min}}^{\infty}\sum_{j=l_{\min}}^{\infty} b^l_k(a\omega)b^{l'}_j(a\omega)\langle skm|\xi|sjm\rangle \\ &= \sum_{k=l_{\min}}^{\infty}\sum_{j=l_{\min}}^{\infty} b^l_k(a\omega)b^{l'}_j(a\omega)J_{skjm}(0) \\ &= \sum_{k=l_{\min}}^{\infty}\sum_{j=l_{\min}}^{\infty} b^l_k(a\omega)b^{l'}_j(a\omega)\sqrt{\frac{2j+1}{2k+1}}\langle j, 1, m, 0|k, m\rangle\langle j, 1, -s, 0|k, -s\rangle \end{aligned}$$

$$= \sum_{k=l_{\min}}^{\infty} \left[b_k^l(a\omega) b_{k-1}^{l'}(a\omega) \sqrt{\frac{2k-1}{2k+1}} \langle k-1,1,m,0|k,m\rangle \right.$$
$$\times \langle k-1,1,-s,0|k,-s\rangle + b_k^l(a\omega) b_k^{l'}(a\omega) \langle k,1,m,0|k,m\rangle \langle k,1,-s,0|k,-s\rangle$$
$$\left. + b_k^l(a\omega) b_{k+1}^{l'}(a\omega) \sqrt{\frac{2k+3}{2k+1}} \langle k+1,1,m,0|k,m\rangle \langle k+1,1,-s,0|k,-s\rangle \right] . \quad \text{(B.48)}$$

On the last line we've used the fact that $\langle j,1,m,0|k,m\rangle \neq 0$ only for $j \in [|k-1|, k, |k+1|]$; this converts the double sum into a single sum. When evaluating these sums, it's necessary to keep in mind that the spin-weighted spherical harmonic ${}_sY_{lm}$ is non-zero only for $l \geq \min(|m|,|s|)$. The first term of the final formula (the contribution at $j = k-1$) will thus be zero when $k = l_{\min}$.

Let us similarly evaluate $I_{sll'mm'}(a\omega, a\omega')$:

$$I_{sll'mm'}(a\omega, a\omega') = 2\pi \int_{-1}^{1} {}_sS_{lm}(\xi; a\omega) {}_sS_{l'm'}(\xi; a\omega') \sqrt{1-\xi^2}\, d\xi$$
$$= \sum_{k=l_{\min}}^{\infty} \sum_{j=l'_{\min}}^{\infty} b_k^l(a\omega) b_j^{l'}(a\omega') \langle skm|\sqrt{1-\xi^2}|sjm'\rangle$$
$$= \sum_{k=l_{\min}}^{\infty} \sum_{j=l'_{\min}}^{\infty} b_k^l(a\omega) b_j^{l'}(a\omega') I_{skjmm'}(0,0)$$
$$= \pm \sum_{k=l_{\min}}^{\infty} \sum_{j=l'_{\min}}^{\infty} b_k^l(a\omega) b_j^{l'}(a\omega') \sqrt{\frac{4j+2}{2k+1}} \langle j,1,m',\mp 1|k,m\rangle \langle j,1,-s,0|k,-s\rangle$$
$$= \sum_{k=\pm \min(l_{\min}, l'_{\min})}^{\infty} \left[b_k^l(a\omega) b_{k-1}^{l'}(a\omega') \sqrt{\frac{4k-2}{2k+1}} \langle k-1,1,m',\mp 1|k,m\rangle \right.$$
$$\times \langle k-1,1,-s,0|k,-s\rangle + b_k^l(a\omega) b_k^{l'}(a\omega') \sqrt{2} \langle k,1,m',\mp 1|k,m\rangle \langle k,1,-s,0|k,-s\rangle$$
$$\left. + b_k^l(a\omega) b_{k+1}^{l'}(a\omega') \sqrt{\frac{4k+6}{2k+1}} \langle k+1,1,m',\mp 1|k,m\rangle \langle k+1,1,-s,0|k,-s\rangle \right] . \quad \text{(B.49)}$$

Note that $\omega \equiv \omega_{mk}$, $\omega' \equiv \omega_{(m\pm 1)k}$. When evaluating Eq. (B.49), we again have to be careful to handle terms at the lower end of the sum — some will be zero by the rules governing the harmonics.

Appendix C
Formulas for the last stable orbit

The inner-most stable circular orbit (ISCO) for orbits in the equatorial plane of a Kerr black hole is given by [73]

$$\tilde{r}_{\rm isco}(\tilde{a}) = 3 + Z_2 - {\rm sign}(\tilde{a})\sqrt{(3-Z_1)(3+Z_1+2Z_2)}\ , \tag{C.1a}$$

$$Z_1 = 1 + (1-\tilde{a}^2)^{1/3}[(1+\tilde{a})^{1/3} + (1-\tilde{a})^{1/3}]\ , \tag{C.1b}$$

$$Z_2 = (3\tilde{a}^2 + Z_1^2)^{1/2}\ , \tag{C.1c}$$

where $-1 \leq \tilde{a} \leq 1$ and $\tilde{a} < 0$ refers to retrograde orbits.

A simple analytic fit to the equation for the ISCO can easily be derived. It comes from noticing that the plot of Eq. (C.1a) resembles $\sqrt{1-\tilde{a}}$. A good guess for a simple function to replace (C.1a) is

$$\tilde{r}_{\rm isco} \approx b\sqrt{1-\tilde{a}} + c\tilde{a} + d\ . \tag{C.2}$$

From knowing only $\tilde{r}_{\rm isco}(0) = 6$, $\tilde{r}_{\rm isco}(1) = 1$, and $\tilde{r}_{\rm isco}(-1) = 9$, one can determine the 3 constants b, c, d. Plugging in and solving the simple linear system, we get $b = 2+\sqrt{2}$, $c = \sqrt{2}-3$, and $d = 4-\sqrt{2}$. Interestingly, this formula agrees surprisingly well with Eq. (C.1a)—better than 7% for all values of $\tilde{a}$, and *much* better for $\tilde{a} \lesssim 0.8$. Agreement is better than 1% for $\tilde{a} \leq 0.6$.

The last stable orbit (LSO) is the analog of the ISCO for more general orbits. For circular but inclined orbits, the LSO can be fit surprisingly well by [155]

$$\tilde{r}_{\rm LSO}(\hat{a} \geq 0, \iota) \simeq |\tilde{r}_{\rm isco}(-\hat{a})| + \frac{1}{2}(1+\cos\iota)[\tilde{r}_{\rm isco}(\hat{a}) - |\tilde{r}_{\rm isco}(-\hat{a})|] \tag{C.3}$$

where ι is the inclination angle defined by

$$\cos\iota = \frac{L_z}{\sqrt{L_z^2+Q}}\ , \tag{C.4}$$

L_z is the orbital angular momentum, and Q is the Carter constant. Here the spin parameter $\hat{a}$ is strictly non-negative. Prograde orbits correspond to $\iota = 0$ and retrograde orbits correspond to $\iota = \pi$.

We can use Eq. (C.2) to simplify the equation for the LSO as well:

$$\tilde{r}_{\rm LSO} \approx \frac{1}{2} b(\sqrt{1+\hat{a}} + \sqrt{1-\hat{a}}) + \frac{1}{2}\cos\iota[b(\sqrt{1-\hat{a}} - \sqrt{1+\hat{a}}) + 2c\hat{a}] + d\,. \quad \text{(C.5)}$$

This formula likewise agrees with Eq. (C.3) to better than 7%.

Appendix D
Equations of Motion for the Plunge

The black hole perturbation theory calculation of the recoil discussed in Section 2.4 and Appendix B becomes invalid as one approaches the inner-most circular orbit (ISCO). The reasons for this are two-fold: we solve the Teukolsky equation in the frequency-domain (by Fourier-transforming the partial differential equation for Ψ_4) and under the assumption that the orbit evolves adiabatically (radiation reaction acts slowly enough that the particle smoothly transitions from one geodesic of the Kerr spacetime to another). At the ISCO both of these approximations break down. Past the ISCO the geodesics that "plunge" into the horizon are not periodic. Our frequency-domain decomposition of the Teukolsky equation requires that the geodesic orbits be periodic with well-defined frequencies. Near the ISCO the orbit is no longer evolving slowly, so the adiabatic assumption is invalid as well. Fortunately, the break down of adiabaticity lends itself to another approximation: After it has passed through the ISCO, the particle's motion is largely governed by the effective-potential of the Kerr spacetime. While the radiation-reaction forces are strong near the ISCO, the plunge happens very quickly so they do not have a strong effect on the particle's motion (in the limit where $q \ll 1$; see [74] for further discussion). The plunge happens in ~ 1 to a few orbital cycles, during which time the constants of the motion (E, L, Q) change very little. This allows us to assume that (up to finite mass ratio corrections) the particle motion is entirely geodesic during the plunge. To describe this motion, we use the following modified form of the geodesic equations, specialized to motion in the equatorial plane (see e.g. Shapiro & Teukolsky [133]):

$$\frac{dt}{d\tau} = \frac{(r^3 + a^2 r + 2Ma^2)E - 2aML}{\mu r \Delta} , \tag{D.1a}$$

$$\frac{d\phi}{d\tau} = \frac{(r-2M)L + 2aME}{\mu r \Delta} \,, \tag{D.1b}$$

$$\mu \frac{dr}{d\tau} = -\sqrt{R(E,L,r)/r^3} \,, \tag{D.1c}$$

$$R \equiv E^2(r^3 + a^2 r + 2Ma^2) - 4aMEL - (r-2M)L^2 - \mu^2 r\Delta \,, \tag{D.1d}$$

$$E = E(\tau) = \left(\frac{dE}{dt}\right)_{r_0}^{\rm inspiral} \frac{dt}{d\tau}(r_0, E_0, L_0)\tau + E_0 \,, \tag{D.1e}$$

$$L = L(\tau) = \left(\frac{dL}{dt}\right)_{r_0}^{\rm inspiral} \frac{dt}{d\tau}(r_0, E_0, L_0)\tau + L_0 \,, \tag{D.1f}$$

where $\Delta = r^2 + a^2 - 2Mr$, E and L are the energy and angular momentum of the particle (as viewed by an observer at spatial infinity), (t, r, ϕ) are the Boyer-Lindquist coordinates, M is the large black hole mass, a is the Kerr spin parameter (defined such that the BH has spin angular momentum $|\mathbf{S}| = aM$), and μ is the mass of the small particle (which we will think of as a small Schwarzschild black hole of radius 2μ). Note the minus sign in Eq. (D.1c), which is chosen so that the orbits plunge into the BH. These equations (and those below) can be put in dimensionless form by the following change of variables: $\tau = \tilde{\tau}M$, $t = \tilde{t}M$, $r = \tilde{r}M$, $a = \tilde{a}M$, $E = \tilde{E}\mu$, and $L = \tilde{L}\mu M$ (or by simply setting $M = \mu = 1$). Note that we have modified the geodesic equations by allowing the constants of the motion to vary with proper time τ. In practice the energy and angular momentum vary slowly during the plunge, so our results would not change much if we chose $E = E_0$, $L = L_0$. The rates of change of the energy $(dE/dt)_{r_0}^{\rm inspiral}$ and angular momentum $(dL/dt)_{r_0}^{\rm inspiral}$ are determined from the inspiral calculation and evaluated at the initial radius r_0 of the plunge evolution. For circular, equatorial orbits at a radius r, the energy and angular momentum may be determined by solving $R = 0$, $\partial R/\partial r = 0$ (Bardeen, Press, & Teukolsky [73]):

$$\tilde{E}_{\rm circ} = \frac{1 - 2/\tilde{r} + \tilde{a}/\tilde{r}^{3/2}}{\sqrt{1 - 3/\tilde{r} + 2\tilde{a}/\tilde{r}^{3/2}}} \,, \tag{D.2a}$$

$$\tilde{L}_{\rm circ} = {\rm sign}(\tilde{a}) \frac{\tilde{r}^{1/2} - 2\tilde{a}/\tilde{r} + \tilde{a}^2/\tilde{r}^{3/2}}{\sqrt{1 - 3/\tilde{r} + 2\tilde{a}/\tilde{r}^{3/2}}} \ , \tag{D.2b}$$

where in the above equations we extend the spin parameter $\tilde{a} = a/M$ to the range $-1 \leq \tilde{a} \leq 1$, with negative values corresponding to retrograde orbits (orbital angular momentum counter-aligned with black hole spin). Note that in Eqs.(D.1) above, a is taken to be strictly positive, while L can have either sign depending on whether the orbit is prograde or retrograde.

With these equations in hand, our goal is to generate a plunge geodesic that matches onto the previously calculated inspiral worldline. This involves picking the correct initial values for the coordinates as well as the constants of motion of the orbit, E_0 and L_0. To do this we pick the following initial conditions: $t(\tau = 0) = 0$, $\phi(\tau = 0) = \phi_0$, $r(\tau = 0) \equiv r_0 = r_{\rm ISCO} + \delta r$, where (r_0, ϕ_0) are the coordinates of the particle near the end of the inspiral calculation, shortly before the particle reaches the ISCO ($r_0 \gtrsim r_{\rm ISCO}$). To fully specify a plunging geodesic, we must also make a choice for the initial values of the energy and angular momentum (E_0, L_0). One might first think to choose $E_0 = E_{\rm circ}(r_0)$, $L_0 = L_{\rm circ}(r_0)$, but such a choice would lead to an orbit that remains circular and never plunges. So we use the following procedure to determine values for E_0 and L_0 that lead to a plunging orbit: First pick $E_0 = E_{\rm circ}(r_0)$, and then solve the following equations for L_0:

$$\mu^2 r_0^3 \left[\left(\frac{dr}{dt} \right)_0 \left(\frac{dt}{d\tau} \right) \Big|_{(r_0, E_0, L_0)} \right]^2 = R(r_0, E_0, L_0) \ , \tag{D.3a}$$

$$\left(\frac{dr}{dt} \right)_0 = \left(\frac{dE}{dt} \right)_{r_0}^{\rm inspiral} \left(\frac{dE_{\rm circ}}{dr} \right)^{-1} \ . \tag{D.3b}$$

This has the solution

$$L_0 = \frac{p_1 + {\rm sign}(\tilde{a}) \sqrt{p_3}}{p_2} \ , \tag{D.4}$$

where

$$p_1 = (2aME_0)\left[r_0\left(\frac{dr}{dt}\right)_0^2(r_0^3 + a^2 r_0 + 2Ma^2) - \Delta_0^2\right] , \tag{D.5a}$$

$$p_2 = (2Ma)^2 r_0\left(\frac{dr}{dt}\right)_0^2 + \Delta_0^2(r_0 - 2M) , \tag{D.5b}$$

$$p_3 = r_0\Delta_0^3\Bigg\{\Delta_0^2\left[r_0E_0^2 - \mu^2(r_0 - 2M)\right] - r_0\left(\frac{dr}{dt}\right)_0^2\Big[(2\mu Ma)^2 + r_0E_0^2(r_0^3 + a^2r_0 + 2Ma^2)\Big]\Bigg\} , \tag{D.5c}$$

where $\Delta_0 = r_0^2 + a^2 - 2Mr_0$. The quantity $(dE/dt)_{\rm r_0}^{\rm inspiral}$ [and also $(dL/dt)_{\rm r_0}^{\rm inspiral}$] are determined by the output of our code that solves the Teukolsky equation. This method for choosing L_0 incorporates information on the radially-inward component of the particle motion. One makes little error by simply neglecting the $O(\tau)$ correction terms in Eqs. (D.1e) and (D.1f). When applying the above equations it is important to note that $dE_{\rm circ}/dr$ diverges at the ISCO, which means that r_0 cannot be taken to be too close to the ISCO. Other ways of choosing a plunge trajectory are possible. For example, one could have chosen $L_0 = L_{\rm circ}(r_0)$ and solved equations similar to the ones above for E_0. A method similar to this was implemented by Blanchet, Qusailah, and Will [6] in their treatment of the plunge recoil.

D.0.1 Alternate scheme for radiation reaction

As an alternative to using values for $(dE/dt)_{r_0}^{\rm inspiral}$ and $(dL/dt)_{r_0}^{\rm inspiral}$ obtained from a Teukolsky code, one can also use the following prescription, based on the quadrupole formula [74]: The energy flux for nearly circular orbits near the ISCO can be written as

$$\frac{d\tilde{E}}{d\tilde{t}} = -\frac{32}{5}q\tilde{\Omega}^{10/3}\dot{\mathcal{E}}_{\rm GR}(\hat{a}) , \tag{D.6}$$

where the orbital frequency is given by the geodesic equation

$$\tilde{\Omega} = \frac{d\phi}{d\tilde{t}} = \frac{d\phi}{d\tilde{\tau}} \left(\frac{d\tilde{t}}{d\tilde{\tau}} \right)^{-1} , \tag{D.7}$$

and the energy and angular momentum fluxes are related by

$$\frac{d\tilde{L}}{d\tilde{t}} = \frac{1}{\tilde{\Omega}} \frac{d\tilde{E}}{d\tilde{t}} , \tag{D.8}$$

where $\mathcal{E}_{\rm GR}$ is a general-relativistic correction factor computing by solving the Teukolsky equation (see Table I of Ori & Thorne[74]). For circular and equatorial orbits, we can simplify these equations by using the formula

$$\tilde{\Omega} = \frac{\mathrm{sign}(\hat{a})}{\tilde{r}^{3/2} + \hat{a}} . \tag{D.9}$$

Equations (D.6) and (D.8) may then we used in Eqs. (D.1e), (D.1f), and (D.3b) in place of $(dE/dt)^{\rm inspiral}_{r_0}$ or $(dL/dt)^{\rm inspiral}_{r_0}$.

The scheme for evolving plunge orbits presented in this appendix was originally motivated by the equations of motion for the transition from inspiral to plunge derived by Ori & Thorne [74]. The Ori-Thorne approximation consists of Taylor expanding the radial effective potential $R(r, E, L)/r^3$ to third order in $(r - r_{\rm ISCO})$ and first order in $L - L_{\rm ISCO}$, and evaluating all other quantities at the ISCO. This approximation works well during the transition region, which extends from $r - r_{\rm ISCO} \sim \pm(\text{several})\mu^{2/5}M^{3/5}$, but breaks down as the particle gets deeper into the plunge region.

Appendix E
Details of the lower-limit calculation for the recoil during the plunge

Once we have calculated the plunge trajectory of the particle $[r(\tau), \phi(\tau)]$, we can proceed to calculate the momentum flux. While the procedure described in Appendix D accurately describes the orbit of a point-particle in the strong-field region around a Kerr hole, accurately describing the radiation field of such a particle is a more difficult task and must be treated using black hole perturbation theory. Ideally one would like to solve the Teukolsky equation to compute the momentum radiated during the plunge. However, our frequency-domain Teukolsky solver requires a sequence of geodesics with well defined orbital frequencies, which plunge trajectories lack. To get around this we resort to a crude estimate of the radiated momentum. This will form the basis of our "lower limit" computation for the kick velocity.

Our approximation scheme is a "semi-relativistic" or "hybrid" one that combines relativistic and non-relativistic elements. It is similar to (but formulated independently from) recent schemes for computing "kludged" templates for gravitational waves [157, 158]. This scheme uses fully relativistic formulas to model the orbit, but it truncates the multipole expansion of the momentum flux. Because we ignore higher multipole contributions, we underestimate the total radiated momentum.

To model the momentum flux we use the lowest-order multipole expansion

$$\frac{dP_j^{\rm GW}}{dt} = \left(\frac{2}{63} \langle {}^{(4)}\mathcal{I}_{jab} {}^{(3)}\mathcal{I}_{ab} \rangle + \frac{16}{45} \langle \epsilon_{jpq} {}^{(3)}\mathcal{I}_{pa} {}^{(3)}\mathcal{S}_{qa} \rangle \right) , \tag{E.1}$$

where $P_j^{\rm GW}$ is the linear momentum in the GWs, and t is the time coordinate of an observer far from the source. In the asymptotically-flat region far from the source

$P_j^{\rm GW}$ behaves like the space-component of the special-relativistic 4-momentum. The resulting linear momentum of the source is simply $P_j = -P_j^{\rm GW}$. Since the recoil velocity is much less than c for astrophysically plausible scenarios, we can take the momentum to be $P_j = \gamma M V^j_{\rm recoil} \approx M V^j_{\rm recoil}$, where $\gamma = 1/\sqrt{1 - V^2_{\rm recoil}}$, and M is the asymptotic mass of the emitting system. (Since we are working in an asymptotically Cartesian coordinate system, spatial indices can be raised and lowered freely.) The angle brackets that appear in Eq. (E.1) mean to average over several gravitational wavelengths. This is necessary for computing a well-defined momentum flux. However, since we are interested in the total radiated momentum

$$P_j^{\rm GW} = \int_{-\infty}^{t} \frac{dP_j^{\rm GW}}{dt'}\, dt' \,, \tag{E.2}$$

explicit averaging over the expression for dP_j/dt is not necessary. Such averaging is automatically performed by the integration process in Eq. (E.2).

To compute the momentum flux to lowest order, we use the simple Newtonian-order definitions for the multipole moments in Eq. (E.1), restricting to the case of a point-particle with mass $\mu \ll M$:

$$\mathcal{I}_{ab} = \mu \left(x_a x_b\right)^{\rm STF} = \mu \left(x_a x_b - \frac{r^2}{3}\delta_{ab} \right) \,, \tag{E.3a}$$

$$\mathcal{I}_{jab} = \mu \left(x_j x_a x_b\right)^{\rm STF} = \mu \left[x_j x_a x_b - \frac{r^2}{5}\left(\delta_{ja}x_b + \delta_{jb}x_a + \delta_{ab}x_j\right) \right] \,, \tag{E.3b}$$

$$\mathcal{S}_{ab} = \mu \left(\epsilon_{apq} x_p x_b v^q\right)^{\rm STF} = \mu \frac{x_p v^q}{2}\left(\epsilon_{apq}x_b + \epsilon_{bpq}x_a\right) \,, \tag{E.3c}$$

where ϵ_{jpq} is the Levi-Civita permutation symbol, $v^j = dx^j/dt$ and STF means "take the symmetric, trace-free part". The coordinates x_j that appear in the multipole moments are defined in terms of the Boyer-Lindquist coordinates of the particle by the ordinary polar-coordinate transformation rule:

$$x(\tau) = r(\tau)\cos\phi(\tau)\,, \tag{E.4a}$$

$$y(\tau) = r(\tau)\sin\phi(\tau)\,, \tag{E.4b}$$

$$z(\tau) = 0\,, \tag{E.4c}$$

where our motion is confined to the equatorial plane.

Although all of our functions are computed in terms of the particle's proper time τ, the time derivatives appearing in (E.1) are with respect to the coordinate time t. They are computed by repeatedly applying $d/dt = (dt/d\tau)^{-1}d/d\tau$ to the coordinate transformation (E.4) and the orbit equations of motion (D.1). The expansion of all the time derivatives of $r(\tau)$, $\phi(\tau)$, $E(\tau)$, and $L(\tau)$ that come from Eq. (E.1) becomes exceedingly complicated and is performed using the computer algebra program MAPLE. The expansion of the momentum flux and multipole moments in terms of the coordinates x_j was carried out using the tensor manipulation package GRTENSORII.

We express all the resulting time derivatives analytically. The first derivatives are given by the geodesic equations themselves [Eqs. (D.1)]:

$$\frac{dr}{dt} = \frac{dr}{d\tau}\left(\frac{dt}{d\tau}\right)^{-1}\,, \tag{E.5a}$$

$$\frac{d\phi}{dt} = \frac{d\phi}{d\tau}\left(\frac{dt}{d\tau}\right)^{-1}\,. \tag{E.5b}$$

The higher order derivatives come from differentiating both sides of the geodesic equations. Since $dE/d\tau$ and $dL/d\tau$ are constants [cf. Eqs. (D.1)] and the geodesic equations are independent of $\phi(\tau)$, all of our time derivatives can be expressed as functions of $r(\tau)$, $E(\tau)$, and $L(\tau)$. This allows us to write the time derivative of any function $F(r, E, L)$ as

$$\frac{d}{dt}(F) = \left(\frac{dt}{d\tau}\right)^{-1}\left[\frac{dr}{d\tau}\frac{\partial F}{\partial r} + \frac{dE}{d\tau}\frac{\partial F}{\partial E} + \frac{dL}{d\tau}\frac{\partial F}{\partial L}\right]\,. \tag{E.6}$$

Using this formula for d/dt, the higher order derivatives are defined by:

$$2\frac{dr}{dt}\frac{d^2r}{dt^2} = \frac{d}{dt}\left[\frac{R(r,E,L)}{\mu^2 r^3}\left(\frac{dt}{d\tau}\right)^{-2}\right] , \tag{E.7a}$$

$$\frac{d^2\phi}{dt^2} = \frac{d}{dt}\left(\frac{d\phi}{dt}\right) , \tag{E.7b}$$

$$\frac{d^3r}{dt^3} = \frac{d}{dt}\left(\frac{d^2r}{dt^2}\right) , \tag{E.7c}$$

$$\frac{d^3\phi}{dt^3} = \frac{d}{dt}\left(\frac{d^2\phi}{dt^2}\right) , \tag{E.7d}$$

$$\frac{d^4r}{dt^4} = \frac{d}{dt}\left(\frac{d^3r}{dt^3}\right) , \tag{E.7e}$$

$$\frac{d^4\phi}{dt^4} = \frac{d}{dt}\left(\frac{d^3\phi}{dt^3}\right) . \tag{E.7f}$$

One must then define derivatives of $x(\tau)$ and $y(\tau)$ in terms of the derivatives of $r(\tau)$ and $\phi(\tau)$. This is done by straight forwardly differentiating the coordinate transformation law (E.4). The resulting equations are enormous, especially for d^3r/dt^3 and d^4r/dt^4, which is why MAPLE is used. This method is advantageous because there is no need to compute the time derivatives numerically, which can lead to numerical errors. In this approach, all the derivatives are defined in terms of the functions $r(\tau)$, $\phi(\tau)$, $E(\tau)$, and $L(\tau)$, which are themselves determined by numerically solving the system of ODEs in Eqs. (D.1).

When computing the recoil velocity we need to perform a time integration of the momentum flux in Eq. (E.1). However, the time coordinate t is poorly behaved near the event horizon. Instead we integrate with respect to proper time τ. The total recoil velocity is then given by

$$V^j_{\rm recoil} = -\frac{1}{M}\int_{t_0}^{T}\frac{dP^j_{\rm GW}}{dt}\frac{dt}{d\tau}\,d\tau + V^j_{\rm inspiral} , \tag{E.8}$$

where $V^j_{\rm inspiral}$ is the recoil accumulated up to time t_0 as calculated using our Teukolsky code. It is evaluated at the point $r = r_0$ where we match the plunging geodesic

to the inspiral worldline. This point is taken to be slightly larger than the ISCO radius. There is some error associated with the choice of this matching point. This error is $\lesssim 20\%$ for low or moderate spins, but can be larger for rapid spins ($|\tilde{a}| > 0.8$). The recoil computed above in the test-mass limit is proportional to $V_{\rm recoil} \propto q^2$, where $q = \mu/M$. We have shown numerically that, to within an error of $\sim 20\%$, the function $V_{\rm recoil}/q^2$ is independent of the mass ratio. Following Fitchett and Detweiler [19], we scale our results to higher mass ratios using Fitchett's scaling function $q^2 \to f(q)$ [Eq. (2.5)].

The integral above is terminated at the time T when the Boyer-Lindquist coordinate radius of the point particle is $r = r_{\rm horizon} + 2\mu$, where $r_{\rm horizon}$ is the location of the event horizon. This corresponds in a "quasi-Newtonian" sense to the radius where the horizons of the two black holes touch. This choice also has an associated error. Part of this error comes from the neglect of the ringdown contribution to the recoil. This error has been estimated to be $\sim 15\%$ by Damour and Gopakumar [8]. The other piece of this error is related to the scaling to higher mass ratios. When this scaling is performed, the value of μ that determines the cutoff time T is not adjusted. In our prescription, a larger mass ratio merger would have an earlier cutoff time than a smaller mass ratio merger. But the calculations assume a small mass ratio merger when computing T. The scaling to larger mass ratios only modifies the leading factor of q^2 in the momentum flux.

Appendix F
Justification of metric expansion and equations of motion

The purpose of this appendix is to justify the form of the metric in Eq. (3.1) and the neglect of certain 1PN terms in the metric and hydrodynamics equations (3.9).

F.0.2 Metric expansion

The purpose of our metric expansion (3.1) is to provide a coordinate system in which the properties of a star (specifically, the change in central density) interacting with a binary companion can be studied. In this coordinate system the binary companion (labelled B here and denoted with a prime in the main text) interacts with the star (labelled A here) only through tidal interactions. Since we wish to study only the leading-order corrections to the change in central density due to post-Newtonian interactions, we throw away certain 1PN terms; this is justified below. Our approximation amounts to keeping only the 1PN gravitomagnetic tidal corrections to the metric. The justification for the form of our metric will rely heavily on the formalism introduced in Racine and Flanagan [65]. The tidal pieces of our metric are merely the $l = 2$ tidal pieces of the Newtonian and gravitomagnetic parts of the "body-adapted frame" metric derived there. We specialize the general treatment given in [65] to the limited context of a Newtonian star interacting with quadrupolar tidal fields. The reader is referred to that paper for further details.

Begin by considering the 1PN expansion of the metric in terms of the standard PN parameter $\hat{\varepsilon} \equiv 1/c$:

$$ds^2 = -\{1 + 2\hat{\varepsilon}^2\Phi_g(\hat{\varepsilon}T, \boldsymbol{X}) + 2\hat{\varepsilon}^4[\Phi_g^2(\hat{\varepsilon}T, \boldsymbol{X}) + \psi_g(\hat{\varepsilon}T, \boldsymbol{X})] + O(\hat{\varepsilon}^6)\}dT^2$$

$$+ [2\hat{\varepsilon}^3\zeta_i^g(\hat{\varepsilon}T, \boldsymbol{X}) + O(\hat{\varepsilon}^5)]dTdX^i + [\delta_{ij} - 2\hat{\varepsilon}^2\Phi_g(\hat{\varepsilon}T, \boldsymbol{X})\delta_{ij} + O(\hat{\varepsilon}^4)]dX^i dX^j \ . \tag{F.1}$$

This metric describes the global coordinate system of the binary. The coordinate system is conformally Cartesian and asymptotically flat (since we specify that the global potentials Φ_g, ζ_i^g, and ψ_g go to zero far from the binary). We also assume global harmonic gauge,

$$4\frac{\partial\Phi_g}{\partial(\hat{\varepsilon}T)} + \frac{\partial\zeta_i^g}{\partial X^i} = 0 \ . \tag{F.2}$$

(Note that our notation differs from that used in [65] and that our time coordinates differ from theirs by a factor of $1/\hat{\varepsilon}$. Time derivatives of a quantity introduce additional factors of $\hat{\varepsilon}$. See Sec. II of [65].)

In the vicinity of star A, there exist local coordinate systems $(t, \boldsymbol{x})$ in which the metric has an expansion of the same form as (A1),

$$\begin{aligned} ds^2 = &-\{1 + 2\hat{\varepsilon}^2\Phi_{\rm loc}(\hat{\varepsilon}t, \boldsymbol{x}) + 2\hat{\varepsilon}^4[\Phi_{\rm loc}^2(\hat{\varepsilon}t, \boldsymbol{x}) + \psi_{\rm loc}(\hat{\varepsilon}t, \boldsymbol{x})] + O(\hat{\varepsilon}^6)\}dt^2 \\ &+ [2\hat{\varepsilon}^3\zeta_i^{\rm loc}(\hat{\varepsilon}t, \boldsymbol{x}) + O(\hat{\varepsilon}^5)]dtdx^i + [\delta_{ij} - 2\hat{\varepsilon}^2\Phi_{\rm loc}(\hat{\varepsilon}t, \boldsymbol{x})\delta_{ij} + O(\hat{\varepsilon}^4)]dx^i dx^j \ , \end{aligned} \tag{F.3}$$

and in which the gauge condition also has the same form as in (F.2). The potentials in both coordinate systems satisfy the standard, 1PN Einstein equations in harmonic gauge. However, the metric in the local frame of the star is not asymptotically flat as the local potentials $\Phi_{\rm loc}$, $\zeta_i^{\rm loc}$, and $\psi_{\rm loc}$ diverge at large distances from the star due to the tidal contribution to the potentials.

The local and global coordinate frames are related by a 1PN coordinate transformation of the form

$$T(t, x^j) = t + \hat{\varepsilon}\alpha(\hat{\varepsilon}t, x^j) + \hat{\varepsilon}^3\beta(\hat{\varepsilon}t, x^j) + O(\hat{\varepsilon}^5) \ , \tag{F.4a}$$

$$X^i(t, x^j) = x^i + z^i(\hat{\varepsilon}t) + \hat{\varepsilon}^2 h^i(\hat{\varepsilon}t, x^j) + O(\hat{\varepsilon}^4) \ , \tag{F.4b}$$

where z^i is the Newtonian order spatial vector that relates the global frame to the local frame.[1] The standard coordinate transformation of the metric components, along with the gauge conditions (F.2) in both frames, relate the potentials in the global and local frames and provide the functional form of α, β, and h^i up to several freely specifiable functions of time and one solution of Laplace's equation (see Sec. IIB of [65]). In the vacuum region outside the star (but far from the binary companion), the local potentials $\Phi_{\rm loc}$, $\zeta_i^{\rm loc}$, and $\psi_{\rm loc}$ can be expressed as a multipole expansion in powers of r^l and $1/r^{l+1}$, where $r = (x_i x^i)^{1/2}$ and l is the angular harmonic index of the expansion [see Eq. (3.28) of [65]]. These multipole expansions are characterized in terms of body moments (the coefficients in front of the $1/r^{l+1}$ terms), tidal moments (the coefficients in front of the r^l terms), and gauge moments (coefficients that appear in front of both types of terms and contain information about the coordinate system, but which do not contain gauge-invariant information about the stars). Racine and Flanagan [65] show that the freely-specifiable pieces of the functions that appear in the coordinate transformation (F.4) can be chosen in such a way that (i) all the gauge moments vanish, (ii) the full 1PN mass dipole moment of the star vanishes, and (iii) all the tidal moments with $l < 2$ vanish (see Table I of [65] and the associated discussion). These choices uniquely specify a body-adapted harmonic coordinate system.

We further restrict the metric (F.3) by throwing away the nonlinear 1PN terms $\hat{\varepsilon}^4(\Phi_{\rm loc}^2 + \psi_{\rm loc})$. We argue below that these terms will not affect the central density at the order in which we are interested. Since the remaining potentials satisfy linear partial differential equations, they can be unambiguously split into terms

[1] Terms in the coordinate transformation at higher order in $\hat{\varepsilon}$ do not affect the metric at 1PN order. Also, terms at $O(\hat{\varepsilon}^2)$ in $T(t, x^j)$ and $O(\hat{\varepsilon})$ in $X^i(t, x^j)$ produce only constant shifts of the coordinate systems and can be set to zero.

that depend on the self-gravity of the star and terms that depend on the external tidal field,

$$\Phi^{\rm loc} = \Phi^{\rm self} + \Phi^{\rm ext} \ , \tag{F.5}$$

$$\zeta_i^{\rm loc} = \zeta_i^{\rm self} + \zeta_i^{\rm ext} \ . \tag{F.6}$$

(In the body of this paper $\Phi^{\rm self} \equiv \Phi$.) The external potentials satisfy the vacuum Einstein equations

$$\nabla^2 \Phi^{\rm ext} = \nabla^2 \zeta_i^{\rm ext} = 0 \tag{F.7}$$

and are given by the r^l pieces of the multipole expansions of $\Phi^{\rm loc}$ and $\zeta_i^{\rm loc}$. In Racine and Flanagan [65], the self pieces of the potentials also satisfy the vacuum equations as in (F.7) and are given by the $1/r^{l+1}$ pieces of the multipole expansion. Such an expansion diverges at the center of the coordinate system (when $r \to 0$). Since they are interested in treating the dynamics of strongly gravitating bodies, the "body-adapted" coordinates of [65] are only valid in the weak-field "buffer region" that exists outside the body but far from the companion. In this paper we wish to treat the internal dynamics of a weakly gravitating fluid star. To do this we use the slightly modified body-adapted frame described in the last paragraph of Sec. III D of [65], which extends smoothly into the star's interior. The self potentials are given by the usual Poisson integrals associated with the equations

$$\nabla^2 \Phi^{\rm self} = 4\pi\rho \quad \text{and} \tag{F.8}$$

$$\nabla^2 \zeta_i^{\rm self} = 16\pi\rho v_i \ , \tag{F.9}$$

where ρ is the mass density and v_i is the fluid velocity.

Since we are interested in the oscillation modes of the star, the explicit form of the metric outside the star does not concern us. To find the explicit form of the self potentials inside star, one would simply solve Equations (F.8) and (F.9) along with

the hydrodynamic equations. However, for our purposes we can also ignore the $\zeta_i^{\rm self}$ piece of the metric as it will not affect our calculation of the change in central density; this is justified below. To explicitly compute the external potentials (both inside and outside the star), one can use the formulas found in Sec. V of [65]. Computing only the lowest order ($l = 2$) piece of those potentials yields

$$\Phi^{\rm ext} = \frac{1}{2}\mathcal{E}_{ij}x^i x^j \tag{F.10}$$

and

$$\zeta_i^{\rm ext} = -\frac{1}{2}Y_{ijk}x^j x^k \ . \tag{F.11}$$

In the notation of [65], $\mathcal{E}_{ij} = -{}^nG^A_{ij}$ and, for a two-body system, is given by

$$\mathcal{E}_{ij} = \frac{M_B}{d^3}\left(\delta_{ij} - 3\frac{z_i^{BA}z_j^{BA}}{d^2}\right) \ , \tag{F.12}$$

where M_B is the mass of the companion (M' in the body of this paper), and z_i^{BA} is the separation vector pointing from body B to body A. The tidal moment Y_{ijk} is given by

$$Y_{ijk} = A_{ijk} - A_{<ijk>} \ , \tag{F.13}$$

where

$$A_{ijk} = -4\mathcal{E}_{jk}V_i^{BA} + \frac{6}{5}\left(\delta_{ij}\dddot{z}^A_k + \delta_{ik}\dddot{z}^A_j\right) - \frac{4}{5}\delta_{jk}\dddot{z}^A_i \ , \tag{F.14}$$

and $<>$ means to symmetrize and remove traces on the enclosed indices. Using the definitions $\mathcal{B}_{ij} = -\frac{1}{2}\nabla_{(j}B_{i)}$ and $\boldsymbol{B} = \nabla \times \boldsymbol{\zeta}^{\rm ext}$, the magnetic-type tidal field $\mathcal{B}_{ij}$ can be related to the Y_{ijk} tidal moments by

$$\mathcal{B}_{ij} = \frac{1}{4}(\epsilon_{iab}Y_{baj} + \epsilon_{jab}Y_{bai}) \ , \tag{F.15}$$

and the external gravitomagnetic potential can be expressed as

$$\zeta_i^{\rm ext} = -\frac{2}{3}\epsilon_{iaj}\mathcal{B}^a{}_k x^j x^k \ . \tag{F.16}$$

Racine and Flanagan [131] give an equivalent but simpler formula for the tidal field:

$$\mathcal{B}_{ij} = 6M_B z^{BA}_{(i}\epsilon_{j)kl} z^{BA}_k V^{BA}_l / d^5 \ . \tag{F.17}$$

In the above equations, z^A_i is the position vector of body A relative to the center of mass of the binary, $V^{BA}_i = \dot{z}^{BA}_i$ is the relative velocity of the bodies, $z^{BA}_i = z^B_i - z^A_i$, $d = |z^{BA}_i|$, and $\ddot{z}^A_i = M_B z^{BA}_i / d^3$. For a circular, Newtonian orbit in the x-y plane, z^{BA}_i has the Cartesian components

$$z^{BA}_i = d[\cos\omega_{\rm orb}t, \sin\omega_{\rm orb}t, 0] \ , \tag{F.18}$$

where $\omega_{\rm orb} = [(M_A + M_B)/d^3]^{1/2}$ and $z^A_i = -M_B z^{BA}_i/(M_A + M_B)$. In this case the components of $\mathcal{E}_{ij}$ and $\mathcal{B}_{ij}$ are given by Eqs. (3.42) and (3.43).

We note that the expression (F.10) and (F.16) for the external pieces of the metric are identical to standard expressions for the metric in the vicinity of a point particle in an arbitrary gravitational field expressed in Fermi normal coordinates [190, 191]. In this language, consider the worldline $z^\alpha(t)$ of an observer moving on a geodesic near a gravitating body. Manasse and Misner [190] have shown that one can introduce a coordinate system in which $g_{\mu\nu} = \eta_{\mu\nu}$ and $\Gamma^\mu{}_{\nu\sigma} = 0$ are satisfied all along this worldline. Such coordinate systems are called Fermi normal coordinates and describe the proper reference frame of a freely falling observer. Near the origin of this coordinate system in a specific choice of gauge, the metric can be expanded as a power series in the distance $|x^j|$ from the observer as [190, 64]

$$ds^2 = (-1 - R_{0i0j}x^i x^j)dt^2 + \left(\frac{4}{3}R_{0ijk}x^i x^j\right)dtdx^k + \left(\delta_{kl} - \frac{1}{3}R_{ikjl}x^i x^j\right)dx^k dx^l + O(|x^j|^3)dx^\alpha dx^\beta \ , \tag{F.19}$$

where the coordinate time t is also the proper time along the observer's worldline, and $R_{\alpha\beta\gamma\delta}$ are components of the Riemann tensor evaluated along the geodesic

worldline $z^\alpha(t)$. Some of these components can be expressed in terms of the tidal moments $\mathcal{E}_{ij}(t) \equiv R_{0i0j}$ and $\mathcal{B}_{ij}(t) \equiv \frac{1}{2}\epsilon_{iqp}R_{0jpq}$. These moments describe the tidal field of a strongly relativistic object, but in the PN (weak-field) limit they reduce to the tidal moments described above [Eqs. (F.12) and (F.15)]. Higher order tidal moments are defined in terms of the derivatives of the Riemann tensor evaluated along the worldline. Ishii et al. [191] have recently extended the metric expansion (F.19) to $O(|x^j|^4)$. For the extension to accelerated and rotating observers, see Ni and Zimmermann [192] and Li and Ni [193].

The post-Newtonian limit of the metric (F.19) is equivalent to keeping only the $\Phi^{\rm ext}$ and $\zeta_i^{\rm ext}$ terms in the metric of Eq. (3.1). To arrive at the full metric (3.1) for a Newtonian star in a tidal field, we must include the Newtonian potential $\Phi^{\rm self}$. Since we treat the star's self-gravity at Newtonian order and neglect all nonlinear gravitational terms, the superposition principle allows this extension to be achieved by simply adding the appropriate $\Phi^{\rm self}$ terms to the time-time and space-space pieces of the metric (F.19). The resulting metric and the hydrodynamic equations that are derived using it are often used in studies of the tidal disruption of an ordinary star or compact object [see [191] and references therein, and also their Eq. (127)].

F.0.3 Neglecting 1PN terms in initially unperturbed stars

We now explain why certain 1PN terms will not affect our calculations and can be dropped from the equations of motion. For the case in which the star is initially unperturbed (Sec. 3.3), three facts help us to justify dropping the irrelevant terms: First, since the change in central density is due only to tidal interactions, $\delta\rho_c/\rho_c$ must be constructed from specific combinations of tidal moments. Since these

combinations must have even parity, the change in central density must have the form

$$\frac{\delta\rho_c}{\rho_c} = c_1\mathcal{E}_{ij}\mathcal{E}^{ij} + c_2\mathcal{B}_{ij}\mathcal{B}^{ij} + c_3\mathcal{E}_{ijk}\mathcal{E}^{ijk} + c_4\mathcal{B}_{ijk}\mathcal{B}^{ijk} + \cdots \,, \tag{F.20}$$

where the coefficients $c_1, c_2, \cdots$ depend on M, R, and the equation of state. Terms of the form $\mathcal{E}_{ij}\mathcal{B}^{ij}$ are excluded because they are parity odd. Since we are interested in only the leading-order correction to the Newtonian tidal-stabilization term—the $\mathcal{B}_{ij}\mathcal{B}^{ij} \sim O(\alpha^7)$ term in (F.20)—it is clear that any 1PN tidal terms that depend on electric-type tidal fields $\mathcal{E}_{a_1a_2\cdots a_l}$ can be excluded. This immediately excludes all the terms in $a_i^{\rm ext}$ that depend on $\Phi^{\rm ext}$ [see Eq. (3.10)]. It also excludes the tidal pieces of $\Phi_{\rm loc}^2 + \psi_{\rm loc}$.

Second, we are uninterested in $O(\epsilon)$ corrections to each of the terms in (F.20). For example, several terms in the 1PN hydrodynamics equations will effect the change in central density by adding corrections to the first two terms in (F.20) that scale like $\delta\rho_c/\rho_c \sim [O(1) + O(\epsilon)]\alpha^6 + [O(\epsilon^2) + O(\epsilon^3)]\alpha^7 + O(\alpha^8)$. We drop terms that contribute to these $O(\epsilon)$ and $O(\epsilon^3)$ corrections.[2]

Third, any acceleration terms in the equations of motion whose angle-averaged radial piece $\langle \boldsymbol{n}\cdot\boldsymbol{a}\rangle$ vanishes cannot contribute at linear order to the change in central density. Such terms are also dropped [except in the linearized hydrodynamic equations (3.15)–(3.17)]. All 1PN terms are excluded from the metric (3.1) or equations of motion (3.9) and (3.10) because of one or more of these three reasons.

For example, let us consider some of the terms appearing in the 1PN Euler's equation in detail. In the absence of tidal forces (for a static star), the 1PN terms

[2]The change in density caused by an acceleration term $\sim a$ in the perturbed 1PN Euler equations has the scaling $\delta\rho/\rho \sim \xi/R \sim a/(R\omega^2) \sim (R^2/M)a$, where ξ is the displacement of the star caused by the acceleration a, and $\omega^2 \sim M/R^3$ is the characteristic frequency response of the star.

modify the equations of hydrostatic equilibrium [Eqs. (3.14)], causing $O(\epsilon)$ changes to the background structure of the star, including the mass and radius. This will lead to $O(\epsilon)$ corrections to the mode functions and to the leading-order coefficients in (F.20). They can therefore be excluded. Now consider perturbations to the 1PN terms due to tidal interactions. The nonlinear 1PN terms $\Phi_{\rm loc}^2 + \psi_{\rm loc}$ are dropped because their pieces either modify only the background star at $O(\epsilon)$, or contain only electric-type tidal interactions that either lead to $O(\epsilon)$ corrections to the $O(\alpha^6)$ piece of $\delta\rho_c/\rho_c$ or have vanishing $\langle \boldsymbol{n}\cdot\boldsymbol{a}\rangle$. Consider next the acceleration term $a_i \sim \dot{\zeta}_i^{\rm self}$ which is driven by the velocity $v_i^{(1)}$ induced in the star. This term scales like $\dot{\zeta}_i^{\rm self} \sim R^2\omega_{\rm orb}\rho^{(0)}v_i^{(1)} \sim \epsilon^3\alpha^5/R$ and causes a change in density $\delta\rho/\rho \sim \epsilon^2\alpha^5$. However, the change in central density from this term vanishes because $\langle \boldsymbol{n}\cdot\boldsymbol{\zeta}^{\rm self}\rangle = \langle \boldsymbol{n}\cdot\boldsymbol{v}^{(1)}\rangle = 0$ [since $v^{(1)}$ is purely axial; see Sec. 3.3.2]. The acceleration term $\boldsymbol{v}^{(1)}\times(\nabla\times\boldsymbol{\zeta}^{\rm self})$ scales like $\sim R\rho^{(0)}{v^{(1)}}^2 \sim \epsilon^4\alpha^7/R$ and has a change in density that scales like $\delta\rho/\rho \sim \epsilon^3\alpha^7$, providing an $O(\epsilon)$ correction to the $O(\alpha^7)$ compression term. Terms in the metric and equations of motion that depend on $\zeta_i^{\rm self}$ can therefore be safely neglected.

Terms in the 1PN Euler's equation [see Eq. (9.8.15) of [132]] proportional to $(P/\rho)\nabla_i\Phi$, $(\Phi/\rho)\nabla_i P$ and $\Phi\nabla_i\Phi$, where $\Phi \equiv \Phi^{\rm self}$, are dropped because they involve only electric-type tidal perturbations. Terms that are quadratic in the fluid velocity such as $v^2\nabla_i\Phi$, $v_i(v^k\nabla_k)\Phi$, $\rho^{-1}\nabla_k[v_kv_i(P-2\rho\Phi+\Phi v^2)]$, and $\rho^{-1}\partial/\partial t(\rho v^2 v_i)$ add corrections to the central density at higher orders than concern us (or vanish completely). Terms that are linear in the fluid velocity like $\rho^{-1}\partial/\partial t[v_i(P-2\rho\Phi)]$ and $v_i\dot{\Phi}$ are also either higher order or vanish identically [since $\boldsymbol{n}\cdot\boldsymbol{v}^{(1)}=0$].

Except for terms proportional to $\zeta_i^{\rm ext}$, none of the 1PN terms can contribute to the pieces of the central density that we seek, so they are safely dropped from the

metric and equations of motion. The resulting equations of motion that we use [the continuity equation, Poisson's equation, and Euler's equation supplemented by gravitomagnetic terms involving $\zeta_i^{\rm ext}$; Eqs. (3.9) and (3.11)] are identical to the weak-field, $l = 2$ tidal-order limit of the equations used by Ishii et al. [191] in their Fermi normal coordinate description of a Newtonian star interacting with a black hole tidal field [see Eq. (127) of [191] and the surrounding discussion].

Appendix G
Vector spherical harmonics and STF integrals

In this appendix we supply useful formulae regarding vector spherical harmonics and STF integrals that we use throughout this paper. See Sec. II of Thorne [44] for a more detailed discussion.

We begin with the expansion of the scalar spherical harmonics in terms of radial unit vectors,

$$Y^{lm}(\theta,\phi) = \mathcal{Y}^{lm}_{A_l} N_{A_l}, \tag{G.1}$$

where $A_l \equiv (a_1 a_2 \cdots a_l)$, $N_{A_l} = n_{a_1} n_{a_2} \ldots n_{a_l}$ and $n_j = x_j/r$. The coefficients of this expansion, $\mathcal{Y}^{lm}_{A_l}$, are symmetric trace-free tensors of rank l (STF-l tensors). An explicit formula for the STF-l tensors $\mathcal{Y}^{lm}_{A_l}$ is given in Eq. (2.12) of Thorne [44]. Their explicit components up to $l = 2$ in a Cartesian coordinate basis $[\boldsymbol{e}_x, \boldsymbol{e}_y, \boldsymbol{e}_z]$ are:

$$\mathcal{Y}^{00} = \frac{1}{\sqrt{4\pi}}\,, \tag{G.2a}$$

$$\mathcal{Y}^{10}_j = \sqrt{\frac{3}{4\pi}}\,[0,0,1]\,, \tag{G.2b}$$

$$\mathcal{Y}^{11}_j = -\sqrt{\frac{3}{8\pi}}\,[1,i,0]\,, \tag{G.2c}$$

$$\mathcal{Y}^{1-1}_j = \sqrt{\frac{3}{8\pi}}\,[1,-i,0]\,, \tag{G.2d}$$

$$\mathcal{Y}^{20}_{jk} = \frac{1}{2}\sqrt{\frac{5}{4\pi}}\begin{bmatrix} -1 & 0 & 0 \\ 0 & -1 & 0 \\ 0 & 0 & 2 \end{bmatrix}\,, \tag{G.2e}$$

$$\mathcal{Y}^{21}_{jk} = -\frac{1}{2}\sqrt{\frac{15}{8\pi}}\begin{bmatrix} 0 & 0 & 1 \\ 0 & 0 & i \\ 1 & i & 0 \end{bmatrix} , \tag{G.2f}$$

$$\mathcal{Y}^{2-1}_{jk} = \frac{1}{2}\sqrt{\frac{15}{8\pi}}\begin{bmatrix} 0 & 0 & 1 \\ 0 & 0 & -i \\ 1 & -i & 0 \end{bmatrix} , \tag{G.2g}$$

$$\mathcal{Y}^{22}_{jk} = \frac{1}{2}\sqrt{\frac{15}{8\pi}}\begin{bmatrix} 1 & i & 0 \\ i & -1 & 0 \\ 0 & 0 & 0 \end{bmatrix} , \tag{G.2h}$$

$$\mathcal{Y}^{2-2}_{jk} = \frac{1}{2}\sqrt{\frac{15}{8\pi}}\begin{bmatrix} 1 & -i & 0 \\ -i & -1 & 0 \\ 0 & 0 & 0 \end{bmatrix} . \tag{G.2i}$$

The scalar spherical harmonics satisfy the eigenvalue equation

$$\nabla^2 Y^{lm} = -\frac{l(l+1)}{r^2} Y^{lm} , \tag{G.3}$$

and the orthonormality relation

$$\int Y^{lm} Y^{l'm'*} \, d\Omega = \delta_{ll'}\delta_{mm'} . \tag{G.4}$$

The *pure-spin* vector harmonics are defined by [44]:

$$\boldsymbol{Y}^{E,lm} = \frac{r\boldsymbol{\nabla} Y^{lm}}{\sqrt{l(l+1)}} = -\boldsymbol{n} \times \boldsymbol{Y}^{B,lm} , \tag{G.5a}$$

$$\boldsymbol{Y}^{B,lm} = \frac{\boldsymbol{x} \times \boldsymbol{\nabla} Y^{lm}}{\sqrt{l(l+1)}} = \boldsymbol{n} \times \boldsymbol{Y}^{E,lm} , \tag{G.5b}$$

$$\boldsymbol{Y}^{R,lm} = \boldsymbol{n} Y^{lm} . \tag{G.5c}$$

They satisfy the orthonormality relation

$$\int \boldsymbol{Y}^{J,lm} \cdot \boldsymbol{Y}^{J',l'm'*} \, d\Omega = \delta_{JJ'}\delta_{ll'}\delta_{mm'} , \tag{G.6}$$

where $J = E, B,$ or R, and their complex conjugates satisfy

$$\boldsymbol{Y}^{J,lm*} = (-1)^m \boldsymbol{Y}^{J,l\,-m} \,. \tag{G.7}$$

These vector spherical harmonics can also be expressed in terms of the STF-l tensors:

$$Y_j^{E,lm} = \sqrt{\frac{l}{l+1}} \left[\mathcal{Y}^{lm}_{jA_{l-1}} N_{A_{l-1}} - n_j \, \mathcal{Y}^{lm}_{A_l} N_{A_l} \right], \tag{G.8a}$$

$$Y_j^{B,lm} = \sqrt{\frac{l}{l+1}} \, \epsilon_{jpq} n_p \mathcal{Y}^{lm}_{qA_{l-1}} N_{A_{l-1}} \,, \tag{G.8b}$$

$$Y_j^{R,lm} = n_j \mathcal{Y}^{lm}_{A_l} N_{A_l} \,. \tag{G.8c}$$

The gradient, divergence, and curl of the vector harmonics are given by the following formulas:

$$\nabla_j Y_i^{E,lm} = \frac{r}{\sqrt{l(l+1)}} \nabla_j \nabla_i Y^{lm} \,, \tag{G.9a}$$

$$\nabla_j Y_i^{B,lm} = \frac{1}{r} \epsilon_{ijk} Y_k^{E,lm} + \epsilon_{ilk} n_l \nabla_j Y_k^{E,lm} \,, \tag{G.9b}$$

$$\nabla_j Y_i^{R,lm} = \frac{1}{r} \left[(\delta_{ij} - n_i n_j) Y^{lm} + \sqrt{l(l+1)} n_i Y_j^{E,lm} \right] \,, \tag{G.9c}$$

$$\nabla \cdot \boldsymbol{Y}^{E,lm} = -\frac{\sqrt{l(l+1)}}{r} Y^{lm} \,, \tag{G.10a}$$

$$\nabla \cdot \boldsymbol{Y}^{B,lm} = 0 \,, \tag{G.10b}$$

$$\nabla \cdot \boldsymbol{Y}^{R,lm} = \frac{2}{r} Y^{lm} \,, \tag{G.10c}$$

$$\nabla \times \boldsymbol{Y}^{E,lm} = 0 \,, \tag{G.11a}$$

$$\nabla \times \boldsymbol{Y}^{B,lm} = \boldsymbol{n} (\nabla \cdot \boldsymbol{Y}^{E,lm}) - \frac{2}{r} \boldsymbol{Y}^{E,lm} - (\boldsymbol{n} \cdot \nabla) \boldsymbol{Y}^{E,lm} \,, \tag{G.11b}$$

$$\nabla \times \boldsymbol{Y}^{R,lm} = -\frac{\sqrt{l(l+1)}}{r} \boldsymbol{Y}^{B,lm} \,. \tag{G.11c}$$

When performing angular integrals over STF-l tensors, the following integrals over products of unit vectors are useful:

$$\oint N_{A_{2l+1}}\, d\Omega = 0 \;, \tag{G.12a}$$

$$\oint N_{A_{2l}}\, d\Omega = \frac{4\pi}{(2l+1)!!}[\delta_{a_1a_2}\delta_{a_3a_4}\cdots\delta_{a_{2l-1}a_{2l}} + \text{ all distinct permutations}] \;. \tag{G.12b}$$

More explicitly, the first few nonvanishing integrals are:

$$\oint n_a n_b\, d\Omega = \frac{4\pi}{3}\delta_{ab} \;, \tag{G.13a}$$

$$\oint n_a n_b n_c n_d\, d\Omega = \frac{4\pi}{15}\left(\delta_{ab}\delta_{cd} + \delta_{ac}\delta_{bd} + \delta_{ad}\delta_{bc}\right), \tag{G.13b}$$

$$\begin{aligned}\oint n_a n_b n_c n_d n_e n_f\, d\Omega = {}& \\ & \frac{4\pi}{105}\left(\delta_{ab}\delta_{cd}\delta_{ef} + \delta_{ab}\delta_{ce}\delta_{df} + \delta_{ab}\delta_{cf}\delta_{de}\right. \\ & + \delta_{ac}\delta_{bd}\delta_{ef} + \delta_{ac}\delta_{be}\delta_{df} + \delta_{ac}\delta_{bf}\delta_{de} \\ & + \delta_{ad}\delta_{bc}\delta_{ef} + \delta_{ad}\delta_{be}\delta_{cf} + \delta_{ad}\delta_{bf}\delta_{ce} \\ & + \delta_{ae}\delta_{bc}\delta_{df} + \delta_{ae}\delta_{bd}\delta_{cf} + \delta_{ae}\delta_{bf}\delta_{cd} \\ & \left. + \delta_{af}\delta_{bc}\delta_{de} + \delta_{af}\delta_{bd}\delta_{ce} + \delta_{af}\delta_{be}\delta_{cf}\right) \;.\end{aligned} \tag{G.13c}$$

We also frequently use the identity

$$\epsilon_{ijk}\epsilon_{ilm} = \delta_{jl}\delta_{km} - \delta_{jm}\delta_{kl} \;. \tag{G.14}$$

Appendix H
Relativistic circulation and the irrotational approximation

The purpose of this appendix is to explain why fluids that satisfy the relativistic irrotational condition can nonetheless have Newtonian vorticity. We also provide an alternative derivation of the gravitomagnetically induced velocity (3.19).

Begin by considering the relativistic definition of circulation [194]

$$\mathcal{C} = \oint_\lambda h u_\alpha \, d\lambda^\alpha \,, \tag{H.1}$$

where h is the specific enthalpy, u_α is the fluid four-velocity, and the integral is taken around a closed spacelike curve λ. Kelvin's circulation theorem states that the relativistic circulation is conserved for a curve λ that moves with the fluid. If we work in the PN limit and assume that our closed curve λ is purely spatial $d\lambda^\alpha = (0, dx^i)$, we can use Stokes' theorem to write the circulation as

$$\mathcal{C} = \oint_\lambda (hu_i) dx^i = \int_S (\nabla \times h\boldsymbol{u})_i \cdot dS^i \,, \tag{H.2}$$

where $\boldsymbol{u} \equiv u_j$ and dS^i is the normal to the surface S whose boundary is λ. In the relativistic irrotational approximation, $hu_\alpha = \nabla_\alpha \Psi$, so $\mathcal{C} = 0$. So while the irrotational condition in Newtonian theory is simply[1] $\boldsymbol{\omega} \equiv \nabla \times \boldsymbol{v} = 0$ (where $\boldsymbol{v}$ is the coordinate velocity $d\boldsymbol{x}/dt$), its relativistic generalization is [130]

$$h(\nabla \times \boldsymbol{u}) + \nabla h \times \boldsymbol{u} = 0 \,. \tag{H.3}$$

[1] A more precise definition of the relativistic irrotational condition is that the relativistic vorticity tensor, $\omega_{\mu\nu} = \nabla_\nu(hu_\mu) - \nabla_\mu(hu_\nu)$, vanishes [121]. Using Euler's equation for a perfect fluid in the form $u^\mu \nabla_\mu(hu_\nu) + \nabla_\nu h = 0$, one can show that $u^\mu \omega_{\mu\nu} = 0$ and $\pounds_{\vec{u}} \omega_{\mu\nu} = 0$, where $\pounds_{\vec{u}}$ is the Lie derivative along the fluid 4-velocity. This last equation is the differential version of Kelvin's circulation theorem.

This indicates that a relativistic, irrotational fluid can have nonvanishing Newtonian circulation so long as the fluid velocity is restricted by (H.3).

At 1PN order we can write the circulation $\mathcal{C}$ more explicitly: Using the metric expansion (F.3), $u_i = g_{i\alpha}u^\alpha$, $u^j = u^0 v^j$, $u^0 = 1 + \hat{\varepsilon}^2(v^2 - \Phi_{\rm loc}) + O(\hat{\varepsilon}^4)$, and (for polytropes) $h = 1 + \hat{\varepsilon}^2(\epsilon_0 + P/\rho)$, we have

$$hu_i = \hat{\varepsilon} v^i + \hat{\varepsilon}^3 \left[\zeta_i^{\rm loc} + v^i \left(\frac{1}{2} v^2 - 3\Phi_{\rm loc} + \epsilon_0 + \frac{P}{\rho} \right) \right] + O(\hat{\varepsilon}^5) \,, \tag{H.4}$$

where v^i is the fluid 3-velocity, ρ is the mass density, $\rho\epsilon_0$ is the internal energy density, and P is the pressure. Substituting (H.4) into (H.2) gives the circulation up to 1PN order. Formally, this 1PN expansion assumes the scalings $v^i \sim \hat{\varepsilon} \sim (M/R)^{1/2} \sim (M/d)^{1/2}$. However, when the fluid velocity is generated by tidal interactions, its scaling is actually much smaller: $v^i \sim (M/R)^{1/2}(R/d)^{9/2}$ for electric-type tidal interactions and $v^i \sim (M/R)^{3/2}(R/d)^{7/2}$ for magnetic-type tidal interactions. This allows us to ignore all but the first two terms on the right-hand-side of (H.4) as well as the contribution from $\zeta_i^{\rm self}$, yielding

$$\mathcal{C} = \int_S [\nabla \times (\boldsymbol{v} + \boldsymbol{\zeta}^{\rm ext})]_i \, dS^i \,, \tag{H.5}$$

[see also Eq. (8) of Shapiro [104]]. By Kelvin's circulation theorem, an irrotational fluid satisfies $\mathcal{C} = 0$ for all times, and $\nabla \times \boldsymbol{v} = -\nabla \times \boldsymbol{\zeta}^{\rm ext}$. This has the solution $\boldsymbol{v} = -\boldsymbol{\zeta}^{\rm ext} + \nabla\Lambda$ for any scalar function Λ. The boundary condition that $\boldsymbol{v}$ and $\boldsymbol{\zeta}^{\rm ext} \to 0$ at early times yields the solution given in Eq. (3.19).

Appendix I
Definitions of Newtonian and Gravitomagnetic Love numbers

Here we briefly review the definition of the Newtonian Love number k_2 which relates the induced mass quadrupole moment $\mathcal{I}_{ij}$ to the external Newtonian tidal field $\mathcal{E}_{ij}$. We also show how the gravitomagnetic Love number γ_2 is related to the equation of state of a star.

Consider a fluid star with mass M and mean radius R, interacting with the tidal field of a distant companion with mass M' located at position $\boldsymbol{x}' = (r' = d, \theta', \phi')$ in a coordinate system centered on the first star's center of mass. The distant companion tidally deforms the fluid star, giving it a mass quadrupole moment $\mathcal{I}_{ij}$. Near the star but outside its surface, the tidal expansion of the Newtonian potential up to $l = 2$ is

$$\Phi = -\frac{M}{r} - k_2 \frac{M' R^5}{d^3} \frac{P_2(\cos\Theta)}{r^3} - \frac{M'}{d^3} r^2 P_2(\cos\Theta) \; . \tag{I.1}$$

Here P_2 is a Legendre polynomial and Θ is the angle between $\boldsymbol{x}$ and $\boldsymbol{x}'$ [see Eqs. (4.121) and (4.155) of [105]]. The tidal Love number k_2 is *defined* to be the dimensionless coefficient of the $1/r^3$ piece of the expansion of the potential of a tidally deformed, nonrotating body. To show how k_2 is related to the STF moments $\mathcal{I}_{ij}$ and $\mathcal{E}_{ij}$, expand the Newtonian potential as

$$\Phi = -\frac{M}{r} - \frac{3}{2}\frac{\mathcal{I}_{ij} n^i n^j}{r^3} + \frac{1}{2} r^2 \mathcal{E}_{ij} n^i n^j \tag{I.2}$$

[this is equivalent to Eq. (I.1) expressed in different notation]. Expanding the Legendre polynomial as

$$P_2(\cos\Theta) \;\; = \;\; \frac{4\pi}{5} \sum_{m=-2}^{2} Y^{2m*}(\theta', \phi') Y^{2m}(\theta, \phi) \tag{I.3}$$

$$= \frac{4\pi}{5} \sum_{m=-2}^{2} \mathcal{Y}_{ab}^{2m*} n'^a n'^b \mathcal{Y}_{ij}^{2m} n_i n_j \tag{I.4}$$

and equating the corresponding $1/r^3$ and r^2 terms in Eqs. (I.1) and (I.2), it is easily shown that the mass quadrupole moment and Newtonian tidal moment are related to the Love number k_2 by

$$\mathcal{I}_{ij} = -\frac{1}{3} k_2 R^5 \mathcal{E}_{ij} \ . \tag{I.5}$$

The value of the Love number k_2 depends on the equation of state of the star. To determine this dependence, one must solve for the structure of the deformed star. Lai, Rasio, & Shapiro [195] have done this for the case of tidally deformed, compressible ellipsoids. For ellipsoids with a polytropic EOS with index n, the moments of inertia are

$$I_{ij} = \int \rho x_i x_j \, d^3x = \frac{1}{5} \kappa_n M a_i^2 \delta_{ij} \quad \text{(no sum)} \ , \tag{I.6}$$

where $a_i = R(1 + \alpha_i)$ are the axes of the ellipsoid, and, for a tidal field along the x-axis [22],

$$\alpha_1 = \frac{5}{2} q_n \frac{M'}{M} \left(\frac{R}{r} \right)^3 \ , \tag{I.7}$$

$$\alpha_2 = \alpha_3 = -\frac{1}{2} \alpha_1 \ .$$

In these equations EOS information is contained in the coefficients

$$\kappa_n = \frac{5}{3} \frac{\int_0^{\xi_1} \xi^4 \theta^n \, d\xi}{\xi_1^4 |\theta'(\xi_1)|} \tag{I.8}$$

and $q_n = \kappa_n (1 - n/5)$. Here $\theta(\xi)$ is a solution of the Lane-Emden equations, ξ_1 is the first root of this solution, and $\theta' \equiv d\theta/d\xi$.

Expanding (I.6) to linear order in α_i, taking the STF piece, and using the form for $\mathcal{E}_{ij}$ due to a point mass on the x-axis gives the relation

$$\mathcal{I}_{ij} = -\frac{1}{2} \kappa_n^2 \left(1 - \frac{n}{5} \right) R^5 \mathcal{E}_{ij} \ . \tag{I.9}$$

The Love number is therefore related to the structure of the star by

$$k_2 = \frac{3}{2}\kappa_n^2 \left(1 - \frac{n}{5}\right) \ . \tag{I.10}$$

For a uniform density star, $k_2 = 3/2$; for a $\Gamma = 2$ polytrope, $k_2 = (10/3)(1 - 6/\pi^2)^2 \approx 0.5124$.

For a nonrotating star immersed in a magnetic-type tidal field, we have shown in Sec. 3.3.2 that a current-quadrupole moment is induced and is related to the tidal field by

$$\mathcal{S}_{ij} = \gamma_2 M R^4 \mathcal{B}_{ij} \ . \tag{I.11}$$

Here γ_2 is the *gravitomagnetic Love number* analogous to k_2. For a spherical, Newtonian polytrope,

$$\gamma_2 = \frac{2}{15} \frac{\int_0^{\xi_1} \xi^6 \theta^n \, d\xi}{\xi_1^6 |\theta'(\xi_1)|} \ . \tag{I.12}$$

To show this, perform the change of variables $\rho = \rho_c \theta^n$ and $r = R\xi/\xi_1$ in Eq. (3.22) and use $\rho_c = \xi_1/(4\pi|\theta'(\xi_1)|)(M/R^3)$. For a uniform density star, $\gamma_2 = 2/35$; for a $\Gamma = 2$ polytrope $\gamma_2 = 2(\pi^4 - 20\pi^2 + 120)/(15\pi^4) \approx 0.0274$. As is the case with the Newtonian Love number, the gravitomagnetic Love number becomes smaller as the star becomes more centrally condensed. See Poisson [196] for an extension of the concept of gravitomagnetic Love numbers to tidally distorted black holes.

Appendix J
Tidal stabilization for a nonrotating Newtonian star at order $O(\alpha^6)$

To compute the change in central density at order $O(\alpha^6)$, one could follow a perturbative procedure similar to that used in Sec. 3.3 above, expanding in $\varepsilon_{\mathcal{E}}$ (with $\varepsilon_{\mathcal{B}} = 0$). However, the solutions at order $O(\varepsilon_{\mathcal{E}}^1)$ are more complicated than those at order $O(\epsilon_{\mathcal{B}}^1)$. A simpler method based on an energy variational principle was used by Lai [22]. In this appendix we provide a concise derivation of the leading-order contribution to the change in central density using the method described by Lai [22], but specialized to nonrelativistic stars. The resulting analytic expression for $\delta\rho_c/\rho_c$ is not provided in [22] but approximates the analytic result of Taniguchi & Nakamura [94] which was arrived at by a more difficult method.

The energy $E(\rho_c)$ of an isolated, nonrotating star with baryon mass M, radius R, and polytropic EOS $P = K\rho^{1+1/n}$, as a function of its central density ρ_c, is

$$E(\rho_c) = E_{\rm int}(\rho_c) + E_{\rm grav}(\rho_c) \ , \tag{J.1}$$

where

$$E_{\rm int} \equiv \int u\, dm = k_1 K M \rho_c^{1/n} = \frac{n}{5-n}\frac{M^2}{R} \tag{J.2}$$

is the star's internal energy, and

$$E_{\rm grav} \equiv -\int \frac{m}{r}\, dm = -k_2 M^{5/3}\rho_c^{1/3} = -\frac{3}{5-n}\frac{M^2}{R} \tag{J.3}$$

is its gravitational potential energy (see chapter 6 of [133]). In the above equations $u = nP/\rho$ is the internal energy per unit mass, $m = m(r)$ is the enclosed mass as a function of radial coordinate r (satisfying $dm/dr = 4\pi r^2\rho$), and the various constants are given by

$$k_1 = \frac{n(n+1)}{5-n}\xi_1|\theta'(\xi_1)| = \frac{1}{2} \ , \tag{J.4}$$

$$k_2 = \frac{3}{5-n}\left|\frac{4\pi\theta'(\xi_1)}{\xi_1}\right|^{1/3} = \left(\frac{27}{16\pi}\right)^{1/3} \approx 0.8129 \ . \tag{J.5}$$

As in Appendix I, the function $\theta(\xi)$ is a solution to the Lane-Emden equation, ξ_1 is the first root of this solution, and $\theta' \equiv d\theta/d\xi$. The numerical values here and below are for $n = 1$. (In this section k_2 is not to be confused with the Newtonian Love number defined in Appendix I.)

The equilibrium central density for a stable star, $\rho_{c,0}$, lies at the stable minimum of $E(\rho_c)$—where $dE/d\rho_c = 0$ and $d^2E/d\rho_c^2 > 0$. Placing the star in an electric-type tidal field modifies the total energy to

$$\tilde{E}(\rho_c) = E_{\rm int}(\rho_c) + E_{\rm grav}(\rho_c) + W_t(\rho_c) \ , \tag{J.6}$$

where W_t accounts for the interaction energy between the tidal field and the star's induced mass quadrupole moment, as well as the modification to the star's self-gravitational potential energy due to the redistribution of mass by the tidal field (the kinetic energy of internal fluid oscillations is neglected). For an ellipsoidal star [22][195],

$$W_t = -\lambda\frac{M'^2}{R}\left(\frac{R}{d}\right)^6 = -\lambda'\left(\frac{M}{\rho_c}\right)^{5/3}\frac{M'^2}{d^6} \ , \tag{J.7}$$

where

$$\lambda = \frac{3}{4}\kappa_n^2\left(1-\frac{n}{5}\right) = \frac{5}{3\pi^4}(\pi^2-6)^2 \approx 0.2562 \ , \tag{J.8}$$

$$\begin{aligned}\lambda' &= \frac{3}{4}\kappa_n^2\left(1-\frac{n}{5}\right)\left(\frac{\xi_1}{4\pi|\theta'(\xi_1)|}\right)^{5/3} \\ &= \frac{5(4\pi^5)^{1/3}}{48\pi^4}(\pi^2-6)^2 \approx 0.1713 \ ,\end{aligned} \tag{J.9}$$

and

$$\kappa_n = \frac{5}{3}\frac{\int_0^{\xi_1}\xi^4\theta^n\,d\xi}{\xi_1^4|\theta'(\xi_1)|} = \frac{5}{3}\left(1-\frac{6}{\pi^2}\right) \approx 0.6535 \ . \tag{J.10}$$

In the above equations, we have used $M/R^3 = 4\pi\rho_c|\theta'(\xi_1)|/\xi_1$. The central density in the presence of a binary companion can then be determined from $d\tilde{E}/d\rho_c =$

$dE/d\rho_c + dW_t/d\rho_c = 0$, the roots of which must generally be found numerically. Alternatively, one can Taylor expand $dE/d\rho_c$ about the density for an isolated star,

$$\frac{dE}{d\rho_c} = \left.\frac{dE}{d\rho_c}\right|_{\rho_{c,0}} + \left.\frac{d^2E}{d\rho_c^2}\right|_{\rho_{c,0}} \delta\rho_c + O(\delta\rho_c^2) \,, \tag{J.11}$$

where $\delta\rho_c \equiv \rho_c - \rho_{c,0}$. This yields the change in central density,

$$\frac{\delta\rho_c}{\rho_c} = -\left[\frac{1}{\rho}\frac{(dW_t/d\rho_c)}{(d^2E/d\rho_c^2)}\right]_{\rho_{c,0}} \,, \tag{J.12}$$

where

$$\rho_{c,0} = \left(\frac{n}{3}\frac{k_2}{k_1}\frac{M^{2/3}}{K}\right)^{3n/(3-n)} \,. \tag{J.13}$$

The polytropic constant can be expressed in terms of the mass and radius by

$$K = \left(\frac{4\pi}{\xi_1^{n+1}|\theta'(\xi_1)|^{n-1}}\right)^{1/n} \frac{M^{1-1/n}R^{3/n-1}}{n+1} \,. \tag{J.14}$$

Since $d^2E/d\rho_c^2$ and $dW_t/d\rho_c$ are both positive, we see that at order $O(\alpha^6)$ stars are stabilized by an external tidal field. For $n = 1$, $K = 2R^2/\pi$ and Eq. (J.12) reduces to

$$\frac{\delta\rho_c}{\rho_c} = -\frac{50}{3\pi^4}(\pi^2 - 6)^2 \left(\frac{M'}{M}\right)^2 \left(\frac{R}{d}\right)^6 \,. \tag{J.15}$$

Taniguchi & Nakamura [94] also calculated the leading-order change in central density. Instead of an energy variational principle for an ellipsoidal star, they solved the Newtonian fluid equations perturbatively up to order $O(\alpha^6)$ for irrotational stars. Their result for the change in central density is

$$\frac{\delta\rho_c}{\rho_c} = -\frac{45}{2\pi^2} \left(\frac{M'}{M}\right)^2 \left(\frac{R}{d}\right)^6 \,, \tag{J.16}$$

which agrees with Eq. (J.15) to $\sim 10\%$.

Appendix K
Fundamental Radial mode of a $\Gamma = 2$ Newtonian Polytrope

Since changes to a star's central density occur along the fundamental radial mode of oscillation, we will need to compute the frequency of this mode and its corresponding eigenfunction. We specialize to a Newtonian polytrope with EOS $P = K\rho^\Gamma$ and $\Gamma = 2$.

For a $\Gamma = 2$ polytrope the Lane-Emden equations (see e.g., chapter 3 of [133]) yield the following solutions for the internal density, pressure, gravitational potential, and mass distribution:

$$\rho(u) = \rho_c \frac{\sin u}{u} \ , \tag{K.1a}$$

$$P(u) = \frac{2}{\pi}\rho_c^2 R^2 \frac{\sin^2 u}{u^2} \ , \tag{K.1b}$$

$$\Phi(u) = -\frac{4}{\pi}\rho_c R^2 \left(1 + \frac{\sin u}{u}\right) \ , \tag{K.1c}$$

$$m(u) = \frac{4}{\pi^2}\rho_c R^3 \left(\sin u - u\cos u\right) \ , \tag{K.1d}$$

where $u = \pi r/R$ and the central density is $\rho_c = (\pi/4)M/R^3$. A $\Gamma = 2$ polytrope also satisfies $M/R = 2K\rho_c$ and $R = (\pi K/2)^{1/2}$. (In this section u is the renormalized radial coordinate and the symbol ξ is reserved for the mode function.)

The oscillations of a Newtonian star are described by the eigenvalue equation (3.34), where

$$\rho\mathcal{L}[\boldsymbol{\xi}] = \nabla_i\left(\Gamma_1 P \nabla_j \xi^j\right) - \left(\nabla_j \xi^j\right)\nabla_i P + \left(\nabla_i \xi^j\right)\nabla_j P - \rho\xi^j \nabla_j \nabla_i \Phi - \rho\nabla_i \delta\Phi \ . \tag{K.2}$$

For radial perturbations $\boldsymbol{\xi} = \xi(r)\boldsymbol{n}$, this equation simplifies to

$$\frac{d}{dr}\left[\Gamma_1 P \frac{1}{r^2}\frac{d}{dr}\left(r^2\xi\right)\right] - \frac{4}{r}\frac{dP}{dr}\xi + \omega^2\rho\xi = 0 \ , \tag{K.3}$$

(see chapter 6 of [133]). In the above equations Γ_1 is the adiabatic index for the perturbations, which we will take to be $\Gamma_1 = \Gamma = 2$ throughout the star. Mode indices are ignored throughout this section. For a $\Gamma = 2$ polytrope we can use Eqs. (K.1) to rewrite (K.3) as

$$u^2 \sin u\, \xi_{,uu} + 2u^2 \cos u\, \xi_{,u} + \left[4\left(1 - \frac{2}{\Gamma_1}\right) u \cos u - 2\left(3 - \frac{4}{\Gamma_1}\right) \sin u + A u^3 \right] \xi = 0\,, \tag{K.4}$$

where $\xi_{,u} \equiv d\xi/du$ and $A \equiv \omega^2/(2\pi\Gamma_1\rho_c)$.

The boundary conditions Eq. (K.3) must satisfy are $\xi(r=0) = 0$ and $\xi(r=R)$ is finite. However, more specific boundary conditions are needed in order to solve the eigenvalue problem. To determine these conditions we analytically explore the solutions to Eq. (K.4) near the origin and the stellar surface. Near $u = 0$ we Taylor expand $\cos u = 1 - u^2/2 + u^4/24 - \cdots$ and $\sin u = u(1 - u^2/6 + u^4/120 - \cdots)$ and look for a series solution of the form $\xi = \sum_{n=0}^{\infty} a_n u^n$. Substituting into (K.4) and solving order by order we arrive at the recursion relation

$$\frac{a_{n+2}}{a_n} = \frac{n^2 + 5n - 6\beta}{6(n+4)(n+1)}\,, \tag{K.5a}$$

$$a_0 = a_2 = a_4 = \cdots = 0\,, \tag{K.5b}$$

where $\beta = A - 1 + 8/(3\Gamma_1)$. The approximate solution near the origin is therefore $\xi(u) \approx a_1 u + a_3 u^3 + \cdots$. To find a solution near the surface we use a similar procedure: Taylor expand (K.4) about $u = \pi$ and look for a power series solution of the form $\xi = \sum_{m=0}^{\infty} b_m (\pi - u)^m$. The resulting leading-order terms are $\xi(u) \approx b_0 + b_1(\pi - u) + \cdots$, where

$$\frac{b_1}{b_0} = \frac{2}{\pi}\left(1 - \frac{2}{\Gamma_1}\right) - \frac{\pi A}{2}\,. \tag{K.6}$$

The constants a_1 and b_0 are undetermined.

We now outline a numerical "shooting" method to compute the eigenvalue A and the eigenfunction $\xi(u)$: (1) Pick an initial guess for A. (2) Since the eigenfunctions are only defined up to a normalization constant, choose $a_1 = 1$. Integrate Eq. (K.4) as an initial value problem, starting a small distance $u = \delta$ from the center of the star with initial conditions $\xi(\delta) = \delta$ and $\xi_{,u}(\delta) = 1$. (3) Integrate to $u = \pi$ and compute the boundary condition

$$\xi_{,u}(\pi) + (b_1/b_0)\xi(\pi) = 0 \; . \tag{K.7}$$

Initially this equation will not be satisfied. (4) Choose a new value for A such that, when the equations are integrated again, Eq. (K.7) is more closely satisfied. (5) Repeat this procedure until (K.7) is satisfied to the desired precision.

To determine the fundamental radial mode, we want to choose a low enough value for A so that the eigenfunction has no nodes. Higher frequency radial modes can be found by choosing A such that n nodes appear in the eigenfunction (where n is the radial quantum number for the mode). Following the above procedure we find $A = 0.3804$ for the eigenvalue. Fitting a seventh-order polynomial to the eigenfunction gives

$$\xi(u) = u - 0.001119u^2 + 0.03302u^3 - 0.006397u^4 + 0.005408u^5 - 0.001502u^6 + 0.0002397u^7 \; . \tag{K.8}$$

This function is related to the mode function in Sec. 3.3.3 by

$$\boldsymbol{\xi}_0(\boldsymbol{x}) = (C/\sqrt{4\pi})(R/\pi)\xi(u)\boldsymbol{n}. \tag{K.9}$$

The normalization constant is found from Eq. (3.33):

$$C = 2\pi^2 \left[\int_0^\pi u\xi^2(u) \sin u \, du \right]^{-1/2} \approx 4.756 \; . \tag{K.10}$$

In computing the inner product in Eq. (3.41), we also make use of the integral

$$\int_0^\pi u^4 \xi(u) \sin u \, du \approx 76.93 \; . \tag{K.11}$$

Appendix L
Change in central density for rotating stars

In this appendix, we briefly discuss how one would extend our computations in Sec. 3.3 to an initially unperturbed, slowly-rotating star with uniform angular velocity $\eta\boldsymbol{\Omega}$. We show that gravitomagnetic contributions to the change in central density vanish at orders $O(\varepsilon_{\mathcal{B}}^1\eta^1)$ and $O(\varepsilon_{\mathcal{B}}^1\eta^2)$, but do not necessarily vanish at orders $O(\varepsilon_{\mathcal{B}}^2\eta^1)$ and $O(\varepsilon_{\mathcal{B}}^2\eta^2)$.

Along the lines of Eqs. (3.12), we expand the fluid variables in two dimensionless parameters, η and ε, that characterize the spin of the star and the external tidal field acting on it:

$$\rho(t,\boldsymbol{x}) = \sum_{n,m=0}^{\infty} \varepsilon^n \eta^m \rho^{(n,m)}(t,\boldsymbol{x}) \,, \tag{L.1}$$

and similar equations for P, Φ, and $\boldsymbol{v}$. These expansions are plugged into the fluid equations (3.9) and solved at each order in ε and η. We set $\varepsilon = \varepsilon_{\mathcal{B}}$ and ignore electric-type tidal interactions.[1]

At order $O(\varepsilon_{\mathcal{B}}^n\eta^0)$ for $n \leq 2$, the results are the same as in Sec. 3.3.2 with the relabelling $(n) \to (n,0)$. At order $O(\varepsilon_{\mathcal{B}}^0\eta^1)$ the velocity perturbation is unconstrained and chosen to be uniform rotation, $\boldsymbol{v}^{(0,1)} = \boldsymbol{\Omega}\times\boldsymbol{x}$. The density and other fluid variables are unchanged at this order: $\rho^{(0,1)} = P^{(0,1)} = \Phi^{(0,1)} = 0$.

At order $O(\varepsilon_{\mathcal{B}}^0\eta^2)$, we find the usual decrease in central density due to rotation. This can be calculated explicitly using the methods of Sec. 3.3.2. The perturbation

[1] Combined electric-type/magnetic-type tidal couplings cannot change the central density up to order $O(\alpha^7\Omega^2)$. Any changes to the central density up to this order must have the form $\delta\rho_c/\rho_c \sim \mathcal{E}_{ij}\mathcal{B}_{ij}$ & $\epsilon_{abc}\mathcal{E}_{ad}\mathcal{B}_{bd}\Omega_c$ & $\mathcal{E}_{ab}\mathcal{B}_{bc}\Omega_a\Omega_c$, where "&" means "plus terms of the form". Parity considerations force all these terms to vanish: Under a parity transformation ($x_j \to -x_j$), $\delta\rho_c/\rho_c \to \delta\rho_c/\rho_c$, while $\mathcal{E}_{ij} \to \mathcal{E}_{ij}$, $\mathcal{B}_{ij} \to -\mathcal{B}_{ij}$, $\Omega_i \to -\Omega_i$, and $\epsilon_{ijk} \to -\epsilon_{ijk}$. All three of the above terms are parity odd while the change in central density is parity even.

equations at this order become

$$\frac{\partial \rho^{(0,2)}}{\partial t} + \nabla_i[\rho^{(0,0)} v_i^{(0,2)}] = 0 \ , \tag{L.2a}$$

and

$$\frac{\partial v_i^{(0,2)}}{\partial t} + \frac{\nabla_i P^{(0,2)}}{\rho^{(0,0)}} + \nabla_i \Phi^{(0,2)} + \frac{\rho^{(0,2)}}{\rho^{(0,0)}} \nabla_i \Phi^{(0,0)} = a_i^{(0,2)} \ , \tag{L.2b}$$

where

$$a_i^{(0,2)} = -[\boldsymbol{v}^{(0,1)} \cdot \nabla] v_i^{(0,1)} = \Omega^2 x_i - (\boldsymbol{\Omega} \cdot \boldsymbol{x}) \Omega_i \ . \tag{L.3}$$

The change in central density is then determined by converting to an equation for the Lagrangian displacement of the fundamental radial mode (Sec. 3.3.3). The angular integral of $\boldsymbol{n} \cdot \boldsymbol{a}^{(0,2)}$ is $(8/3)\pi r \Omega^2$, and the resulting inner product with $\boldsymbol{\xi}_0$ is

$$\langle \boldsymbol{\xi}_0, \boldsymbol{a}^{(0,2)} \rangle = 0.4163 M R^2 \Omega^2 \ , \tag{L.4}$$

where we have computed the following radial integral for a $\Gamma = 2$ polytrope using the techniques in appendix K:

$$\int_0^\pi u^2 \xi(u) \sin u \, du \approx 14.43 \ . \tag{L.5}$$

Solving the analog of Eq. (3.35), and using Eq. (3.38) and the condition that $q_0, \dot{q}_0 \to 0$ at $t \to -\infty$ yields the change in central density at this order,

$$\frac{\rho^{(0,2)}(t,0)}{\rho^{(0,0)}(t,0)} = -0.4462 \left(\frac{\Omega}{\Omega_c} \right)^2 \ , \tag{L.6}$$

where $\Omega_c \equiv (M/R^3)^{1/2}$.

At order $O(\varepsilon_{\mathcal{B}}^1 \eta^1)$ the fluid equations are the same as Eqs. (L.2) with $(0,2) \to (1,1)$ and the driving acceleration replaced by

$$a_i^{(1,1)} = -[\boldsymbol{v}^{(0,1)} \cdot \nabla] v_i^{(1,0)} - [\boldsymbol{v}^{(1,0)} \cdot \nabla] v_i^{(0,1)} + [\boldsymbol{v}^{(0,1)} \times \boldsymbol{B}]_i = I_{ijk} x^j x^k \ , \tag{L.7}$$

where

$$I_{ijk} = \frac{2}{3}\left(2\mathcal{B}_{jk}\Omega_i - \mathcal{B}_{ij}\Omega_k - \mathcal{B}_{aj}\Omega_a\delta_{ik} - \epsilon_{abj}\epsilon_{ick}\mathcal{B}_{ac}\Omega_b\right) \ . \tag{L.8}$$

Since the angle average of $\boldsymbol{n}\cdot\boldsymbol{a}^{(1,1)}$ vanishes, there is no change in central density at this order. [If we consider electric-type tidal interactions, there should also be no change in central density at order $O(\varepsilon^1_{\mathcal{E}}\eta^1)$. This follows from the fact that it is impossible to construct a scalar that is linear in both $\mathcal{E}_{ij}$ and Ω_i.]

At order $O(\varepsilon^1_{\mathcal{B}}\eta^2)$, the driving acceleration becomes

$$a_i^{(1,2)} = -[\boldsymbol{v}^{(0,1)}\cdot\nabla]v_i^{(1,1)} - [\boldsymbol{v}^{(1,1)}\cdot\nabla]v_i^{(0,1)} - [\boldsymbol{v}^{(1,0)}\cdot\nabla]v_i^{(0,2)} - [\boldsymbol{v}^{(0,2)}\cdot\nabla]v_i^{(1,0)} + [\boldsymbol{v}^{(0,2)}\times\boldsymbol{B}]_i \ . \tag{L.9}$$

At each order, the Lagrangian perturbation of the star is approximately given by $\ddot{\xi}_i^{(n,m)} + \omega^2_{(n,m)}\xi_i^{(n,m)} \approx a_i^{(n,m)}$, so the velocity perturbations scale like $v_i^{(n,m)} \propto \dot{a}_i^{(n,m)}/\omega^2_{(n,m)}$. The density perturbations scale like $\rho^{(n,m)} \sim -\rho^{(0,0)}\nabla^i\xi_i^{(n,m)}$. To determine if the change in central density vanishes at a given order, one can compute the angle average of $\boldsymbol{n}\cdot\boldsymbol{a}^{(n,m)}$. Since each of the terms in $\boldsymbol{n}\cdot\boldsymbol{a}^{(1,2)}$ is proportional to an odd power of n_i, their angular integrals vanish and one finds that there is no change in central density at order $O(\varepsilon^1_{\mathcal{B}}\eta^2)$. One can also argue that at order $O(\varepsilon^1_{\mathcal{B}}\eta^2)$ the change in central density must be proportional to $\mathcal{B}_{ij}\Omega_i\Omega_j$ and must vanish because it is parity odd. (If electric-type tidal interactions were included, a change in central density proportional to $\mathcal{E}_{ij}\Omega_i\Omega_j$ would be allowed.)

Following the same procedure at order $O(\varepsilon^2_{\mathcal{B}}\eta^1)$, one finds the total acceleration

$$a_i^{(2,1)} = -[\boldsymbol{v}^{(1,1)}\cdot\nabla]v_i^{(1,0)} - [\boldsymbol{v}^{(1,0)}\cdot\nabla]v_i^{(1,1)} - [\boldsymbol{v}^{(2,0)}\cdot\nabla]v_i^{(0,1)} - [\boldsymbol{v}^{(0,1)}\cdot\nabla]v_i^{(2,0)} + [\boldsymbol{v}^{(1,1)}\times\boldsymbol{B}]_i \ . \tag{L.10}$$

In this case, the change in central density must be proportional to $\epsilon_{abc}\mathcal{B}_{ad}\mathcal{B}_{bd}\Omega_c$, which does *not* obviously vanish from parity arguments. A change in central

density at this order is therefore possible. If electric-type tidal interactions are considered, a central density change at order $O(\varepsilon_{\mathcal{E}}^2\eta^1)$ proportional to $\epsilon_{abc}\mathcal{E}_{ad}\mathcal{E}_{bd}\Omega_c$ is also allowed.

At order $O(\varepsilon_{\mathcal{B}}^2\eta^2)$ the central density must be proportional to $\Omega^2\mathcal{B}_{ij}\mathcal{B}_{ij}$ or $\mathcal{B}_{ij}\mathcal{B}_{ik}\Omega_j\Omega_k$. Similarly, for electric-type tidal fields the change in central density at order $O(\varepsilon_{\mathcal{E}}^2\eta^2)$ must be proportional to $\Omega^2\mathcal{E}_{ij}\mathcal{E}_{ij}$ or $\mathcal{E}_{ij}\mathcal{E}_{ik}\Omega_j\Omega_k$. These terms have even parity and need not vanish.

To summarize, we have shown by simple arguments that in rotating stars the change in central density vanishes at orders $O(\varepsilon_{\mathcal{E}}^0\eta^1)$, $O(\varepsilon_{\mathcal{B}}^0\eta^1)$, $O(\varepsilon_{\mathcal{E}}^1\eta^0)$, $O(\varepsilon_{\mathcal{B}}^1\eta^0)$, $O(\varepsilon_{\mathcal{E}}^1\eta^1)$, $O(\varepsilon_{\mathcal{B}}^1\eta^1)$, and $O(\varepsilon_{\mathcal{B}}^1\eta^2)$. Determining the change in central density at other orders would require more explicit calculations.

Appendix M
Adiabatic and post-adiabatic corrections in the post-Newtonian equations of motion

When working in the context of perturbation theory, the adiabatic approximation to the equations of motion appears to have a well-defined meaning: Instead of solving the full equation-of-motion (4.9) above, solve $a^\mu = \varepsilon a^\mu_{1,\rm diss}$ instead. How is the adiabatic approximation similarly implemented in the post-Newtonian equations of motion? Up to 2.5 PN order and neglecting spins, the PN equations of motion can be expressed in the schematic form as,

$$a = a^{(0)}(M)\Big\{1 + \epsilon^2[a^{(1,0)}(M) + \eta a^{(1,1)}(M)] + \epsilon^4[a^{(2,0)}(M) + \eta a^{(2,1)}(M) + \eta^2 a^{(2,2)}(M)] + \epsilon^5 \eta a^{2.5,1}(M)\Big\}\,, \quad \text{(M.1)}$$

where $\epsilon \sim v \sim \sqrt{M/r}$, $M = m_1 + m_2$, $\eta = \mu/M = \varepsilon/(1+\varepsilon)^2$ is the reduced mass ratio, and the expansion in η is exact at each order in ϵ. In this equation $a^{(p,q)}$ refers to terms that occur at order $O(\epsilon^{2p}\eta^q)$. In the limit $\varepsilon = m_2/m_1 \ll 1$ the above equation can be expanded in ε [and in $\epsilon \to (m_1/r)^{1/2}$] to yield:

$$a = a^{(0)}(m_1)\Big\{1 + \varepsilon + \epsilon^2[a^{(1,0)}(m_1) + \varepsilon \hat{a}^{(1,1)}(m_1) + O(\varepsilon^2)] + \epsilon^4[a^{(2,0)}(m_1) + \varepsilon \hat{a}^{(2,1)}(m_1) + \varepsilon^2 \hat{a}^{(2,2)}(m_1)] + \epsilon^5[\varepsilon a^{2.5,1}(m_1) + O(\varepsilon^2)]\Big\}\,. \quad \text{(M.2)}$$

Here the terms $\hat{a}^{(r,s)}$ occur at order $O(\epsilon^{2r}\varepsilon^s)$ and are composed of combinations of the $a^{(p,q)}$ terms in (M.1) with $r = p$ and $s \le q$. The adiabatic approximation consists of throwing away all the $O(\varepsilon)$ terms except for the $O(\epsilon^5\varepsilon)$ radiation-reaction term (ie., throwing out all the hatted terms). This 2.5 PN term can be identified with the dissipative piece of the self-force $a^\mu_{1,\rm diss}$. The conservative pieces $a^\mu_{1,\rm cons}$ are

the remaining $O(\varepsilon)$ pieces in (M.2). Note that these conservative pieces come in even at Newtonian order $[O(\epsilon^0)]$. These arguments can be extended to the 3.5PN equations of motion as well.

Appendix N
The generalized quasi-Keplerian formalism and post-Newtonian formulae for eccentric binary orbits

In this appendix we briefly review the generalized quasi-Keplerian formalism and briefly list post-Newtonian formulas for the orbital energy, the energy loss rate due to GW emission, and the rates of change of the orbital frequency and eccentricity.

The generalized quasi-Keplerian description of binary orbits was developed by Damour, Deruelle, Schäfer, and Wex [178, 180, 179]. It has recently been extended to 3PN order by Memmesheimer, Gopakumar, and Schäfer [182]. This formalism is an extension of the Keplerian description of elliptical orbits that is common in the celestial mechanics literature [182]:

$$r = a_r(1 - e\cos u)\ , \tag{N.1a}$$

$$\phi - \phi_0 = v \equiv \arctan\left[\left(\frac{1+e}{1-e}\right)^{1/2}\tan\frac{u}{2}\right]\ , \tag{N.1b}$$

$$l \equiv n(t - t_0) = u - e\sin u\ . \tag{N.1c}$$

In the above equations r and ϕ are the polar coordinates of the relative separation vector of the masses in the orbital plane, a_r is the semi-major axis, e is the eccentricity, l is the *mean anomaly*, $n = 2\pi/P$ is the *mean motion* (essentially the angular frequency of the motion), P is the orbital period, u is the *eccentric anomaly*,[1] v is the *true anomaly*,[2] and ϕ_0 is the polar angle at some initial time t_0

[1]The eccentric anomaly is the angle between the periastron and the projection perpendicular to the semi-major axis of the relative separation vector (the position of the reduced mass particle) onto the circle that circumscribes the orbital ellipse. The angle is measured from the center of the ellipse.

[2]The true anomaly is the angle between the periastron and the position of the reduced mass particle, measured from the focus of the ellipse.

(see figure 1 of [182] and associated discussion). In these equations u and l behave like time variables and v acts an angle variable. The orbital elements a_r, e, and n are related to the conserved quantities of the center of mass motion—the orbital energy per unit reduced mass,[3] $c_1 = E = E_{\rm physical}/\mu$, and the reduced angular momentum $c_2 = |c_2^i| = |L_i| = L = L_{\rm physical}/(M\mu)$, where $M = m_1 + m_2$ and $\mu = m_1 m_2/M$—by the following Newtonian expressions:

$$a_r = \frac{M}{(-2E)} \,, \tag{N.2a}$$

$$e^2 = 1 + 2EL^2 \,, \tag{N.2b}$$

$$n = \frac{(-2E)^{3/2}}{M} \,. \tag{N.2c}$$

At 3PN order the dynamics are described by an extension of the above set of equations: [181, 183]:

$$r = S(l; c_1, c_2) = a_r(1 - e_r \cos u) \,, \tag{N.3a}$$

$$\dot{r} = n\frac{\partial S}{\partial l} \,, \tag{N.3b}$$

$$\phi = \lambda + W(l; c_1, c_2) \,, \tag{N.3c}$$

$$\dot{\phi} = (1+k)n + n\frac{\partial W}{\partial l} \,, \tag{N.3d}$$

$$W(l; c_1, c_2) = (1+k)(v - l) + \frac{f_\phi}{c^4}\sin 2v + \frac{g_\phi}{c^4}\sin 3v + O(c^{-6}) \,, \tag{N.3e}$$

$$v = 2\arctan\left[\left(\frac{1+e_\phi}{1-e_\phi}\right)^{1/2}\tan\frac{u}{2}\right] \,, \tag{N.3f}$$

$$l = u - e_t \sin u + \frac{f_t}{c^4}\sin v + \frac{g_t}{c^4}(v - u) + O(c^{-6}) \,. \tag{N.3g}$$

[3]Note that unlike the energy that appears in the Kerr geodesic equations, the energy per reduced mass in post-Newtonian contexts usually does not include the rest mass of the particle. In this appendix orbital energies are expressed in units of the reduced mass μ.

Here a_r is a 3PN accurate semimajor axis, and there are three different eccentricities, e_t, e_r, e_ϕ which are related to each other. The functions $W(l)$ and $S(l)$ and their derivatives are 2π periodic in l. The mean motion is still denoted by $n = 2\pi/P$, but P here is the radial (or periastron to periastron) period. The quantity $k = \Delta\Phi/(2\pi)$, where $\Delta\Phi$ is the angle that the periastron advances through in the time P. The angles l and λ satisfy $\dot{l} = n$ and $\dot{\lambda} = (1+k)n$ and integrate to

$$l = n(t - t_0) + c_l \ , \tag{N.4a}$$

$$\lambda = (1+k)n(t - t_0) + c_\lambda \ , \tag{N.4b}$$

where c_l and c_λ are the values of those angles at time t_0. The parameters n, k, a_r, e_t, e_r, e_ϕ, f_t, f_ϕ, g_t, g_ϕ are functions of the 3PN conserved energy and angular momentum per unit reduced mass. They can also be expressed in terms of the mean motion n and the time-eccentricity e_t (see Refs. [181, 182, 183] for the explicit expressions and further details). These formulas provide parametric solutions for the conservative aspects of the motion up to 3PN order.

In Refs. [181, 183] the effects of the 2.5PN and 3.5PN radiation-reaction effects are included in order to determine the phasing of the GW polarizations. The essential problem in computing this phasing is determining the functions $r(t)$, $\phi(t)$ and their derivatives. When only the conservative motion is needed, those functions are given by Eqs. (N.3) above. To the compute the effects of the 2.5PN and 3.5PN dissipative terms, the method of variation of constants is used in Refs. [181, 183]. Instead of directly solving the 3.5PN equations of motion, the functional form of the 3PN conservative solution [Eqs. (N.3)] is used as a leading-order solution, and the 2.5PN and 3.5PN terms act as a perturbation that cause the constants of the motion in Eqs. (N.3) to vary with time. Specifically, the energy and angular momentum vary with time, $c_1 = c_1(t)$, $c_2 = c_2(t)$, and the angles in Eqs. (N.4) are

now given by

$$l \equiv \int_{t_0}^{t} n(t')\,dt' + c_l(t)\ , \tag{N.5a}$$

$$\lambda \equiv \int_{t_0}^{t} [1 + k(t')]n(t')\,dt' + c_\lambda(t)\ . \tag{N.5b}$$

Instead of solving a first order system of differential equations involving $r(t)$, $\phi(t)$, $\dot{r}(t)$, and $\dot{\phi}(t)$, a new first order system is solved in which the dynamical variables are $c_\alpha(t) = [c_1(t),\, c_2(t),\, c_l(t),\, c_\lambda(t)]$. In this system the "constants" c_1 and c_2 need not be the energy or angular momentum. They are more conveniently chosen to be the mean motion n and the time eccentricity e_t (which can be related to the energy and angular momentum). To solve for these variables, the system of equations is first written in the form

$$\frac{dc_\alpha}{dl} = G_\alpha(l; c_a)\ , \tag{N.6}$$

where G_α is a periodic function of l and $a = 1, 2$. Since G_α contains both fast, periodic oscillations as well as slowly varying pieces [from the $c_a(t)$], the solution is split into a slowly varying piece $\bar{c}_\alpha(l)$ and a rapidly varying piece $\tilde{c}_\alpha(l)$,

$$c_\alpha(l) = \bar{c}_\alpha(l) + \tilde{c}_\alpha(l)\ . \tag{N.7}$$

The rapidly-oscillating terms $\tilde{c}_\alpha(l)$ will always be smaller than the slowly-varying ones $\bar{c}_\alpha(l)$. The time evolution of the angles $l(t)$ and $\lambda(t)$ can be similarly split into secular and oscillatory pieces. Using this splitting Refs. [181, 183] then show how to solve for the quantities $\bar{n}$, $\bar{e}_t$, $\bar{c}_l$, $\bar{c}_\lambda$, $\tilde{n}$, $\tilde{e}_t$, $\tilde{c}_l$, $\tilde{c}_\lambda$ which are expressed as functions of l, u, or t. We will list here only those components of the solution that are necessary for our calculations of the gravitational wave phase in Chapter 4.

The primary expressions that we need are the differential equations that determine the secular changes in $\bar{n}$ and $\bar{e}_t$. (The other constants of the motion are

found to have no secular variations, $\dot{\bar{c}}_l = \dot{\bar{c}}_\lambda = 0$.) These results are derived up to 2PN order and in harmonic gauge in [183], and in ADM gauge in [181]. Differences between these two gauges affect these formulae at 2PN and higher orders. We list here the harmonic gauge evolution equations for $\bar{n}$ and $\bar{e}_t$ as given in [183]: Defining $\bar{\xi} \equiv M\bar{n}$, the 2PN accurate evolution equations for $\bar{n}$ and $\bar{e}_t$ are:

$$\frac{d\bar{n}}{dt} = \bar{\xi}^{5/3}\,\bar{n}^2\,\eta\left\{\dot{\bar{n}}^{\rm N} + \dot{\bar{n}}^{\rm 1PN} + \dot{\bar{n}}^{\rm 1.5PN} + \dot{\bar{n}}^{\rm 2PN}\right\}\,, \tag{N.8a}$$

$$\frac{d\bar{e}_t}{dt} = -\bar{\xi}^{5/3}\,\bar{n}\,\eta\,\bar{e}_t\left\{\dot{\bar{e}}_t^{\rm N} + \dot{\bar{e}}_t^{\rm 1PN} + \dot{\bar{e}}_t^{\rm 1.5PN} + \dot{\bar{e}}_t^{\rm 2PN}\right\}\,, \tag{N.8b}$$

where the "instantaneous" contributions to 2PN order $\dot{\bar{n}}^{\rm N}$, $\dot{\bar{n}}^{\rm 1PN}$, $\dot{\bar{n}}^{\rm 2PN}$, $\dot{\bar{e}}_t^{\rm N}$, $\dot{\bar{e}}_t^{\rm 1PN}$, and $\dot{\bar{e}}_t^{\rm 2PN}$ are given by [183]

$$\dot{\bar{n}}^{\rm N} = \frac{1}{5(1-\bar{e}_t^2)^{7/2}}\left\{96 + 292\bar{e}_t^2 + 37\bar{e}_t^4\right\}\,, \tag{N.9a}$$

$$\begin{aligned}\dot{\bar{n}}^{\rm 1PN} = {}& \frac{\bar{\xi}^{2/3}}{280(1-\bar{e}_t^2)^{9/2}}\Big\{20368 - 14784\eta + (219880 - 159600\eta)\bar{e}_t^2 \\ & + (197022 - 141708\eta)\bar{e}_t^4 + (11717 - 8288\eta)\bar{e}_t^6\Big\}\,,\end{aligned} \tag{N.9b}$$

$$\begin{aligned}\dot{\bar{n}}^{\rm 2PN} = {}& \frac{\bar{\xi}^{4/3}}{30240(1-\bar{e}_t^2)^{11/2}}\Big\{12592864 - 13677408\eta + 1903104\eta^2 + (133049696 \\ & - 185538528\eta + 61282032\eta^2)\bar{e}_t^2 + (284496744 - 411892776\eta \\ & + 166506060\eta^2)\bar{e}_t^4 + (112598442 - 142089066\eta + 64828848\eta^2)\bar{e}_t^6 \\ & + (3523113 - 3259980\eta + 1964256\eta^2)\bar{e}_t^8 + 3024(96 + 4268\bar{e}_t^2 + 4386\bar{e}_t^4 \\ & + 175\bar{e}_t^6)(5-2\eta)\sqrt{1-\bar{e}_t^2}\Big\}\,,\end{aligned} \tag{N.9c}$$

$$\dot{\bar{e}}_t^{\rm N} = \frac{1}{15(1-\bar{e}_t^2)^{5/2}}\left\{304 + 121\bar{e}_t^2\right\}\,, \tag{N.9d}$$

$$\begin{aligned}\dot{\bar{e}}_t^{\rm 1PN} = {}& \frac{\bar{\xi}^{2/3}}{2520(1-\bar{e}_t^2)^{7/2}}\Big\{340968 - 228704\eta + (880632 - 651252\eta)\bar{e}_t^2 \\ & + (125361 - 93184\eta)\bar{e}_t^4\Big\}\,,\end{aligned} \tag{N.9e}$$

$$\begin{aligned}\dot{\bar{e}}_t^{\rm 2PN} = {}& \frac{\bar{\xi}^{4/3}}{30240(1-\bar{e}_t^2)^{9/2}}\Big\{20815216 - 25375248\eta + 4548096\eta^2 + (87568332\end{aligned}$$

$$- 128909916\eta + 48711348\eta^2)\bar{e}_t^2 + (69916862 - 93522570\eta + 42810096\eta^2)\bar{e}_t^4$$
$$+ (3786543 - 4344852\eta + 2758560\eta^2)\bar{e}_t^6 + 1008(2672 + 6963\bar{e}_t^2$$
$$+ 565\bar{e}_t^4)(5 - 2\eta)\sqrt{1 - \bar{e}_t^2}\Big\} . \tag{N.9f}$$

The tail contributions $\dot{\bar{n}}^{1.5\mathrm{PN}}$ and $\dot{\bar{e}}_t^{1.5\mathrm{PN}}$ were derived in Sec. VI of DGI [181] using the Keplerian orbital parametrization and the tail corrections to the orbital averaged expressions for the far-zone energy and angular momentum fluxes derived in [197, 198]:

$$\left(\frac{d\bar{n}}{dt}\right)\bigg|_{\mathrm{Tail}} = \frac{384}{5}\frac{\bar{\xi}^{14/3}\,\pi\,\eta}{M^2}\,\kappa_{\mathrm{E}}\,, \tag{N.10a}$$
$$\left(\frac{d\bar{e}_t^2}{dt}\right)\bigg|_{\mathrm{Tail}} = -\frac{256}{5}\frac{\bar{\xi}^{11/3}\,\pi\,\eta}{M}\Big\{(1 - \bar{e}_t^2)\,\kappa_{\mathrm{E}} - \sqrt{1 - \bar{e}_t^2}\,\kappa_{\mathrm{J}}\Big\}\,, \tag{N.10b}$$

where κ_{E} and κ_{J} are expressed in terms of infinite sums involving quadratic products of Bessel functions $J_p(p\,\bar{e}_t)$ and its derivative $J'_p(p\,\bar{e}_t) \equiv \frac{dJ_p(p\,\bar{e}_t)}{d(p\,\bar{e}_t)}$:

$$\kappa_{\mathrm{E}} = \sum_{p=1}^{+\infty}\frac{p^3}{4}\Bigg\{(J_p(p\,\bar{e}_t))^2\left[\frac{1}{\bar{e}_t^4} - \frac{1}{\bar{e}_t^2} + \frac{1}{3} + p^2\left(\frac{1}{\bar{e}_t^4} - \frac{3}{\bar{e}_t^2} + 3 - \bar{e}_t^2\right)\right]$$
$$+ p\left[-\frac{4}{\bar{e}_t^3} + \frac{7}{\bar{e}_t} - 3\,\bar{e}_t\right]J_p(p\,\bar{e}_t)\,J'_p(p\,\bar{e}_t) + (J'_p(p\,\bar{e}_t))^2\left[\frac{1}{\bar{e}_t^2} - 1\right.$$
$$\left. + p^2\left(\frac{1}{\bar{e}_t^2} - 2 + \bar{e}_t^2\right)\right]\Bigg\}\,, \tag{N.11a}$$
$$\kappa_{\mathrm{J}} = \sum_{p=1}^{+\infty}\frac{p^2}{2}\sqrt{1 - \bar{e}_t^2}\Bigg\{p\left[\frac{3}{\bar{e}_t^2} - \frac{2}{\bar{e}_t^4} - 1\right](J_p(p\,\bar{e}_t))^2 + \left[\frac{2}{\bar{e}_t^3} - \frac{1}{\bar{e}_t}\right.$$
$$\left. + 2\,p^2\left(\frac{1}{\bar{e}_t^3} - \frac{2}{\bar{e}_t} + \bar{e}_t\right)\right]J_p(p\,\bar{e}_t)\,J'_p(p\,\bar{e}_t) + 2\,p\left(1 - \frac{1}{\bar{e}_t^2}\right)(J'_p(p\,\bar{e}_t))^2\Bigg\}\,. \tag{N.11b}$$

Note that $\kappa_{\mathrm{E}}(\bar{e}_t = 0) = \kappa_{\mathrm{J}}(\bar{e}_t = 0) = 1$. Expanding these functions in the limit of small $\bar{e}_t$ gives

$$\kappa_{\mathrm{E}} = 1 + \frac{2335}{192}\bar{e}_t^2 + \frac{42955}{768}\bar{e}_t^4 + \frac{6204647}{36864}\bar{e}_t^6 + O(\bar{e}_t^8)\,, \tag{N.12a}$$
$$\kappa_{\mathrm{J}} = 1 + \frac{209}{32}\bar{e}_t^2 + \frac{2415}{128}\bar{e}_t^4 + \frac{730751}{18432}\bar{e}_t^6 + O(\bar{e}_t^8)\,. \tag{N.12b}$$

The time evolution of $\bar{n}$ and $\bar{e}_t$ can be directly determined by solving Eqs. (N.8). This evolution is "adiabatic" in the post-Newtonian sense of the term: it neglects rapidly varying pieces that average to zero on an orbital timescale. The rapidly oscillating solutions $\tilde{n}, \tilde{e}_t, \tilde{c}_l, \tilde{c}_\lambda$, along with oscillatory contributions $\tilde{l}(l; \bar{c}_a)$ and $\tilde{\lambda}(l; \bar{c}_a)$ to the angles $l(t)$ and $\lambda(t)$ are given by functions of $u = u(l, \bar{n}, \bar{e}_t)$, $\bar{n}$, and $\bar{e}_t$. We list here only their scalings with ξ and η [181, 183]:

$$(\tilde{n}/\bar{n}, \tilde{e}_t, \tilde{c}_l, \tilde{c}_\lambda, \tilde{l}, \tilde{\lambda}) \sim \xi^{5/3}\eta\big[O(1) + O(\xi^{2/3}) + O(\xi^{2/3}\eta)\big] \ . \tag{N.13}$$

For the purposes of computing the first-post-adiabatic scalings of the GW phase, the contributions from the rapidly oscillating pieces in Eq. (N.13) can be ignored. They will contribute at post-post-adiabatic order. For example, consider the scaling of the phase variable $\phi(\lambda, l) = \lambda + W(l)$, which is closely related to the GW phase. The leading-order contribution from $\tilde{\lambda}$ is of order $O(\varepsilon)$ and is thus a post-post-adiabatic effect.

In addition to Eqs. (N.8) we also need to relate the radial angular frequency (the mean motion n) with the angular frequency ω_ϕ corresponding to the ϕ-motion. The ω_ϕ frequency naturally arises from the Fourier transform of the $\cos[2\phi(t)]$ and $\sin[2\phi(t)]$ terms in the GW polarizations h_+ and $h_\times$ [see Eqs. (6) of DGI [181]]. This frequency is given by the orbit average of Eq. (N.3d),

$$\omega_\phi = \langle \dot{\phi} \rangle = (1 + k)n \ , \tag{N.14}$$

where the $\partial W/\partial l$ term vanishes when averaged over a radial period P [due to the periodicity of $W(l)$]. This equation equivalently states that the angular frequency of periastron precession $\omega_{\rm peri} = \Delta\Phi/P = nk$ is just the difference between the angular and radial frequencies,

$$\omega_{\rm peri} = \omega_\phi - \omega_r \ , \tag{N.15}$$

where $\omega_r \equiv n$. Up to 3PN order the periastron advance parameter is given by [183]

$$k = \frac{3\xi^{2/3}}{1-e_t^2} + \frac{\xi^{4/3}}{4(1-e_t^2)^2}\left[78 - 28\eta + (51-26\eta)e_t^2\right] + \frac{\xi^2}{128(1-e_t^2)^3}\Big\{18240 \\ - 25376\eta + 492\pi^2\eta + 896\eta^2 + (28128 - 27840\eta + 123\pi^2\eta + 5120\eta^2)e_t^2 \\ + (2496 - 1760\eta + 1040\eta^2)e_t^4 + \left[1920 - 768\eta + (3840 - 1536\eta)e_t^2\right]\sqrt{1-e_t^2}\Big\}. \tag{N.16}$$

N.1 Formulas for the Orbital Energy and GW Luminosity

We will also find the following formulas useful in our derivations: The conserved orbital energy per unit reduced mass is given to 3PN order by [183]

$$E = -\frac{\xi^{2/3}}{2}\Big\{1 + \frac{\xi^{2/3}}{12}(15-\eta) + \frac{\xi^{4/3}}{24}\left[15 - 15\eta - \eta^2 + \frac{24}{\sqrt{1-e_t^2}}(5-2\eta)\right] \\ + \frac{\xi^2}{5184}\Big[-4995 - 6075\eta - 450\eta^2 - 35\eta^3 + \frac{864}{\sqrt{1-e_t^2}}(15 + 23\eta - 20\eta^2) \\ + \frac{18}{(1-e_t^2)^{3/2}}\left(11520 - 15968\eta + 123\pi^2\eta + 2016\eta^2\right)\Big]\Big\}. \tag{N.17}$$

Note that the $e_t \to 0$ limit of this equation does not yield the formula for the 3PN circular orbit energy given by Eq. (5) of Blanchet, Faye, Iyer, & Joguet [176]:

$$E_{\rm circ} = -\frac{\xi_\phi^{2/3}}{2}\Big\{1 + \xi_\phi^{2/3}\left(-\frac{3}{4} - \frac{\eta}{12}\right) + \xi_\phi^{4/3}\left(-\frac{27}{8} + \frac{19}{8}\eta - \frac{\eta^2}{24}\right) \\ + \xi_\phi^2\left(-\frac{675}{64} + \left[\frac{34445}{576} - \frac{205}{96}\pi^2\right]\eta - \frac{155}{96}\eta^2 - \frac{35}{5184}\eta^3\right)\Big\}, \tag{N.18}$$

where $\xi_\phi \equiv M\omega_\phi$. This discrepancy arises because the two dimensionless frequencies ξ and ξ_ϕ are not identical even in the $e_t \to 0$ limit. In this limit the frequencies are related by

$$\xi_\phi = \xi \lim_{e_t\to 0}(1+k) = \xi\Big\{1 + 3\xi^{2/3} + \xi^{4/3}\left(\frac{39}{2} - 7\eta\right) \\ + \xi^2\left[\frac{315}{2} + \left(\frac{123}{32}\pi^2 - \frac{817}{4}\right)\eta + 7\eta^2\right]\Big\}. \tag{N.19}$$

Plugging this equation into (N.18) and series expanding yields the $e_t \to 0$ limit of (N.17).

We will also find expressions for the GW luminosity $\mathcal{L}_{\rm GW} = -\mu \dot{E}$ useful in our calculations. For circular orbits this luminosity has been computed up to 3.5PN order [176]. For eccentric orbits published luminosities currently exist only up to 2PN order [199] (although those published expressions may contain errors at 2PN order due to errors in the transformation between harmonic and ADM coordinates ; see Ref. [32] of DGI [181]). We list here the luminosity for eccentric orbits only up to 1.5PN order:

$$\mathcal{L}_{\rm GW} = \mathcal{L}^{\rm N}_{\rm GW} + \mathcal{L}^{\rm 1PN}_{\rm GW} + \mathcal{L}^{\rm 1.5PN}_{\rm GW} + \cdots \ . \tag{N.20}$$

At Newtonian order the GW luminosity was derived by Peters and Mathews [200]:

$$\mathcal{L}^{\rm N}_{\rm GW} = \frac{1024}{5}\eta^2(-E)^5 f(e_r) = \frac{32}{5}\eta^2 \left(\frac{M}{a_r}\right)^5 f(e_r) \ , \tag{N.21}$$

where

$$f(e) = \sum_{p=1}^{\infty} g(p,e) = \frac{1+\frac{73}{24}e^2+\frac{37}{96}e^4}{(1-e^2)^{7/2}} \ , \tag{N.22}$$

and $g(p,e)$ is given in Eq. (N.27) below. The GW luminosity formulas are usually expressed in terms of the radial eccentricity e_r. The radial and time eccentricities are related by Eqs. (48b) of [181] and (21a) of [182] (in ADM coordinates) and by Eq. (26a) of [182] (in harmonic coordinates). The contribution to the luminosity at 1PN order is [see Eq. (4.20) of Blanchet & Schäfer [201] or Eq. (4.15) of [199]],

$$\mathcal{L}^{\rm 1PN}_{\rm GW} = \mathcal{L}^{\rm N,\,circ}_{\rm GW} \left\{ \frac{-E}{168(1-e_r^2)^{9/2}} \left[13 - 6414 e_r^2 - \frac{27405}{4} e_r^4 - \frac{5377}{16} e_r^6 \right.\right. \\ \left.\left. + \left(-840 - \frac{6419}{2} e_r^2 - \frac{5103}{8} e_r^4 + \frac{259}{8} e_r^6 \right) \eta \right] \right\} \ , \tag{N.23}$$

where

$$\mathcal{L}^{\rm N,\,circ}_{\rm GW} = \mathcal{L}^{\rm N}_{\rm GW}/f(e_r) \ . \tag{N.24}$$

The 1.5PN tail contribution to the luminosity is given by Eq. (81) of Rieth & Schäfer [198] or Eq. (5.10) of Blanchet & Schäfer [197]:

$$\mathcal{L}_{\rm GW}^{\rm 1.5N} = 4\pi \mathcal{L}_{\rm GW}^{\rm N}\, \xi\, \bar{\varphi}(e) = 4\pi \mathcal{L}_{\rm GW}^{\rm N} \left(\frac{M}{a_r}\right)^{3/2} \bar{\varphi}(e)\ , \tag{N.25}$$

$$\bar{\varphi}(e) = \frac{1}{f(e)} \sum_{p=1}^{\infty} \frac{p}{2} g(p,e)\ , \tag{N.26}$$

$$\begin{aligned} g(p,e) = \frac{p^2}{2} \Bigg\{ &\left[\frac{1}{e^4} - \frac{1}{e^2} + \frac{1}{3} + p^2 \left(\frac{1}{e^4} - \frac{3}{e^2} + 3 - e^2\right)\right] (J_p(pe))^2 \\ &+ p\left(-\frac{4}{e^3} + \frac{7}{e} - 3e\right) J_p(pe) J_p'(pe) + \left[\frac{1}{e^2} - 1 + p^2\left(\frac{1}{e^2} - 2 + e^2\right)\right] (J_p'(pe))^2 \Bigg\}\ . \end{aligned} \tag{N.27}$$

In the 1.5PN expression for the luminosity the choice of eccentricity parameter will not effect the total GW luminosity until 2.5PN and higher orders.

BIBLIOGRAPHY

[1] A. G. Wiseman, Phys. Rev. D. **46**, 1517 (1992).

[2] D. Merritt, M. Milosavljević, M. Favata, S. A. Hughes, and D. E. Holz, Astrophys. J. Lett. **607**, L9 (2004).

[3] K. Oohara and T. Nakamura, Phys. Lett. **94A**, 349 (1983).

[4] M. Favata, S. A. Hughes, and D. E. Holz, Astrophys. J. Lett **607**, L5 (2004), astro-ph/0402056.

[5] M. Campanelli, Class. Quantum Grav. **22**, S387 (2005), astro-ph/0411744.

[6] L. Blanchet, M. S. S. Qusailah, and C. M. Will, Astrophys. J. **635**, 508 (2005), astro-ph/0507692.

[7] F. Herrmann, D. Shoemaker, and P. Laguna, (2006), gr-qc/0601026.

[8] T. Damour and A. Gopakumar, (2006), gr-qc/0602117.

[9] J. G. Baker *et al.*, (2006), astro-ph/0603204.

[10] G. J. Mathews and J. R. Wilson, Phys. Rev. D **61**, 127304 (2000), gr-qc/9911047.

[11] J. R. Wilson, G. J. Mathews, and P. Marronetti, Phys. Rev. D **54**, 1317 (1996), gr-qc/9601017.

[12] M. Favata, Phys. Rev. D **73**, 104005 (2006), astro-ph/0510668.

[13] R. A. Hulse and J. H. Taylor, Astrophys. J. Lett. **195**, L51 (1975).

[14] LIGO http://www.ligo.caltech.edu.

[15] GEO600 http://www.geo600.uni-hannover.de.

[16] TAMA300 http://tamago.mtk.nao.ac.jp.

[17] VIRGO http://www.virgo.infn.it.

[18] K. S. Thorne, *Black holes and time warps: Einstein's outrageous legacy* (Commonwealth Fund Book Program, New York, NY: W.W. Norton and London: Picador, —c1994, 1994).

[19] M. J. Fitchett and S. Detweiler, Mon. Not. R. Astron. Soc. **211**, 933 (1984).

[20] M. S. Turner, Physica Scripta Volume T **85**, 210 (2000), astro-ph/9901109.

[21] M. C. Miller and E. J. M. Colbert, Int. J. Mod. Phys. **D13**, 1 (2004), astro-ph/0308402.

[22] D. Lai, Phys. Rev. Lett. **76**, 4878 (1996), astro-ph/9605095.

[23] É. É. Flanagan, Phys. Rev. Lett. **82**, 1354 (1999), astro-ph/9811132.

[24] D. Kennefick, Social Studies of Sciences **30**, 5 (2000).

[25] H. Fang and G. Lovelace, Phys. Rev. D **72**, 124016 (2005).

[26] A. Pound, E. Poisson, and B. G. Nickel, Phys. Rev. D **72**, 124001 (2005).

[27] W. B. Bonnor and M. A. Rotenberg, Proc. R. Soc. London **A265**, 109 (1961).

[28] A. Peres, Phys. Rev. **128**, 2471 (1962).

[29] A. Papapetrou, C. R. Acad. Sci. Paris **255**, 1578 (1962).

[30] A. Papapetrou, Ann. Inst. H. Poincaré **14**, 79 (1971).

[31] J. D. Bekenstein, Astrophys. J. **183**, 657 (1973).

[32] F. I. Cooperstock, Physical Review **165**, 1424 (1968).

[33] F. I. Cooperstock and D. J. Booth, Physical Review **187**, 1796 (1969).

[34] F. I. Cooperstock, Astrophys. J. **213**, 250 (1977).

[35] W. H. Press, Phys. Rev. D **15**, 965 (1977).

[36] D. J. Booth, International Journal of Theoretical Physics **13**, 363 (1975).

[37] D. J. Booth, International Journal of Theoretical Physics **10**, 333 (1974).

[38] D. D. Dionysiou, Int. J. Theor. Phys. **10**, 355 (1974).

[39] D. D. Dionysiou, Lett. Nuovo Cim. **13**, 86 (1975).

[40] W. B. Campbell and T. Morgan, Physica **53**, 264 (1971).

[41] D. D. Dionysiou, Journal of Physics A Mathematical General **10**, 969 (1977).

[42] D. D. Dionysiou, Astrophys. Space Sci. **52**, 17 (1977).

[43] W. B. Bonnor and M. A. Rotenberg, Proc. R. Soc. London A **A289**, 247 (1966).

[44] K. S. Thorne, Rev. Mod. Phys. **52**, 299 (1980).

[45] W. B. Bonnor and M. S. Piper, Classical and Quantum Gravity **14**, 2895 (1997).

[46] V. Moncrief, Astrophys. J. **238**, 333 (1980).

[47] C. T. Cunningham, R. H. Price, and V. Moncrief, Astrophys. J. **224**, 643 (1978).

[48] C. T. Cunningham, R. H. Price, and V. Moncrief, Astrophys. J. **230**, 870 (1979).

[49] S. Brandt and P. Anninos, Phys. Rev. D. **60**, 084005 (1999).

[50] E. R. Harrison and E. Tademaru, Astrophys. J. **201**, 447 (1975).

[51] D. Lai, D. F. Chernoff, and J. M. Cordes, Astrophys. J. **549**, 1111 (2001).

[52] M. J. Fitchett, Mon. Not. R. Astron. Soc. **203**, 1049 (1983).

[53] T. Nakamura and M. P. Haugan, Astrophys. J. **269**, 292 (1983).

[54] Z. Andrade and R. H. Price, Phys. Rev. D. **56**, 6336 (1997).

[55] P. Anninos and S. Brandt, Physical Review Letters **81**, 508 (1998).

[56] C. O. Lousto and R. H. Price, Phys. Rev. **D69**, 087503 (2004), gr-qc/0401045.

[57] H. Pietila, P. Heinamaki, S. Mikkola, and M. J. Valtonen, Celestial Mechanics and Dynamical Astronomy **62**, 377 (1995).

[58] W. Junker and G. Schaefer, Mon. Not. R. Astron. Soc. **254**, 146 (1992).

[59] L. Blanchet, Phys. Rev. D **55**, 714 (1997).

[60] L. E. Kidder, Phys. Rev. D. **52**, 821 (1995).

[61] J. P. A. Clark and D. M. Eardley, Astrophys. J. **215**, 311 (1977).

[62] Y. Kojima and T. Nakamura, Prog. Theor. Phy. **71**, 79 (1984).

[63] T. Nakamura, K. Oohara, and Y. Kojima, Prog. Theor. Phy. Supp. **90**, 1 (1987).

[64] C. W. Misner, K. S. Thorne, and J. A. Wheeler, *Gravitation* (Freeman, San Francisco, 1973).

[65] É. Racine and É. É. Flanagan, Phys. Rev. D **71**, 044010 (2005), gr-qc/0404101.

[66] L. D. Landau and E. M. Lifshitz, *The classical theory of fields* (Butterworth Heinemann, Oxford, 1975).

[67] R. A. Isaacson, Physical Review **166**, 1272 (1968).

[68] T. Damour, Phys. Rev. D. **64**, 124013 (2001).

[69] L. Smarr, Gauge conditions, radiation formulae, and the two black hole collision, in *Sources of Graviational Radiation*, edited by L. Smarr, Cambridge, 1978, Cambridge University Press.

[70] S. A. Teukolsky, Astrophys. J. **185**, 635 (1973).

[71] S. A. Hughes, Phys. Rev. D. **61**, 084004 (2000).

[72] S. A. Hughes, Phys. Rev. D **64**, 064004 (2001).

[73] J. M. Bardeen, W. H. Press, and S. A. Teukolsky, Astrophys. J. **178**, 347 (1972).

[74] A. Ori and K. S. Thorne, Phys. Rev. D. **62**, 124022 (2000).

[75] G. Khanna, Phys. Rev. **D69**, 024016 (2004), gr-qc/0309107.

[76] K. Martel, Phys. Rev. **D69**, 044025 (2004), gr-qc/0311017.

[77] R. Barkana and A. Loeb, Phys. Rep. **349**, 125 (2001).

[78] M. Volonteri, F. Haardt, and P. Madau, Astrophys. J. **582**, 559 (2003), astro-ph/0207276.

[79] P. Madau, M. J. Rees, M. Volonteri, F. Haardt, and S. P. Oh, Astrophys. J. **604**, 484 (2004), astro-ph/0310223.

[80] I. H. Redmount and M. J. Rees, Comments on Astrophysics **14**, 165 (1989).

[81] B. Abbott et al. (The LIGO Scientific Collaboration), Phys. Rev. D **69**, 122001 (2004), gr-qc/0308069.

[82] B. Abbott et al. (The LIGO Scientific Collaboration), Phys. Rev. D **72**, 082001 (2005), gr-qc/0505041.

[83] C. Cutler and K. S. Thorne, An overview of gravitational-wave sources, in *Proceedings of the 16th International Conference on General Relativity and Gravitation*, edited by N. T. Bishop and S. D. Maharaj, Singapore, 2002, World Scientific, gr-qc/0204090.

[84] L. Blanchet, Living Rev. Relativity **5**, 3 (2002), gr-qc/0202016.

[85] T. W. Baumgarte and S. L. Shapiro, Phys. Rept. **376**, 41 (2003), gr-qc/0211028.

[86] M. Shibata, K. Taniguchi, and K. Uryū, Phys. Rev. D **71**, 084021 (2005), gr-qc/0503119.

[87] F. A. Rasio and S. L. Shapiro, Class. Quantum Grav. **16**, R1 (1999), gr-qc/9902019.

[88] S. Kobayashi and P. Mészáros, Astrophys. J. **589**, 861 (2003), astro-ph/0210211.

[89] J. R. Wilson and G. J. Mathews, Phys. Rev. Lett. **75**, 4161 (1995).

[90] P. R. Brady and S. A. Hughes, Phys. Rev. Lett. **79**, 1186 (1997), gr-qc/9704019.

[91] É. É. Flanagan, Phys. Rev. D **58**, 124030 (1998), gr-qc/9706045.

[92] K. S. Thorne, Phys. Rev. D **58**, 124031 (1998), gr-qc/9706057.

[93] A. G. Wiseman, Phys. Rev. Lett. **79**, 1189 (1997), gr-qc/9704018.

[94] K. Taniguchi and T. Nakamura, Phys. Rev. Lett. **84**, 581 (2000), astro-ph/9911426.

[95] J. C. Lombardi, F. A. Rasio, and S. L. Shapiro, Phys. Rev. D **56**, 3416 (1997), astro-ph/9705218.

[96] T. W. Baumgarte, G. B. Cook, M. A. Scheel, S. L. Shapiro, and S. A. Teukolsky, Phys. Rev. Lett. **79**, 1182 (1997), gr-qc/9704024.

[97] T. W. Baumgarte, G. B. Cook, M. A. Scheel, S. L. Shapiro, and S. A. Teukolsky, Phys. Rev. D **57**, 6181 (1998), gr-qc/9705023.

[98] T. W. Baumgarte, G. B. Cook, M. A. Scheel, S. L. Shapiro, and S. A. Teukolsky, Phys. Rev. D **57**, 7299 (1998), gr-qc/9709026.

[99] S. Bonazzola, E. Gourgoulhon, and J.-A. Marck, Phys. Rev. Lett. **82**, 892 (1999), gr-qc/9810072.

[100] K. Taniguchi and E. Gourgoulhon, Phys. Rev. D **66**, 104019 (2002), gr-qc/0207098.

[101] M. Shibata, T. W. Baumgarte, and S. L. Shapiro, Phys. Rev. D **58**, 023002 (1998), gr-qc/9805026.

[102] K. Uryū and Y. Eriguchi, Phys. Rev. D **61**, 124023 (2000), gr-qc/9908059.

[103] K. Uryū, M. Shibata, and Y. Eriguchi, Phys. Rev. D **62**, 104015 (2000), gr-qc/0007042.

[104] S. L. Shapiro, Phys. Rev. Lett. **77**, 4487 (1996).

[105] C. D. Murray and S. F. Dermott, *Solar System Dynamics* (Cambridge University Press, Cambridge, 1999).

[106] D. Lai, Mon. Not. R. astr. Soc. **270**, 611 (1994), astro-ph/9404062.

[107] J. R. Wilson and G. J. Mathews, *Relativistic Numerical Hydrodynamics* (Cambridge University Press, Cambridge, 2003).

[108] J. R. Wilson, G. J. Mathews, and J. D. Salmonson, Nuovo Cimento B **117**, 1257 (2002).

[109] G. B. Cook, S. L. Shapiro, and S. A. Teukolsky, Phys. Rev. D **53**, 5533 (1996), gr-qc/9512009.

[110] J. R. Wilson and R. W. Mayle, Phys. Rep. **227**, 97 (1993).

[111] R. W. Mayle, M. Tavani, and J. R. Wilson, Astrophys. J. **418**, 398 (1993).

[112] J. D. Salmonson, J. R. Wilson, and G. J. Mathews, Astrophys. J. **553**, 471 (2001), astro-ph/0002312.

[113] G. J. Mathews, P. Marronetti, and J. R. Wilson, Phys. Rev. D **58**, 043003 (1998), gr-qc/9710140.

[114] M. Shibata and K. Taniguchi, Phys. Rev. D **56**, 811 (1997), gr-qc/9705028.

[115] S. L. Shapiro, Phys. Rev. D **57**, 908 (1998), gr-qc/9710094.

[116] M. D. Duez, E. T. Engelhard, J. M. Fregeau, K. M. Huffenberger, and S. L. Shapiro, Phys. Rev. D **60**, 104024 (1999), gr-qc/9904011.

[117] K. Alvi and Y. T. Liu, Gen. Rel. Grav. **34**, 1067 (2002), gr-qc/0110091.

[118] J. R. Wilson and G. J. Mathews, Astrophys. J. **610**, 368 (2004), astro-ph/0307337.

[119] J. D. Salmonson and J. R. Wilson, Astrophys. J. **578**, 310 (2002), astro-ph/0203349.

[120] P. Marronetti, G. J. Mathews, and J. R. Wilson, Phys. Rev. D **60**, 087301 (1999), gr-qc/9906088.

[121] S. A. Teukolsky, Astrophys. J. **504**, 442 (1998), gr-qc/9803082.

[122] S. Bonazzola, E. Gourgoulhon, and J.-A. Marck, Evolutionary sequences of irrotational binary neutron stars, in *Proceedings of the XIX Texas Symposium in Relativistic Astrophyics and Cosmology*, edited by J. Paul, T. Montmerle, and E. Aubourg, Paris, France, 1999, CEA Saclay, gr-qc/9904040.

[123] K. Taniguchi and E. Gourgoulhon, Phys. Rev. D **68**, 124025 (2003), gr-qc/0309045.

[124] E. Gourgoulhon, P. Grandclément, K. Taniguchi, J.-A. Marck, and S. Bonazzola, Phys. Rev. D **63**, 064029 (2001), gr-qc/0007028.

[125] J. R. Wilson, Phys. Rev. D **66**, 084015 (2002).

[126] P. Marronetti, G. J. Mathews, and J. R. Wilson, Binary neutron stars systems: Irrotational quasi-equilibrium sequences, in *Proceedings of the XIX Texas Symposium in Relativistic Astrophyics and Cosmology*, edited by J. Paul, T. Montmerle, and E. Aubourg, Paris, France, 1999, CEA Saclay, gr-qc/9903105.

[127] P. Marronetti, private communication, 2005.

[128] C. S. Kochanek, Astrophys. J. **398**, 234 (1992).

[129] L. Bildsten and C. Cutler, Astrophys. J. **400**, 175 (1992).

[130] P. Marronetti and S. L. Shapiro, Phys. Rev. D **68**, 104024 (2003), gr-qc/0306075.

[131] É. Racine and É. É. Flanagan, Phys. Rev. D (2006), gr-qc/0601029, (in press).

[132] S. Weinberg, *Gravitation and Cosmology: Principles and Applications of the General Theory of Relativity* (Wiley, New York, 1972).

[133] S. L. Shapiro and S. A. Teukolsky, *Black Holes, White Dwarfs, and Neutron Stars* (Wiley, New York, 1983).

[134] K. S. Thorne, R. H. Price, and D. A. Macdonald, *Black Holes: The Membrane Paradigm* (Yale University Press, New Haven, 1986).

[135] J. M. Bardeen, W. H. Press, and S. A. Teukolsky, Astrophys. J. **178**, 347 (1972).

[136] X.-H. Zhang, Phys. Rev. D **31**, 3130 (1985).

[137] P. Purdue, Phys. Rev. D **60**, 104054 (1999), gr-qc/9901086.

[138] M. Favata, Phys. Rev. D **63**, 064013 (2001), gr-qc/0008061.

[139] I. S. Booth and J. D. E. Creighton, Phys. Rev. D **62**, 067503 (2000), gr-qc/0003038.

[140] N. Andersson, Astrophys. J. **502**, 708 (1998), gr-qc/9706075.

[141] L. Lindblom, B. J. Owen, and S. M. Morsink, Phys. Rev. Lett. **80**, 4843 (1998), gr-qc/9803053.

[142] B. J. Owen *et al.*, Phys. Rev. D **58**, 084020 (1998), gr-qc/9804044.

[143] J. R. Wilson, private communication, 2005.

[144] L. Lindblom, J. E. Tohline, and M. Vallisneri, Phys. Rev. Lett. **86**, 1152 (2001), astro-ph/0010653.

[145] P. Gressman, L.-M. Lin, W.-M. Suen, N. Stergioulas, and J. L. Friedman, Phys. Rev. D **66**, 041303 (2002), gr-qc/0301014.

[146] N. Stergioulas and J. A. Font, Phys. Rev. Lett. **86**, 1148 (2001), gr-qc/0007086.

[147] M. Miller, (2005), gr-qc/0510020.

[148] C. Cutler, D. Kennefick, and E. Poisson, Phys. Rev. D **50**, 3816 (1994).

[149] M. Freitag, Astrophys. J. Lett. **583**, L21 (2003), astro-ph/0211209.

[150] L. S. Finn and K. S. Thorne, Phys. Rev. D **62**, 124021 (2000).

[151] P. C. Peters, Physical Review **136**, 1224 (1964).

[152] L. Barack and C. Cutler, Phys. Rev. D **69**, 082005 (2004).

[153] J. R. Gair *et al.*, Classical and Quantum Gravity **21**, 1595 (2004).

[154] S. Drasco, É. É. Flanagan, and S. A. Hughes, Classical and Quantum Gravity **22**, 801 (2005).

[155] S. A. Hughes and R. D. Blandford, Astrophys. J. Lett. **585**, L101 (2003).

[156] S. Drasco and S. A. Hughes, Phys. Rev. D **73**, 024027 (2006).

[157] K. Glampedakis, S. A. Hughes, and D. Kennefick, Phys. Rev. D **66**, 064005 (2002).

[158] S. Babak, H. Fang, J. R. Gair, K. Glampedakis, and S. A. Hughes, (2006), gr-qc/0607007.

[159] Y. Mino, M. Sasaki, and T. Tanaka, Phys. Rev. D **55**, 3457 (1997).

[160] T. C. Quinn and R. M. Wald, Phys. Rev. D **56**, 3381 (1997).

[161] E. Poisson, Living Reviews in Relativity **7**, 6 (2004).

[162] E. Poisson, The gravitational self-force, available at http://www.physics.uoguelph.ca/poisson/research/self.pdf.

[163] L. Barack and A. Ori, Phys. Rev. Lett. **90**, 111101 (2003).

[164] K. Glampedakis and D. Kennefick, Phys. Rev. D **66**, 044002 (2002).

[165] K. Glampedakis, Class. Quantum Grav. **22**, S605 (2005).

[166] Y. Mino, Phys. Rev. D **67**, 084027 (2003).

[167] S. Detweiler and B. F. Whiting, Phys. Rev. D **67**, 024025 (2003).

[168] S. A. Hughes, S. Drasco, É. É. Flanagan, and J. Franklin, Physical Review Letters **94**, 221101 (2005).

[169] N. Sago, T. Tanaka, W. Hikida, and H. Nakano, Progress of Theoretical Physics **114**, 509 (2005).

[170] N. Sago, T. Tanaka, W. Hikida, K. Ganz, and H. Nakano, ArXiv General Relativity and Quantum Cosmology e-prints (2005), arXiv:gr-qc/0511151.

[171] T. Hinderer and E. E. Flanagan, in preparation.

[172] L. M. Burko, Phys. Rev. D **67**, 084001 (2003).

[173] C. Cutler and É. E. Flanagan, Phys. Rev. D **49**, 2658 (1994).

[174] S. Droz, D. J. Knapp, E. Poisson, and B. J. Owen, Phys. Rev. D **59**, 124016 (1999).

[175] A. Królak, K. D. Kokkotas, and G. Schäfer, Phys. Rev. D **52**, 2089 (1995).

[176] L. Blanchet, G. Faye, B. R. Iyer, and B. Joguet, Phys. Rev. D **65**, 061501 (2002).

[177] L. Blanchet, G. Faye, B. R. Iyer, and B. Joguet, Phys. Rev. D **71**, 129902(E) (2005).

[178] T. Damour and N. Deruelle, Ann. Inst. Henri Poincaré **43**, 107 (1985).

[179] T. Damour and G. Schäfer, Nuovo Cimento **101B**, 127 (1988).

[180] G. Schäfer and N. Wex, Phys. Lett. A **174**, 196 (1993).

[181] T. Damour, A. Gopakumar, and B. R. Iyer, Phys. Rev. D **70**, 064028 (2004).

[182] R.-M. Memmesheimer, A. Gopakumar, and G. Schäfer, Phys. Rev. D **70**, 104011 (2004).

[183] C. Königsdörffer and A. Gopakumar, Phys. Rev. D **73**, 124012 (2006).

[184] D. Whitbeck and B. J. Owen, (in preparation).

[185] W. Schmidt, Classical and Quantum Gravity **19**, 2743 (2002).

[186] S. Drasco and S. A. Hughes, Phys. Rev. D **69**, 044015 (2004).

[187] M. Favata and S. A. Hughes, in preparation.

[188] C. Cohen-Tanoudji, B. Diu, and F. Lalo, *Quantum Mechanics* (Wiley Interscience, New York, 1977).

[189] W. H. Press and S. A. Teukolsky, Astrophys. J. **185**, 649 (1973).

[190] F. K. Manasse and C. W. Misner, J. Math. Phys. **4**, 735 (1963).

[191] M. Ishii, M. Shibata, and Y. Mino, Phys. Rev. D **71**, 044017 (2005), gr-qc/0501084.

[192] W.-T. Ni and M. Zimmermann, Phys. Rev. D **17**, 1473 (1978).

[193] W.-Q. Li and W.-T. Ni, J. Math. Phys. **20**, 1473 (1979).

[194] A. H. Taub, Ann. Rev. Fluid Mech. **10**, 301 (1978).

[195] D. Lai, F. A. Rasio, and S. L. Shapiro, Astrophys. J. Suppl. Ser. **88**, 205 (1993).

[196] E. Poisson, Phys. Rev. D **70**, 084044 (2004), gr-qc/0407050.

[197] L. Blanchet and G. Schafer, Classical and Quantum Gravity **10**, 2699 (1993).

[198] R. Rieth and G. Schäfer, Classical and Quantum Gravity **14**, 2357 (1997).

[199] A. Gopakumar and B. R. Iyer, Phys. Rev. D **56**, 7708 (1997).

[200] P. C. Peters and J. Mathews, Physical Review **131**, 435 (1963).

[201] L. Blanchet and G. Schaefer, Mon. Not. R. Astron. Soc. **239**, 845 (1989).